Synthesis and Study of Polyazine Bridged Mixed Metal Dyads: Electrochemical, Photophysical, and Photochemical Properties of a New Supramolecular Architecture

by

David Francis Zigler

Dissertation submitted to the faculty of the Virginia Polytechnic Institute and State University in partial fulfillment of the requirements for the degree of

Doctor of Philosophy

In

Department of Chemistry

Karen J. Brewer, Chair

Brenda S. J. Winkel

Paul A. Deck

Gordon T. Yee

James M. Tanko

October 28, 2008

Blacksburg, VA

Keywords: supramolecules, mixed-metal, polyazine, DNA, photochemistry, osmium, ruthenium, rhodium

Synthesis and Study of Polyazine Bridged Mixed Metal Dyads: Electrochemical, Photophysical, and Photochemical Properties of a New Supramolecular Architecture

David F. Zigler

ABSTRACT

A series mixed metal supramolecular complexes were synthesized and studied by electrochemistry, photophysics and photochemistry. The complexes consisted of a single Ru^{II} or Os^{II} polyazine light absorber bound to a *cis*-$Rh^{III}Cl_2$ moiety through a polyazine bridging ligand. A related class of supramolecule is known to perform photoinitiated electron collection, photocatalysis of hydrogen from water, DNA photomodification and is known to kill mammalian cells; all with visible light irradiation. The complexes studied herein, $[(bpy)_2Ru(bpm)RhCl_2(phen)](PF_6)_3$, $[(bpy)_2Ru(dpp)RhCl_2(phen)](PF_6)_3$, $[(bpy)_2Os(dpp)RhCl_2(phen)](PF_6)_3$, and $[(tpy)OsCl(dpp)RhCl_2(phen)](PF_6)_2$ were synthesized in moderate yields (54-84%) by reaction of the appropriate monometallic visible light absorbing subunit with a slight excess of $K[(phen)RhCl_4]\cdot 3H_2O$ (bpy = 2,2'-bipyridine, bpm = 2,2'-bipyrimidine, 1,10-phenanthroline, dpp = 2,3-bis(2-pyridyl)pyrazine, and tpy = 2,2':6',2''-terpyridine). Voltammetric analysis of $[(bpy)_2Ru(bpm)RhCl_2(phen)](PF_6)_3$ revealed a reversible oxidation at 1.76 V (vs. Ag/AgCl) ($Ru^{III/II}$). A reversible reduction at −0.14 V ($bpm^{0/-}$), and quasi-reversible reductions at −0.77 V and −0.91 V each corresponded to a one electron process, $bpm^{0/-}$, $Rh^{III/II}$ and $Rh^{II/I}$. The electrochemistry of $[(bpy)_2Ru(dpp)RhCl_2(phen)](PF_6)_3$ showed a reversible oxidation at 1.61 V ($Ru^{III/II}$), and quasi-reversible reductions at −0.39 V, −0.74 V and −0.98 V. The first two reductive couples corresponded to two electrons, consistent with Rh reduction. $[(bpy)_2Os(dpp)RhCl_2(phen)](PF_6)_3$, and $[(tpy)OsCl(dpp)RhCl_2(phen)](PF_6)_2$ each exhibited reductions similar to the dpp bridged Ru,Rh dyad, but with $Os^{III/II}$ based oxidations at 1.24 V and 0.83 V, respectively. The complexes $[(bpy)_2Ru(bpm)RhCl_2(phen)](PF_6)_3$ and $[\{(bpy)_2Ru(bpm)\}_2RhCl_2](PF_6)_5$ display Ru(dπ)→bpm(π*) CT (MLCT) transitions at 581 nm and at 594 nm, respectively. The dpp bridged Ru,Rh bimetallic and Ru,Rh,Ru trimetallic display Ru(dπ)→dpp(π*) CT transitions at 509 nm and 518 nm, respectively. Similarly, $[(bpy)_2Os(dpp)RhCl_2(phen)](PF_6)_3$ absorbs strongly at 520 nm versus 534 nm for $[\{(bpy)_2Os(dpp)\}_2RhCl_2](PF_6)_5$, both with low energy tails at 800 nm indicative of Os centered MLCT transitions. Overlapping Os(dπ)→dpp(π*) and Os(dπ)→tpy(π*) transitions occur at 536

nm with low energy tails at 856 nm for both $[(tpy)OsCl(dpp)RhCl_2(phen)](PF_6)_2$ and $[\{(tpy)OsCl(dpp)\}_2RhCl_2](PF_6)_3$. Emission from $[\{(bpy)_2Ru(dpp)\}RhCl_2](PF_6)_5$ and $[(bpy)_2Ru(dpp)RhCl_2(phen)](PF_6)_3$ at room temperature and 77 K was red shifted and less intense than emission from $[(bpy)_2Ru(dpp)Ru(bpy)_2](PF_6)_4$, consistent with quenched emission from a Ru(dπ)→dpp(π*) ^{3}MLCT state. Transient absorption spectroscopy supported assignment of the emissive state as Ru(dπ)→dpp(π*) CT in nature. The complexes $[(bpy)Ru(dpp)RhCl_2(phen)](PF_6)_3$ (τ =18 ns) and $[\{(bpy)_2Ru(dpp)\}_2RhCl_2](PF_6)_5$ (τ = 16 ns) each exhibit shorter lived ^{3}MLCT states than the Ru,Ru dyad (τ = 125 ns) in acetonitrile consistent with favorable electron transfer to Rh(III) to generate a metal to metal charge transfer (^{3}MMCT) state. The photochemistry of $[\{(bpy)_2Ru(dpp)\}_2RhCl_2]Cl_5$, $[\{(tpy)OsCl(dpp)\}_2RhCl_2]Cl_3$, $[(bpy)_2Ru(dpp)RhCl_2(phen)]Cl_3$, and $[(tpy)OsCl(dpp)RhCl_2(phen)]Cl_2$ with DNA was investigated using gel electrophoresis and selective precipitation of a DNA/metal complex adduct. An array of high intensity LEDs was designed, constructed and validated to accommodate these high throughput photochemical experiments with DNA. Each of the metal complexes is suggested to undergo photobinding with DNA as well as to photocleave DNA. A ^{3}MMCT state or a thermally accessible Rh centered ^{3}LF state each are proposed as leading to photobinding, while a ^{3}MMCT state is thought to be involved in DNA photocleavage.

Thesis Statement

The aim of this research is to explore the electrochemical, photophysical and photochemical properties of supramolecular complexes with a single Ru^{II} or Os^{II} polyazine visible light absorber bonded to a *cis*-$Rh^{III}Cl_2$ moiety via bridging polyazine ligands. The new bimetallic architecture is analogous to previously studied trimetallic supramolecules with interesting electronic excited state dynamics and capable of photochemistry with DNA.

Acknowledgements

Many people were involved in shaping my knowledge, passion and work ethic. First, I thank my parents. My mother Karen M. Zigler encouraged me to pursue all my interests. My father, Eric H. Zigler, I thank for the seemingly endless discussions on various topics, including: astronomy, modern theoretical physics, electronics, philosophy, biology, medicine, music, language, politics and anything else that presented itself. I thank my high school Chemistry teacher, Steve Johnson, for using explosions and fire to make Chemistry cool. I thank T. Howard Black, Professor Emeritus at Eastern Illinois University, for introducing me to undergraduate research. I thank Professor Edward M. Treadwell, also of EIU, for allowing me to work long hours in the lab and for his patience. I thank Professors Emeritus Richard L. and Ellen A. Keiter for introducing me to Chemistry with metals. I thank the kitchen crew at Roc's Blackfront in Charleston, IL for encouraging my work ethic. Thanks to the Brewer research group, past and present, for helpful discussions. I especially thank the undergraduates that I was fortunate to work with, including: Aaron J. (A.J.) Prussin for helping develop the LED array experiments; Julie Heinecke for synthesizing a useful starting ligand, Lilit Stepanyan and Judy Chu for performing the early DNA studies with the bimetallics, Geoff Lewis for his work on the osmium containing supramolecules project and Elizabeth Spencer for synthesizing and studying a new complex during a grueling semester. I also thank Prof. Matthew T. Mongelli, Dr. Shamindri M. Arachchige, and Jared R. Brown for their collaborative efforts on a number of projects. I thank my advisory committee, Professors Paul A. Deck, James M. Tanko, and Gordon T. Yee, for their contribution to my professional development and especially for their attention to detail when reviewing me or my works. I thank Professor Brenda S. J. Winkel, an unofficial co-chair on my advisory committee, for providing external perspective on ideas and papers needing a touch of biological understanding. Thanks to my advisor, Prof. Karen J. Brewer, for her support, encouragement and advice, and for helping me to see that sometimes the most selfless acts that make us seem vulnerable only make us stronger.

Table of Contents

List of Figures

List of Tables

List of Abbreviations

5,6-Me_2phen = 5,6-dimethyl-1,10-phenanthroline
bpm = 2,2'-bipyrimidine
bpy = 2,2'-bipyridine
dpp = 2,3-bis(2-pyridyl)pyrazine
dppz = dipyrido[3,2-*a*:2',3'-*c*]phenazine
EA = electron acceptor
ED = electron donor
en = excited state energy transfer
ES = excited state light absorber
et = excited state electron transfer
f = fluorescence
GS = ground state light absorber
HAT = 1,4,5,8,9,12-hexaazatriphenylene
HOMO = highest occupied molecular orbital
ic = internal conversion
IL = internal ligand
isc = intersystem crossing
k_x = rate constant of process "x"
LA = ground state light absorber
*LA = excited state light absorber
LF = ligand field
LUMO = lowest unoccupied molecular orbital
MLCT = metal to ligand charge transfer
MMCT = metal to metal charge transfer
MMLCT = metal-metal to ligand charge transfer
nr = non-radiative decay
p = phosphorescence
PDT = photodynamic therapy
Ph_2phen = 4,7-diphenyl-1,10-phenanthroline
phen = 1,10-phenanthroline
phi = 9,10-phenanthrenequinone diimine
q = bimolecular deactivation
Q = quencher
rxn = photochemical reaction
τ = electronic excited state lifetime
TAP = 1,4,5,8-tetraazaphenanthrene
tpy = 2,2':6',2''-terpyridine
Φ_x = quantum yield of process "x"

Preface

This dissertation describes one seminal study completed by the author. During his graduate career, the author has worked on other projects, resulting in several publications, which go beyond the scope of this dissertation. Following is a list of the publications to date resulting from the graduate work. Works relevant to the dissertation work are marked with an asterisk.

"Toward Photodynamic Therapy of Cancer with Platinum Group Metal Polyazine Complexes," in Metal Complexes—DNA Interactions, David F. Zigler, Karen J. Brewer Blackwell Publishing Ltd, Oxford, in press.

*"Ruthenium(II)-Polyazine Light Absorbers Bridged to Reactive *cis*-Dichlororhodium(III) Centers in a Bimetallic Molecular Architecture," David F. Zigler, Jing Wang, Karen J. Brewer *Inorg. Chem.* **2008,** in press.

"Multifunctional DNA Interactions by Design: Ground and Excited State Properties of a Mixed Metal Supramolecular Complex that Binds and Photocleaves DNA $[\{(bpy)_2Ru(dpp)\}_2Ru(dpp)PtCl_2](PF_6)_6$," Ran Miao, David F. Zigler, Brenda S. J. Winkel, Karen J. Brewer, **2008,** submitted for publication.

"Design Considerations for a System for Photocatalytic Hydrogen Production from Water Employing Mixed-Metal Photochemical Molecular Devices for Photoinitiated Electron Collection," Shamindri M. Arachchige, Jared R. Brown, Eric Chang, Avijita Jain, David F. Zigler, Krishnan Rangan, Karen J. Brewer **2008**, submitted for publication.

*"Photochemical Methods to Assay DNA Photocleavage using Supercoiled pUC18 DNA and LED or Xenon Arc Lamp Excitation," Aaron J. Prussin II, David F. Zigler, Avijita Jain, Jared R. Brown, Brenda S. J. Winkel, Karen J. Brewer *J. Inorg. Biochem.* **2008,** *102,* 731-9.

"Photobiological Impact of $[\{(bpy)_2Ru(dpp)\}_2RhCl_2]Cl_5$ and $[\{(bpy)_2Os(dpp)\}_2RhCl_2]Cl_5$ [bpy = 2,2'-bipyridine, dpp = 2,3-bis(2-pyridyl)pyrazine] on Vero Cells," Alvin A. Holder, David F. Zigler, Maria T. Tarrago-Trani, Brian Storrie, Karen J. Brewer *Inorg. Chem.* **2007,** *46,* 4760-2.

*"A Trimetallic Supramolecular Complex of Osmium(II) and Rhodium(III) Displaying MLCT transitions in the Near-IR," David F. Zigler, Matthew T. Mongelli, Matthew Jeletic, Karen J. Brewer *Inorg. Chem. Commun.* **2007,** *10,* 295-8.

"Supramolecular Complexes as Photoinitiated Electron Collectors: Applications in Solar Hydrogen Production," Mark Elvington, Jared R. Brown, David F. Zigler, Karen J. Brewer *Proc. SPIE* **2006,** *6340,* 63400W/1.

*"Analytical Methods Development for Supramolecular Design in Solar Hydrogen Production," Jared R. Brown, Mark Elvington, Matthew T. Mongelli, David F. Zigler, Karen J. Brewer *Proc. SPIE* **2006,** *6340,* 634017/1.

"A Multifunctional Tetrametallic Ru-Pt Supramolecular Complex Exhibiting Both DNA Binding and Photocleavage," Ran Miao, Matthew T. Mongelli, David F. Zigler, Brenda S. J. Winkel, Karen J. Brewer *Inorg. Chem.* **2006,** *45,*10413-5.

"Luminescently Tagged 2,2'-Bipyridine Complex of Fe^{II}: Synthesis and Photophysical Studies of 4-[N-(2-anthryl)carbamoyl]-4'-methyl-2,2'-bipyridine," David F. Zigler, Mark C. Elvington, Julie Heinecke, Karen J. Brewer *Inorg. Chem.* **2006,** *45,* 6565-7.

Chapter 1. Introduction

Supramolecular devices, particularly those that function as photochemical molecular devices (PMD), garner expanding interest in commercial and scientific applications.[1] A more focused direction has been the study of platinum group transition metal complexes containing multiple metal centers bridged by aromatic polyazine ligands. This combination of ligands and metals features rich electrochemistry and photophysics. Each ligand and metal contributes to the properties of the supramolecule, but together they give a device with complex function. Substitution of any component for another in the supramolecular architecture often has significant impact on its physical and chemical properties. Tuning PMDs can therefore be performed through rational synthetic design to give mechanistic insight into their function. Supramolecules within a structurally diverse series can present a range of electronic properties and electronic excited states useful in various photochemical applications. This dissertation examines the subunit tuning of a new molecular architecture within a class of supramolecular devices known to perform DNA photomodification and to kill mammalian cells in the presence of light.

1.1. Definition of Transition Metal Polyazine Supramolecular Complexes

Supramolecules are broadly defined as species consisting of multiple molecular subunits that, when associated by non-covalent interactions (e.g. hydrogen bonding, molecular threading, electrostatic attraction), have more complex functions than the individual subunits. Balzani expanded this definition to include ligand-bridged multinuclear metal complexes with distinct

subunit and supramolecular electronic characteristics.[2] Supramolecular devices from Nature such as the photosystems and ATP synthase provide examples in this arena. Natural examples drive research to develop species that might be exploited as molecular devices.[3] Transition metal complexes incorporating polyazine ligands, Figure 1.1, are one class of PMD that show great promise in this field.[4-7]

Terminal Ligands

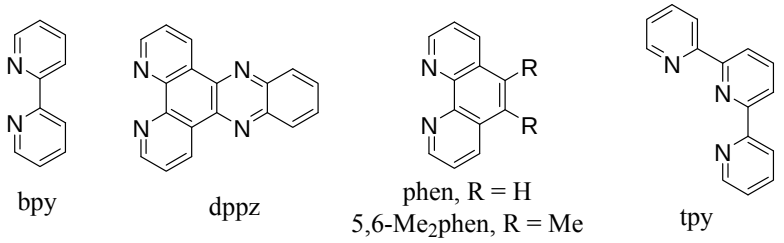

Bridging Ligands

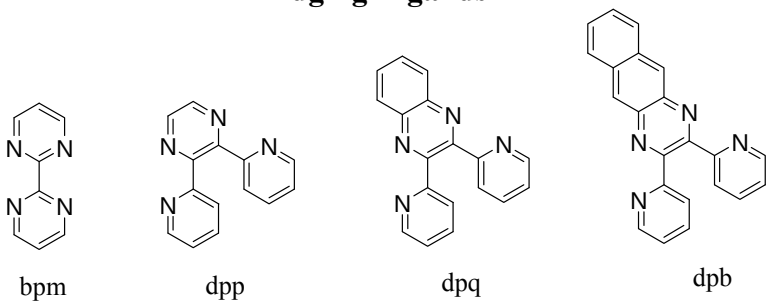

Figure 1.1. Polyazine ligands commonly used in the construction of transition metal based photochemical molecular devices.

1.2. Photochemical Molecular Devices for the Treatment of Cancer

Some PMDs function in the treatment of cancer and vascular diseases as agents for phototherapy (direct photoreaction) and photodynamic therapy (oxygen photosensitization). Both therapies are often abbreviated PDT due to the complicated photochemical mechanisms often involved in their action. Ideal PDT agents absorb light strongly in the red or near-infrared (NIR) region of the spectrum, accumulate within the target tissue, efficiently perform the intended action, have low systemic toxicity, and are eliminated rapidly from the body. Light in the red to NIR region of the spectrum (650-850 nm) is the light that has the greatest depth of penetration in human tissue and is known as the "therapeutic window."[8] Depending on the absorption properties of the tissue, 650 nm can penetrate to about 10 mm in depth. Potent light absorbers with moderately long-lived and reactive electronic excited states are of particular

interest. Chromophores with long-lived electronic excited states have a high probability of approach to a substrate during the excited state lifetime. Excited-state energy and lifetime often are inversely related, with longer wavelength light absorbers having short-lived excited states.[9] The short excited state lifetime is a result of low energy electronic excited states' tendency to be vibronically coupled to the ground state, also known as the Energy Gap Law.[10] Some PDT agents in current clinical usage show cytospecificity, accumulating in tumor cells and enhancing the photosensitizers' therapeutic function.[8] Uptake of the PDT agent is often complicated and is impacted by the size of the chromophore, its charge and its lipophilicity. All three are important characteristics to consider in the design of PDT agents for elimination from the body. PDT agents that have hydrophobic architectures are retained for long periods within the body, leading to prolonged patient photosensitivity.[11]

1.2.1. Inorganic Complexes as PDT Agents

Current PDT treatments employ organic chromophores as photosensitizers, but inorganic chromophores show great promise as PDT agents.[12,13] The first approved PDT agent was a hematoporphyrin derivative, Photofrin®, Figure 1.2. Other photosensitizers have been approved, all of which also are based on organic constructs.[8] PDT has not gained widespread clinical use due in part to the limited knowledge concerning its implementation. In addition, toxicity commonly associated with heavy metal-containing compounds has led to limited use of these promising species as PDT agents. Two metal-containing photosensitizers are in clinical trials, metoxifin lutetium and tin ethyl etiopurpurin. Transition metal-centered complexes with porphyrin, phthalocyanine, naphthalocyanine, or polypyridine type ligands have interesting excited state properties, making them good targets for future therapies. This chapter will focus on inorganic systems with electrochemical and excited state properties, and bioactivity that makes them of interest as future PDT agents.

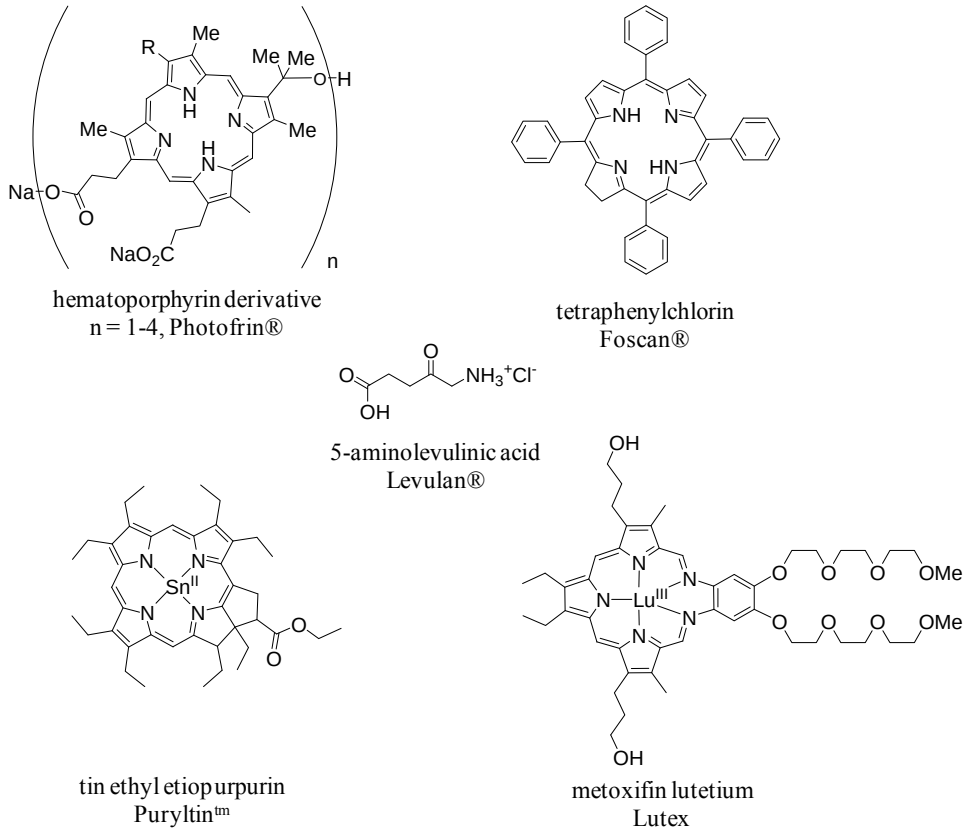

Figure 1.2. Chemicals currently in clinical use (Photofrin®, Foscan®, Levulan®) or clinical trial (Puryltin™, Lutex) as photodynamic therapy (PDT) agents.[11]

1.2.2. Study of Inorganic Complexes' Physical Properties Toward PDT

The physical properties of a potential PDT agent can give insight into its photochemical activity and provide a window into excited state tuning by structural modification. These properties include ground state and excited state species redox properties, light absorbing propeties and photophysical propeties. In addition, the study of these molecules in different solution and substrate environments provides a means to gauge their activity *in vivo.* Synthesis coupled with observation of physical properties provides a means of rational supramolecular design and elucidation of PMDs' photochemical mechanisms.

1.3. Redox Properties of Platinum Group Metal Polyazine Complexes

Octahedral d^6 platinum group metal polyazine complexes, e.g. Ru^{II}, Os^{II}, Rh^{III}, and Ir^{III}, have electrochemical properties characteristic of the polyazine ligand and metal center.

Electrochemistry often is performed using straightforward techniques, but can give important (though difficult to interpret) information about molecules' redox chemistry. The electrochemical properties of Ru^{II} and Os^{II} polyazine complexes are typified by metal based oxidations and ligand based reductions that correlate to the observed visible light absorbing properties of these complexes.[14] Polyazine complexes with a *cis*-$Rh^{III}Cl_2$ center often are characterized by Rh based reductions with reversible ligand reductions more negative,[15] while analogous *cis*-$Ir^{III}Cl_2$ complexes tend to have ligand centered reductions positive of the metal.[16,17] Combining platinum group polyazine complex based subunits into mixed metal supramolecular systems generally results in complexes with electrochemical properties analogous to subunit components, though shifted.[4] The electrochemical properties of mixed metal supramolecules therefore are useful in probing electronic excited states that might not be so easily explored by spectroscopic methods.

1.3.1. Electrochemical Measurements: Theory and Application

Electrochemistry is often used to characterize electroactive transition metal complexes, including those incorporating polyazine ligands. Cyclic voltammetry (CV) is commonly used to evaluate relative energies of various donor and acceptor orbitals of the species of interest. CV also provides information about electron transfer kinetics at the electrode surface and also details about chemical steps competing with electron transfer processes. Bulk electrolysis provides the number of electrons per molecule per electrochemical step and for evaluating the electronic and electronic absorption properties of electrochemical products. Changes to the electronic absorption properties following oxidation or reduction of a light absorbing metal complex (spectroelectrochemistry) are helpful in assigning the nature of electrochemically active orbitals or optical transitions.

1.3.1.1. Cyclic Voltammetry

Cyclic voltammetry is a linear sweep technique that gives important information about the frontier orbitals of an analyte. CV often is a technique performed using a three electrode system that changes the redox state of material at the electrode surface, Figure 1.3. Measurements are made at an inert working electrode. The potential at the working electrode is developed relative to a standard reference electrode that is usually a half cell of known potential.

For example, the saturated calomel electrode is based on the half-reaction shown in Eq. 1.1.

$$Hg_2Cl_{2(s)} + 2e^- \rightleftharpoons 2Hg_{(l)} + 2Cl^-_{(aq)} \qquad 0.2415 \text{ V vs. NHE}^{18} \qquad (1.1)$$

Here NHE is the normal hydrogen electrode, a common reference for reported standard potentials. A third electrode counters the current passed at the working electrode and is appropriately termed the counter or auxiliary electrode. CV experiments are performed by sweeping potential at a constant scan rate and observing the change in current at the working electrode, Figure 1.4. In the absence of an electroactive species, the resulting *i* vs. *E* curve reflects only background current (i_q) due to charging of the working electrode (capacitive current).[18]

$$|i_q| = A\, C_d\, v \qquad (1.2)$$

In equation 1.2, A is the area of the working electrode, C_d is the capacitance of the diffusion layer at the electrode surface and *v* is potential scan rate. Oxidation or reduction of an electroactive species at the electrode surface causes additional current (faradaic current) to pass due to the reaction in Eq. 1.3.

$$LA + e^- \rightleftharpoons LA^- \qquad E°'_{LA} \qquad (1.3)$$

As the potential at the working electrode surface approaches the formal reduction potential, $E°'_{LA}$, the effective "concentration" of electrons increases and perturbs the equilibrium in eq. 1.3. The preceding statement is a generalization of the Butler-Volmer model for heterogeneous electron transfer.[18] Going toward products, the concentration of LA is depleted at the electrode surface and causes a decrease in faradaic current. The cathodic peak current (i_p^c) then can be related by eq. 1.4.[18,19]

$$i_p^c = (2.69\text{x}10^5) n^{3/2} A (D_{LA})^{1/2} [LA]_o v^{1/2} \qquad (1.4)$$

where to the number of electrons (*n*) passed per mole of LA, working electrode area, the light absorber diffusion coefficient under electrolytic conditions (D_{LA}) , the concentration of the light absorber in the bulk solution ($[LA]_o$) and scan rate. Reversal of the scan for a Nerstian (reversible) system results in an *i* vs. *E* curve with an anodic peak current opposite the forward scan ($i_p^a/i_p^c = 1$) and with a characteristic shape, Figure 1.5. Potentials for a reversible system or often reported as the half-wave potential ($E_{1/2}$) which is the average of the cathodic and anodic peak potentials (E_p^c and E_p^a) for a specific couple.

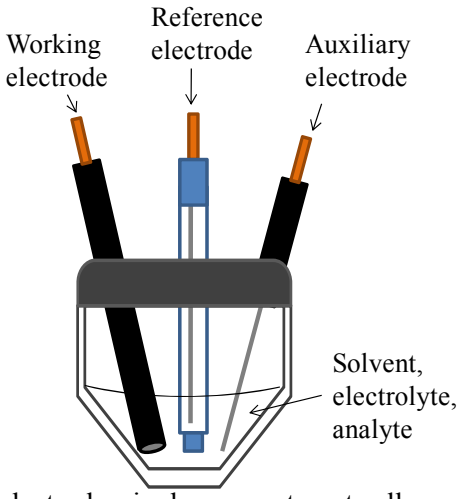

Figure 1.3. The design of a three electrode, single compartment cell commonly employed in transient electrochemical techniques, including cyclic voltammetry.

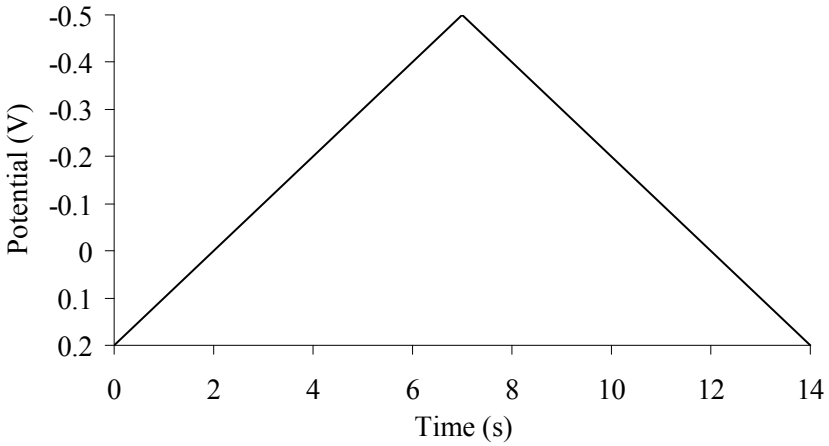

Figure 1.4. Triangular potential sweep function applied in a two segmented cyclic voltammetry experiment like Figure 1.5 at a scan rate (v) of 100 mV/s.

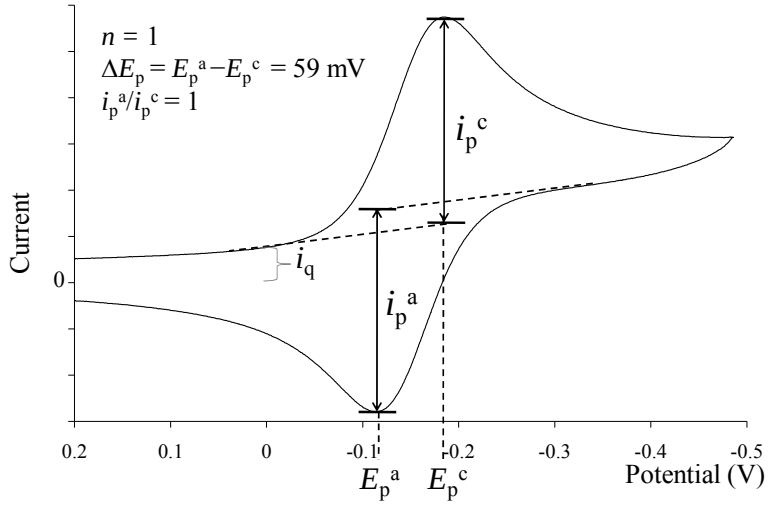

Figure 1.5. Cyclic voltammogram of an $n = 1$ redox couple that follows reversible Nernstian behavior, where cathodic and anodic peak potentials are denoted by E_p^c and E_p^a respectively and the analogous peak currents are i_p^c and i_p^a.

Irreversible chemical and electrochemical processes perturb the cyclic voltammogram giving a characteristic *i* vs. *E* curve. Chemical reactions following an electron transfer step which compete with back electron transfer are identified by a peak current ratio that is scan rate dependent, eq 1.5:

$$LA + e^- \rightleftharpoons LA^- \longrightarrow \text{products} \qquad (1.5)$$

The kinetics of a chemical process following electron transfer (reaction rate, rate constant, etc) is studied by observing i_p^a/i_p^c as a function of scan rate and concentration, generally with i_p^a/i_p^c less than unity at slower scan rates, Figure 1.6.[18,19] Observations in cyclic voltammetry can be more complicated, so it is prudent to couple CV with other techniques. Even with large amounts of electrochemical data, it can be difficult to assign a meaningful electrochemical mechanism for a specific system, especially those with multiple electroactive moieties.

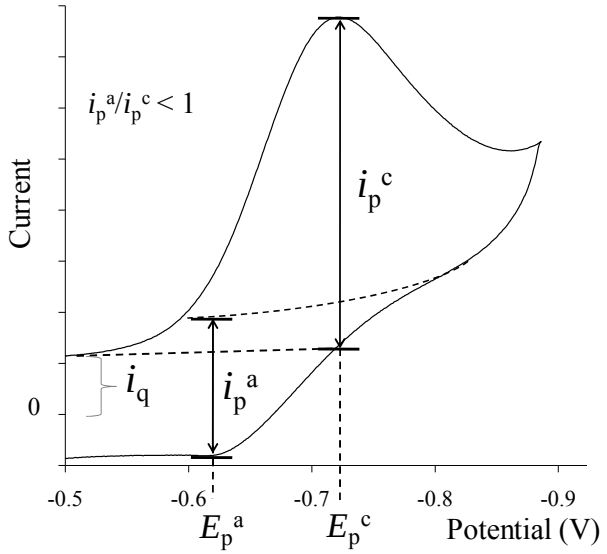

Figure 1.6. Cyclic voltammogram illustrating current response at the electrode surface for a redox couple that has an irreversible chemical step following the initial electron transfer step (EC_i mechanism). The dotted line shows the extrapolated *i* vs. *E* curve. The cathodic peak potential is denoted by E_p^c and the cathodic and anodic peak currents are i_p^c and i_p^a.

1.3.1.2. Bulk Electrolytic Techniques

Bulk electrolytic techniques are methods that result in a net change of the redox state of the bulk sample and are often used to evaluate the electron stoichiometry of an electrochemical process, voltammetry of electroactive redox products and their light absorbing properties.

Similar in design to CV experiments, bulk electrolysis is performed at a working electrode whose potential is set relative to a reference electrode, but with a working electrode of larger surface area to facilitate greater current and faster mass conversion. In contrast to CV, in bulk methods the auxiliary electrode is placed in a different compartment, separated by a semi-permeable barrier that allows for ion flow but limits passage of the electrochemical products, Figure 1.7. The electrochemical reaction is enhanced by choosing a working electrode with a large surface area and by stirring the bulk electrolysis solution. The amount of charge passed can be determined by subtracting the integrated capacitive current decay curve (i_q vs. t) from the total i vs. t curve, eq. 1.6.

$$\mathrm{Q} = \int_0^\infty i(t)dt - \int_0^\infty i_q(t)dt \tag{1.6}$$

$$n = \frac{\mathrm{Q}}{mol_{\mathrm{LA}} \times 96{,}485\,\mathrm{C}/mol} \tag{1.7}$$

In Eq. 1.7, Q is the charge passed in coulombs, n is number of electrons passed, while the elementary charge for a mole of electrons is 96,485 C.

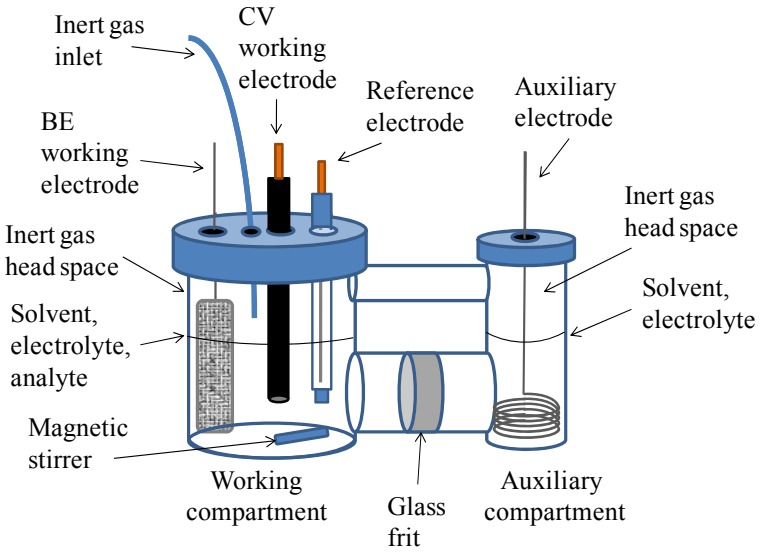

Figure 1.7. Example two compartment cell used in bulk electrolysis experiments using a Pt gauze working electrode for coulometry, Pt disk working electrode for linear sweep techniques that allows for CV study of electrolytic products, Ag/AgCl reference electrode and Pt coil auxiliary electrode. Cell design is adapted from Smith, W. H.; Bard, A. J. *J. Amer. Chem. Soc.* **1975,** *97*, 5203, with permission from the American Chemical Society.[20]

Electrochemical products can have electrochemical and/or structural properties that are unique compared to the starting material, depending on the electrochemical mechanism. The cyclic voltammogram for a quasi-stable redox product that has not undergone chemical reaction often reflects the CV of the non-electrolyzed complex. In the event of a chemical step following initial electron transfer, however, new waves are observed in the voltammogram due to the creation of electroactive by products. Identification of these products can be telling of the nature of the orbital involved in the initial electron transfer step. In addition, electronic transitions arising due to newly occupied or vacant orbitals of the redox product can indicate the nature of the orbitals involved in the electrochemistry.

1.3.2. Electrochemical Properties of Ru^{II} and Os^{II} Polyazine Complexes

The redox properties of low-spin d^6 metal polyazine complexes of octahedral group 8 metal complexes were studied extensively probing ligand tuning of the complexes' oxidation and reduction potentials.[21] Table 1.1 presents a representative list of Ru^{II} and Os^{II} polyazine complexes that are commonly used as mononuclear models for new complexes in the literature.

Table 1.1. Electrochemical properties of Ru^{II} and Os^{II} centered polyazine complexes[a]

Complexes[b]	$M^{III/II}$	$L_1^{0/-}$	$L_2^{0/-}$	$L_3^{0/-}$	Ref
	$E_{1/2}$ (V)	$E_{1/2}$ (V)	$E_{1/2}$ (V)	$E_{1/2}$ (V)	
$[Ru(bpy)_3](PF_6)_2$	1.27	−1.24	−1.43	−1.67	23
$[Ru(tpy)_2](ClO_4)_2$	1.32	−1.15	−1.36	−1.81	25
$[(tpy)RuCl(bpm)](PF_6)$	1.00	−1.15	−1.56	--	26
$[(tpy)RuCl(dpp)](PF_6)$	1.01	−1.21	−1.54	--	26
$[(bpy)_2OsCl_2]$	0.00	−1.57	−1.83	--	24
$[(bpy)_2OsCl(pz)](PF_6)$	0.47	−1.37	−1.60	--	27
$[(tpy)Os(pz)(bpy)](PF_6)_2$	0.98	−1.13	−1.51	--	27
$[Os(bpy)_3](PF_6)_2$	0.85	−1.16	−1.34	−1.65	22,28
$[Os(tpy)_2](PF_6)_2$	1.00	−1.09	−1.34	−1.77	18

[a] Potentials are reported in CH_3CN at v = 100 mV/s (unless otherwise noted) versus Ag/AgCl 3M NaCl reference. Conversion for standard reference potentials to Ag/AgCl: NHE = −0.209 V, SSCE = 0.030 V, SCE = 0.035 V, $FeCp_2^{0/-}$ = 0.461 V, Ag/$AgNO_3$ (10 mM) = 0.34 V.[18]

[b] bpy = 2,2'-bipyridine, bpm = 2,2'-bipyrimidine, dpp = 2,3-bis(2-pyridyl)pyrazine, tpy = 2,2':6',2''-terpyridine, pz = pyrazine.

The metal complexes are typically characterized by reversible metal based oxidations and by reversible ligand centered reductions. Osmium(II) polyazine complexes tend to have a highest occupied molecular orbital (HOMO) at higher energy than the ruthenium(II) analog, e.g. $[Os(bpy)_3]^{2+}$ $E_{1/2}(Os^{III/II})$ = 0.85 V[22] vs. $[Ru(bpy)_3]^{2+}$ $E_{1/2}(Ru^{III/II})$ = 1.27 V[23] (vs. Ag/AgCl). Ligands that destabilize the metal orbitals such as chloride also shift the metal centered oxidation potentials more negative, $[(bpy)_2OsCl_2]$ $E_{1/2}(Os^{III/II})$ = 0.00 V.[22,24] The type of polyazine ligand, with a delocalized π-systems, tends to have less impact on the energy of the metal centered oxidation compared to the number of polyazine nitrogens bound to the metal.[23,25-28]

1.3.3. Electrochemistry of Rh^{III} and Ir^{III} Polyazine Complexes

The electrochemical properties of group 9 metal polyazine complexes have been studied extensively to understand catalytic and photophysical properties. Iridium(III) polyazine complexes are typically more difficult to reduce than their rhodium(III) analogs. The electrochemical mechanisms of each are strongly dependent on the solvent and the polyazine ligands used in their construction. The orbitals involved in the electrochemistry are commonly assigned based on electrochemical behavior. Orbital assignments typically use terminology for localized orbitals with the understanding that orbital mixing does occur and the terminology is meant to provide the primary contribution to the particular molecular orbital.

1.3.3.1. Electrochemical Properties of cis-$Rh^{III}X_2$ Complexes

Rhodium(III) polyazine complexes have been employed in photocatalysis and electrocatalysis, prompting extensive examination of their electrochemical properties. [15,29-38] Selected electrochemical properties of polyazine complexes that exhibit the *cis*-$Rh^{III}X_2$ moiety are presented in Table 1.2. DeArmond, Hanck and coworkers reported that $[(NN)_2RhCl_2]^+$, where NN = bpy or phen, underwent rapid loss of chloride following reduction of the complex by two electrons, Figure 1.8.[15,30] A similar result was reported by Brewer *et al*. for the complexes $[(NN)_2RhBr_2]^+$ where NN were polyazine ligands capable of bridging to an additional metal center.[33] The initial irreversible reduction process for these complexes is typically followed by two reversible $1e^-$ reduction steps. The first three cathodic processes of typical $[(NN)_2RhX_2]^+$ complexes therefore have been assigned as a two $1e^-$ metal localized reduction followed by two strongly coupled $1e^-$ ligand localized reductions.[15,30,39] Reduction at the metal

center proceeds via two $1e^-$ transfers each followed by rapid ligand loss (ECEC) or by two sequential $1e^-$ transfer steps followed by a rapid chemical step (EEC). Regardless of the microscopic kinetics, the first reduction step is widely accepted to result in the square planar Rh^I complex and two equivalents of the monodentate ligand, X.[15,30,40,41]

Table 1.2. Electrochemical properties of Rh^{III} centered polyazine complexes[a]

Complexes[b]	$Rh^{III/II}$	$Rh^{II/I}$	$Rh^{III/II/I}$	$L_1^{0/-}$	$L_2^{0/-}$	Ref
	E_p^c (V)	E_p^c (V)	E_p^c (V)	$E_{1/2}$ (V)	$E_{1/2}$ (V)	
$[(bpy)_2RhCl_2](ClO_4)$	--	--	−0.89[c]	−1.32	−1.62	28
$[(tbb)_2RhCl_2](ClO_4)$	--	--	−0.96[c]	−1.37	−1.65	28
$[Rh(phen)_3](ClO_4)_3$	−0.75	−0.92[c]	--	−1.45[d]	−1.60[d]	29
$[(phen)_2RhCl_2](ClO_4)$	--	--	−0.82[c]	−1.46[d]	−1.62[d]	29
$[Rh(bpy)_3](ClO_4)_3$	--	--	−0.83[c]	−1.42	−1.63	15
$[Rh(bpy)_3](ClO_4)_3$[g]	−0.79	−0.92[c]	--	−1.44	−1.65	15
$[(bpy)_2RhCl_2](ClO_4)$	--	--	−0.80[c]	−1.42	−1.63	15
$[Hbpy][(bpy)RhCl_3(OH)]$	--	--	−0.79[c]	−1.23[c,d]	--	15
$[(bpy)_2Rh(OH_2)_2](ClO_4)_3$	−0.78[e]	+0.25[c,f]	--	--	--	30
$[(bpy)_2Rh(OH)_2](ClO_4)$	−1.26[e]	−0.18[c,f]	--	--	--	30
$[(dmb)_2RhCl_2](BF_4)$	--	--	−0.95[c]	−1.47	−1.71	31
$[(bpy)_2RhBr_2](PF_6)$	--	--	−0.79[c]	−1.30	−1.50	32
$[(bpm)_2RhBr_2](PF_6)$	--	--	−0.62[c]	−1.34[c,d]	−1.70[d]	32
$[(dpp)_2RhBr_2](PF_6)$	--	--	−0.60[c]	−1.05	−1.19	32
$[(dpq)_2RhBr_2](PF_6)$	--	--	−0.44[c]	−0.85	−1.49	32
$[(dpb)_2RhBr_2](PF_6)$	--	--	−0.39[c]	−0.72	−1.24	32
$[\{(tpy)RuCl(dpp)\}_2RhCl_2](PF_6)_3$	--	--	−0.47[c]	−0.87	−1.20	33
$[\{(tpy)RuCl(bpm)\}_2RhCl_2](PF_6)_3$	−0.26	−0.38[c]	--	−0.70	−1.12	33
$[\{(bpy)_2Ru(dpp)\}_2RhCl_2](PF_6)_5$	--	--	−0.39[c]	−0.79	−1.02	33
$[\{(bpy)_2Ru(bpm)\}_2RhCl_2](PF_6)_5$	--	--	−0.78[c,h]	−0.13	−0.26	34
$[\{(bpy)_2Ru(dpq)\}_2RhCl_2](PF_6)_5$	--	--	−0.12[c]	−0.31	--	36
$[\{(bpy)_2Ru(dpb)\}_2RhCl_2](PF_6)_5$	--	--	−0.60[c]	+0.18	--	36
$[(tpy)Ru(tppz)RhCl_3](PF_6)_2$	--	--	−0.23[c]	−0.60	−0.98	37

[a] Potentials are reported in CH_3CN at ν = 100 mV/s (unless otherwise noted) versus Ag/AgCl 3M NaCl reference. Conversion for standard reference potentials versus Ag/AgCl: NHE = −0.209 V, SSCE = 0.030 V, SCE = 0.035 V, $FeCp_2^{0/+}$ = 0.461 V, $Ag/AgNO_3$ (10 mM) = 0.34 V.[18]

[b] bpy = 2,2'-bipyridine, tbb = 4,4'-bis(tert-butyl)-2,2'-bipyridine, phen = 1,10-phenanthroline, dmb = 4,4'-dimethyl-2,2'-bipyridine, bpm = 2,2'-bipyrimidine, dpp = 2,3-bis(2-pyridyl)pyrazine, dpq = 2,3-bis(2-pyridyl)quinoxaline, dpb = 2,3-bis(2-pyridyl)benzoquinoxaline, tpy = 2,2':6',2''-terpyridine, tppz = 2,3,5,6-tetrakis(2-pyridyl)pyrazine.

[c] Determined or assumed to be followed by fast chemical step

[d] E_p^c

[e] In 0.05 M $NaOH_{(aq)}$

[f] Values determined by measured potential, disproportionation rate constant and pKa[31]

[g] ν = 9520 mV/s

[h] Quasi-reversible

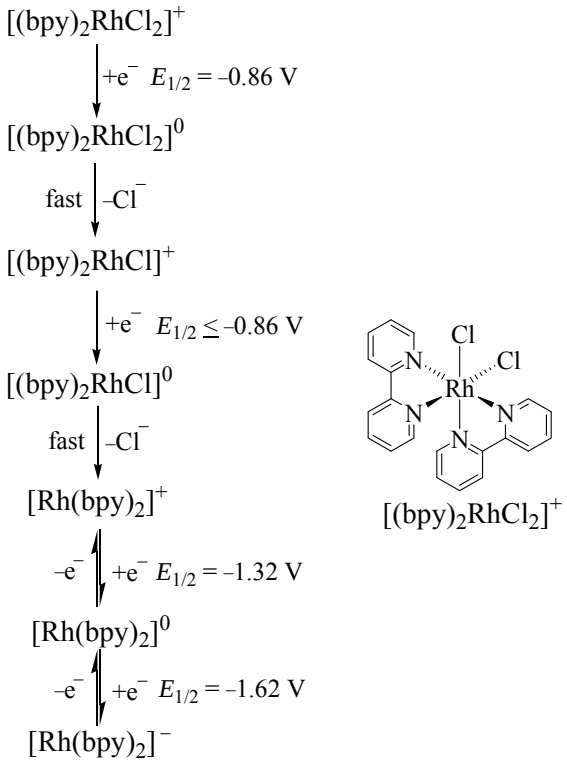

Figure 1.8. Mechanism of the electrochemical reduction of $[(bpy)_2RhCl_2]^+$ in acetonitrile proposed by Kew, DeArmond and Hanck, bpy = 2,2'-bipyridine, potentials are converted to versus Ag/AgCl (−0.035 V versus SCE).[15]

1.3.3.2. Ligand Effects on Rhodium Reduction Potential

Polyazine ligands with more delocalized π-systems tend to give complexes that are easier to reduce. For example, the complex $[(bpy)_2RhBr_2](PF_6)$ has reductive couples at −0.79 V, −1.30 V and −1.50 V vs. Ag/AgCl, while a complex with weaker donor ligands, $[(dpb)_2RhBr_2](PF_6)$ where dpb = 2,3-bis(2-pyridyl)benzoquinoxaline, has couples at −0.39 V, -−0.74 V, and −1.24 V.[33] Further stabilization of the polyazine ligands causes apparent orbital inversion and was observed for few examples of *cis*-$[(NN)_2RhX_2]^+$ complexes. The complexes $[\{(bpy)_2Ru(bpm)\}_2RhCl_2](PF_6)_5$[36] and $[\{(bpy)_2Ru(dpb)\}_2RhCl_2](PF_6)_5$,[42] exhibit reversible reductions (−0.13 V, −0.26 V for BL = bpm, and +0.18 V for BL = dpb, vs. Ag/AgCl) prior to the irreversible $Rh^{III/II/I}$ (−0.78 V and −0.60 V, respectively). A third system, $[\{(tpy)RuCl(bpm)\}_2RhCl_2](PF_6)_3$, is the only *cis*-$[(NN)_2RhCl_2]^+$ complex of this type to exhibit separation of the metal based reduction steps (−0.26 V and −0.38 V).[34] The peak separation could indicate that chloride loss is competitive with heterogeneous electron transfer at the scan rate studied (EEC mechanism), a property previously unreported for a *cis*-$[(NN)_2RhCl_2]^+$ center.

1.3.3.3. Electrochemical Properties of Iridium(III) Polyazine Complexes

The mechanism of electrochemical reduction of *cis*-$[(NN)_2IrCl_2]^+$ complexes is more complicated than that of their rhodium analogs, with a stronger apparent dependence on solvent and nature of the polyazine ligand, NN. Compared to *cis*-$[(NN)_2RhX_2]^+$ systems, the metal and ligand orbitals of *cis*-$[(NN)_2IrCl_2]^+$ are inverted, Table 1.3. DeArmond and Hanck, [17,43] and Roffia and Ciano[16] studied the effect of the terminal polyazine ligand on the observed electrochemistry compared to the rhodium centered analogs. Halide loss was found to have a strong solvent dependence,[44] consistent with observations from photo-induced dissociation experiments.[45] The electrochemical processes observed for the different *cis*-$[(NN)_2IrCl_2]^+$ systems may have relevance toward the observed electrochemical behavior of some of the Rh^{III} centered systems.

Table 1.3. Electrochemical reduction potentials of *cis*-$Ir^{III}Cl_2$ centered polyazine complexes[a]

Complexes[b]	E_p^c (V)	E_p^c (V)	E_p^c (V)	E_p^c (V)	Ref
$[(bpy)IrCl_2](NO_3)$	−1.02[c]	−1.30	−1.44[c]	−1.59[d]	17
$[(bpy)_2IrCl_2](PF_6)$	−1.25	−1.47	--	−2.12[d]	32
$[(phen)_2IrCl_2](NO_3)$	−1.15[c]	−1.36	--	−1.88[d]	44
$[(5,6\text{-}Me_2phen)_2IrCl_2]Cl$	−1.19[c]	−1.37	−1.52[d]	−1.92[d]	44
$[(bpm)_2IrCl_2](PF_6)$	−0.79	−0.97	--	−1.65[d]	32
$[(dpp)_2IrCl_2](PF_6)$	−0.86	−1.09	--	−1.75[d]	32
$[(dpq)_2IrCl_2](PF_6)$	−0.50	−0.70	--	−1.50[d]	32
$[(dpb)_2IrCl_2](PF_6)$	−0.39	−0.60	--	−1.34[d]	32
$[\{(bpy)_2Ru(dpp)\}_2IrCl_2](PF_6)_5$	−0.39[e]	−0.54[e]	−1.06[e]	−1.22[e]	43
$[\{(bpy)_2Ru(bpm)\}_2IrCl_2](PF_6)_5$	−0.08[e]	−0.21[e]	−0.90[e]	−1.07[e]	34
$[\{(bpy)_2Ru(dpq)\}_2IrCl_2](PF_6)_5$	−0.12[e]	−0.26[e]	−0.90[e]	−1.22[e]	43
$[\{(bpy)_2Ru(dpb)\}_2IrCl_2](PF_6)_5$	+0.03[e]	−0.12[e]	−0.71[e]	−0.98[e]	43

[a] Electrochemical properties recorded in 0.1 M electrolyte solutions in acetonitrile unless otherwise noted, all potentials versus Ag/AgCl (3M NaCl). Conversion of standard reference potentials versus Ag/AgCl: NHE = −0.209 V, SSCE = 0.030 V, SCE = 0.035 V, $FeCp_2^{0/+}$ = 0.461 V, $Ag/AgNO_3$ (10 mM) = 0.34 V.[18] Redox couple assignments varied between sources and are omitted.

[b] bpy = 2,2'-bipyridine, phen = 1,10-phenanthroline, 5,6-Me_2phen = 5,6-dimethyl-1,10-phenanthroline, bpm = 2,2'-bipyrimidine, dpp = 2,3-bis(2-pyridyl)pyrazine, dpq = 2,3-bis(2-pyridyl)quinoxaline, dpb = 2,3-bis(2-pyridyl)benzoquinoxaline

[c] Electron transfer step followed by slow halide loss

[d] Two electron transfer step followed by fast halide loss

[e] Reported as $E_{1/2}$ values for reversible reductions

1.3.3.4. Ligand Effect on the Iridium Reduction Potential of cis-$[(NN)_2IrCl_2]^+$

Polyazine ligands with more delocalized π-systems stabilize ligand and metal centered redox processes of iridium(III), much like the rhodium(III) analogs. Brewer and coworkers reported cyclic voltammetric results for a series of *cis*-$[(NN)_2IrCl_2]^+$ complexes where NN = bpy, bpm, dpp, dpq, or dpb, Table 1.3.[33] Significant stabilization of the ligand acceptor orbital is noted for the weaker acceptor dpb of the system *cis*-$[(dpb)_2IrCl_2]^+$ (E_p^c = −0.39 V) compared to what was measured for *cis*-$[(bpy)_2IrCl_2]^+$ (E_p^c = −1.25 V). Following two reversible couples attributed to each ligand, an irreversible third couple is noted for each complex negative of the first two reductions. For the complexes where NN is a polyazine ligand capable of bridging; bpm,[36] dpp, dpq, and dpb;[42] the ligand acceptor orbitals are further stabilized upon attachment to

a Ru^{II} center. In fact, four reversible one electron couples are observed prior to any irreversible Ir reduction.

The electrochemical reduction of *cis*-$[(NN)_2IrCl_2]^+$ complexes (NN = bpy or phen) involves metal and ligand centered orbitals, the relative energies of that are difficult to assign from the observed electrochemistry.[43,46] The first reduction results in a chloride labile redox state, consistent with metal localized orbital.[17,43] Roffia and Ciano, however, indicated the first reduction steps to be ligand centered.[16] Divisia-Blohorn confirmed that the first two cathodic waves were reversible at fast scan rate and in solvents that inhibited solvation of chloride.[44] In polar solvents, however, these waves are irreversible regardless of scan rate. Chloride loss from the electronic excited state of *cis*-$[(bpy)_2IrCl_2]^+$ is known to be $>10^4$ slower in acetonitrile and DMF than water.[45] Ultimately, DeArmond and Hanck were able to show that passage of $3e^-$ yielded two chlorides and $[Ir(NN)_2]^-$ when electrolyzed at ca. −1.7 V.[43,46] These electrochemical observations taken together may indicate that metal and ligand acceptor orbitals are similar in energy for these complexes.

1.3.4. Correlation of Electrochemical Properties of Ru^{II},Rh^{III} and Os^{II},Rh^{III} Supramolecular Complexes to their Electronic Excited States

The electrochemical properties of some polyazine bridged mixed metal complexes predict interesting electronic excited states and means for excited state tuning. Polyazine complexes of Ru^{II} or Os^{II} (M^{II}) are characterized by metal based oxidations, consistent with a HOMO of primarily $M^{II}(d\pi)$ character and reductions consistent with a ligand(π^*) LUMO. Most *cis*-$[(NN)_2RhX_2]^+$ complexes on the other hand have lowest energy reductions consistent with a Rh($d\sigma^*$) LUMO. These electrochemical results predict polyazine bridged supramolecules containing Ru^{II} or Os^{II} centered light absorbers connected to a *cis*-$Rh^{III}Cl_2$ to possess a low lying $M^{II}(d\pi)$-to-$Rh^{III}(d\sigma^*)$ charge transfer (MMCT) electronic excited state, where M = Ru or Os. Such an MMCT state would be interesting due to the reactive M^{III} and Rh^{II} centers created in the charge separated state. In addition, tuning the supramolecules by constructing these species with different bridges caused orbital inversion, giving *cis*-$Rh^{III}Cl_2$ centered complexes with electrochemical properties more like those of a *cis*-$[(NN)_2IrCl_2]^+$ complex.[34,36,37,42] The electrochemical properties of these complexes can provide a useful tool in the design, construction and study of mixed metal supramolecules as PMDs.

1.4. Study of Photochemistry and Photophysics

An explanation of general photophysical processes is a necessary prerequisite for the discussion of transition metal polyazine complex photochemistry and photophysics. Absorption of a photon by a light absorber (LA) causes an electronic transition and populates an electronic excited state (*LA). There are several internal pathways by which *LA might relax. The decay processes of electronically excited transition metal polyazine complexes have been the subject of study for decades and continue to be a strong focus in research.[5-7] Thorough studies of transition metal polyazine chromophores have led to many applications of the complexes in photochemistry. Photochemistry includes photosynthetic schemes, photosensitization/modification of substrate molecules and photocatalytic reactions.

1.4.1. Electronic Excitation

Absorption of a photon of light by a LA in its electronic ground state (GS) is coincident with an electronic transition, populating an electronic excited state (ES) of the LA. The electronic transition promotes an electron from a low energy occupied orbital to an unoccupied orbital of higher energy, Figure 1.9. The lowest energy transition promotes an electron from the highest occupied molecular orbital (HOMO) to the lowest unoccupied molecular orbital (LUMO). The orbitals involved in the transition must be electronically coupled to allow electronic transition. The probability of an electronic transition is governed by selection rules. The symmetry selection rule for intensity of an electronic transition is expressed in (eq. 1.8):[47]

$$f \propto \int \psi_{e1}^{ES} \boldsymbol{\mu} \, \psi_{e1}^{GS} d\nu \tag{1.8}$$

where *f*, the oscillator strength, is proportional to the integral of the product of the GS and ES wavefunctions (ψ). The electric dipole moment operator, $\boldsymbol{\mu}$, is defined as:

$$\boldsymbol{\mu} = -e\sum_i \mathrm{r}_i + \sum_j q_j \mathrm{R}_j \tag{1.9}$$

or the sum of all electron charge and vector position ($-e$r) and all nuclei charge and position (qR), where $q = eZ$. The spin selection rule states that for an electronic transition to be allowed, the spin multiplicity of the ground state and excited state must be the same. Electronic transitions that are allowed by donor-acceptor orbital electronic coupling, symmetry, and electron spin are the most intense, with extinction coefficients, ε, of $\geq 10^3\ M^{-1}cm^{-1}$. Transitions that are allowed by spin, but formally forbidden by symmetry have ε between 10^0 and $10^2\ M^{-}$

$^1cm^{-1}$. Truly spin-forbidden transitions are not observed. Relaxation of the selection rules can give rise to observation of transitions that are formally forbidden. In the presence of a heavy atom, spin-orbit coupling relaxes the spin-selection rule, giving rise to absorptions that are formally spin forbidden displaying ε as high as 10^3 $M^{-1}cm^{-1}$.

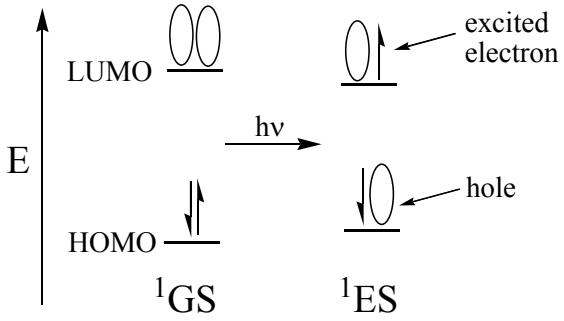

Figure 1.9. The change in electronic configuration following excitation by light (h*ν*) of a singlet ground state chromophore (^{1}GS) to a singlet electronic excited state (^{1}ES) (HOMO = highest occupied molecular orbital, LUMO = lowest unoccupied molecular orbital). Reproduced from Zigler, D. F.; Brewer, K. J. "Toward Photodynamic Therapy of Cancer with Platinum Group Metal Polyazine Complexes" in *Metal-Complexes-DNA Interactions*, Wiley-Blackwell, In press, with permission from Wiley-Blackwell.[48]

Electronic transitions often are accompanied by vibronic excitation. The conversion between electronic energy surfaces, moving from the ^{1}GS to the ^{1}ES, is dictated by the Franck-Condon principle, Figure 1.10. Electronic transitions following absorption of a photon, hν, are rapid, populating the ^{1}ES in a nuclear configuration consistent with the ^{1}GS. The ^{1}ES is populated in a hot vibronic state (ν_n, where n is an integer > 0). Vibronic relaxation to the lowest vibronic states is rapid with a rate constant of $k_{vib} > 10^{12}$ s^{-1}. Emission from ^{1}ES, hν', is Stokes shifted relative to absorption, in line with the Franck-Condon principle. Depopulation of the ^{1}ES to the ^{1}GS occurs at varying rates, with rate constants of the decay processes greatly depending on the nature of the ^{1}ES.

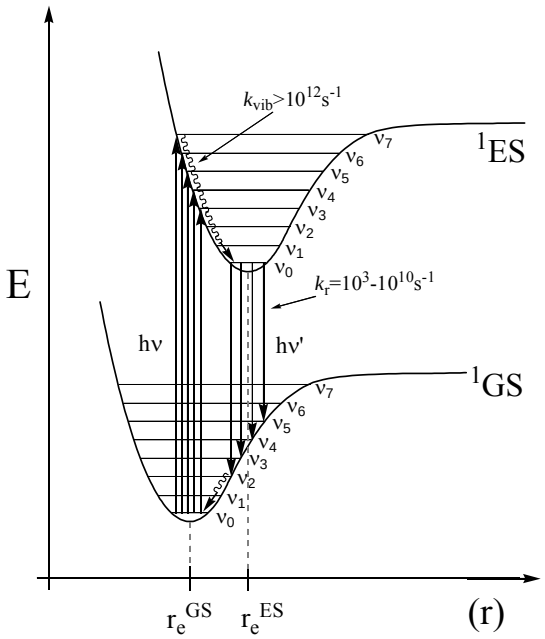

Figure 1.10. Morse potential energy (*E*) surface diagram for electronic states (^{1}GS, ^{1}ES) and vibrational (ν_n) states of a chromophore. Included are typical first order rate constants. k_{vib} = vibronic relaxation rate constant, k_r = rate constant of emission of light with average energy hν′, r = internuclear distance, r_e^{GS} = GS equilibrium internuclear distance, r_e^{ES} = ES equilibrium internuclear distance. Reproduced from Zigler, D. F.; Brewer, K. J. "Toward Photodynamic Therapy of Cancer with Platinum Group Metal Polyazine Complexes" in *Metal-Complexes-DNA Interactions*, Wiley-Blackwell, In press, with permission from Wiley-Blackwell.[48]

1.4.2. Unimolecular Electronic Excited State Decay

The quantum efficiency of ES processes is an important relation of ES decay kinetics. Decay from the ES by a specific pathway, x, is quantified by the quantum yield, Φ_x. The quantum yield is the probability of a molecule in its excited state to decay by a specific pathway. Quantum yield is defined as the ratio of observed first order rate constant of the process of interest, k_x, divided by sum of the rate constants of all pathways depopulating that state, Σk, eq. 1.10:

$$\Phi_x = \Phi_{ES} \frac{k_x}{\sum k} \tag{1.10}$$

where Φ_{ES} is the quantum efficiency of population of the reactive ES. An important descriptor of the electronic excited state is its inherent lifetime, τ^o, simply defined as $(\Sigma k)^{-1}$.

Conversion between electronic states is typically represented with Jablonski or state diagrams. These diagrams are simplified versions of the Morse potential energy surfaces as

shown in Figure 1.10, where each electronic state is represented as a line instead of a surface. Decay processes of electronic excited states, ES, may occur by multiple pathways, Figure 1.11. Radiative processes are typically represented as straight arrows (⟶) and non-radiative processes are presented as wavy arrows (⇝). Internal conversion, k_{ic}, is non-radiative relaxation without change in electron spin while intersystem crossing, k_{isc}, is accompanied by change in spin. A molecular orbital depiction of the processes is shown in Figure 1.12. Fluorescence, k_f, is defined as emission of a photon and decay to the ground state without change in spin multiplicity. Radiative decay with a change in spin state is defined as phosphorescence, k_p. It should be noted that several examples in the literature incorrectly define fluorescence or phosphorescence by the lifetime of the emitting ES. Non-radiative relaxation of an ES to the ground state by intersystem crossing is sometimes expressed by k_{nr}.

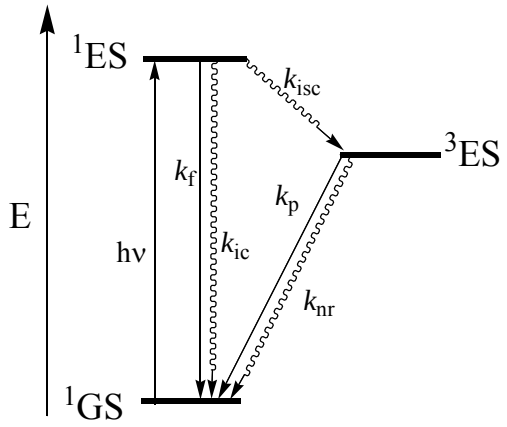

Figure 1.11. Jablonski diagram illustrating relative energies of states. Each bar (▬) represents the potential energy surface of an electronic state. Lines depicting vibronic states are omitted for clarity. ES are excited states and GS is the ground state. Arrows represent electronic excited state decay via fluorescence (k_f), internal conversion (k_{ic}), intersystem crossing (k_{isc}), and phosphorescence (k_p). The rate constant of non-radiative decay (k_{nr}) describes intersystem crossing to the ground state. Reproduced from Zigler, D. F.; Brewer, K. J. "Toward Photodynamic Therapy of Cancer with Platinum Group Metal Polyazine Complexes" in *Metal-Complexes-DNA Interactions*, Wiley-Blackwell, In press, with permission from Wiley-Blackwell.[48]

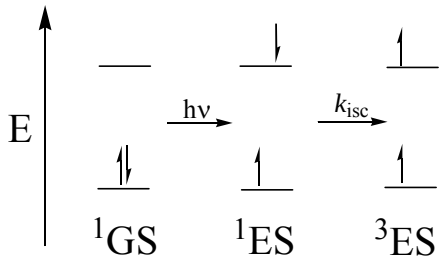

Figure 1.12. Orbital representation of intersystem crossing (k_{isc}) from singlet excited state (^{1}ES) to triplet excited state (^{3}ES). Reproduced from Zigler, D. F.; Brewer, K. J. "Toward Photodynamic Therapy of Cancer with Platinum Group Metal Polyazine Complexes" in *Metal-Complexes-DNA Interactions*, Wiley-Blackwell, In press, with permission from Wiley-Blackwell.[48]

1.4.3. Electronic Excited States and Unimolecular Decay of Transition Metal Polyazine

Transition metal polyazine complexes are potent light absorbers in the ultraviolet (UV) and visible region of the spectrum.[14] Table 1.4 summarizes the photophysical properties of a representative set of transition metal polyazine complexes. All polyazine complexes absorb UV light strongly due to intense internal ligand (IL) transitions of the aromatic ligands, Figure 1.13. Ruthenium(II)[5] and osmium(II)[6] polyazine complexes absorb strongly in the visible region and have low-lying ES that are typically emissive, long-lived, and reactive.[21] These low-lying ES are typically metal-to-ligand charge transfer (MLCT) in nature with some localization of the donor orbital on the metal and the acceptor orbital on the polyazine ligand. Mononuclear Rh^{III} polyazine complexes absorb strongly in the UV region due to IL transitions.[7] The ES of rhodium(III) and dirhodium(II) polyazine complexes have reactivity that is strongly coupled to the type of polyazine ligands employed. Combining chromophores into supramolecules gives complexes with photophysical properties that are unique compared to the mononuclear analogs.[2] Tuning the ES properties of the transition metal polyazine complexes allows for tuning of their photochemical properties including their photomodification of DNA.[49-60]

Table 1.4. Photophysical properties of a representative set platinum group metal polyazine complexes used in DNA photomodification schemes[a]

Complex[b]	λ_{max}^{abs} (nm)	$\lambda_{max}^{em,RT}$ (nm)	$\lambda_{max}^{em,77K,c}$ (nm)	τ^{RT} (μs)	ES[d]	DNA Photorxn[e]	Ref
cis-$[(bpy)_2Ru(NH_3)_2](BF_4)_2$	345, 490	--	741[f]	0.052[f]	^{3}LF	PB-M	51,52
$[Ru(bpy)_3]Cl_2$	452	610	--	0.385	^{3}MLCT	Type II-PC	51,53
$[Ru(phen)_3]Cl_2$	462	596	--	0.421	^{3}MLCT	Type I & II-PC	51,53, 54
$[Os(bpy)_3](PF_6)_2$	478[g]	743	710	0.060	^{3}MLCT	--	55,56
$[(phen)Ru(HAT)_2]Cl_2$	466	645	--	0.835	^{3}MLCT	PB-L Type I-PO Type II-PC	51,57
$[(phen)_2Rh(phi)]Cl_3$	358	--	--	--	^{3}IL	PB-M, Type I-PC	58
cis-$[(phen)_2RhCl_2]Cl$	355	--	723	--	^{3}LF	PB-M	59
cis-$[Rh_2(\mu\text{-}O_2CMe)_2(dppz)(bpy)](O_2CMe)_2$	432	--	--	--	^{3}MMLCT	Type I & II-PC	60
$[\{(bpy)_2Ru(dpp)\}_2Ru(dpp)PtCl_2](PF_6)_6$	542	--	--	--	^{3}MLCT	Type II-PC	61
$[\{(bpy)_2Ru(dpp)\}_2RhCl_2](PF_6)_5$	525	--	--	--	^{3}MMCT	PC	62

[a] Absorption maxima and room temperature emission maxima, reported in aqueous solutions, unless otherwise noted.

[b] bpy = 2,2'-bipyridine; phen = 1,10-phenanthroline; dppz = dipyrido[3,2-*a*:2',3'-*c*]phenazine; HAT = 1,4,5,8,9,12-hexaazatriphenylene; dpp = 2,3-bis(2-pyridyl)pyrazine; phi = 9,10-phenanthrenequinone diimine

[c] In 4:1 EtOH/MeOH

[d] LF = ligand field, MLCT = metal-to-ligand charge transfer, IL = internal ligand, MMLCT = metal-metal to ligand charge transfer, MMCT = metal to metal charge transfer

[e] Mechanism of DNA photomodification: PB-M = photobinding to metal, PB-L = photobinding to ligand, Type I = direct ES & DNA reaction following electron transfer, Type II = photosensitized oxygen mediated reactions, PC = photocleavage, PO = photooxidation

[f] 157 K.

[g] In room temperature acetonitrile

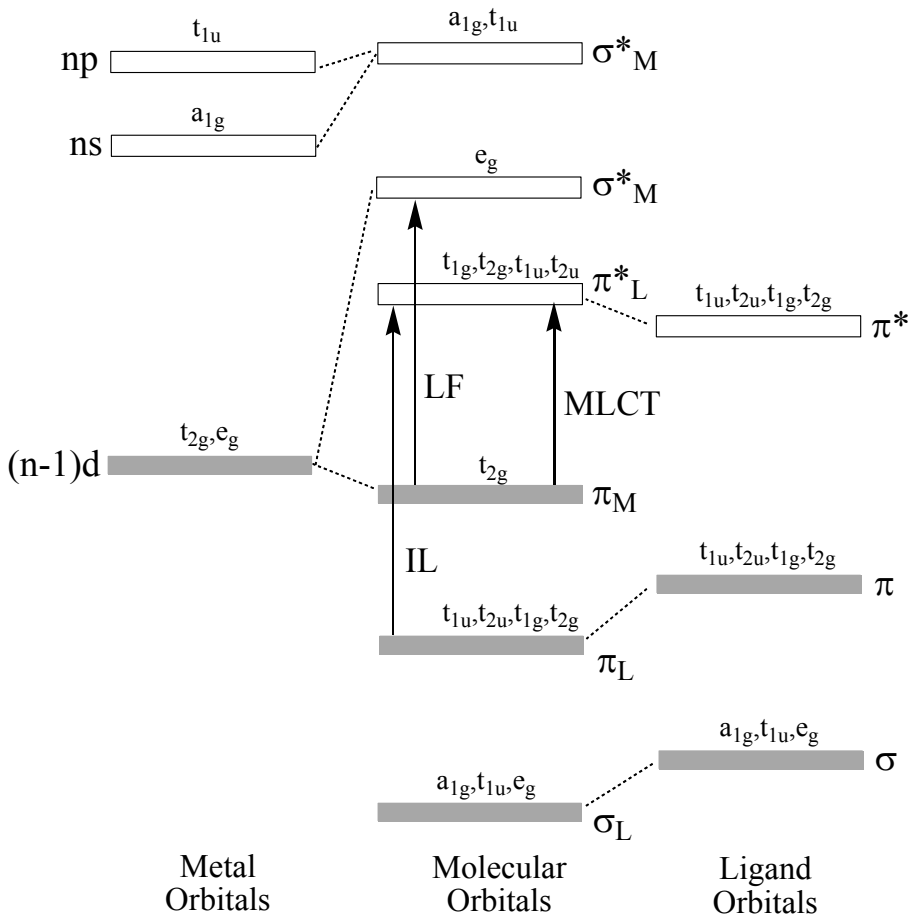

Figure 1.13. Molecular orbital diagram of an octahedral metal complex with π-acceptor ligands, depicting common electronic transitions associated with transition metal (M) complexes with polyazine ligands (L) (IL = internal ligand, MLCT = metal to ligand charge transfer, LF = ligand field). Reproduced from Zigler, D. F.; Brewer, K. J. "Toward Photodynamic Therapy of Cancer with Platinum Group Metal Polyazine Complexes" in *Metal-Complexes-DNA Interactions*, Wiley-Blackwell, In press, with permission from Wiley-Blackwell.[48]

1.4.3.1. Excited States of Ruthenium(II) and Osmium(II) Polyazine Complexes

Ru^{II} and Os^{II} complexes are interesting as photosensitizers as they possess reactive ES that are easily tuned by modification of their ligand coordination sphere.[5,6,21] Mononuclear Ru^{II} polyazine complexes typically have an absorption band in the 400-500 nm region due to the Ru(dπ)→TL(π*) charge transfer transition (MLCT), where TL = terminal polyazine ligand. The electronic absorption spectrum of $[Ru(bpy)_3]^{2+}$, bpy = 2,2'-bipyridine, is presented in Figure 1.14. The initially populated ^{1}MLCT state undergoes intersystem crossing with unit efficiency ($\Phi_{isc} \approx 1$) to give the ^{3}MLCT state, Figure 1.15.[61] For tris(chelate) polyazine complexes of Ru^{II}, the ^{3}MLCT state is long-lived at room temperature (τ° = 10-1000 ns) and displays strong phosphorescence ($\Phi_p \approx 0.10$).[21] The ES populated following metal-centered d→d excitation is

the ligand field state (LF). Though higher in energy, the non-emissive ^{3}LF state is thermally accessible at room temperature from the ^{3}MLCT state. Thermal population of the ^{3}LF state competes with phosphorescence or non-radiative decay pathways of the ^{3}MLCT state as a decay pathway. The long excited state lifetime, visible light excitation and efficient emission make the ^{3}MLCT state of Ru^{II} polyazine complexes interesting for schemes involving photochemistry, photo-induced energy transfer and photo-induced electron transfer.

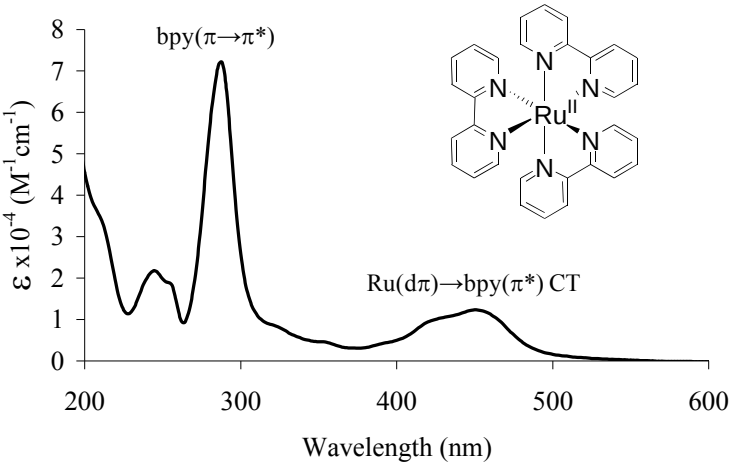

Figure 1.14. Electronic absorption spectrum of tris(2,2'-bipyridine)ruthenium(II), $[Ru(bpy)_3]^{2+}$, in CH_3CN at RT. Extinction coefficients are average values reported in the review by Juris, Balzani, Barigletti, Campangna, Belser, and von Zelewsky.[21] Reproduced from Zigler, D. F.; Brewer, K. J. "Toward Photodynamic Therapy of Cancer with Platinum Group Metal Polyazine Complexes" in *Metal-Complexes-DNA Interactions*, Wiley-Blackwell, In press, with permission from Wiley-Blackwell.[48]

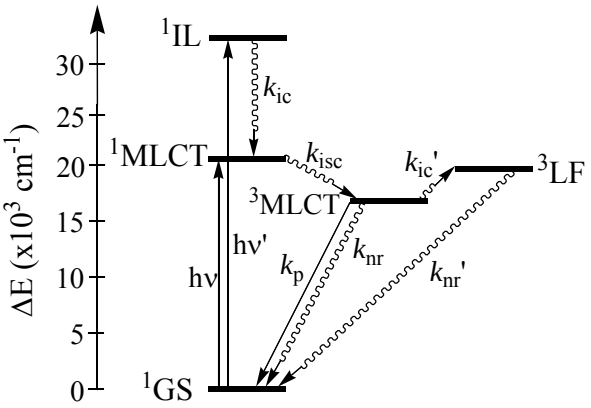

Figure 1.15. Jablonski-type diagram of $[Ru(bpy)_3]^{2+}$. bpy = 2,2'-bipyridine, ^{1}GS = singlet electronic ground state, ^{1}MLCT = singlet metal to ligand charge transfer excited state, ^{3}MLCT = triplet MLCT excited state, ^{1}IL = singlet internal ligand excited state, ^{3}LF = triplet ligand field excited state. Relative energies are adapted from two extensive reviews.[5,21] Reproduced from Zigler, D. F.; Brewer, K. J. "Toward Photodynamic Therapy of Cancer with Platinum Group Metal Polyazine Complexes" in *Metal-Complexes-DNA Interactions*, Wiley-Blackwell, In press, with permission from Wiley-Blackwell.[48]

Modification of the coordination environment of Ru^{II} polyazine systems modulates the electronic properties of the chromophore.[5] Bis(chelate) polyazine complexes of Ru^{II} with a *cis*-$Ru(TL)_2$ moiety tend to have absorption spectral features similar to the tris(chelate) systems. Emission quantum efficiencies from the ^{3}MLCT states of these complexes, however, are often orders of magnitude smaller. For example, the Φ_p of $[Ru(bpy)_3]^{2+}$ at room temperature is 0.06 versus $\Phi_p = 0.002$ reported for $[(bpy)_2Ru(NH_3)_2]^{2+}$ at 157 K.[21,50] This reduction in emission for $[(bpy)_2Ru(NH_3)_2]^{2+}$ is due to the more rapid interstate conversion between the ^{3}MLCT state and lower-lying ^{3}LF state, Figure 1.16. Excitation directly into higher LF states was linked to photoaquation of complexes with the *cis*-$Ru^{II}(TL)_2$ moiety, where complexes such as $[(bpy)_2RuCl_2]$ photochemically generate $[(bpy)_2RuCl(OH_2)]^+$ and $[(bpy)_2Ru(OH_2)_2]^{2+}$.[62]

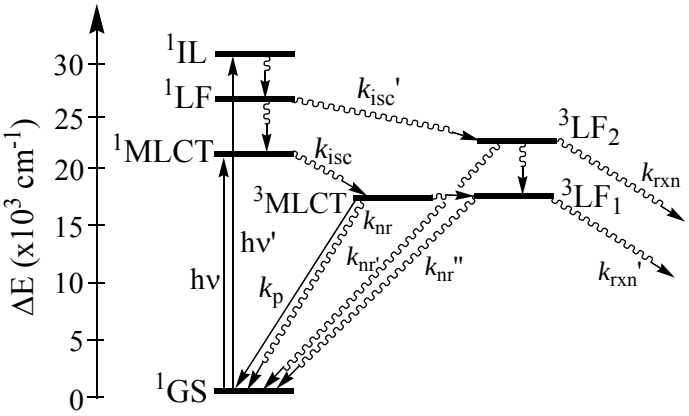

Figure 1.16. Jablonski-type diagram of $[(bpy)_2Ru(NH_3)_2]^{2+}$. bpy = 2,2'-bipyridine, ^{1}GS = singlet electronic ground state, ^{1}MLCT = singlet metal to ligand charge transfer excited state, ^{3}MLCT = triplet MLCT excited state, ^{1}IL = singlet internal ligand excited state, ^{3}LF = triplet ligand field excited state. Rate constants of internal conversion (k_{ic}^x) for the following processes are omitted for clarity: $^1IL \rightarrow {}^1LF$, $^1IL \rightarrow {}^1MLCT$, $^1LF \rightarrow {}^1MLCT$, $^3MLCT \rightarrow {}^3LF_1$ and $^3LF_2 \rightarrow {}^3LF_1$. Relative state energies are from Singh and Turro.[50] Reproduced from Zigler, D. F.; Brewer, K. J. "Toward Photodynamic Therapy of Cancer with Platinum Group Metal Polyazine Complexes" in *Metal-Complexes-DNA Interactions*, Wiley-Blackwell, In press, with permission from Wiley-Blackwell.[48]

Tris(chelate) polyazine complexes of Os^{II} generally absorb visible light at longer wavelengths but result in electronic excited states with decreased emission efficiency and shorter lifetimes than the Ru^{II} centered analogs.[6,9,54] A shorter ^{3}MLCT state lifetime (and smaller Φ_p) is a result of several contributing factors. The energy gap law states that as the difference in energy of two electronic states decreases, the vibronic coupling of the states increases, enhancing k_{nr}

leading to more efficient ES deactivation.[10,54] The large spin-orbit coupling of Os^{II} versus Ru^{II} results in significant relaxation of the spin selection rule and enhanced decay from the ^{3}MLCT state. The large spin orbit coupling of Os^{II} also gives rise to a low energy "tail" of the visible region electronic absorption spectra of Os^{II} polyazine complexes. The low energy tail is due to direct population of ^{3}MLCT state, Figure 1.17.[54] Unlike the Ru^{II} counter parts, Os^{II} polyazine ^{3}LF states are not thermally accessible from the ^{3}MLCT state. Therefore, excitation of the Os^{II} chromophore with visible light generally does not result in ligand substitution. Chromophores based on Ru^{II} and Os^{II} polyazine complexes have found great utility in the study of PMDs for DNA photomodification.

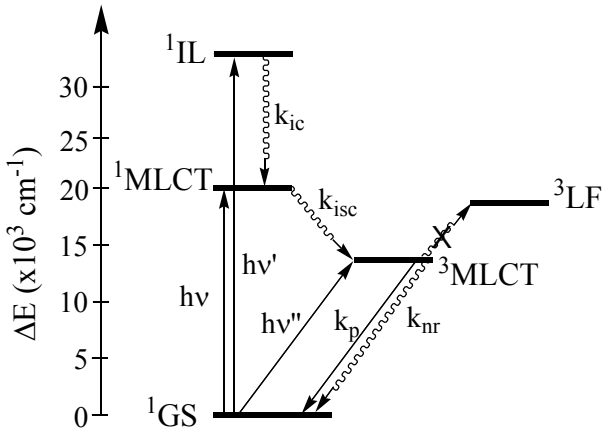

Figure 1.17. Jablonski-type diagram of $[Os(bpy)_3]^{2+}$. bpy = 2,2'-bipyridine, ^{1}GS = singlet electronic ground state, ^{1}MLCT = singlet metal to ligand charge transfer excited state, ^{3}MLCT = triplet MLCT excited state, ^{1}IL = singlet internal ligand excited state. Relative state energies are estimated from Kober, Caspar, Lumpkin and Meyer.[54] Reproduced from Zigler, D. F.; Brewer, K. J. "Toward Photodynamic Therapy of Cancer with Platinum Group Metal Polyazine Complexes" in *Metal-Complexes-DNA Interactions*, Wiley-Blackwell, In press with permission from Wiley-Blackwell.[48]

1.4.3.2. Rhodium Polyazine Complexes

Rhodium polyazine complexes have distinct, reactive electronic excited states that make them attractive in PMD architectural schemes.[7] As with other transition metal polyazine complexes discussed in this chapter, the ligand environment around the central rhodium has major impact on the ES properties. Mononuclear tris(chelate) Rh^{III} polyazine complexes are potent light absorbers in the UV region of the spectrum due to strong IL transitions. These Rh^{III} complexes lack the visible light absorption bands as their MLCT transitions occur at much higher energy than analogous Ru^{II} and Os^{II} systems, Figure 1.18.[63,64] Coincidently, the complexes emit from an ^{3}IL state.[64]

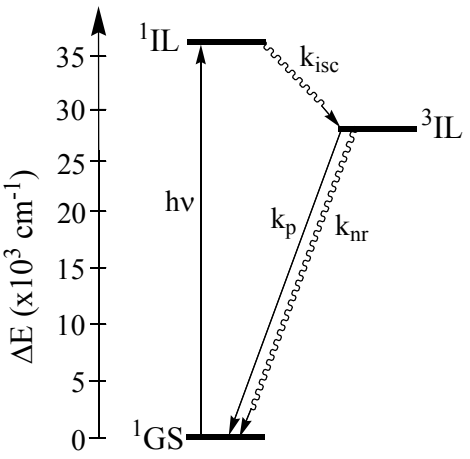

Figure 1.18. Jablonski-type diagram of $[Rh(phen)_3]^{3+}$. phen = 1,10-phenathroline, ^{1}GS = singlet electronic ground state, ^{1}IL = singlet internal ligand excited state. Relative state energies are adapted from Crosby and Elfring.[64] Reproduced from Zigler, D. F.; Brewer, K. J. "Toward Photodynamic Therapy of Cancer with Platinum Group Metal Polyazine Complexes" in *Metal-Complexes-DNA Interactions*, Wiley-Blackwell, In press, with permission from Wiley-Blackwell.[48]

Bis(chelate) polyazine complexes of Rh^{III} with a *cis*-$Rh^{III}X_2$ moiety, where X is a halide, also absorb only in the UV and are emissive in low temperature glasses.[65] A weak absorption band observed between 350-400 nm arises from LF transitions for the $[(NN)_2RhX_2]^+$ systems. The emission from these complexes when excited into the IL or LF bands is broad and significantly Stokes shifted relative the lowest absorption band (~14,000 cm^{-1}).[63] The initially populated ^{1}LF state intersystem crosses to an upper $^3LF_2$ state, Figure 1.19. The $^3LF_2$ state decays by internal conversion to the emissive $^3LF_1$ state. At room temperature, photoaquation (k_{rxn}) competes with non-radiative decay to give the mono- and di-substituted solvato complexes, $[(NN)_2RhX(S)]^{2+}$ and $[(NN)_2Rh(S)_2]^{3+}$ (S = solvent).[62,66] Morrison and coworkers exploit this decay pathway to photobind to DNA, mimicking the DNA thermal binding properties of the well known complex *cis*-$[Pt(NH_3)_2Cl_2]$, better known as cisplatin.[57,67]

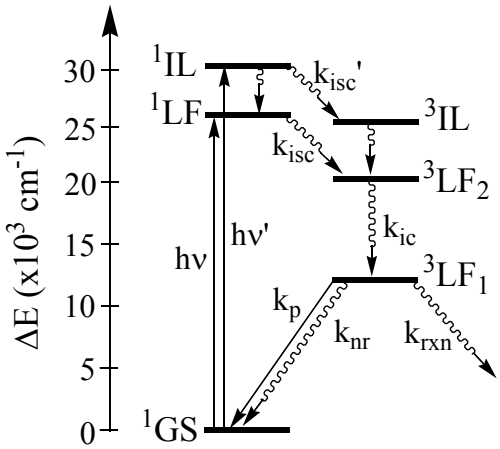

Figure 1.19. Jablonski-type diagram of $[(phen)_2RhCl_2]^+$. phen = 1,10-phenathroline, ^{1}GS = singlet electronic ground state, ^{1}IL = singlet internal ligand excited state, ^{3}LF = triplet ligand field excited state. Rate constants of internal conversion (k_{ic}^x) for the ^{1}IL→^{1}LF and ^{3}IL→^{3}LF processes are omitted for clarity. Relative state energies are adapted from Demas and Crosby.[65] Reproduced from Zigler, D. F.; Brewer, K. J. "Toward Photodynamic Therapy of Cancer with Platinum Group Metal Polyazine Complexes" in *Metal-Complexes-DNA Interactions*, Wiley-Blackwell, In press, with permission from Wiley-Blackwell.[48]

Dirhodium(II) complexes possess unique ESs compared to the mononuclear Rh^{III} complexes due to the strong electronic coupling of the two metal centers. Complexes of the form $[Rh_2(\mu\text{-}O_2CCH_3)_4]$ absorb weakly in the near UV region owing to a low lying Rh-Rh(dπ*) → Rh-Rh(dσ*) (MM-MM) transitions, Figure 1.20.[68] Inclusion of ligands with stabilized π*-acceptor orbitals, e.g. dibenzo[*h*,*j*]dipyrido[3,2-*a*:2',3'-*c*]phenazine (dppz), gives complexes with transitions at ca. 430 nm attributed to IL transitions and Rh-Rh(dπ*)→dppz(π*) charge transfer transitions (MMLCT).[69] The ^{3}MMLCT state is thought to be a long-lived state with an oxidized dirhodium core. These complexes display DNA photooxidation reactions, consistent with reaction of the ^{3}MMLCT state.

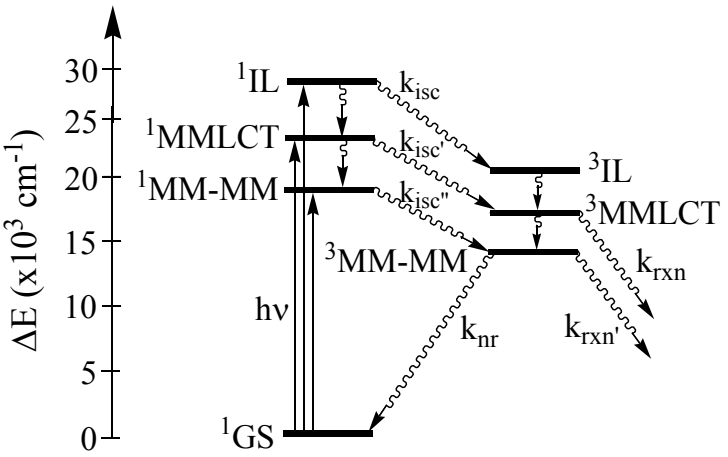

Figure 1.20. Jablonski-type diagram of *cis*-$[Rh_2(\mu\text{-}O_2CCH_3)_2(dppz)_2]^{2+}$. dppz = dipyrido[3,2-*a*:2',3'-*c*]phenazine, ^{1}GS = singlet electronic ground state, ^{1}IL = singlet internal ligand excited state, ^{1}MMLCT = singlet metal-metal to ligand charge transfer state, ^{1}MM-MM = Rh-Rh(dπ*-dσ*) state. Rate constants of internal conversion (k_{ic}^{x}) for the ^{1}IL→^{1}MMLCT, ^{1}IL→^{1}MM-MM, ^{1}MMLCT→^{1}MM-MM, ^{3}IL→^{3}MMLCT, ^{3}IL→^{3}MM-MM and ^{3}MMLCT→^{3}MM-MM processes are omitted for clarity. Relative state energies are adapted from Angeles-Boza, Bradley, Fu, Wicke, Bacsa, Dunbar, Turro.[58,69] Reproduced from Zigler, D. F.; Brewer, K. J. "Toward Photodynamic Therapy of Cancer with Platinum Group Metal Polyazine Complexes" in *Metal-Complexes-DNA Interactions*, Wiley-Blackwell, In press, with permission from Wiley-Blackwell.[48]

1.4.3.3. Excited States of Polyazine Bridged Ru,Rh Complexes

Polyazine bridged, mixed-metal supramolecules have been developed that incorporate multiple metal centers and have more complicated photophysics than the mononuclear analogs.[70] The mixed-metal complexes often retain some ES properties of the subunits used to assemble the supramolecule. Metal centers with strong electronic coupling, e.g. di-Rh^{II} complexes above, have electronic transitions that involve orbitals delocalized over the metal centers. At the other extreme, metal centers that are covalently linked, but without strong electronic coupling, behave like the mononuclear analogs. Ru^{II},Rh^{III} dyads linked via an alkyl tether have electronic properties consistent with each subunit, indicating weak electronic interaction between coupled chromophores.[71-75] The polyazine bridged complexes have inter-component interactions, giving rise to states that are unique to the supramolecular complex without full delocalization of orbitals.

Mixed-metal supramolecules that have weakly to moderately coupled metal centers exhibit unique ESs with interesting ES dynamics, giving rise to useful photophysical properties. Metals bridged by 2,3-bis(2-pyridyl)pyrazine (dpp) electronically couple through the aromatic pyrazine ring.[76] Mononuclear Ru^{II} complexes with dpp have a strong, visible MLCT transition

and a LUMO localized on the pyrazine ring of the dpp ligand (e.g. $[(bpy)_2Ru(dpp)]^{2+}$, λ_{max}^{abs} = 480 nm in water). Bridging the complex to another metal center stabilizes the dpp(π*) LUMO, shifting the MLCT transition to lower energy (e.g. $[(bpy)_2Ru(dpp)Ru(bpy)_2]^{4+}$, λ_{max}^{abs} = 526 nm). Trimetallic complexes with Ru^{II}(dpp) subunits bridged to a *cis*-$Rh^{III}Cl_2$ such as $[\{(bpy)_2Ru(dpp)\}_2RhCl_2]^{5+}$ center have interesting properties, Figure 1.21.[37] The HOMO of these trimetallic complexes is localized on the Ru like other Ru^{II} polyazine complexes, but the LUMO is Rh(dσ*) in nature. Direct Ru(dπ)→Rh(dσ*) charge transfer (MMCT) excitation is forbidden by symmetry and the relatively weak HOMO-LUMO electronic coupling. Irradiation with visible light, however, populates the ^{1}MLCT state. Intersystem crossing generates the ^{3}MLCT state that is higher in energy than the ^{3}MMCT state.[34] Coupling of the dpp(π*) and Rh(dσ*) acceptor orbitals facilitates intramolecular electron transfer to give the ^{3}MMCT state. These trimetallic complexes, which function as photoinitiated electron collectors,[77] have been shown to photocatalyze the production of hydrogen from water[78] and to photocleave DNA.[60,79]

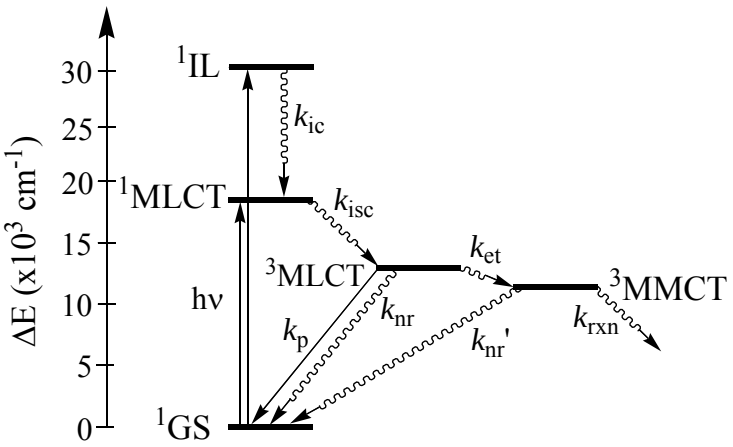

Figure 1.21. Jablonski-type diagram of $[\{(bpy)_2Ru(dpp)\}_2RhCl_2]^{5+}$. bpy = 2,2'-bipyridine, dpp = 2,3-bis(2-pyridyl)pyrazine, ^{1}GS = singlet electronic ground state, ^{1}MLCT = singlet metal to ligand charge transfer, ^{3}MLCT = triplet MLCT, ^{1}IL = singlet internal ligand excited state. Relative state energies adapted from Molnar, Jensen, Vogler, Jones, Laverman, Bridgewater, Richter and Brewer.[41] Reproduced from Zigler, D. F.; Brewer, K. J. "Toward Photodynamic Therapy of Cancer with Platinum Group Metal Polyazine Complexes" in *Metal-Complexes-DNA Interactions*, Wiley-Blackwell, In press, with permission from Wiley-Blackwell.[48]

1.4.4. Reactions of Electronic Excited States

Ground state light absorbers (LA) and their electronic excited states (*LA) are interesting for study, but it is the interaction of *LA with substrate molecules such as DNA that interests developers of PDT treatments. Bimolecular interactions resulting in quenching of *LA following excitation (eq. 1.11) and competing with unimolecular radiative decay (eq. 1.12) and non-radiative decay (eq. 1.13) can be classified into basic groups: bimolecular deactivation, k_{nr}' (eq. 1.14); excited state electron transfer, k_{et}, to (eq. 1.15) or from (eq. 1.16) *LA; excited state energy transfer, k_{en} (Eq. 1.17); and photochemical reaction, k_{rxn} (Eq. 1.18); where Q = quencher, ED = electron donor, EA = electron acceptor.

$$LA + h\nu \xrightarrow{I_a} {}^*LA \tag{1.11}$$

$${}^*LA \xrightarrow{k_r} LA + h\nu' \tag{1.12}$$

$${}^*LA \xrightarrow{k_{nr}} LA \tag{1.13}$$

$${}^*LA + Q \xrightarrow{k_{nr}'} LA + Q \tag{1.14}$$

$${}^*LA + ED \xrightarrow{k_{et}} LA^- + ED^+ \tag{1.15}$$

$${}^*LA + EA \xrightarrow{k_{et}'} LA^+ + EA^- \tag{1.16}$$

$${}^*LA + Q \xrightarrow{k_{en}} LA + {}^*Q \tag{1.17}$$

$${}^*LA + \text{reactant} \xrightarrow{k_{rxn}} \text{photoproducts} \tag{1.18}$$

Current research efforts aimed at developing new, more effective PMDs study the photochemistry of an excited chromophore with the substrate of interest. Transition metal polyazine complexes have a rich photochemical history, focusing strong research efforts. These efforts have given rise to recent discoveries of previously unknown photochemistry including site specific DNA photocleavage,[80] oxygen independent DNA photomodification[60,81] and covalent binding of a metal complex DNA through an appended polyazine ligand.[55] The field is expanding rapidly to accommodate increasing interest in DNA photochemical modification and inorganic based PDT. In addition, information about fundamental photophysical properties is being uncovered.

1.4.4.1. Excited State Electron Transfer Theory

Reductive and oxidative quenching of *LA is driven by the relative redox potentials of the excited LA (*LA) relative to the ED or EA and *LA. The *LA reduction $E(*LA^n/LA^{n-1})$ and *LA oxidation $E(*LA^n/LA^{n+1})$ potentials are estimated with the following equations:[4]

$$E(*LA^n/LA^{n-1}) \approx E(LA^n/LA^{n-1}) - E^{00} \quad (1.19)$$

$$E(*LA^n/LA^{n+1}) \approx E(LA^n/LA^{n+1}) + E^{00} \quad (1.20)$$

Here, $E(LA^n/LA^{n-1})$ and $E(LA^n/LA^{n+1})$ are the respective first reduction and oxidation potentials in V of the GS chromophore, E^{00} is the difference of energy between lowest vibronic states of the GS and ES in eV (see Figure 1.10). The E^{00} is commonly estimated from the λ_{max}^{em} with a Stokes shift applied to account for the shift of the excited state energy surface relative to the ground state. The rate of ES quenching is governed by the driving force of electron transfer as described by Marcus.[82] For a bimolecular reaction under pseudo-first order conditions,

$$[ED]_o \text{ or } [EA]_o >> [ES]$$

the observed rate constant of electron transfer ($k_{obs,et}$) is defined as

$$k_{obs,et} = \nu_N \kappa \exp(-\Delta G^{\ddagger}/RT) \quad (1.21)$$

where ν_N is the nuclear frequency factor and κ is the electron transfer coefficient. The free energy of activation for electron transfer between neutral species, $\Delta G^{\ddagger}$, is expressed in Eq. 1.22.

$$\Delta G^{\ddagger} = \frac{\lambda}{4}\left(1 + \frac{\Delta G^{o}}{\lambda}\right)^2 \quad (1.22)$$

Here, λ is the reorganizational energy and $\Delta G°$ is the change in standard free energy of redox reactants and products. Experimentally k_{et} can be determined by Stern-Volmer kinetic analysis as described below.[83]

1.4.4.2. An Example of Excited State Electron Transfer: Type I Photooxidation of DNA

Reductive quenching of an excited photosensitizer by DNA constitutes a Type I photooxidation reaction as defined by Foote.[84] For example, consider the mechanism of decay of the ^{3}MLCT state of $[(phen)Ru(HAT)_2]^{2+}$ in the presence of DNA, phen = 1,10-phenanthroline, HAT = 1,4,5,8,9,12-hexaazatriphenylene, given that $\Phi_{isc} \cong 1$.

$$[(phen)Ru(HAT)_2]^{2+} + h\nu \xrightarrow{I_a} *[(phen)Ru(HAT)_2]^{2+} \quad (1.23)$$

$$*[(\text{phen})\text{Ru}(\text{HAT})_2]^{2+} \xrightarrow{k_{nr}} [(\text{phen})\text{Ru}(\text{HAT})_2]^{2+} \quad (1.24)$$

$$*[(\text{phen})\text{Ru}(\text{HAT})_2]^{2+} \xrightarrow{k_p} [(\text{phen})\text{Ru}(\text{HAT})_2]^{2+} + h\nu' \quad (1.25)$$

$$*[(\text{phen})\text{Ru}(\text{HAT})_2]^{2+} + \text{DNA} \xrightarrow{k_q} [(\text{phen})\text{Ru}(\text{HAT})_2]^{2+} + \text{DNA} \quad (1.26)$$

$$*[(\text{phen})\text{Ru}(\text{HAT})_2]^{2+} + \text{DNA} \xrightarrow{k_{et}} [(\text{phen})\text{Ru}(\text{HAT})_2]^{+} + \text{DNA}^{+} \quad (1.27)$$

The quantum yield of the electron transfer reaction (eq. 1.28) can be expressed as:

$$\Phi_{et} = \Phi_{isc} \frac{k_{et}[\text{DNA}]}{k_p + k_{nr} + (k_{et} + k_q)[\text{DNA}]} \quad (1.28)$$

where Φ_{et} is the quantum yield of electron transfer, Φ_{isc} is the efficiency of population of the ^{3}MLCT state, k_p and k_{nr} are the respective unimolecular phosphorescence and non-radiative decay rate constants, k_{et} is the rate constant of electron transfer, k_q is rate constant of bimolecular deactivation, and [DNA] is the effective concentration of the DNA quencher in molarity of base pairs. Efficiency and rates of excited state reactions can be determined by probing the quantum yield of phosphorescence Φ_p,

$$\frac{\Phi_p^{\,o}}{\Phi_p} = 1 + \tau^o (k_{et} + k_q)[\text{DNA}] \quad (1.29)$$

with Φ_p being the quantum yield of phosphorescence in the presence of quencher and $\Phi_p°$ is the phosphorescence yield in the absence of quencher. Stern-Volmer analysis consists of plotting $\Phi_p°/\Phi_p$ as a function of [DNA] times the ES lifetime τ^o in the absence of quencher, providing a linear relationship with a slope equal to k_{SV}, where $k_{SV} = k_{et} + k_q$. In the absence of measurable ES emission, k_{SV} may be determined by observing the change in ES lifetime as measured by transient absorption spectroscopy because:

$$\Phi_p°/\Phi_p = \tau/\tau^o \quad (1.30)$$

where τ is the excited state lifetime in the presence of quencher. Transient absorption spectroscopy can differentiate electron transfer quenching and other decay pathways probing the formation of the electron transfer product. Measuring the rate of formation of the product can also allow for the determination of k_{et}.

1.4.4.3. Excited State Energy Transfer Theory

Two mechanisms of excited state energy transfer (eq. 1.16) have been described and involve either ES dipole resonance coupling or electron exchange between the *LA donor and quencher, Q. These two mechanisms have been described individually by Förster[85] and Dexter.[86] The electronic excited states of polyazine bridged platinum group metal complexes have been shown to be reactive toward either mechanism of ES energy transfer, depending on condtions.[70]

Förster described *LA quenching by excited state energy transfer through space by a Q.[85] Resonant coupling of the chromophore and quencher excited state dipoles allow for radiationless energy transfer from the *LA donor to the acceptor Q (k_{SS}). Förster energy transfer efficiency is governed by the spectral overlap of *LA emission and Q absorption (J_F), inter-chromophore distance (d_{DA}), and relative dipole orientation (κ), (eq 1.31):

$$k_{SS} = \frac{8.79 \text{ x } 10^{-25}\kappa^2\phi_f}{n^4\tau_S {d_{DA}}^6} J_F \tag{1.31}$$

$$\kappa = \cos\theta_{DA} - 3\cos\theta_D \cos\theta_A \tag{1.32}$$

$$J_F = \int_0^\infty \frac{F_D(\nu)\varepsilon_A(\nu)}{\nu^4} d\nu \tag{1.33}$$

where n is the refractive index of the solvent. [70,85,87] The ES donor (D) and ES acceptor (A) dipole orientation factor defined by eq. 1.33 considers the mutual 3-dimensional ES dipole orientation. The spectral overlap integral is defined by eq. 1.34, where ν is the average wavenumber frequency, $F_D(\nu)$ is the donor ES emission spectrum normalized to $\varepsilon_A(\nu)$, the extinction coefficient of the overlapping acceptor absorption spectrum.[85,87] Förster excited state energy transfer is the dominant pathway when *LA→LA and Q→*Q transitions are spin allowed. Förster excited state energy transfer is the governing principle of fluorescence resonance energy transfer (FRET) techniques used in confocal microscopy.

A mechanism of excited state energy transfer, described by Dexter, involves electron exchange between the *LA and Q.[86,88] Electron exchange requires some electronic coupling of the *LA donor and the Q acceptor orbitals (eq. 1.35):

$$k_{TT} = \frac{2\pi |V_o|^2 \, e^{-\beta(d_{DA} - R_o)}}{\hbar} J_D \tag{1.34}$$

$$J_D = \int_0^\infty P_D(\nu)\varepsilon_A(\nu)d\nu \tag{1.35}$$

The orbital overlap term is derived from a combination of the electronic coupling matrix element, V_o,[88] and the exponent containing the distance difference between d_{DA} and the critical distance (R_o). R_o is often estimated as the sum of the van der Waal's radii of the *LA and Q.[86,88,89] The entire orbital overlap term is reasonably approximated using semi-empirical calculations, (e.g. ZINDO, INDO, CNDO).[88,90] The β term accounts for solvent reorganization and can be ignored for small change in dipole moment $\Delta\mu$ ($\Delta\mu = |\mu_{ES} - \mu_{GS}|$).[88,91] The spectral overlap term J_D is defined in eq. 1.36, where $P_D(\nu)$ is the $\varepsilon_A(\nu)$ normalized phosphorescence spectrum. Dexter transfer is not bound by the spin selection rule and is thought to be the dominant mechanism of *LA energy transfer when there is poor spectral overlap of *LA emission and Q absorption, e.g. photosensitization of $^3O_2 \rightarrow {}^1O_2$.

Study of excited state energy transfer quenching dynamics can be performed using Stern-Volmer kinetic analysis.[87] Details of this analysis are outlined above for excited state electron transfer. In some instances, observation of the rise-time and/or decay of the *Q state can also be observed and aids in understanding this bimolecular interaction for a specific system.

1.4.4.4. An Example of Excited State Energy Transfer: Type II Photooxidation of DNA

Type II photooxidation reactions of biomolecules as defined by Foote[84] involves photosensitization of molecular oxygen ($^3O_2$), generating singlet oxygen ($^1O_2$) that reacts with a biologically important substrate molecule. Photosensitization of $^1O_2$ from $^3O_2$ requires excited state energy transfer by the Dexter mechanism. Following near unit population the ^{3}MLCT state of $[Ru(phen)_3]^{2+}$, excited state energy transfer produced $^1O_2$ from $^3O_2$ (eq. 1.37).[92]

$$[Ru(phen)_3]^{2+} + h\nu \xrightarrow{I_a} *[Ru(phen)_3]^{2+} \tag{1.36}$$

$$*[Ru(phen)_3]^{2+} \xrightarrow{k_{nr}} [Ru(phen)_3]^{2+} \tag{1.37}$$

$$*[Ru(phen)_3]^{2+} \xrightarrow{k_p} [Ru(phen)_3]^{2+} + h\nu' \tag{1.38}$$

$$*[Ru(phen)_3]^{2+} + {}^3O_2 \xrightarrow{k_{en}} [Ru(phen)_3]^{2+} + {}^1O_2 \tag{1.39}$$

$${}^1O_2 \xrightarrow{k_{nr}'} {}^3O_2 \tag{1.40}$$

$$^1O_2 \xrightarrow{k_p'} {}^3O_2 + h\nu'' \quad (1.41)$$

$$DNA + {}^1O_2 \xrightarrow{k_{rxn}} DNA\ photoproduct \quad (1.42)$$

Using the steady-state approximation on the [$^1O_2$], the quantum efficiency of oxygen mediated photomodification of DNA (Φ_{rxn}) can be described by Eq. 1.43.

$$\Phi_{rxn} = \Phi_{isc}\left(\frac{k_{en}[^3O_2]}{k_p + k_{nr} + k_{en}[^3O_2]}\right)\left(\frac{k_{rxn}[DNA]}{k_{nr}'+k_p'+k_{rxn}[DNA]}\right) \quad (1.43)$$

Here Φ_{isc} is the quantum yield of population of the ^{3}MLCT state (typically 1); k_{en} is the rate constant for ES energy transfer to oxygen, $^3O_2$, dissolved in solution; k_{rxn} is the rate constant for the reaction of $^1O_2$ with DNA, where [DNA] is expressed as concentration of DNA base pairs. The rate constant k_{en} is determined experimentally by measuring emission from the ^{3}MLCT state of $[Ru(phen)_3]^{2+}$ in the absence of DNA, at different concentrations of $^3O_2$. The rate constant k_{rxn} can be elucidated from DNA photoproduct analysis or by observing $^1O_2$ emission decay.

1.4.5. Intramolecular Excited State Interactions: Supramolecular Complexes

Coupling LA and ED or EA subunits together to form supramolecular complexes gives species with interstate interactions that exhibit first order kinetic pathways. The normally emissive electronic excited states of Ru^{II} and Os^{II} polyazine complexes tend to be quenched when covalently attached to energy or electron transfer quencher. The kinetic expression for these types of systems can be generalized with eq 1.44:

$$\Phi'_p = \Phi_{isc}\frac{k_p}{k_p + k_{nr} + k_{en} + k_{et}} \quad (1.44)$$

where Φ'_p is the phosphorescence quantum yield when considering additional specific decay pathways, intramolecular energy transfer quenching (k_{en}) and electron transfer quenching (k_{et}).

1.4.5.1. Kinetics of the Interstate Interactions of Polynuclear Polyazine Complexes

Polyazine bridging ligands (BL) have been employed to build multimetallic supramolecules containing Ru^{II} centered light absorbers with Rh^{III} centered electron acceptors.[93-97] These supramolecules undergo interesting intramolecular interactions governed by the nature of the connecting linkage.[4,70-75,98-101] The Ru^{II} centered ^{3}MLCT state emission is quenched by

intramolecular excited state electron transfer to generate the Ru(dπ)→Rh(dσ*) CT state (metal to metal charge transfer state, MMCT).[71-75,100-104] Electronic coupling of the Ru^{II} donor and Rh^{III} acceptor and thermodynamic driving force dictate the rate of electron transfer.[34,105,106] Endicott and coworkers reported one of the first Ru, Rh dyads, $[(CN)(bpy)_2Ru(\mu\text{-}CN)Rh(NH_3)_4(L)]^{n+}$ with L = NH_3 (n = 3) or L = Br^-, I^-, CN^- (n = 2).[107] Furue, Kinoshita *et al.* reported the heterodyad $[(bpy)_2Ru(Mebpy\text{-}CH_2CHOHCH_2\text{-}Mebpy)Rh(NN)_2]^{5+}$, NN = bpy or phen, which exhibited an intramolecular electron transfer rate constant (k_{et}) of ca. 10^6 s^{-1}.[71] The shorter alkyl tether of $[(4,7\text{-}Me_2phen)_2Ru(Mebpy\text{-}CH_2CH_2\text{-}Mebpy)Rh(dmb)]^{5+}$, where dmb = 4,4'-dimethyl-2,2'-bipyridine, reported by Indelli *et al.* had $k_{et} = 1.7 \times 10^8$ s^{-1}.[72] Decreasing the distance between excited state donor and electron acceptor appeared to enhance intramolecular excited state electron transfer. A series of complexes of the form $[(ttpy)Ru(tpy\text{-}Ph_n\text{-}tpy)Rh(ttpy)]^{5+}$, where ttpy = 4'-(*p*-tolyl)-2,2':6′,2"-terpyridine and n = 1, or 2, also exhibit a distance dependent k_{et}.[98,102,103]

Systems with polyazine BLs between the Ru^{II} and Rh^{III} have photophysical characteristics unlike either monometallic analog and often are compared to the Ru-BL-Ru analogs. Indelli *et al.* studied the complex $[(ttpy)Ru(tpy\text{-}tpy)Rh(ttpy)]^{5+}$, which has a lowest MLCT state red shifted relative to $[Ru(ttpy)_2]^{2+}$.[102,103] The complex $[(ttpy)Ru(tpy\text{-}tpy)Ru(ttpy)]^{4+}$ has a 600 ns excited state lifetime, which upon changing a Ru^{II} to Rh^{III} decreases to 17 ns.[103] The excited state lifetimes measured at 77 K were similar (ca. 12.5 μs). Kalyanasundaram and coworkers reported similar results for the complex $[(bpy)_2Ru(dpp)Rh(bpy)_2]^{5+}$ when compared to $[(bpy)_2Ru(dpp)Ru(bpy)_2]^{4+}$.[73] In solid matrix at 77 K, both the Ru,Rh complexes and Ru,Ru analog display broad, lowly structured emissions centered at ca. 700 nm. At room temperature $[(bpy)_2Ru(dpp)Rh(bpy)_2]^{5+}$ had an emission significantly lower in energy and red shifted relative to the model complex, which the authors attribute to the presence of additional emissive excited state decay pathways, $k_q = 1.48 \times 10^7$ s^{-1}.

More recently polyazine bridged Ru,Os polynuclear complexes were shown to undergo facile intramolecular electronic excited state interactions consistent with rapid Förster energy transfer. Researchers reported on tetranuclear polyazine complexes consisting of three Ru^{II} polyazine subunits bridged to a single Os^{II} core.[108,109] When excited at the higher lying Ru based MLCT transition the authors report unit efficiency of excited state energy transfer yielding the Os centered ^{3}MLCT as the lowest lying electronic excited state.[108] Surprisingly, energy transfer

from the donor ^{1}MLCT of Ru was determined to compete with rapid intersystem crossing to the analogous ^{3}MLCT state ($k_{en} \geq 1.7 \times 10^{13}$ s^{-1}).[109] The newly discovered electronic excited state decay pathways may extend to other platinum group polyazine supramolecules containing excited state donors and acceptors.[110,111] Additional decay pathways might explain some of the poorly understood photochemical reactions of this class of supramolecule.

1.5 Photochemical Reactions of Metal Complexes with DNA

DNA is central to protein expression (transcription) and cell replication. Damage to DNA disrupts cell function by causing carcinogenesis, mutagenesis, apoptosis, and cell death. There are several reported mechanisms of excited state photosensitizer reactions inducing DNA damage.[49,80,81,112-114] Careful design of DNA photochemical experiments can yield surprising amounts of information about the mechanism of DNA/metal complex interaction as well as information about the chromophore's excited state dynamics. Characteristic changes to DNA are observed for photobinding of metal complex, photooxidation of nucleobases, and photocleavage of the sugar phosphate backbone. Knowledge of the decomposition pathways of DNA photolyzed with a metal complex helps to understand a possible mechanism of PDT action.

1.5.1. General Structure of DNA

DNA is a supramolecular polymer with complex structure that dictates its interactions with molecules of interest. Helpful descriptions of DNA structure and analysis can be found in the book by Calladine.[115] The backbone of a single strand of DNA is a phosphodiester-linked chain of deoxyribose subunits linked at the 3' and 5' position, Figure 1.22. The 1' position is covalently bound to a purine (adenine, guanine) or pyrimidine (thymine, cytosine). Hydrogen bonding between complimentary bases (A to T, G to C) on separate strands of DNA gives double stranded DNA (ds-DNA). The secondary structure of DNA is the characteristic double helix, with handedness and pitch dictated by solution conditions (e.g. ionic strength). B-DNA is the most prevalent in biological systems with a right-handed helix and about 10.4 bases per helical turn. B-DNA has hydrophobic major and minor grooves each edged by anionic sugar-phosphate backbones, Figure 1.22. This complex surface structure gives DNA its interesting behavior with potential PDT agents

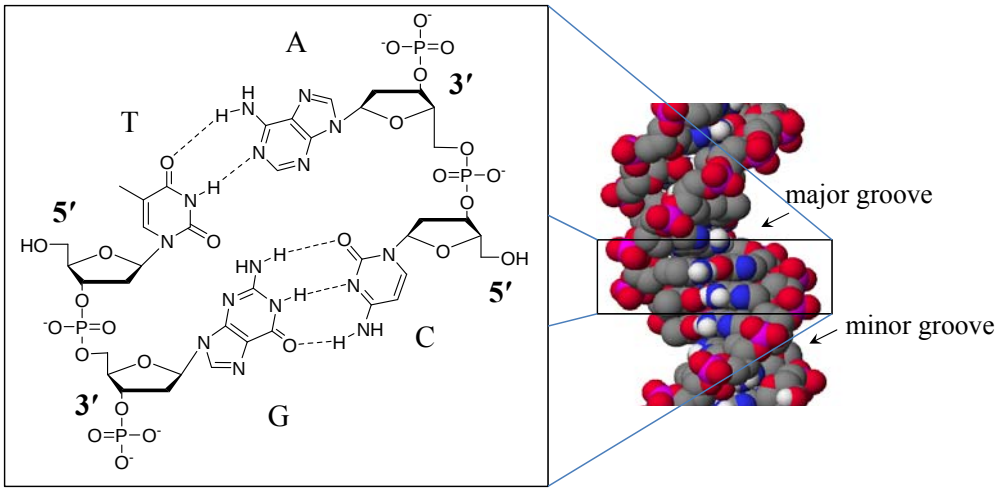

Figure 1.22. Complimentary pairs of nucleotides that make up double helix DNA (Inset, A = adenine, T = thymine, G = guanine, C = cytosine, DNA = deoxyribonucleic acid). Atoms are carbon (gray), hydrogen (white), nitrogen (blue), oxygen (red) and phosphorous (pink). Reproduced from Zigler, D. F.; Brewer, K. J. "Toward Photodynamic Therapy of Cancer with Platinum Group Metal Polyazine Complexes" in *Metal-Complexes-DNA Interactions*, Wiley-Blackwell, In press, with permission from Wiley-Blackwell.[48]

1.5.2. DNA Targets and Analysis

Study of the photochemical reactions of metal complexes with DNA requires careful choice of the type of DNA used and method of analysis. Mono- and oligonucleotides are used as targets with chemical analysis techniques such as mass spectrometry (MS) and nuclear magnetic resonance (NMR) spectroscopy. Mononucleotides are available commercially and have found utility as models for DNA/metal complex binding and in ES quenching studies. Oligonucleotides (oligos) are short strands of DNA (15-100 base pairs) that have known sequence and structural properties. Oligos are better models for chromosomal DNA because they can be obtained as double stranded DNA. High-resolution poly(acrylamide) gel electrophoresis (HR-PAGE) is instrumental in understanding sequence specificity of photochemical reactions with oligonuclear DNA leading to irreversible changes. Circular plasmid DNA extracted from bacteria is obtained with a supercoiled (Form I) tertiary structure that makes this type of DNA an excellent target for photomodification schemes, Figure 1.23.[116,117] Changes to the topological nature of supercoiled circular plasmid DNA are indicative

of several decomposition pathways that can be analyzed using agarose gel electrophoresis, Figure 1.24. The DNA topoisomers are separated by size in the gel with supercoiled (Form I) as the most compact migrating the furthest. Supercoiled circular plasmid DNA relaxes to the bulkier open circular form (Form II) when the DNA backbone is nicked. Two nicks, occurring on opposite strands and in close proximity, cause the circular DNA to open into its linear form (Form III), which migrates faster than the open circular form and slower than the supercoiled form in gel electrophoresis. Finally, genomic DNA is commercially available as a freeze dried extract from various tissue sources and is high molecular weight, with > 10^6 base pairs per molecule. Genomic DNA is used to understand DNA-metal interactions that require large volumes and/or high DNA concentrations for analysis using selective precipitation, changes to spectroscopy and viscosity measurements. Each form of DNA has specific advantages and disadvantages toward use in photochemical experiments and multiple types are required to get a more complete understanding of the metal complex-DNA photochemical mechanism.

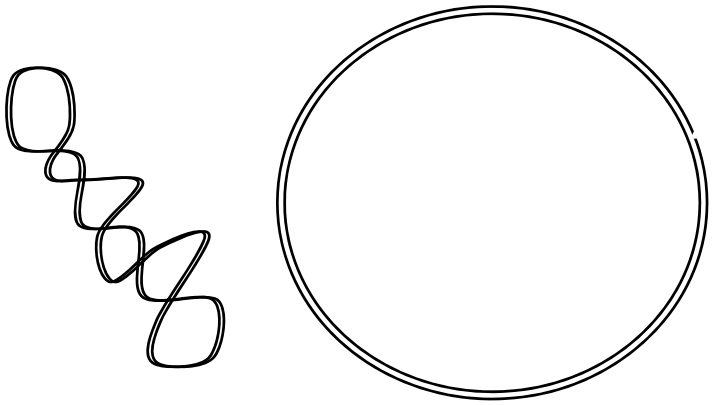

Form I Form II

Figure 1.23. Cartoon of closed circular plasmid DNA, like pUC18 DNA, in its supercoiled form (Form I) and its nicked, relaxed form (Form II).

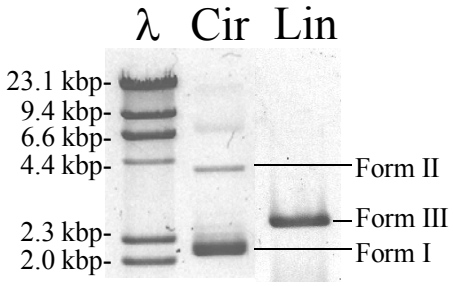

Figure 1.24. Photograph of a typical 0.8% agarose gel illustrating the electrophoretic migration (moving from top to bottom) of three different forms of plasmid DNA. The lanes from left to right are as follows: λ is a Lambda DNA/*Hin*dIII digest molecular weight marker (kbp = 1,000 base-pairs), Cir is circular plasmid DNA containing native supercoiled (Form I) and open-circular (Form II) plasmid DNA, and Lin is linear plasmid DNA (Form III). Band assignments are based on Vinograd and Lebowitz.[116] Reproduced from Zigler, D. F.; Brewer, K. J. "Toward Photodynamic Therapy of Cancer with Platinum Group Metal Polyazine Complexes" in *Metal-Complexes-DNA Interactions*, Wiley-Blackwell, In press, with permission from Wiley-Blackwell.[48]

1.5.3. Designing Transition Metal Polyazines for DNA Photomodification

Photomodification of DNA by transition metal polyazine complexes is attractive because of the structural diversity of this class of complexes.[14,21] Two major design considerations for chromophores applicable as DNA photomodification agents are: the impact of structural changes on the interaction of the chromophore with DNA and the impact of chromophore structure on the efficiency and mechanism of their DNA photochemistry. Recent reports present photochemical mechanisms that help elaborate previously described photochemistry, Table 1.4 (Section 1.4.3.), and have prompted cell studies to explore application in PDT.

1.5.3.1. Ground State Interactions of Transition Metal Polyazine Complexes and DNA

The mechanism of DNA modification by photosensitizers is often multi-step with the first step involving some form of metal complex/DNA association.[49,81,112] Figure 1.25 illustrates the polyazine ligands used in complexes discussed in this section. Smaller, compact polyazine transition metal complexes tend to have an electrostatic interaction with DNA.[51] Lipophilic substituents on the polyazine ligands gives complexes that bind in the hydrophobic minor or major groove of the DNA double helix.[118] Ligands with extended, planar aromatic substituents favor intercalation between DNA bases.[80,112] More recently metal complexes have been shown

to displacing a base pair upon insertion between strands of the double helix, a behavior that is previously not described.[112] Binding of transition metal polyazine complexes to DNA is enantioselective, a reflection of the chiral nature of DNA and the often chiral nature of polyazine chelated metal complexes. Barton has pioneered exploiting the different binding modes as shape selective probes of DNA and RNA structure.[56,80,112,119] The strength of the DNA/metal complex interactions has a direct impact on the photosensitizer function as a DNA modification tool.

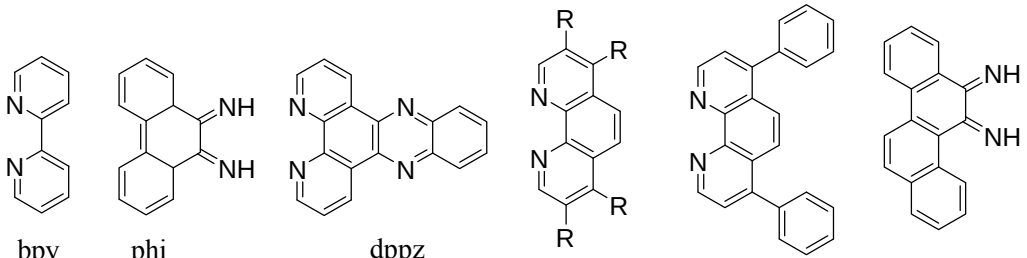

Figure 1.25. Polyazine ligands used in the construction of metal complexes that bind to DNA.

Electrostatic interaction of cationic transition metal polyazine complexes with DNA can be described by the polyelectrolyte approximation of counter ion condensation theory.[120] DNA is polyanionic with a single negative charge per nucleotide in aqueous solution. Usually Na^+ acts as the counter ion to the DNA negative charge. Transition metal polyazine complexes studied for DNA photomodification can have large negative to large positive charges. Exchange efficiency of Na^+ by an incoming complex ion at the DNA surface is a factor of the charge of the complex, the concentration of free metal complex, and Na^+ concentration (ionic strength). Complexes with large positive charges that are structurally compact have stronger electrostatic interactions with DNA. The prototypical transition metal polyazine complex $[Ru(bpy)_3]^{2+}$ exhibits ionic binding to DNA.[51]

Groove binding of transition metal polyazine complexes to DNA is controlled by complex lipophilicity and molecular shape. Also known as surface binding, groove binding is association of a species with the hydrophobic pocket formed between the sugar-phosphate backbones of each strand. The complex $[Ru(Me_4phen)_3]^{2+}$ is a well known groove binder.[118] The methyl substituents on the phen ligand contribute to the complex's overall lipophilicity, but

provide steric bulk that prevents more intimate interactions with the DNA.

Extended, planar polyazine ligands that can intercalate into the base stack of DNA have been shown to enhance metal complex/DNA electronic interactions prior to photolysis.[80,112] Two ligands often included in a metal complex's architecture that promote intercalation are dppz and 9,10-phenanthrenequinone diimine (phi). Emission in water of Ru(II)-polyazine complexes with the dppz ligand is notably weak due to low lying n $\rightarrow\pi^*$ ^{3}IL state(s) that quenches the emission from the ^{3}MLCT state possibly through hydrogen bonding of the water to the lone pairs on the nitrogens on the dppz ligand. Intercalation into DNA, however, protects the nitrogens on dppz from water, decreasing quenching of the ^{3}MLCT state and greatly enhancing emission. Therefore Ru(II)-complexes with dppz are often called "DNA light switches."[121]

Complexes with bulky planar ligands bind by an alternative mechanism. The complex $[(phen)_2Rh(chrysi)]^{3+}$ reported by Barton and coworkers inserts its α-chrysenequinone diimine (chrysi) ligand into the base stack accompanied by displacement of a base pair. Photocleavage of DNA by metallo-insertor complexes was shown to be an effective method of identifying base mismatches in the DNA.[122]

It is important to note that the mode of DNA/metal complex interaction prior to photolysis is not always clear. The reader is referred to a review by Kirsch De-Mesmeaker, Lecompte and Kelly for a historical account of "The controversial case of $[Ru(phen)_3]^{2+}$."[49]

Hexacoordinate transition metal complexes with two or three bidentate ligands tend to have strongly enantioselective binding interactions with DNA.[119] DNA in its most common B form is a right-handed double helix, Figure 1.22, interacting more strongly with Δ enantiomers of tris(chelate) metal complexes. Barton has shown that the complex Δ-$[Ru(Ph_2phen)_3]^{2+}$ binds strongly in the major groove of the double-helix, intercalating the base pairs. The other enantiomer Λ-$[Ru(Ph_2phen)_3]^{2+}$ does not bind as strongly, owing to the steric repulsion of the bulky ancillary ligands with the sugar-phosphate backbone of DNA.

1.5.3.2. Mechanisms of DNA Photochemical Degradation

The study of DNA photochemical degradation is pursued to better understand the complicated and sometimes unclear mechanisms deleterious damage to the DNA. The mechanisms of DNA degradation under photolytic or oxidative stress have been thoroughly reviewed.[113,114,123] Photoinitiated binding of metal complexes was studied, coined "photo-

cisplatin" agents. Photobinding through an ancillary ligand also leads to DNA covalent modification. Oxidation of the DNA bases by ES electron transfer reaction and hydrogen atom abstraction are important to the photochemical function of some transition metal polyazine complexes. Photocleavage of DNA by the transition metal polyazine ES in the presence or absence of dissolved $^3O_2$ exhibits a separate mechanisms of action. Many of the transition metal polyazine complexes studied for their photochemical interaction with DNA exhibit multiple ES reactions with DNA.

1.5.4. Design Aspects: Toward Photobinding DNA through a Metal Center

Ruthenium(II) complexes of the form *cis*-$[(TL)_2RuX_2]^{n+}$, where X = halide (n = 0) and X = H_2O, NH_3, or aliphatic amine (n = 2), have been investigated for their DNA thermal binding properties and more recently as DNA photobinding agents.[124] The complexes *cis*-$[(bpy)_2RuCl_2]$ and *cis*-$[(bpy)_2Ru(OH_2)_2]^{2+}$ readily covalently bind to DNA under physiological conditions. Photobinding to DNA of *cis*-$[(bpy)_2RuCl_2]$ and *cis*-$[(bpy)_2Ru(OH_2)_2]^{2+}$ shows little enhancement over thermal binding pathways.[125] Singh and Turro reported the DNA photobinding properties of *cis*-$[(bpy)_2Ru(NH_3)_2]^{2+}$, but have shown that the complex did not appreciably thermally bind DNA.[50] The mononuclear complex absorbs strongly at 290 nm and 243 nm, consistent with IL transitions. MLCT transitions in the visible region occur at λ_{max}^{abs} = 490 nm. The complex undergoes photoaquation when irradiated with near-UV light (λ_{max}^{ex} = 350 nm or 400 nm, Φ_{aq} = 0.024±2 or 0.018±2). Excitation with light > 450 nm however did not lend to an observable chemical reaction. The photoaquation takes place from a ^{3}LF state that is thermally inaccessible from the ^{3}MLCT state. A photoproduct of 400 nm excitation of *cis*-$[(bpy)_2Ru(NH_3)_2]^{2+}$, *cis*-$[(bpy)_2Ru(OH_2)_2]^{2+}$, was demonstrated to undergo ligand substitution with mononucleotides and was shown to bind readily to double stranded (ds) and single stranded (ss) DNA. The authors predict that the interacting electronic excited states can be tuned by modifying the complex structure to favor photoaquation following visible light excitation.

Octahedral polyazine complexes of Rh(III) with a *cis*-dihalide moiety are also known to undergo ligand substitution upon photolysis with near-UV light.[62,66] Morrison and coworkers have studied the DNA photobinding properties of *cis*-$[(TL)_2RhCl_2]^+$.[57,126-128] They demonstrated that $[(phen)_2RhCl_2]^+$, when irradiated with 308 nm light, photobound to ss- or dsDNA with $\Phi_b \approx$ 0.006 and 0.001, respectively.[57] Dark controls confirm that electronic excitation of the metal

complex is required for $[(phen)_2RhCl_2]^+$ to bind DNA. The authors have also proposed that a photooxidation step is necessary to initiate the sequence giving the photosubstitution products.[126] The photolabile state of $[(phen)_2RhCl_2]^+$ was previously assigned to the lowest ^{3}LF state.[66] Exchanging phen for 3,4,7,8-tetramethyl-1,10-phenanthroline (Me_4phen) or 5,6-dimethyl-1,10-phenanthroline (5,6-Me_2phen) had varying impact on the photochemistry.[128] The lowest absorption band of $[(5,6\text{-}Me_2phen)_2RhCl_2]^+$ is red shifted compared to both $[(phen)_2RhCl_2]^+$ and $[(Me_4phen)_2RhCl_2]^+$. Enhanced photoaquation was observed for $[(Me_4phen)_2RhCl_2]^+$ (Φ_{aq} = 0.63) compared to $[(phen)_2RhCl_2]^+$ (Φ_{aq} = 0.03) when photolyzed with 347 nm light. A similar complex, $[(phen)(dppz)RhCl_2]^+$ was shown to both photobind and photocleave DNA when irradiated at 311 nm. The planar dppz ligand is known to facilitate intercalative binding of the metal complex to DNA. The Φ_{aq} of $[(phen)(dppz)RhCl_2]^+$ when irradiated with 355 nm light is reported to be 0.068, reduced compared to $[(phen)_2RhCl_2]^+$ (Φ_{aq} = 0.087). Competitive decay to a low lying n→π* state localized on the dppz ligand is possible in the dppz containing complex. The authors noted photocleavage by $[(phen)(dppz)RhCl_2]^+$ may occur through a low lying ^{3}IL state.

1.5.5. Design Aspects: Toward Photocleavage of DNA

Photoinitiated scission of DNA can occur by reaction of DNA with $^1O_2$, by hydrogen atom abstraction from a sugar, and by excited state electron transfer.[49,113,114,123] Early studies indicated that the ^{3}MLCT states of $[Ru(bpy)_3]^{2+}$ under anoxic and hypotonic conditions are quenched along with single strand cleavage of circular plasmid DNA, $\Phi_{rxn} = 1.2 \times 10^{-6}$ when $[DNA]/[Ru(bpy)_3]^{2+} = 9$. Hydrogen atom abstraction from a sugar of DNA by $*[(phen)_2Rh(phi)]^{3+}$ initiates a reaction cascade ending with single strand scission.[56] Recently the complex $[(TAP)_2Ru(dppz)]^{2+}$ with DNA was reported showing mixed photochemical pathways.[129] The authors noted a mechanism by which the complex photobinds to DNA through a TAP ligand in addition to nicking the backbone.

The ability of a chromophore excited state to oxidize DNA depends on the redox properties of DNA bases and of the excited chromophore. Guanine is the DNA nitrogenous base with the strongest reducing power [$E(G/G^+) \approx 0.92$ V vs. Ag/AgCl].[130-133] When incorporated in dsDNA, oxidation occurs preferentially at the 5'-G of a multi-G stack, resulting from a destabilization of the 5'-G donor orbitals and shifting the oxidation potential ($E°$) of 5'-GGG-3' to

ca. 0.42 V (vs. Ag/AgCl).[123] Radical cations of the oxidized bases decompose by multiple pathways, including cleavage of the sugar phosphate backbone and base-labile nucleotide oxidation products.[113]

1.5.5.1. Oxygen Mediated Photocleavage of DNA

Photocleavage of DNA represents a major research effort in the study of DNA photomodifications with application to the development of new PDT agents. Several mechanisms of DNA photocleavage by platinum group metal polyazine complexes have been proposed that require $^3O_2$. DNA photocleavage was reported for $[Ru(TL)_3]^{2+}$, TL = bpy, phen, in aerated solution.[52] Mongelli, Brewer and coworkers reported a series of mononuclear Ru(II) complexes containing a dpp; $[(TL)_2Ru(dpp)]^{2+}$, where TL = bpy, phen or Ph_2phen.[134] Enhancement of DNA photocleavage was noted for complexes with more lipophilic terminal ligands, $[(Ph_2phen)_2Ru(dpp)]^{2+}$ being the most active, consistent with earlier reports by Barton for $[Ru(Ph_2phen)_3]^{2+}$.[51] Hergueta-Bravo, Orellana and coworkers investigated the $^3O_2$ dependence of DNA photocleavage by a series of Ru(II) complexes incorporating the intercalating ligand dibenzo[*h*,*j*]dipyrido[3,2-*a*:2',3'-*c*]phenazine (ddz).[135] The ^{3}MLCT of $[(bpy)_2Ru(ddz)]^{2+}$ state is a less efficient photosensitizer of $^1O_2$ generation relative to $[Ru(bpy)_3]^{2+}$. Enhanced DNA photocleavage by $[(bpy)_2Ru(ddz)]^{2+}$ however was noted. The increase in DNA photocleavage by $[(bpy)_2Ru(ddz)]^{2+}$ was attributed to strong intercalative binding to the DNA prior to photolysis. A similar observation was made for the complex $[(bpy)_2Ru(DAP)]^{+}$, DAP = 1,12-diazaperylene.[136]

The coupling of Ru polyazine chromophores to a *cis*-$Pt^{II}Cl_2$ site provides a means to attach a DNA photocleavage unit to a DNA covalent binding unit. This attachment provides a means to deliver the Ru polyazine chromophore to the DNA target. An example of such a complex, $[\{(bpy)_2Ru(dpp)\}_2Ru(dpp)PtCl_2]^{6+}$, binds to DNA through the Pt(II) center and photcleaves DNA via an oxygen mediated pathway.[59]

1.5.6.2. Oxygen Independent Photocleavage of DNA

Swavey, Holder, and Brewer examined DNA photocleavage using polyazine bridged supramolecules comprising of two Ru(II) or two Os(II) light absorber subunits connected to a central *cis*-$Rh^{III}Cl_2$ moiety.[34,79] A wide array of supramolecules constructed with a dpp

molecular bridge produced nicks in supercoiled circular plasmid DNA with > 450 nm light photolysis. The gel showing the photocleavage of DNA by a member of this series, $[\{(bpy)_2Ru(dpp)\}_2RhCl_2]^{5+}$, is shown in Figure 1.26. The mechanism of DNA photocleavage is unclear, but this complex functions as a DNA photocleavage agent in the presence or absence of dissolved $^3O_2$. DNA photocleavage is proposed to result from intramolecular ES electron transfer quenching of the ^{3}MLCT state by the *cis*-$RhCl_2$ center. The resultant metal to metal charge transfer (^{3}MMCT) state has a formally oxidized Ru center and a formally reduced Rh center, both of which are capable of mediating DNA cleavage in the absence of $^3O_2$. Importantly, nicks in the DNA backbone caused by most types of photocleavage often are irreparable by the repair enzyme DNA ligase.[114]

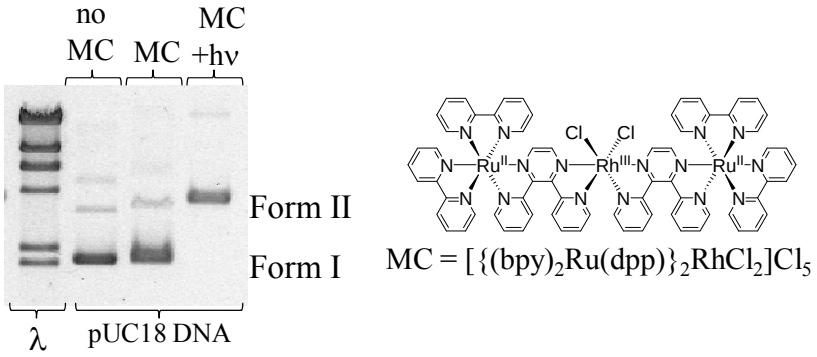

Figure 1.26. Photograph of electrophoresis gel imaged with ethidium bromide showing the efficient photocleavage of pUC18, supercoiled circular plasmid DNA (Form I), with the metal complex $[\{(bpy)_2Ru(dpp)\}_2RhCl_2]Cl_5$, generating open circular pUC18 DNA (Form II) [bpy = 2,2'-bipyridine, dpp = 2,3-bis(2-pyridyl)pyrazine]. DNA was photolyzed with 460 nm centered light from a 5W LED. From left to right the lanes are: Lambda DNA/*Hin*dIII digest molecular weight marker (λ), pUC18 DNA without treatment with metal complex (no MC), pUC18 DNA incubated with metal complex in the dark at 5:1 base pairs to metal complex (MC), and pUC18 DNA photolyzed in the presence of metal complex at 5:1 base pairs to metal complex (MC+hν).[137] Reproduced from Zigler, D. F.; Brewer, K. J. "Toward Photodynamic Therapy of Cancer with Platinum Group Metal Polyazine Complexes" in *Metal-Complexes-DNA Interactions*, Wiley-Blackwell, In press, with permission from Wiley-Blackwell.[48]

1.6. Statement of Problem

Trimetallic supramolecules with two Ru^{II} or two Os^{II} polyazine light absorbers bridged to a *cis*-$Rh^{III}Cl_2$ center are interesting due to their interstate dynamics and photochemical activity, including photochemistry with DNA. New molecular architectures that have a single light absorber attached to a *cis*-$Rh^{III}Cl_2$ center offer similar interesting properties while simplifying the overall structure of these complexes. Described herein is the preparation of this new structural motif as an electrochemical, photophysical, and photochemical model of more complicated supramolecular architectures.

Chapter 2. Experimental

2.1. Materials

All commercial materials and solvents were used without further purification. The inorganic starting material $[(bpy)_2RuCl_2]\cdot 2H_2O$ was purchased from Strem Chemical (Newburyport, MA). The bridging ligand 2,3-bis(2-pyridyl)pyrazine (dpp), the terminal ligand 2,2':6',2"-terpyridine (tpy) and starting material $RhCl_3\cdot xH_2O$ (38.87% Rh) were purchased from Sigma-Aldrich (St. Louis, MO). The bridging ligand 2,2'-bipyrimidine (bpm) was purchased from Alfa-Aesar (Ward Hill, MA). The terminal ligand 1,10-phenanthroline monohydrate (phen) and supporting electrolyte tetra(*n*-butyl)ammonium hexafluorophosphate (Bu_4NPF_6, electrochemical grade) were from Fluka (Steinheim, Switzerland). Ethanol (200 proof) was from Aaper Alcohol and Chemical Company (Shelbyville, KY). Adsorption alumina (80-200 mesh), diethyl ether, 12 M HCl and HPLC Grade methanol, acetonitrile, toluene, and acetone were all from Fisher (Fair Lawn, NJ). All biochemicals and materials for biochemical experiments were used as received. Plasmid (pUC18) DNA was purchased from Bayou Biolabs (Harahan, LA). *Lambda* DNA/*Hin*dIII molecular marker was obtained from Promega (Madison, WI). Electrophoresis grade boric acid, agarose, and molecular biology grade tris(hydroxymethyl)aminomethane (TRIS) and glycerol were all obtained from Fisher Scientific (Pittsburgh, PA). Ethidium bromide and bromophenol blue were from Sigma-Aldrich (St. Louis, MO). Sodium dihydrogen phosphate was obtained from Acros Organics (New Jersey). Reverse osmosis water was used to prepare all solutions and was obtained from an in house water source.

2.2. Syntheses

2.2.1. Monometallic Synthons

2.2.1.1. Synthesis of $[(bpy)_2Ru(bpm)](PF_6)_2$

The synthetic procedures were adapted from Nallas *et al*.[36] In 45 mL of deoxygenated 2:1 v/v ethanol/water, 0.50 g (1.0 mmol) of $[(bpy)_2RuCl_2]\cdot 2H_2O$ and 0.49 g (3.1 mmol) of bpm were heated at reflux for 3 hours. The resulting orange-brown solution was added dropwise to a stirring aqueous 2 M NH_4PF_6 (ca. 10 mL) to induce precipitation of the product. Following isolation by vacuum filtration, reprecipitation from acetone (5 mL) into diethyl ether (400 mL), and vacuum filtration, the orange solid was purified via column chromatography (2 columns, 40 mm x 15 cm each) on methanol deactivated adsorption alumina, eluting with 3:2 v/v

toluene/acetonitrile. The leading orange band was concentrated by rotary evaporation, dissolved in a minimal amount of acetone, added to diethyl ether to induce precipitation and filtered through fine porosity frit to give 0.48 g of $[(bpy)_2Ru(bpm)](PF_6)_2$ as a bright orange solid (0.53 mmol, 52% yield). Electrochemical and electronic absorption spectroscopic data were consistent with the previously reported values.[36] CV (Pt-disc) in acetonitrile: $E_{1/2}$ = 1.43, −0.99, −1.42 V versus Ag/AgCl. UV-Vis (acetonitrile): 430, 286, 249 nm.

2.2.1.2. Synthesis of $[(bpy)_2Ru(dpp)](PF_6)_2$

The synthesis of this monometallic synthon was adapted from Gafney *et al.*[138] Under argon, a solution 0.50 g (1.0 mmol) of $[(bpy)_2RuCl_2]\cdot 2H_2O$ and 0.74 g (3.2 mmol) of dpp in 45 mL 2:1 v/v ethanol/water was heated at reflux for 3 hours. The crude product was precipitated by dropwise addition of the reaction mixture to a stirring 2 M aqueous solution of NH_4PF_6(20 mL). The orange solid was removed via vacuum filtration through a fine porosity fritted glass funnel, taken into 5 mL of acetone and reprecipitated in 500 mL of diethyl ether. After isolation via vacuum filtration, the crude powder was purified by column chromatography on methanol deactivated adsorption alumina, eluting with 3:2 v/v toluene/acetonitrile (3 columns, 40 mm x 15 cm each). The leading orange band was collected, reduced by rotary evaporation. The orange residue was taken into a minimal amount of acetone (ca. 5 mL) and added to 500 mL of diethyl ether to induce precipitation. Vacuum filtration gave the product as a brick red solid (0.76 g, 0.81 mmol, 79% yield) with electrochemical, electronic absorption and excited state emission properties consistent with the literature reported values.[138] CV (Pt-disc) in acetonitrile: $E_{1/2}$ = 1.35, −1.02, −1.46 V versus Ag/AgCl. UV-Vis (λ, acetonitrile): 470, 290, 250 nm. RT Emission (λ^{ex} = 470 nm): 640 nm.

2.2.1.3. Synthesis of $[(bpy)_2OsCl_2]$

The synthesis of $[(bpy)_2OsCl_2]$ was similar to the synthesis reported by Kober *et al.*[24] A mixture of 1.0 g (2.4 mmol) of $(NH_4)_2[OsCl_6]$ and 0.76 g (4.8 mmol, 2.0 eq) of bpy in 50 mL of well deoxygenated ethylene glycol were heated at reflux under argon atmosphere for 1 hour. After cooling, 75 mL of a concentrated $Na_2S_2O_4$ solution in water was added and stirred for ca. 20 min at room temperature under argon. The resulting purple-black solid was removed via vacuum filtration through a coarse frit, resuspended in ca. 20 mL of water, sonicated for 10 min

and filtered. The sonication/filtration step was repeated twice to finally give 1.1 g (1.8 mmol, 77%) of a fine black microcrystalline solid with no observed emission when excited at 480 nm indicating negligible $[Os(bpy)_3]^{2+}$ impurity.

2.2.1.4. Synthesis of $[(bpy)_2Os(dpp)](PF_6)_2$

The synthesis of this osmium containing synthon was a modified synthesis from Richter and Brewer.[139] The bridging ligand dpp (0.51 g, 2.2 mmol, ca. 2.5 eq) was dissolved in 25 mL of warmed, deoxygenated ethylene glycol. Solid $[(bpy)_2OsCl_2]$ (0.50 g, 0.87 mmol) was added in one portion with vigorous mixing. The mixture was heated at reflux for ca. 30 min, after which time the heat was removed and the reaction was allowed to come to room temperature. The resulting brown solution was then added dropwise to 20 mL of 2 M aqueous NH_4PF_6 to induce precipitation. The crude material was removed via vacuum filtration and reprecipitated from 5 mL of acetone in 500 mL in diethyl ether. Chromatography on methanol deactivated adsorption alumina, eluting with 3:2 toluene/acetonitrile (2 columns, 40 mm x 15 cm each), gave the intended product as the leading brown band. Eluting solvent was removed via rotary evaporation and the brown residue taken into minimal ca. 5 mL of acetone and dropped into ca. 500 mL of diethyl ether to induce precipitation. Vacuum filtration gave $[(bpy)_2Os(dpp)](PF_6)_2$ as a fine brown powder with electronic absorption and electrochemical properties consistent with the literature (0.52 g, 0.50 mmol, 58%).[139] CV (Pt-disc) in acetonitrile: $E_{1/2}$ = 0.94, −1.02, −1.38, −1.58 V versus Ag/AgCl.

2.2.1.5. Synthesis of $[(tpy)OsCl_3]$

This synthesis is modeled after one reported by Meyer *et al.*[27] A solution of 1.01 g (2.30 mmol) of $(NH_4)_2[OsCl_6]$ and 0.542 g (2.32 mmol, 1.01 eq) of tpy in 70 mL ethylene glycol were heated at reflux for ca. 2 h. The reaction mixture was cooled to room temperature and diluted with 200 mL of 3:1 v/v ethanol/water. The dark mixture was stored at -20 °C overnight. Filtration through a coarse porosity frit and washing with copious amounts of water followed by 30 mL of diethyl ether and drying in vacuo gave 0.981 g (1.85 mmol, 81% yield) of $[Os(tpy)Cl_3]$ as a black, microcrystalline solid.

2.2.1.6. Synthesis of [(tpy)OsCl(dpp)](PF$_6$)

A suspension of 0.428 g (1.82 mmol, 1.20 eq.) of dpp in 50 mL of ethylene glycol was heated until all of the dpp dissolved. The solution was cooled slightly and 0.806 g (1.52 mmol) of [(tpy)OsCl$_3$] suspended in 20 mL of room temperature ethylene glycol was added in one portion. The mixture was heated at reflux for ca. 20 min, after which time the solution was allowed to cool to room temperature. The mixture was filtered to remove 0.428 g (0.808 mmol, 53%) of unreacted [(tpy)OsCl$_3$]. The reaction was scaled down and repeated using the recovered starting material. The violet-burgundy crude product was precipitated with a 70% saturated aqueous solution of KPF$_6$ (ca. 50 mL). Chromatography on a methanol deactivated adsorption alumina column with 1:1 acetonitrile/toluene eluent gave [(tpy)OsCl(dpp)](PF$_6$) as the leading burgundy band. The combined fractions were rotary evaporated, taken into a minimal amount of acetonitrile (ca. 10 mL), flash precipitated into diethyl ether (400 mL), and collected by vacuum filtration to give 0.608 g (0.743 mmol, 49 % yield) of [(tpy)OsCl(dpp)](PF$_6$) as a burgundy solid. FAB+-MS (*m/z*), [M-(PF$_6$)]$^+$ = 694. A cyclic voltammogram is presented in Figure 2.1.

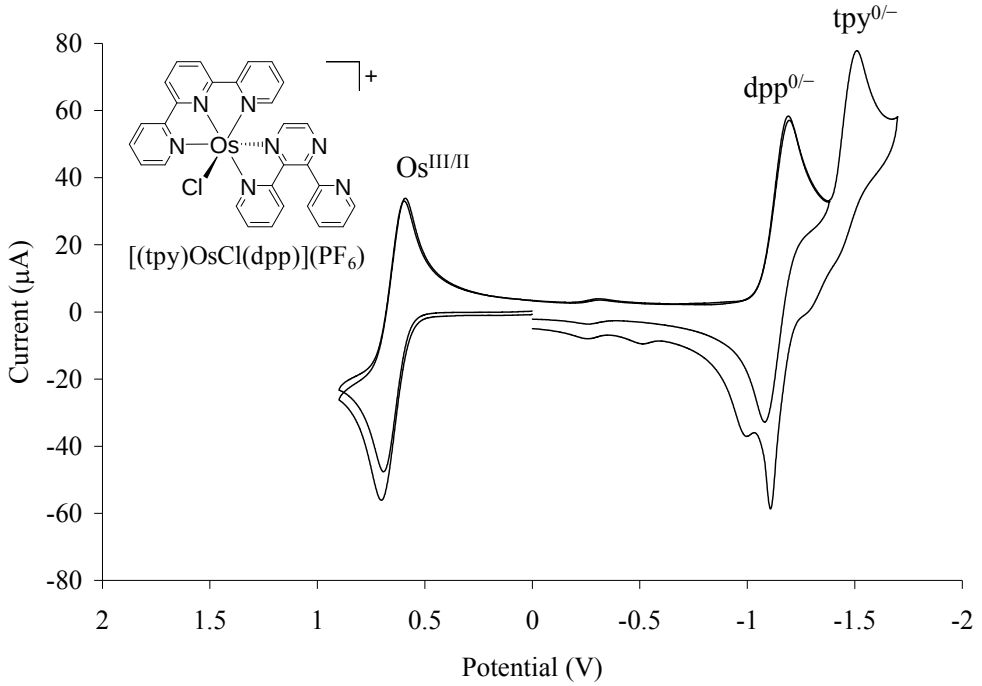

Figure 2.1. Cyclic voltammogram of [(tpy)OsCl(dpp)](PF$_6$) in 0.1 M Bu$_4$NPF$_6$ acetonitrile at a platinum disc working electrode versus Ag/AgCl (3M NaCl) (−0.46 V vs. FeCp$_2^{+/0}$), using a platinum wire counter electrode, tpy = 2,2':6',2"-terpyridine, dpp = 2,3-bis(2-pyridyl)pyrazine.

2.2.1.7. Synthesis of K[(phen)RhCl$_4$]·3H$_2$O

Caution. This synthesis requires the heating of hydrochloric acid solutions in an open vessel, liberating HCl gas. All chemical manipulations were performed in a fume hood. All heating was performed using a stirring hot water bath.

Synthetic procedures for K[(phen)RhCl$_4$]·3H$_2$O were adapted from McKenzie and Plowman.[140] Trichlororhodium(III) hydrate (1.33 g, ~5.00 mmol) was dissolved in 100 mL of hot 2 M HCl. After heating for about 2 hr at 95 °C, 1,10-phenanthroline monohydrate (3.76 g, 19.0 mmol) in 50 mL of 2 M HCl was added drop-wise with vigorous stirring. The opaque salmon colored mixture was stirred for 2.5 hr at 95 °C and then cooled to room temperature. The resulting orange-pink solid was removed via vacuum filtration. The damp solid was heated at 95 °C in 75 mL of 10 M HCl for 1 hour with stirring, followed by hot vacuum filtration to remove any insoluble material. The deep orange filtrate was returned to 95 °C, allowed to cool slowly to room temperature, and then plunged into a CaCl$_2$/ice water bath. The shimmering orange-red crystals were removed by vacuum filtration and rinsed with ca. 20 mL of cold 10 M HCl followed by ca. 20 mL of acetone. The acid salt was dissolved in a minimal amount (ca. 50 mL) of hot 5 M HCl. A saturated solution of KCl in 5 M HCl, ca. 15 mL was added drop-wise to cause precipitation of a bright orange solid. Continued heating followed by slow cooling, vacuum filtration, and an acetone rinse (ca. 20 mL) yielded bright orange needles of K[(phen)RhCl$_4$]·3H$_2$O (1.89 g, 3.66 mmol, 71 %). Rh analysis: Calc Rh 19.9%, Determined 19.9%. The analysis of K[(phen)RhCl$_4$]·3H$_2$O by NMR proved difficult as the spectrum indicated ligand exchange over time in DMSO-d$_6$. Product analysis was performed by the above Rh analysis and by reacting K[(phen)RhCl$_4$]·3H$_2$O and 4,4'-dimethyl-2,2'-bipyridine (dmb) in a 1:1 stoichiometry with subsequent analysis of the ^{1}H-NMR spectrum.

2.2.1.8. Synthesis of [(phen)RhCl$_2$(dmb)](PF$_6$)

K[(phen)RhCl$_4$]·3H$_2$O (0.050 g, 0.11 mmol) and 4,4'-dimethyl-2,2'-bipyridine (0.021 g, 0.11 mmol) were added to 55 mL of stirring, deoxygenated 2:1 ethanol/water. The solution was heated at reflux for 1 hour and then cooled. Metal complex precipitation was induced by slow addition to a 2 M aqueous solution of NH$_4$PF$_6$ (ca. 10 mL). The solid was removed by vacuum filtration and washed with ca. 20 mL each of water, ethanol, and diethyl ether. The pale-yellow [(phen)RhCl$_2$(dmb)](PF$_6$) was dried *in vacuo* (0.053 g, 0.076 mmol, 69 % yield) and analyzed by

^{1}H-NMR. ^{1}H-NMR (d_6-acetone) δ = 10.11 (1H, dt, *J*= 5.4, 1.0 Hz), 9.80 (1H, d, *J*= 5.9 Hz), 9.23 (1H, dd, *J*= 8.3, 1.2 Hz), 8.94 (1H, dd, *J*= 8.3, 1.2 Hz), 8.80 (1H, weak, dd), 8.66 (1H, weak, dd), 8.54 (1H, d, *J*= 8.9 Hz), 8.51 (1H, dd, *J*= 8.2, 5.2 Hz), 8.43 (1H, d, *J*= 8.9 Hz), 8.36 (1H, dt, *J*= 5.4, 1.0 Hz), 8.04 (1H, ddd, *J*= 5.9, 1.9, 0.8 Hz), 7.95 (1H, dd, *J*= 8.2, 5.4 Hz), 7.71 (1H, d, *J*= 6.0 Hz), 7.27 (1H, ddd, *J*= 6.0, 1.8, 0.7 Hz), 2.84 (3H, s), 2.53 (3H, s) ppm. ^{1}H-NMR and ^{1}H-^{1}H COSY are available in the Appendix, Figure A-1.

2.2.2. Bimetallic Complexes

2.2.2.1. Synthesis of [(bpy)$_2$Ru(bpm)RhCl$_2$(phen)](PF$_6$)$_3$·3H$_2$O

A solution of 0.28 g of K[(phen)RhCl$_4$]·3H$_2$O (0.54 mmol, 1.2 eq) and 0.40 g of [(bpy)$_2$Ru(bpm)](PF$_6$)$_2$ (0.46 mmol, 1.0 eq) in ca. 45 mL of deoxygenated 2:1 v/v ethanol/water was warmed to ensure all components had dissolved prior to reaching reaction temperature. The solution was heated at reflux for 45 min, after which time it was cooled and added dropwise to 10 ml of a 2M NH_4PF_6 solution to induce precipitation of [(bpy)$_2$Ru(bpm)RhCl$_2$(phen)](PF$_6$)$_3$ as a green solid. Following isolation by vacuum filtration, the crude material was dissolved in a ca. 5 mL of acetone and precipitated in ca. 400 mL of diethyl ether. The fine green powder was then suspended in ca. 100 mL of absolute ethanol, heated ca. 15 min, allowed to cool and then recovered by vacuum filtration through a medium porosity frit to afford 0.42 g of [(bpy)$_2$Ru(bpm)RhCl$_2$(phen)](PF$_6$)$_3$·3H$_2$O (0.30 mmol, 65% yield) as a dark green powder. Combustion analysis: Calc. C 33.96, H 2.56, N 9.90; Found C 34.34, H 2.74, N 9.96%. (+)ESI-TOF MS: *m/z* = 1215.0 ([M−PF$_6^-$]$^+$). The measured and calculated mass spectra for the molecular ion peak, [M−PF$_6^-$]$^+$ are in the Appendix, Figures A-2 and A-3.

2.2.2.2. Synthesis of [(bpy)$_2$Ru(dpp)RhCl$_2$(phen)](PF$_6$)$_3$·3H$_2$O.

K[(phen)RhCl$_4$]·3H$_2$O (0.20 g, 0.38 mmol, 1.2 eq) was dissolved in deoxygenated 2:1 v/v ethanol/water (45 mL) with continuous stirring under argon flow. To the stirring bright yellow solution was added 0.30 g of [(bpy)$_2$Ru(dpp)](PF$_6$)$_2$ (0.32 mmol, 1.0 eq) followed by 15 mL of 2:1 ethanol/water. The reaction mixture was slowly heated to reach reflux, ensuring all [(bpy)$_2$Ru(dpp)](PF$_6$)$_2$ had dissolved prior to reaching reaction temperature. The solution was heated at reflux for 45 min. The crude mixed metal complex was precipitated using 2 M NH_4PF_6 (10 mL) and isolated via vacuum filtration. The crude [(bpy)$_2$Ru(dpp)RhCl$_2$(phen)](PF$_6$)$_3$ was

taken into a minimal amount of acetone (ca. 15 mL), syringe filtered and precipitated in diethyl ether (ca. 400 mL). The crude purple solid, 0.44 g, was stirred in 100 mL of boiling absolute ethanol for 15 min, followed by slow cooling and vacuum filtration to give a microcrystalline solid. The violet solid was dissolved in ca. 3 mL of acetone, syringe filtered and precipitated into ca. 400 mL of diethyl ether. Vacuum filtration and drying under vacuum afforded the complex $[(bpy)_2Ru(dpp)RhCl_2(phen)](PF_6)_3 \cdot 3H_2O$ (0.34 g, 0.23 mmol, 72% yield). Combustion analysis: Calc. C 37.06, H 2.70, N 9.40%; Found C 37.61, H 2.89, N 9.45%. (+)ESI-TOF MS: *m/z* = 1291.0 ($[M-PF_6^-]^+$). The measured and calculated mass spectra for the molecular ion peak, $[M-PF_6^-]^+$ are in the Appendix, Figures A-4 and A-5.

2.2.2.3. Synthesis of $[(bpy)_2Os(dpp)RhCl_2(phen)](PF_6)_3$

The complexes $K[(phen)RhCl_4] \cdot 3H_2O$ (0.12 g, 0.23 mmol, 1.2 eq) and $[(bpy)_2Os(dpp)](PF_6)_2$ (0.20 g, 0.19 mmol) were stirred in 30 mL of 2:1 v/v ethanol/water under argon flow for 15 minutes. The deoxygenated mixture was heated at reflux for about 75 min, after which the deep purple solution was cooled to room temperature and added to a 2 M NH_4PF_6 solution (10 mL) to induce precipitation. The crude complex salt $[(bpy)_2Os(dpp)RhCl_2(phen)](PF_6)_3$ was collected via vacuum filtration using a medium porosity frit and rinsed with ca. 30 mL of water, then 30 mL of diethyl ether. The purple solid was taken into a minimal amount of dry acetone, ca. 6 mL. The concentrated acetone solution was passed through a 0.2 μm PTFE syringe filter and dropped into 400 mL of stirring diethyl ether to induce precipitation. The violet flocculate was removed via vacuum filtration. The dry solid was added to stirring absolute ethanol (150 mL) with a little acetone (ca. 2 mL) in an open beaker. The contents of the beaker were heated on a hot plate for ca. 15 minutes then allowed to cool slowly to room temperature. The deep violet solid was collected using a coarse porosity frit. Drying in vacuo gave the deep violet solid with a colorless crystal as an impurity. The latter was removed by taking the solid into a ca. 3 mL of very dry acetone and syringe filtering the solution. Flash precipitation followed by vacuum filtration gave 0.25 g (0.16 mmol, 84% yield) of $[(bpy)_2Os(dpp)RhCl_2(phen)](PF_6)_3$. (+)ESI-TOF MS: *m/z* = 1381.1 ($[M-PF_6^-]^+$). The measured and calculated mass spectra for the molecular ion peak, $[M-PF_6^-]^+$ are in the Appendix, Figures A-6 and A-7.

2.2.2.4. Synthesis of [(tpy)OsCl(dpp)RhCl$_2$(phen)](PF$_6$)$_2$

A deoxygenated solution of 0.15 g of [(tpy)OsCl(dpp)](PF$_6$) (0.18 mmol) and 0.10 g of K[(phen)RhCl$_4$]·3H$_2$O (0.20 mmol, 1.1 eq) in 2:1 v/v ethanol/water was heated at reflux for ca. 60 min. The deep violet solution was cooled to room temperature and added dropwise to 10 mL of a stirring 2 M NH_4PF_6 solution to induce precipitation. The violet solid was collected by vacuum filtration and washed with ca. 30 mL of water followed by ca. 30 mL diethyl ether. The dry solid was taken into ca. 10 mL of acetone, passed through a syringe filter, and flash precipitated with diethyl ether. The material recovered by vacuum filtration was then stirred in hot ethanol (ca. 150 mL) for about 15 min, then allowed to slowly cool to room temperature. The resulting material was collected on a coarse porosity frit and rinsed with absolute ethanol (ca. 30 mL) and diethyl ether (ca. 30 mL). The dry solid was then taken into ca. 2 mL of very dry acetone, passed through a syringe filter and dropped into diethyl ether to induce precipitation. Vacuum filtration gave 0.13 g of [(tpy)OsCl(dpp)RhCl$_2$(phen)](PF$_6$)$_2$ (0.097 mmol, 54% yield). (+)ESI-TOF MS: *m/z* = 1192.0 ([M−PF$_6^-$]$^+$). The measured and calculated mass spectra for the molecular ion peak, [M−PF$_6^-$]$^+$ are in the Appendix, Figures A-8 and A-9.

2.2.3. Trimetallic Complexes

2.2.3.1. Synthesis of [{(bpy)$_2$Ru(bpm)}$_2$RhCl$_2$](PF$_6$)$_5$

The synthetic procedures to make this complex were from Nallas *et al.*[36] In 45 mL of 2:1 v/v ethanol/water, 0.30 g (0.35 mmol) of [(bpy)$_2$Ru(bpm)](PF$_6$)$_2$ and 0.046 g (0.17 mmol) of RhCl$_3$·xH$_2$O were heated at reflux under argon for 45 min. Following cooling to room temperature, the mixed metal complex was precipitated by dropwise addition of the reaction mixture to 10 mL of 2 M aqueous NH_4PF_6. The resulting green solid, isolated by vacuum filtration, was taken into a about 5 mL of acetone, which was then added dropwise to 400 mL of diethyl ether to induce precipitation of a fine green powder collected by vacuum filtration. The product was stirred in about 75 mL of boiling absolute ethanol for ca. 15 min, cooled, and recovered by vacuum filtration. The dark green solid was taken into ca. 3 mL dry acetone, passed through a syringe filter and precipitated in ca. 200 mL diethyl ether. Vacuum filtration gave the complex [{(bpy)$_2$Ru(bpm)}$_2$RhCl$_2$](PF$_6$)$_5$ (0.28 g, 0.14 mmol, 79% yield) as a dark green powder with electrochemical properties and an electronic absorption spectrum consistent

with previously reported values.[36] CV (Pt-disc) in acetonitrile: $E_{1/2}$ = 1.70, −0.13, −0.26, −0.78 (E_p^c) V versus Ag/AgCl. UV-Vis (λ, acetonitrile): 594, 412, 278 nm.

2.2.3.2. Synthesis of [{(bpy)$_2$Ru(dpp)}$_2$RhCl$_2$](PF$_6$)$_5$

The synthesis of the trimetallic complex was from Molnar *et al.*[37] To a deoxygenated solution of 0.10 g (0.11 mmol) of [(bpy)$_2$Ru(dpp)](PF$_6$)$_2$ in 15 mL of ethanol was added 7.9 mL of a 7.1 mM solution of $RhCl_3$ in water (0.5 eq). The solution was heated at reflux for 20 min, after which time the heat was removed and the violet solution was cooled to room temperature. Precipitation of the metal complex was caused by slow addition of the reaction mixture to a stirring 2 M aqueous solution of NH_4PF_6 (ca. 10 mL). The resulting violet solid was isolated by vacuum filtration and reprecipitated in 200 mL of diethyl ether from acetone (4 mL). The crude violet product was heated in ca. 150 mL 200 proof ethanol (ca. 80 °C) for 15 min, cooled, and collected on a fritted glass funnel. Dissolution in to ca. 3 mL of dry acetone, followed by syringe filtration and precipitation in 400 mL of diethyl ether gave 0.10 g (0.045 mmol, 81% yield) of [{(bpy)$_2$Ru(dpp)}$_2$RhCl$_2$](PF$_6$)$_5$ as a red violet powder. Metal complex purity was assessed using a combination of electrochemistry, electronic absorption spectroscopy and luminescence spectroscopy, and was consistent with the literature.[37] CV (Pt-disc) in acetonitrile: $E_{1/2}$ = 1.60, −0.39 (E_p^c), −0.79, −1.02 V versus Ag/AgCl. UV-Vis (λ, acetonitrile): 520, 416, 338(sh), 284 nm.

2.2.3.3. Synthesis of [{(bpy)$_2$Os(dpp)}$_2$RhCl$_2$](PF$_6$)$_5$

The synthetic procedures used to make this metal complex were from Holder, Swavey and Brewer.[79] The osmium synthon [(bpy)$_2$Os(dpp)](PF$_6$)$_2$ (0.10 g, 0.097 mmol) and 1.25 mL of a 39 mM solution of $RhCl_3$ in water (0.049 mmol) were heat in deoxygenated 2:1 v/v ethanol/water at reflux for 30 min (total volume = 15 mL). The deep burgundy solution was cooled to room temperature and added dropwise to an NH_4PF_6 solution to induce precipitation of the mixed metal complex, which was collect via vacuum filtration. The complex was dissolved in a minimal volume of acetone, precipitated in diethyl ether, collected on a fritted glass funnel by vacuum filtration, and then purified by stirring in ca. 150 mL of boiling absolute ethanol. The solid was dissolved in 3 mL of acetone, syringe filtered, precipitated in diethyl ether and isolated by vacuum filtration to give 0.076 g (0.032 mmol, 66% yield) of fine violet solid. The

electrochemistry and electronic absorption spectrum was consistent with previous reports of this supramolecule.[79] CV (Pt-disc) in acetonitrile: $E_{1/2}$ = 1.21, −0.39 (E_p^c), −0.76, −1.00 V versus Ag/AgCl. UV-Vis (λ, acetonitrile): 798(br), 534, 412, 336, 284 nm.

2.2.3.4. Synthesis of [{(tpy)OsCl(dpp)}$_2$RhCl$_2$](PF$_6$)$_3$

A solution of 0.089 g (0.11 mmol) of [(tpy)OsCl(dpp)](PF$_6$) in ca. 60 mL of 2:1 ethanol/water and 7.9 mL of a 7.1 mM solution of $RhCl_3 \cdot xH2O$ in water (0.055 mmol) was heated at reflux for 1 hr. The violet reaction mixture was cooled and added to 10 mL of aqueous 2 M NH_4PF_6 to induce precipitation of a violet solid received by vacuum filtration. The solid was rinsed with ca. 30 mL each water, and diethyl ether, dried on the frit, and taken into ca. 2 mL acetone and flash precipitated in 200 mL diethyl ether to give the crude product as a fine powder. The crude was then suspended in ca. 100 mL boiling absolute ethanol and heated for ca. 20 min. The alcoholic mixture was cooled and vacuum filtered to give a deep violet microcrystalline solid. The solid was dissolved in ca. 3 mL of dry acetone, syringe filtered and precipitated in 300 mL of diethyl either to give 0.096 g of [{(tpy)OsCl(dpp)}$_2$RhCl$_2$](PF$_6$)$_3$ (0.048 mmol, 86% yield) as a fine purple powder. (+)ESI-TOF MS: *m/z* = 1851.1 (5%, $[M-PF_6^-]^+$). The measured and calculated mass spectra for the molecular ion peak, $[M-PF_6^-]^+$ are in the Appendix, Figures A-10 and A-11.

2.3. Physical measurements

2.3.1. Nuclear Magnetic Resonance Spectroscopy

Nuclear magnetic resonance spectroscopy was performed on a 400 MHz Varian Inova spectrometer. Samples were prepared in either perdeutero acetonitrile or perdeutero acetone from Cambridge Isotopes and filtered through a glass wool packed Pasture pipette. Chemical shifts were assigned either relative to the residual solvent peaks or to a tetramethylsilane internal standard.

2.3.2. Mass Spectrometry

Mass spectrometry was performed by Richard Davies at M-Scan, Inc of West Chester, PA. Positive ion electrospray mass spectra were obtained on a Waters (Millford, MA) Micromass quadripole-time of flight (Q-TOF) mass spectrometer. The sample in acetonitrile

was directly infused into a preloading capillary at 3.5 kV with a 5 mL/min flow rate. The cone outlet ionization potential of 20 to 50 V was varied to optimize resolution of the molecular ion peak. Reported peaks are the most intense peak within an isotopic group. Ion peak assignments were confirmed using either the Sheffield Chemputer[141] isotopic peak distribution predictor or the chemical analysis function of ChemDraw 8.0.[142] Selected measured and calculated peaks from the mass spectra of the new complexes are presented in the Appendix (Figures A.2-A.11)

2.3.3. Elemental Analysis

Both rhodium metals analysis and CHN combustion analysis were performed on bulk samples (ca. 20 mg) by Galbraith Laboratories, Inc. Rhodium analysis was performed using inductively coupled plasma-atomic emission spectroscopy (ICP-AES).

2.3.4. Electrochemistry

All electrochemistry was performed using a Bioanalytical Systems (BAS) Epsilon potentiostat and three-electrode, single chamber cell, Figure 1.3. Solutions were made in 0.1 M tetra-*n*-butylammonium hexafluorophosphate (Bu_4NPF_6) in spectrophotometric grade acetonitrile (Burdick and Jackson, Muskegon, MI). The working electrode was a Pt disk, the auxiliary electrode was a Pt wire and potentials were measured against either a Ag/AgCl (3M NaCl) reference electrode or Ag wire quasi-reference electrode (QRE), each calibrated against a $FeCp_2^{0/+}$ internal standard (0.46 V versus Ag/AgCl 3M NaCl).[143] Cyclic voltammetry (CV) was typically performed at a scan rate of 100 mV/s. The scan rate dependent electrochemical behavior of some redox processes were examined by changing the potential scan rate (varied from 10 mV/s to 6250 mV/s).

2.3.4.1. Combined Bulk Electrolytic, Controlled Potential Coulometric and Voltammetric Measurements

Three techniques, controlled potential electrolysis (CPE), controlled potential coulometry (CPC), and CV were combined to try to understand the electrochemical properties of the complexes studied. The electrolysis chamber consisted of a 20 mL beaker, graphite cloth working electrode for bulk electrolysis, a Vicor glass tipped Ag/AgCl (3M NaCl) reference electrode, and a platinum disc working electrode for cyclic voltammetry, Figure 2.2. A platinum

coil counter electrode was separated from the electrolysis solution by placing it in a glass tube with a fritted glass bottom. The bottom of the reference electrode was situated between the auxiliary electrode and both working electrodes. The electrodes were arranged to reduce potential and current drops across the graphite cloth during electrolysis. The electrolytic medium was 0.3 M Bu_4N PF_6 in either acetonitrile, 5% v/v H_2O/acetonitrile, or DMF. The analyte solution was blanketed with solvent saturated argon and continuously magnetically stirred during BE. Bulk electrolysis was performed by stepping the graphite cloth electrode to a potential just negative of E_p^c or positive of E_p^a of the process to be studied. Coulometry was performed by integrating the current/time decay curve and subtracting charge transfer due to background current (see eq. 1.6). Cyclic voltammetry was performed prior to and following each bulk electrolytic step by turning off stirring and connecting the platinum disc working electrode.

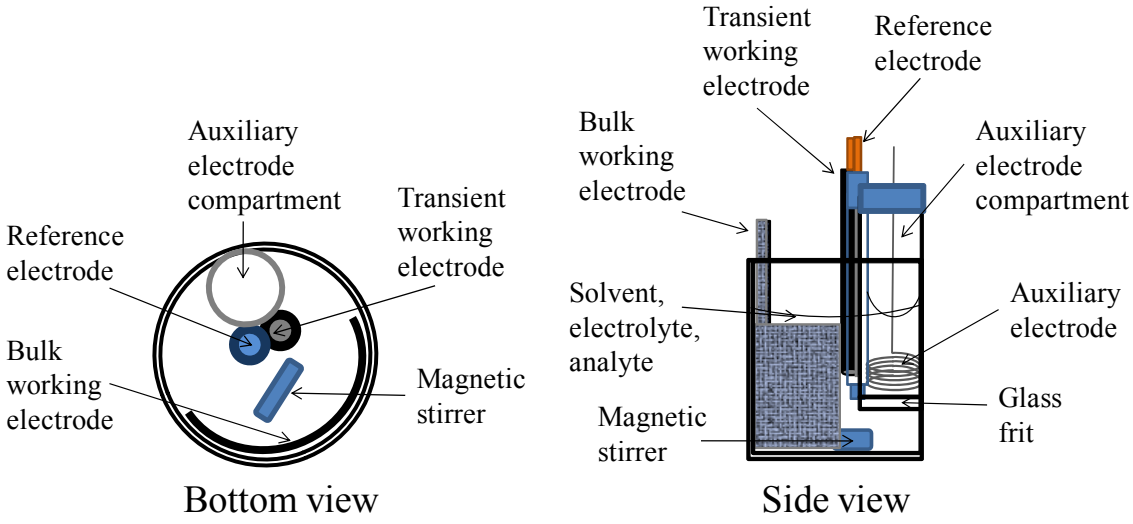

Figure 2.2. A schematic of the two compartment cell used in controlled potential electrolysis experiments using a Pt coil auxiliary electrode, Ag/AgCl (3M NaCl) reference electrode, Pt disk working electrode for *in situ* cyclic voltammetry, and graphite cloth working electrode for bulk electrolysis.

Free chloride in solution following the each electrolytic step was determined by comparing the measured i_p^a of the chloride oxidation at ca. 1.2 V to that of a known concentration. This required a calibration curve for the Pt-disk working electrodes used in the cyclic voltammetry experiments. Two samples of Bu_4NCl, 171.1 ± 0.5 mg and 152.3 ± 0.5 mg, were dissolved in the 25.0 mL of 0.3 M Bu_4NPF_6 acetonitrile. The cyclic voltammogram of each

stock solution, diluted 10-fold and 5-fold, or 10-fold and 20-fold, were obtained at each of two Pt disc working electrodes in duplicate. The auxiliary electrode was platinum wire and a Ag wire was used as a quasi-reference electrode. Cyclic voltammograms were obtained from 0.3 V to 1.6 V, switching after the prominent chloride oxidation. Anodic peak currents were then measure (± 0.5 μA) averaged, and plotted as function of chloride concentration, Figure 2.3.

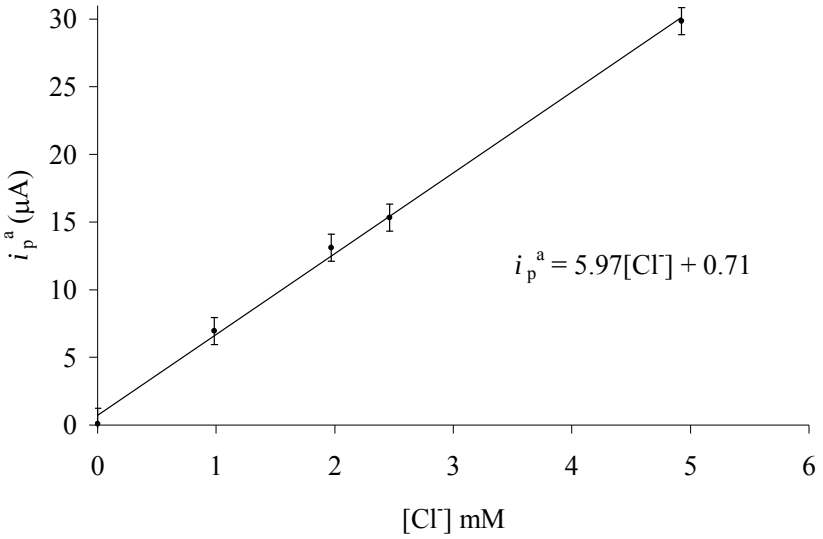

Figure 2.3. Chloride calibration curve charting anodic current (i_p^a) response of the platinum disc working electrode of unknown area used in cyclic voltammetry as a function of "free" chloride concentration, [Cl^-], v = 100 mV/s. Error bars are propagated error based on ±0.5 μA deviation between peak current measurements.

2.3.5. Electronic Absorption Spectroscopy

The electronic absorption spectra were collected using standard techniques. All electronic absorption spectra were obtained in room temperature spectrophotometric grade acetonitrile and using a 1 cm pathlength quartz cuvette (Starna Cells, Inc; Atascadero, CA). Spectra were collected using one of the following UV-Vis spectrophotometers: a Agilent 8453 photodiode array spectrophotometer, Hewlett-Packard 8452A photodiode array spectrophotometer, Ocean Optics photodiode array spectrophotometer, or Varian-Cary 5G UV-Vis-NIR scanning double beam spectrophotometer, all using a solvent reference. Extinction coefficients were determined by averaging the absorption spectra of gravimetric solutions of the title complexes prepared in triplicate.

2.3.5.1. Spectroelectrochemistry

Spectroelectrochemical experiments were performed in an optically transparent, thin layer electrode (OTTLE) cell, Figure 2.4. The cell was constructed from two quartz slides sandwiched around a fine gold mesh working electrode and separated by 0.2 mm Teflon spacers. The slides were clamped in place using binder clips. The electrode assembly was balanced on top of a small glass dish containing the metal complex analyte solution (ca. 80 μM) in 0.3 M Bu_4NPF_6 in acetonitrile. The analyte was drawn into the cell by capillary action. The reference electrode [Ag/AgCl (3M NaCl)] and Pt coil counter electrode were immersed in the analyte pool. The assembly was aligned so that the light path passed through the gold mesh closest to the bottom of the cell. Electrodes of this type typically have increasing potential gradients from top to bottom, with the bottom being closest to the applied potential. The entire assembly was enclosed in a crude dry box formed of cellophane around the spectrophotometer. Dry argon was then pumped into this box in an attempt to limit the concentration of O_2, which interferes with the measurements. Potentials were applied and held using the controlled potential electrolysis (CPE) function of the Epsilon potentiostat. Spectra were recorded at 10 sec intervals using the Agilent 8453A spectrophotometer. Electrolysis was determined to be complete by observing no change in the electronic absorption spectrum, typically within 5 min.

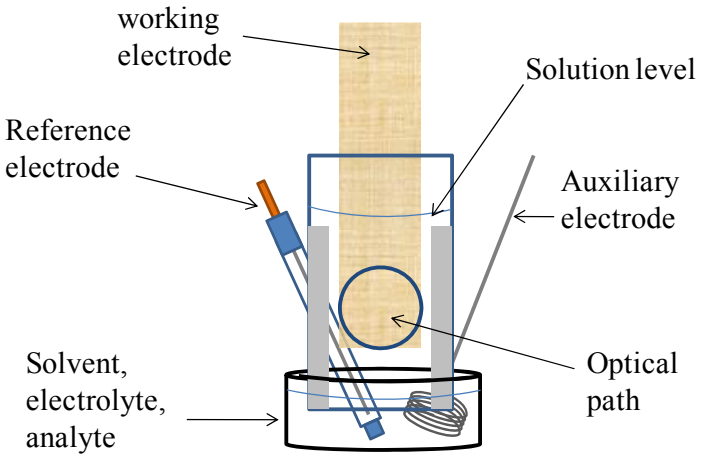

Figure 2.4. Optically transparent thin layer electrode (OTTLE) cell used in the spectroelectrochemical experiments using a transparent gold mesh working electrode, Ag/AgCl (3M NaCl) reference electrode and platinum coil auxiliary electrode. The area enclosed within the circle represents the spectrophotometer light path.

2.3.6. Luminescence Spectroscopy

Steady state emission spectra were measured using standard techniques and recorded with a modified QuantaMaster Model QM-200-4E fluorimeter from Photon Technology International, Inc (Birmingham, NJ). The system was modified to use a water cooled 150 W xenon arc lamp excitation source and the emission was collected at a right angle to the irradiation source by a thermoelectrically cooled Hamamatsu 1527 photomultiplier tube operating in photon counting mode with 0.25 nm resolution. The instrument was controlled with the factory standard Felix Software suite. Emission spectra were recorded in room temperature spectroscopic grade acetonitrile. The emission quantum yields are reported in room temperature acetonitrile against $[(bpy)_2Ru(dpp)Ru(bpy)_2](PF_6)_2$ when exciting absorbance matched solutions at 520 nm (λ^{em} = 0.00138).[77] Low temperature emission spectra were obtained from 4:1 v/v ethanol/methanol glass solutions immersed in a liquid N_2 filled finger Dewar flask (77 K). Spectra were corrected for spectrometer response, Figure 2.5.

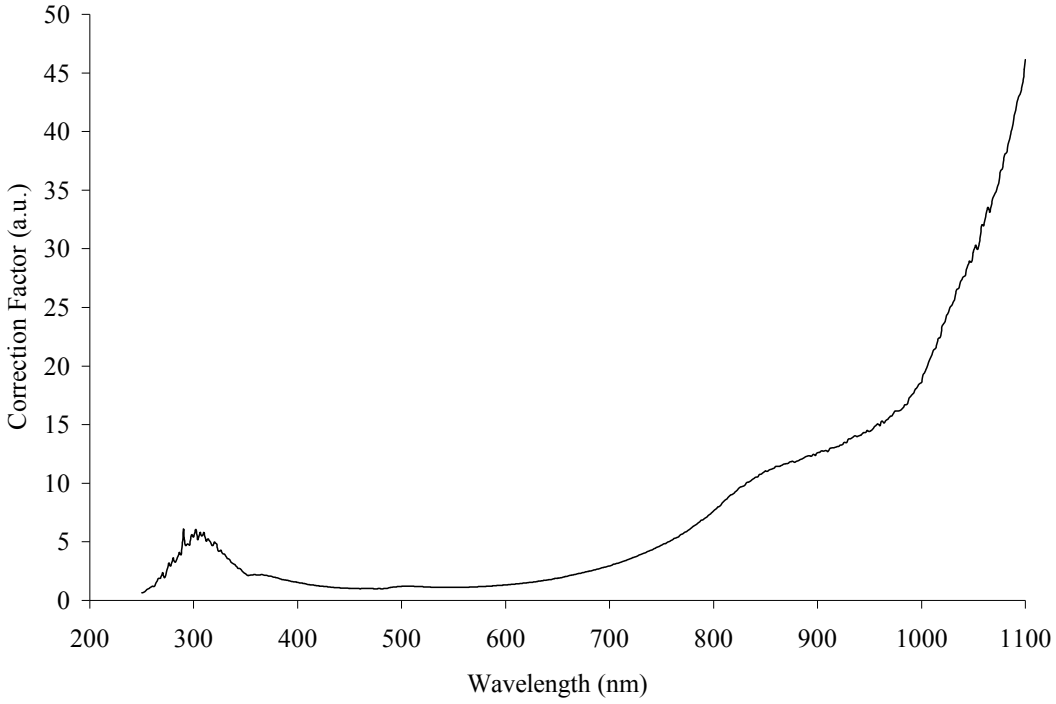

Figure 2.5. Emission correction file used with detection system of QuantaMaster QM-200-4E fluorimeter from PTI, using the 750 nm blaze diffraction grating and Hamamatsu 1527 red sensitive photomultiplier tube.

2.3.7. Time Resolved Emission

Excited state lifetimes were determined using a Photon Technology International, Inc. PL-2300 nitrogen laser equipped with a PL-201 continuously tunable dye laser (Coumarin 500, 490-540 nm) excitation source, Figure 2.6. Emissions were collected at a right angle from the excitation source, passed through a monochromator and detected using a Hamamatsu R928 photomultiplier tube operating in direct analog mode. The signal was recorded using a LeCroy 9361 oscilloscope (2.5 GSa/s), averaging the results of 300 pulses, and transferred to a computer for data analysis. Room temperature measurements were made in acetonitrile solutions, exciting at 520 nm and observing the emission decay at 770 nm. Low temperature measurements were made in 4:1 v/v ethanol/methanol glass solutions immersed in a liquid N_2 filled finger Dewar flask (77 K), exciting at 520 nm and measuring emission decay at 715 nm.

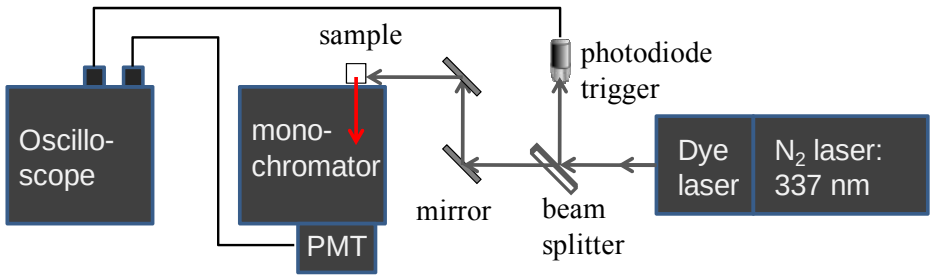

Figure 2.6. A general schematic of the laser path and detection system used for transient emission experiments with gray arrows indicate pump light path, red arrow indicates emission detection path. Laser = Photon Technology International, Inc. (PTI) PL-2300 nitrogen gas laser equipped with a continuously tunable PTI PL-201 dye head, PMT = Hamamatsu R928 photomultiplier tube, oscilloscope = LeCroy 9361 oscilloscope.

2.3.8. Transient Absorption Spectroscopy

Transient absorption spectroscopy was performed during a visit to Tulane University in the laboratory of Professor Russell H. Schmehl.[144] A schematic of the spectrophotometer is presented in Figure 2.7. Samples were pumped with 520 nm laser light from a computer controlled continuously tunable optical parametric oscillator (OPOTEK brand OPO) (470-600 nm) that was driven by frequency tripled light from a Q-switched Quantel Brilliant B Nd:YAG laser (355 nm). The analyte absorbance was probed at a right angle to the pump beam with light from a pulse amplified 75 W Xenon arc lamp. After passing through a computer interfaced monochromator, the transmitted light was detected using a Hamamatsu R928 photomultiplier

tube. The analog signal was recorded as a function of time using an Agilent digital oscilloscope (4.0 GSa/s) and was transferred directly to the interfaced computer (time correlated single photon counting). Decay traces recorded at detection wavelengths at regular intervals were combined to build the transient difference spectra for each sample.

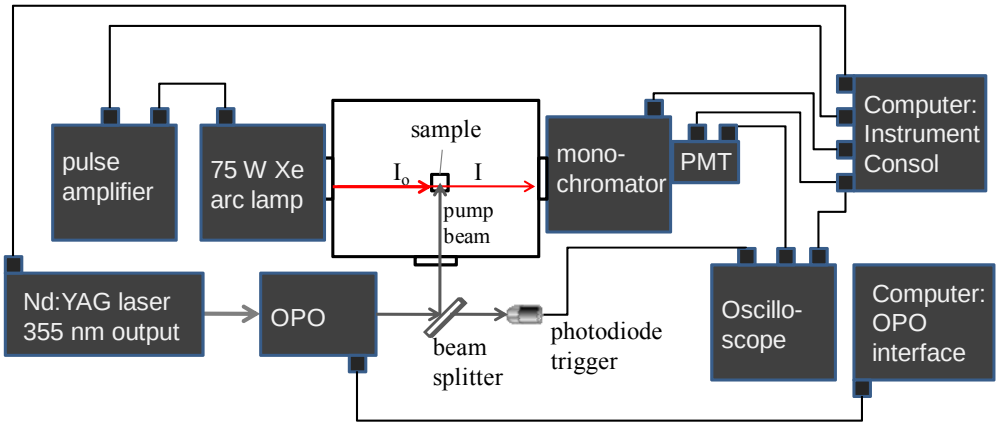

Figure 2.7. Block diagram of the pump/probe instrumentation used for transient absorption spectroscopy with gray arrows to indicate pump light path and red arrows indicate probe light path. OPO = OPOTEK optical parametric oscillator, PMT = Hamamatsu R928 photomultiplier tube.

The transient absorption experiment was performed by timing the shutters, pulse amplified probe beam and laser pump. A generalized pulse sequence used for the transient absorption measurements is presented in Figure 2.8. Analyte solutions were in deoxygenated acetonitrile in a 1 cm optical glass cell and continuously blanketed with flowing nitrogen. The sample solutions were absorbance matched at the probe wavelength ($A^{520\ nm} = 0.60$, [MC] = 2.1 x 10^{-5} M to 4.1 x 10^{-5} M). In the case of $[(bpy)_2Ru(dpp)\}_2RhCl_2](PF_6)_5$, poor signal to noise prompted increase of the sample concentration ($A^{520\ nm} = 0.90$, [MC] = 3.1 x 10^{-5} M), with no evidence of self-quenching due to higher sample concentration. The pulse amplifier was fired, instantaneously doubling the Xe arc lamp output. During the lamp's slow decay (>100 ms) the shutters were opened to allow light to pass through the sample and establishing steady state transmittance (*I*). A 4 ns laser pulse excites a large population chromophores *in situ* causing a rapid and dramatic change in the transmittance of the solution (I'). This is then plotted as change in optical density (aka. absorbance) (ΔOD) as a function of time, where $\Delta OD = -\log(I'/I)$.

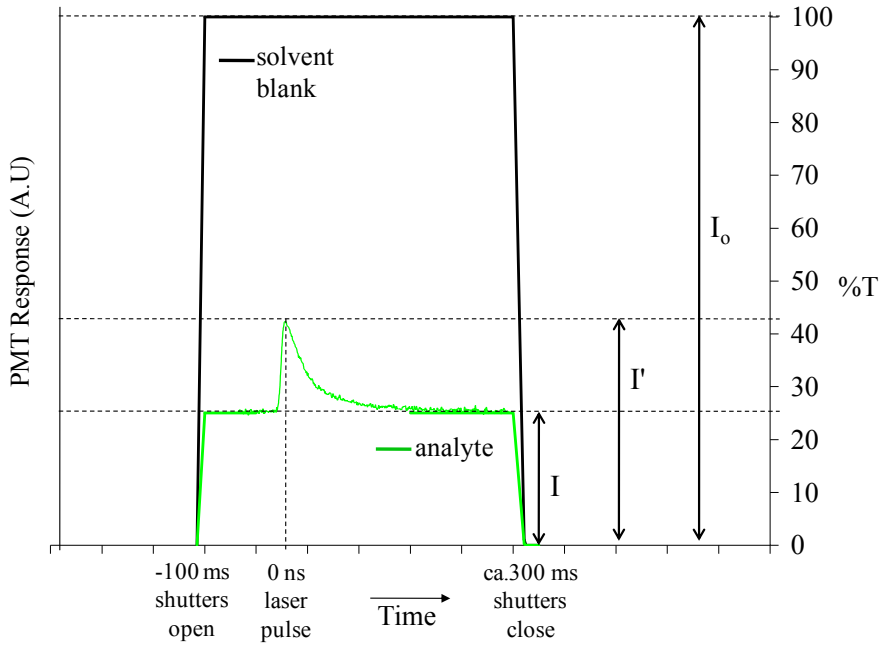

Figure 2.8. A generalized pulse sequence and photomultiplier tube (PMT) response for a typical transient absorption measurement at a strong bleach. Transmittance values (%T) (ground state = I, transient state = I') are presented relative to a solvent blank (A = 0) and where A = 0.6 at $t < 0$ ns and A = 0.4 at $t = 0$ ns.

2.9. Design, Construction and Validation of an LED Array for High-Throughput DNA Photochemical Experiments, LED = Light Emitting Diode

2.9.1. Components Used in the Construction of the LED Array

An LED photolysis array was constructed using the Student Machine Shop (Virginia Tech). A complete detailed list of materials and suppliers can be found in Prussin *et al.*[137]

2.9.2. LED Array Design and Construction

The circuitry used for the LED array employed a design that was developed in our group through sequential improvements of our design and tested for reproducibility.[145] The circuit could be modified to include a number of LED circuits limited by the current of the power supply. Power was drawn from a precision regulated 13.8 V (10 A max) linear AIM power supply purchased from Jameco Electronics. Eight individual circuits were built in parallel off of the main power. The current was passed through a 10 Ω or 7.5 Ω resistor to limit voltage to ca. 5 V or ca.7V, respectively. The current was switched between resistors with a single-pole, double-throw mini toggle switch. The current was passed through a rheostat and a 5 Ω resistor in

parallel that were used to control power output to the LED.

The individual LED holders were built as modular units that interchanged behind the sample, allowing for facile interchange of LED to control excitation wavelength. The holder was machined from 1/8" 6063 angle aluminum to have a base 2"x 2" and a facing side of 1.5"x 1.5". The 5W Luxeon star LED was mounted to the center of the outside face with machine screws and Teflon washers. A heat sink was mounted opposite the LED on the inside face of the LED holder. This promoted efficient cooling of the LED. A power lead made of speaker wire was soldered to the LED pad and connected to the rest of the circuit by an RCA plug. The holder was held in place by a snug channel that was created by the overhang of machined brackets and the base plate.

The sample holder was machined from a single 0.75"x 1.5"x 18" bar of 6061 aluminum. Channels 0.5" deep and 0.5" wide were milled across the width of the bar at 2.5" intervals. These channels held commercial 1 cm pathlength cells snuggly in place and ensured efficient thermal transfer from the analyte solution. Blocks of 6061 aluminum with aluminum tubing threaded through them were mounted to the back of the sample holder. Continuous pieces of aluminum tubing were used so that no joints were near any electronics, successfully separating water cooling and electronics systems. A factory installed fuse in the power supply was designed to break and prevent large current draw in the event of a short circuit.

The entire LED array was designed to photolyze eight samples along a horizontal axis, a modification of previously reported systems.[145-147] This system is optimized for 1 cm optical cells and DNA photocleavage assays. The array was designed to have a linear alignment of each LED with one sample, one On-Off-On switch and one rheostat. The sample holders and base plate of the LED array were cooled by water flowing through attached aluminum tubing.

2.9.3. Chemical Actinometry as an Assay of Array Function

Two separate chemical actinometers were used to study the tuning of the LED array and the reproducibility of photolysis experiments using this device. The potassium tris(oxolato)iron(III) chemical actinometer was used by Aaron J. Prussin of the Brewer Group, following previously reported procedures, to measure photon flux of the LEDs.[148] An additional experiment was performed to generate a mixture of supercoiled (SC) and open-circular (OC) forms of pUC18 plasmid DNA by photolytic single-strand cleavage of the DNA. The

photosensitizer used, $[(bpy)_2Ru(dpp)]Cl_2$, was synthesized using literature adapted procedures.[138] Solutions were 15.3 μM in DNA base pairs, 3.1 μM in $[(bpy)_2Ru(dpp)]Cl_2$ and 10 mM in NaH_2PO_4. Identical solutions (3 mL) were photolyzed at each of the eight LED stations for 26 minutes in aerated solution. Samples for gel electrophoresis were prepared with 50 ng of DNA in a total volume of 12 μL (5 μL analyte, 5 μL 10mM NaH_2PO_4 buffer, 2 μL loading dye). Gel electrophoresis was run on a 0.8% agarose gel, prepared as described in the full paper, at 104 V (~38 mA) for 1.5 hours. Gels were stained with ethidium bromide solution in water and destained with pure water to decrease the background glow of excess ethidium bromide. Photographs of the gel were analyzed by ImageJ using the gel analyzer. This method uses manual peak integration to count pixels, so reported values are an average of three measurements.

2.10. DNA Photochemical Experiments

2.10.1 Stock Solutions

Stock solutions were prepared prior to experimentation. A 5 times concentrate of electrophoresis buffer (5xTB) was made to have 0.45 M each of boric acid and TRIS. Solutions of 0.1 M and 0.01M NaH_2PO_4 were made gravimetrically. The electrophoresis loading dye consisted of a 30% v/v aqueous glycerol solution with 1% w/v bromophenol blue. A 1 mg/mL solution of ethidium bromide was made and stored in the dark. Stock solutions of metal complex of interest as its chloride salt were prepared by dissolving it in water. The concentration of the metal complex master solution was determined spectrophotometrically and typically was between 0.1 mM and 0.5 mM. Fresh metal complex master solutions were made every few days. The calf-thymus DNA used to study photobinding was dissolved into 10 mM NaH_2PO_3 and sonicated to decrease the viscosity of the solution. DNA solutions with 2 mg/ml and with base pair ranges of 300-10,000 base pairs (as determined by gel electrophoresis) were routinely obtained. DNA concentrations in molar base pairs, M (bp), were determined spectrophotometrically using the absorbance at 260 nm ($\varepsilon^{260\ nm} = 13{,}200\ M^{-1}cm^{-1}$ for solutions of ds-DNA).

2.10.2. Equipment Used to Assay DNA Photocleavage

A 1000 W xenon arc lamp and optics was purchased from Oriel Light Sources and

Spectroscopy Instruments (Stratford, CT). Rectangular optical glass cuvettes (1 cm pathlength) were purchased from Starna Cells, Inc. (Atascadero, CA). An Ocean Optics (Dunedin, FL) photodiode array spectrophotometer was used for spectroscopy and LED calibration. Molten agarose gels were prepared using a 1,100 W GE (Louisville, KY) turntable microwave oven (JES632WN 002). Mini-gel (4"x 4") and medium gel (8"x 8") electrophoresis rigs were purchased from Owl Scientific (Portsmouth, NH). Gels were visualized after staining using a Fisher Scientific FBTI-88 UV transilluminator. Photographic records were taken using an Olympus SP-320 digital camera equipped with an ethidium bromide filter purchased from Peca Scientific (Beloit, WI).

2.10.3. Preparation of Sample Solutions for DNA Photocleavage Assays

Each photolysis experiment was performed using solutions with the same metal complex and DNA concentrations. The solutions generally were 10 mM in NaH_2PO_4, 15.3 μM(bp) in pUC18 (bp = base pairs,; pUC18 = 2,686 bp) and metal complex concentrations were absorbance matched to aqueous solutions of 3.1 μM $[\{(bpy)_2Ru(dpp)\}_2RhCl_2](PF_6)_5$. Photolysis solutions were made to a volume of 3 mL, a convenient analyte volume to use with 1 cm pathlength rectangular cuvettes. DNA control samples were made without metal complex and/or photolysis. The DNA controls (C) and metal complex dark controls (MC) were stored in the dark at room temperature during the photolysis experiment. The remaining DNA/MC solutions were photolyzed following the procedures outlined below.

2.10.4. Preparation of Sample Solutions for DNA Photobinding Assays

Solutions were prepared similarly to those used for photocleavage assays, though scaled up. The buffer concentration was increased to 55 mM NaH_2PO_4 and the DNA used was at 120 μM in base pairs. The concentration of $[\{(tpy)OsCl(dpp)\}_2RhCl_2]Cl_5$ was 26 μM. Higher concentrations of buffer and reagents gave identical behavior as observed by gel electrophoresis, suggesting that the DNA photocleavage assay and DNA photobinding conditions were analogous.

2.10.5. DNA Photolysis Using a Xenon Arc Lamp

Note: Light from a xenon arc lamp includes potentially damaging ultra-violet light. Use of a water filter and cut-off filter greatly reduces risk of damage to tissues, but protective eyewear, such as laser goggles, should be worn at all times when working with the xenon arc lamp light source.

Photochemistry experiments were performed using a 1000 W xenon arc lamp. The light from the xenon arc lamp was filtered through a water filter to remove most of the IR components of the light. The light was passed through a high-pass 450 nm cutoff filter (Oriel or Newport Optics, Stratford, CT). Analyte solutions were deoxygenated by bubbling with argon for 15 minutes prior to photolysis. The light was focused on the sample solution in a 1 cm rectangular optical glass cuvette. The samples were photolyzed under slow flow of argon with monitoring by agarose gel electrophoresis and electronic absorption spectroscopy. The temperature of the photolysis sample was regulated by water flow through a thermostated aluminum cell holder. Aliquots were removed at regular intervals and stored at room temperature in the dark. Following photolysis the analyte solutions were prepared for analysis by the method relevant to the photochemical property being studied.

2.10.6. DNA Photolysis Using an LED Array

Analyte samples were photolyzed with the LED array using a protocol analogous to that used in experiments involving the xenon arc source. The LEDs emit nearly monochromatic light that required no additional filtering. LED light intensity output was calibrated using a digital multimeter to obtain roughly equal current being delivered to each LED followed by fine tuning with the relative photonic output measured with a photodiode array. The LEDs used for the photolysis experiment were the 5W Luxeon Royal Blue stars (λ_{max} = 455 nm). Aliquots were removed at regular intervals for analysis by gel electrophoresis or by spectrophotometric methods. The temperature of the photolyzed sample was maintained by thermostated water flowing through the aluminum sample holder.

2.10.7. Agarose Gel Electrophoresis

Note: Electrophoresis requires the use of high voltages. Exercise due caution when performing electrophoresis experiments. Ethidium bromide is a known mutagen. Exercise due

caution when handling solutions and gels containing ethidum bromide.

Agarose gel electrophoresis was used to examine the products of the DNA photolysis experiments. Mini-agarose gels (0.8% agarose) were prepared by combining 0.24 g of agarose with 30 mL of water in a 250 mL narrow mouth Erlenmeyer flask. The mixture was heated for 90 seconds on a power setting of 10 in a microwave. While still hot, water was added to the solution until the total mass of the solution was 24.0 g. 5xTB buffer was added in one portion (6 mL) and the solution was swirled for 30 seconds to ensure even mixing. The molten gel was then poured into the gel mold with a 10 well comb in a mini-gel electrophoresis rig and allowed to solidify over the course of approximately one hour (gel size was 3.5" x 4"). Preparation of medium gels required use of the medium gel rig to form the molten gel and the agarose, water and 5xTB buffer volumes were quadrupled to accommodate the larger rig. The gel was sealed with plastic wrap while it set to prevent excess evaporation from the center of the gel. Non-uniform gel densities can affect the DNA migration rate within the gel for different lanes, impacting interpretation of the results.

Aliquots of the molecular weight marker, controls and photolysis solutions were prepared for loading into the wells of the agarose gel. Lambda DNA/*Hin*dIII digest (2 μL, 500 μg/mL) was diluted to 20 μL using 0.01 M NaH_2PO_4 buffer. Aliquots (4 μL) of each of the samples were placed in microfuge tubes with 2 μl of gel loading dye and 4 μL of 0.01 M NaH_2PO_4 buffer, mixed well, and centrifuged for 30 sec at 10,000 RPM to collect the liquid samples in the bottom of the tube. With the exception of the molecular weight marker, each 10 μL sample contained 40 ng of pUC18.

A general methodology for gel electrophoresis was established that gives good resolution of bands corresponding to supercoiled and relaxed forms of pUC18 in a short electrophoresis time.[60,137] Gel electrophoresis was conducted using TB buffer (5xTB buffer diluted five-fold). Each well of the gel was loaded with prepared analyte sample. Mini-gels were run at 104 V (ca. 35 mA) for 90 min and medium gels were run with 80 V (ca. 35 mA) for 100 min. In a small plastic tray 20 μL of 1 mg/mL ethidium bromide stock solution was diluted into 150 mL of water. Medium gels were cut in half parallel to the wells for easier handling. Following electrophoresis, the gel was stained in the ethidum bromide solution on a shaker at low speed for 45 min. The gel was destained by soaking in water for another 30 min to increase the ethidium bromide/DNA emission signal to background ratio. The gels were visualized on a

transilluminator and photographic records were taken using a digital camera equipped with an ethidium bromide filter. Camera settings commonly used for acquiring photographs were an F-stop of 6.3 and an exposure time of approximately 1.3 seconds. Manual focus was used as the auto focus feature did not work well under low light conditions.

Agarose gel images were examined using the freeware package ImageJ.[149] The raw images were opened with ImageJ, color inverted and converted to 8-bit grayscale images. The resulting images were then calibrated using the "Uncalibrated OD" function. Vertical lanes were selected using the "Gel Analyzer" to generate a histogram display of pixel intensity as a function of migration distance. The peak area of each was measured using the "wand" tool from the tool bar and data was output to Excel for study.

Chapter 3. Results and Discussion

Mixed metal supramolecules containing Ru^{II} or Os^{II} visible light absorbers, polyazine bridges, and redox active *cis*-$Rh^{III}Cl_2$ centers exhibit interesting photochemical properties with DNA. The electronic excited states of these supramolecules are known to be tuned by the terminal polyazine ligands (TL), the visible light absorbing metal center (M) and polyazine bridging ligands (BL). The research described herein seeks to expand the understanding of electronic excited state tuning by replacing an entire TL-M-BL subunit (LA) on the *cis*-$Rh^{III}Cl_2$ center with a chelating polyazine ligand, in this case 1,10-phenanthroline. Bimetallic complexes of the form $[\{LA^{n+}\}RhCl_2(phen)]^{(n+1)+}$, n = 1 or 2, a new structural motif in this class of supramolecular complex (Figure 3.1), exhibit unexpected electrochemical properties. The photophysical properties and photochemistry with DNA of the new supramolecules, however, are surprisingly similar to their $[\{LA^{n+}\}_2RhCl_2]^{(2n+1)+}$ analogs. Synthesis of the new bimetallic complexes therefore offers a new means of structural modification leading to simplified molecular architectures with interesting redox, photophysical and photochemical properties.

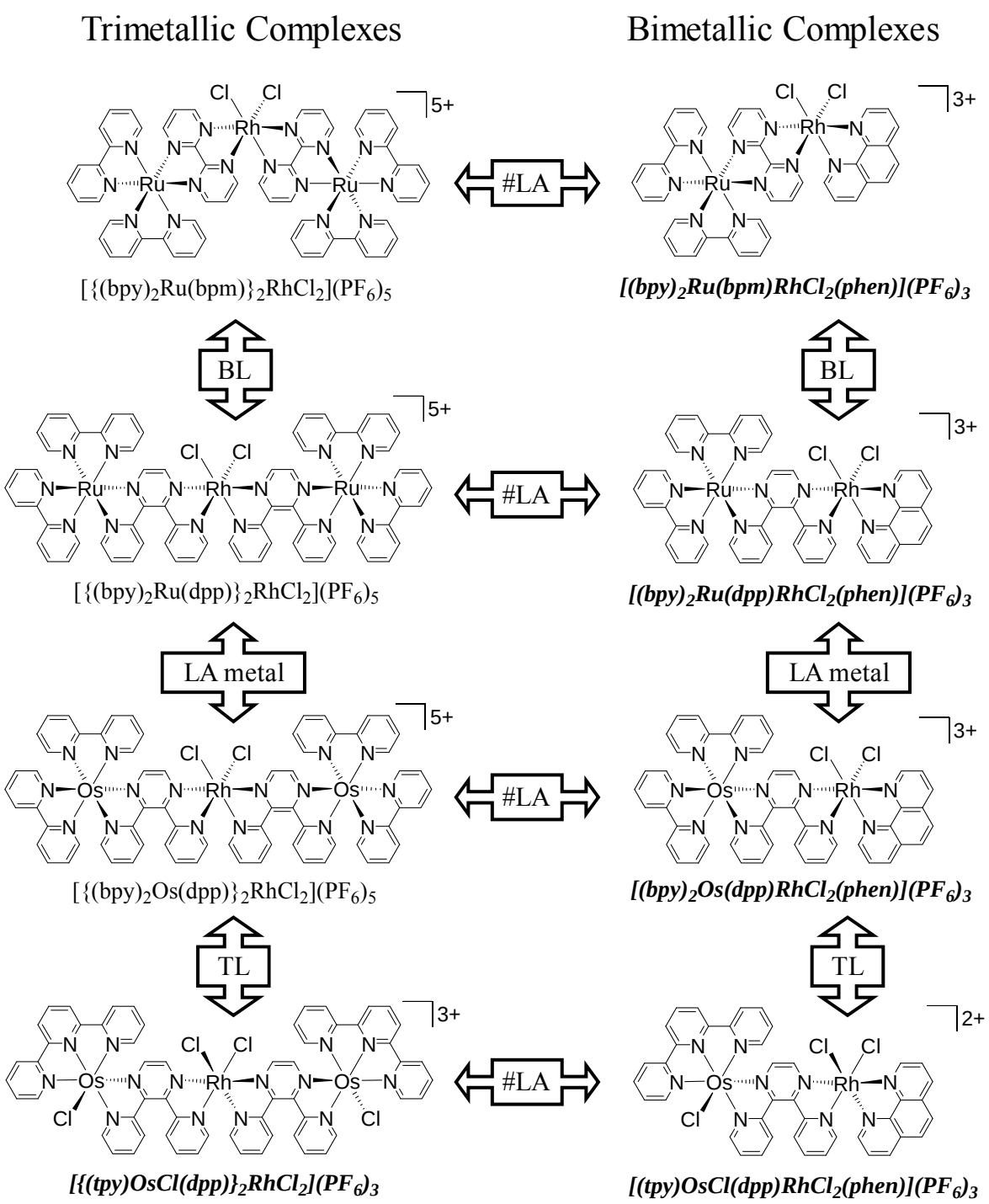

Figure 3.1. A **s**eries of mixed metal complexes known or synthesized herein to investigate the impact on light absorbing and redox properties of changing the number of visible light absorbing subunits (#LA), bridging ligand (BL), metal center of the visible light absorber (LA-metal), and terminal ligand (TL); bpy = 2,2'-bipyridine, bpm = 2,2'-bipyrimidine, dpp = 2,3-bis(2-pyridyl)pyrazine, 2,2':6',2"-terpyridine. New species synthesized during the course of this study are in bold, italics type.

3.1. Synthetic Strategy to Produce Mixed Metal Supramolecules

A series of structurally varied mixed metal supramolecules was synthesized using a building block strategy commonly employed in the production of these complexes. The LA complexes $[(bpy)_2Ru(dpp)](PF_6)_2$,[138] $[(bpy)_2Ru(bpm)](PF_6)_2$,[36] and $[(bpy)_2Os(dpp)](PF_6)_2$[24] were synthesized from $[(bpy)_2MCl_2]$ and BL using modifications of previously reported procedures, M = Ru^{II} or Os^{II}, BL = dpp or bpm. The new complex $[(tpy)OsCl(dpp)](PF_6)$ was synthesized from $[(tpy)OsCl_3]$ and dpp using procedures adapted from the synthesis of $[(tpy)OsCl(bpy)](PF_6)$.[24] The new hetero-bimetallic complexes $[(bpy)_2Ru(dpp)RhCl_2(phen)](PF_6)_3$, $[(bpy)_2Ru(bpm)RhCl_2(phen)](PF_6)_3$, $[(bpy)_2Os(dpp)RhCl_2(phen)](PF_6)_3$, and $[(tpy)OsCl(dpp)RhCl_2(phen)](PF_6)_2$ were synthesized from $K[(phen)RhCl_4]\cdot 3H_2O$ and the appropriate LA subunit starting materials. The syntheses of the trimetallic complexes used in this study, $[\{(bpy)_2Ru(dpp)\}_2RhCl_2](PF_6)_5$,[37] $[\{(bpy)_2Ru(bpm)\}_2RhCl_2](PF_6)_5$,[36] $[\{(bpy)_2Os(dpp)\}_2RhCl_2](PF_6)_5$,[79] were adapted from the literature. The new trimetallic complex, $[\{(tpy)OsCl(dpp)\}_2RhCl_2](PF_6)_3$, was synthesized from two equivalents of $[(tpy)OsCl(dpp)](PF_6)$ and one equivalent of $RhCl_3\cdot 3H_2O$. All of the complexes were readily prepared using a rational synthetic scheme with careful attention to starting material purity and reactant stoichiometry.

3.1.1. Synthesis of [(tpy)OsCl(dpp)](PF$_6$)

Synthesis of the new complex $[(tpy)OsCl(dpp)](PF_6)$ proved difficult due to the tendency of osmium-tpy complexes to undergo ligand scrambling reactions.[150] A synthetic scheme is presented in Figure 3.2. The precursor, $[(tpy)OsCl_3]$ was synthesized in good yield (81%) using ethylene glycol as the reaction solvent instead of DMF as reported in the literature.[27,151,152] The complex was prepared $[(tpy)OsCl(dpp)](PF_6)$ by the reaction of $[(tpy)OsCl_3]$ and excess dpp in refluxing ethylene glycol for ca. 20 minutes. During this time the reaction mixture turned from black to deep purple. Longer reaction times led to a brown, unidentified by-product that was difficult to separate by column chromatography, likely a product of known ligand scrambling reactions of Os tpy complexes.[153] At shorter reaction times not all of the starting $[(tpy)OsCl_3]$ was consumed at the end of the reaction. As $[(tpy)OsCl_3]$ is sparingly soluble in the reaction solvent, most of the unreacted portion was removed by filtration and recycled. The primary reaction products of $[(tpy)OsCl_3]$ and dpp were the desired $[(tpy)OsCl(dpp)](PF_6)$ and the

bimetallic [{(tpy)OsCl}$_2$(dpp)](PF$_6$)$_2$. These compounds separated well using methanol-deactivated adsorption alumina chromatography to give the burgundy monometallic complex as the leading band in moderate yield (49% yield). The 400 MHz ^{1}H-NMR spectrum of [(tpy)OsCl(dpp)](PF$_6$) in CD_3CN was complicated, however peak integration suggested an equimolar ratio of geometric isomers, Figures A-12 and A-13 in the Appendix.

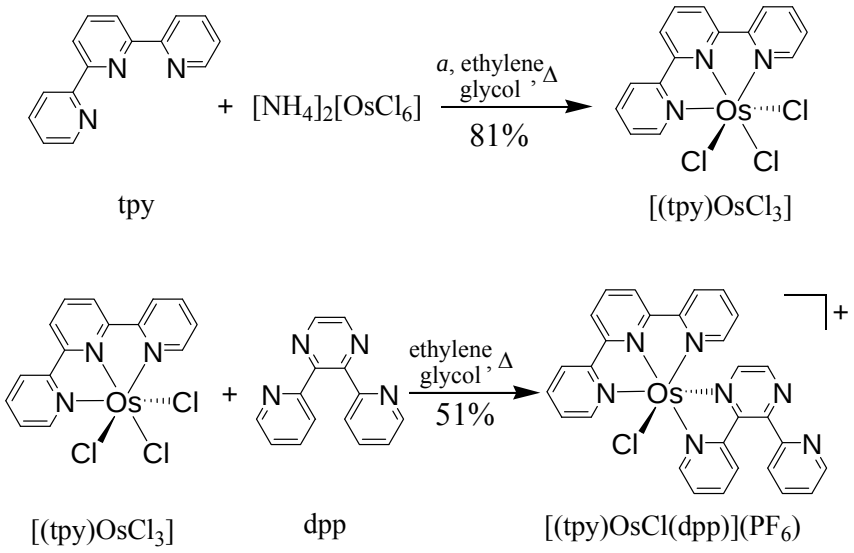

Figure 3.2. Synthetic scheme for the production of [(tpy)OsCl(dpp)](PF$_6$) starting with ammonium hexachloroosmate(IV), tpy = 2,2':6',2"-terpyridine, dpp = 2,3-bis(2-pyridyl)pyrazine. [a] Synthesis adapted from Demadis, Meyer *et al.* synthesis of [(tpy)OsCl(bpy)](PF$_6$).[27]

3.1.2. Synthesis of K[(phen)RhCl$_4$]·3H$_2$O

The complex K[(phen)RhCl$_4$]·3H$_2$O, used in the preparation of the Ru,Rh dyads, was synthesized following procedures adapted from McKenzie and Plowman[140] to accommodate strict purity requirements. The rhodium starting material was synthesized initially as the phenanthrolinium (Hphen$^+$) salt. Hot filtration during the first cation metathesis step removes the unwanted (Hphen)$_{n-1}$[RhCl$_{n+2}$(H$_2$O)$_{4-n}$], n = 0 – 4.[154] Sequential cation metatheses first to the H_3O^+ salt and then the K^+ salt ensured that phen was excluded from the product, which is known to complicate further reaction.[30] The K^+ salt, K[(phen)RhCl$_4$]·3H$_2$O was recovered as a bright orange crystalline material determined to contain 19.9% Rh by mass. Further determination of the purity and identity of K[(phen)RhCl$_4$]·3H$_2$O was performed by product analysis of the reaction of the metal complex with 4,4'-dimethyl-2,2'-bipyridine (dmb), Figure 3.3. Reaction of

$K[(phen)RhCl_4]\cdot 3H_2O$ with one equivalent of dmb in refluxing ethanol, which following addition of NH_4PF_6, gave *cis*-$[(dmb)RhCl_2(phen)](PF_6)$ as a pale yellow solid in good yield and as the only product observed by ^{1}H-NMR in d_6-acetone, Figure A-2 in the Appendix. The clean NMR spectrum is supportive of the metal complex's purity, but does not consider possible insoluble materials or NMR inactive impurities.

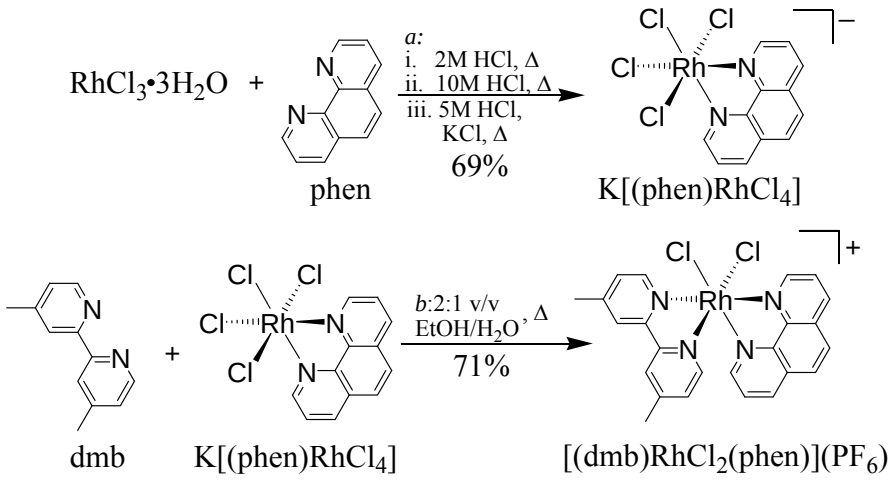

Figure 3.3. Coordination chemistry used in the synthesis of the rhodium(III) synthon $K[(phen)RhCl_4]\cdot 3H_2O$ and heteroleptic rhodium(III) polyazine complex $[(phen)RhCl_2(dmb)](PF_6)$, phen = 1,10-phenanthroline, dmb = 4,4'-dimethyl-2,2'-bipyridine. [a] Adapted from McKenzie and Plowman.[155] [b] Loosely adapted from Menon and Morrison.[127]

3.1.3. Synthesis of Mixed Bimetallic Supramolecules

The polyazine bridged Ru,Rh and Os,Rh dyads were synthesized from a slight excess of $K[(phen)RhCl_4]\cdot 3H_2O$ and either $[(bpy)_2Ru(bpm)]PF_6)_2$, $[(bpy)_2Ru(dpp)](PF_6)_2$, $[(bpy)_2Os(dpp)](PF_6)_2$, or $[(tpy)OsCl(dpp)](PF_6)$, taking advantage of the facile formation of the *cis*-$[(NN)_2Rh^{III}Cl_2]^+$ coordination motif. The reaction conditions used in the synthesis of *cis*-$[(phen)RhCl_2(dmb)](PF_6)$ were optimized and employed in the synthesis of the bimetallic complexes, Figure 3.4. Reaction of a monometallic light absorber with a slight excess of $K[(phen)RhCl_4]\cdot 3H_2O$ gave the deeply colored mixed metal supramolecule in good yield (54−84%). The mixed metal supramolecules were purified by first stirring the solid in hot ethanol, followed by dissolution in minimal acetone, syringe filtration and reprecipitation into diethyl ether. Electrospray ionization-time of flight mass spectrometry (ESI-TOF MS) confirmed the presence of the title complexes $[M\text{-}PF_6]^+$, with experimental isotopic distribution

patterns matching the theoretical values, Figures A.2-A.11 in the Appendix. The ESI-TOF mass spectra of each dyad at higher *m/z* did not show any peaks that could be assigned to possible $[\{LA^{n+}\}_2Rh(phen)](PF_6)_{(3+2n)}$ trimetallic impurities, where n = 1 or 2. Lack of a trimetallic impurity is consistent with previous reports that the *cis*-$[(NN)_2Rh^{III}Cl_2]$ moiety is favored under these reaction conditions.[156-158] The hetero dyads displayed no detectable monometallic emission when excited into the maximal absorbance of the LA starting material. For example, $[(bpy)_2Ru(dpp)](PF_6)_2$ with $\Phi^{em} = 0.06$ is detectable at ≥0.09% when considering for possible diffusion limited second order quenching and with S/N = 2. The Ru,Rh and Os,Rh bimetallic complexes provide limited structural isomerization relative to the previously reported Ru,Rh,Ru or Os,Rh,Os trimetallic analogs. The developed synthetic strategy provides a means to this new structural motif, also allowing for varied coordination at the Rh(III) center while retaining the interesting *cis*-$Rh^{III}Cl_2$ moiety.

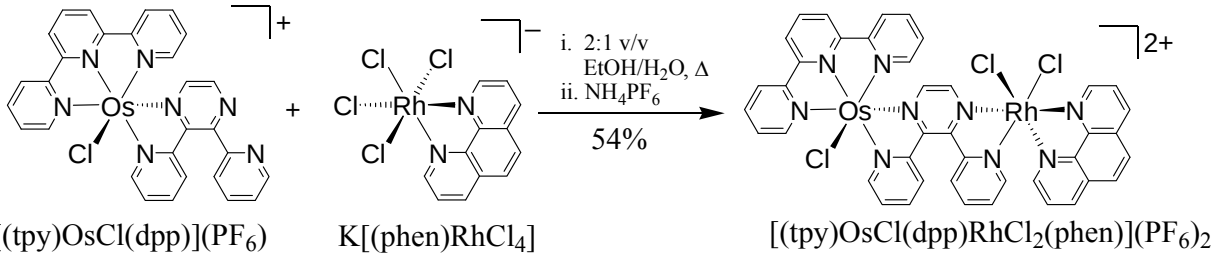

Figure 3.4. Synthesis of the bimetallic complex $[(tpy)OsCl(dpp)RhCl_2(phen)](PF_6)_2$ illustrating the general synthetic methodology for production of Ru,Rh and Os,Rh complexes; tpy = 2,2':6',2"-terpyridine, dpp = 2,3-bis(2-pyridyl)pyrazine, and phen = 1,10-phenanthroline.

3.1.4. Synthesis of $[\{(tpy)OsCl(dpp)\}_2RhCl_2](PF_6)_3$

An existing synthetic strategy mixed trimetallic supramolecules with a *cis*-$Rh^{III}Cl_2$ center was adapted to produce $[\{(tpy)OsCl(dpp)\}_2RhCl_2](PF_6)_3$, Figure 3.5. Each of the trimetallic complexes was synthesized using the same building block approach,[34,37] reacting two equivalents of the appropriate LA with $RhCl_3 \cdot xH_2O$, using modifications reported by Elvington.[159] Production of $[\{(tpy)OsCl(dpp)\}_2RhCl_2](PF_6)_3$ follows this method, with $[(tpy)OsCl(dpp)](PF_6)$ as the LA.

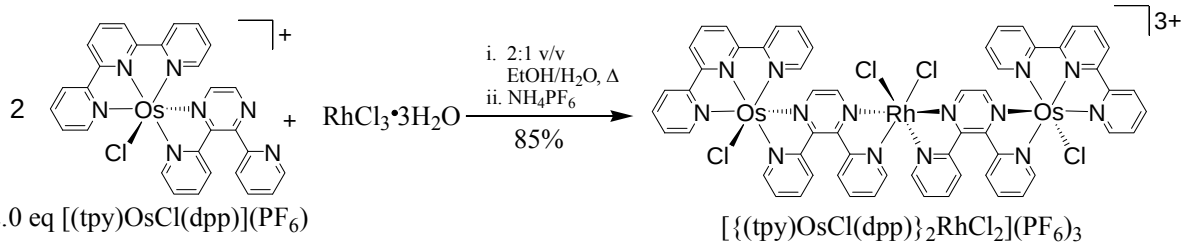

Figure 3.5. A scheme illustrating the synthesis of $[\{(tpy)OsCl(dpp)\}_2RhCl_2](PF_6)_3$, a *cis*-$Rh^{III}Cl_2$ centered trimetallic supramolecular complex, where tpy = 2,2':6',2''-terpyridine, and dpp = 2,3-bis(2-pyridyl)pyrazine.

3.1.5. Supramolecular Structure Considered for Physical Methods

The hetero binuclear and trinuclear complexes have varying numbers of geometric or chiral centers present due to the intrinsic properties of the metals and ligands used in their construction. The two bridging ligands employed, dpp and bpm, are respectively asymmetric (AB) and symmetric (AA) bis-bidentate bridging ligands. The terminal ligand (TL) set generates LA subunits with chiral centers $[(bpy)_2]$ or geometric isomers [(tpy)Cl]. Monometallic complexes of the form $[(NN)_2Ru(BL)]^{2+}$ where NN bpy or phen and BL = dpp or bpm exist as Λ and Δ enantiomers. Metal complexes of the form *cis*-$[(BL)_2RhCl_2]^+$ are also chiral. Geometric isomers of *cis*-$[(dpp)_2RhCl_2]^+$ are possible due to the asymmetric binding mode of dpp, Figure 3.6. The possible geometric isomers either have two chloride ligands trans to two pyridine nitrogens, two pyrazine nitrogens or one of each. $[(tpy)OsCl(dpp)](PF_6)$ also has two possible geometric isomers arising due to the asymmetry of the dpp ligand. Finally, the number of LA subunits attached to the chiral *cis*-$Rh^{III}Cl_2$ contributes to the number isomers possible for each of these complexes. The variable binding modes yield a large array of structural isomers for a given metal and polyazine ligand combination. The bimetallic complexes, with fewer intrinsically chiral or asymmetric subunits, have fewer isomers. The number and types of isomers present for each complex possibly dictates the observed redox, photophysical and photochemical properties.

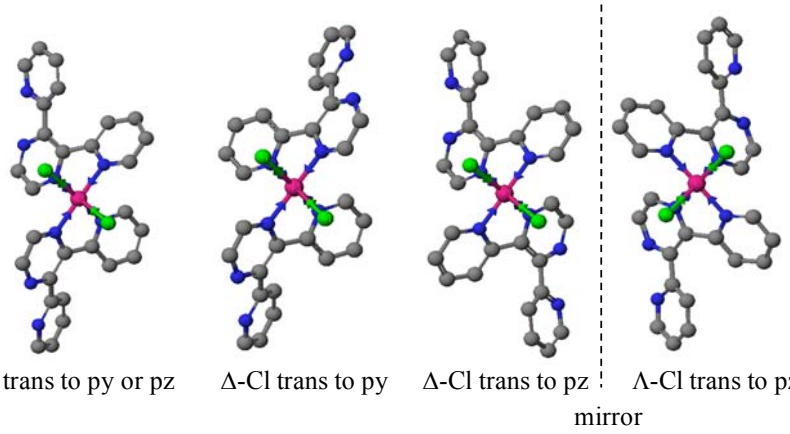

Figure 3.6. Three different geometric isomers possible for *cis*-[(dpp)$_2$Rh^{III}Cl$_2$]. Chloride is illustrated *trans* to pyrazine (pz) and/or pyridine (py) of 2,3-bis(2-pyridyl)pyrazine (dpp). Symmetric species have a C_2 rotation axis perpendicular to the plane of the paper. One geometric isomer (Cl trans to pz) is presented with both Δ and Λ enantiomers.

3.2. Electrochemical Measurements

The electrochemical properties of mixed metal supramolecules give insight into their redox properties, are often indicative of the building blocks incorporated into their structure and are useful to understand electronic excited states and photochemical properties. Mixed metal supramolecules with M(II) and Rh(III) centered polyazine subunits (M = Ru or Os) display electrochemistry with reversible M-based oxidations, irreversible Rh centered reductions and reversible ligand based reductions. Bridging ligands (BL) are typically reduced prior to terminal ligands (NN) due to lower lying π* orbitals that are stabilized upon binding two electropositive metal centers. The Rh(dσ*) orbital energy is sensitive to the Rh ligand set, modulated by ligand σ-donor strength.[33] In the complexes described, BL(π*) and Rh(dσ*) orbitals are often close in energy. The bimetallic supramolecules have interesting electrochemistry as a result of the newly studied ligand environment for a *cis*-Rh^{III}Cl$_2$ moiety.

The electrochemical properties of the trimetallic complexes [{(bpy)$_2$Ru(bpm)}$_2$RhCl$_2$](PF$_6$)$_5$,[36] [{(bpy)$_2$Ru(dpp)}$_2$RhCl$_2$](PF$_6$)$_5$,[34] and [{(bpy)$_2$Os(dpp)}$_2$RhCl$_2$](PF$_6$)$_5$[79] have been discussed elsewhere. The electrochemical properties for these trimetallics, plus the new complex [{(tpy)OsCl(dpp)}$_2$RhCl$_2$](PF$_6$)$_3$, are presented in Table 3.1 for comparison to the bimetallics. The electrochemistry of the new bimetallic structural motif represented by [(bpy)$_2$Ru(bpm)RhCl$_2$(phen)](PF$_6$)$_3$, [(bpy)$_2$Ru(dpp)RhCl$_2$(phen)](PF$_6$)$_3$, [(bpy)$_2$Os(dpp)RhCl$_2$(phen)](PF$_6$)$_3$,

[(tpy)OsCl(dpp)$RhCl_2$(phen)]$(PF_6)_2$ also was studied and their electrochemical properties are presented in Table 3.2. The electrochemical properties of each bimetallic complex are detailed below.

Table 3.1. Electrochemical properties of Ru,Rh,Ru and Os,Rh,Os trimetallic supramolecules in dry acetonitrile

Complex[a]	$E_{1/2}$ (V) [b]	Assignment
[{$(bpy)_2Ru(bpm)\}_2RhCl_2$]$(PF_6)_5$[d]	1.70	$2Ru^{III/II}$
	−0.13	$bpm^{0/-}$
	−0.26	$bpm^{0/-}$
	−0.78[c]	$Rh^{III/II/I}$
[{$(bpy)_2Ru(dpp)\}_2RhCl_2$]$(PF_6)_5$[e]	1.60	$2Ru^{III/II}$
	−0.39[c]	$Rh^{III/II/I}$
	−0.79	$dpp^{0/-}$
	−1.02	$dpp^{0/-}$
[{$(bpy)_2Os(dpp)\}_2RhCl_2$]$(PF_6)_5$[f]	1.21	$2Os^{III/II}$
	−0.39[c]	$Rh^{III/II/I}$
	−0.76	$dpp^{0/-}$
	−1.00	$dpp^{0/-}$
[{(tpy)OsCl(dpp)$\}_2RhCl_2$]$(PF_6)_3$[g]	0.85	$2Os^{III/II}$
	−0.51[c]	$Rh^{III/II/I}$
	−0.86	$dpp^{0/-}$
	−1.20	$dpp^{0/-}$

[a] bpy = 2,2'-bipyridine, dpp = 2,3-bis(2-pyridyl)pyrazine, bpm = 2,2'-bipyrimidine, 2,2':6",2'-terpyridine

[b] Potentials are reported versus Ag/AgCl (3M NaCl)

[c] E_p^c for an irreversible process

[d] From Nallas, Jones and Brewer.[36]

[e] From Swavey and Brewer.[34]

[f] From Holder, Swavey and Brewer.[79]

[g] This work.

Table 3.2. The electrochemical properties of polyazine bridged bimetallic complexes with a *cis*-$Rh^{III}Cl_2$ center

Complex[a]	Couple	$E_{1/2}$ (V)[b]	n[c]
$[(bpy)_2Ru(bpm)RhCl_2(phen)](PF_6)_3$	$Ru^{III/II}$	1.71	*e*
	$bpm^{0/-}$	−0.18	0.9
	$Rh^{III/II}$	−0.75[d]	1.1[f]
	$Rh^{II/I}$	−0.97	1.3[f]
$[(bpy)_2Ru(dpp)RhCl_2(phen)](PF_6)_3$	$Ru^{III/II}$	1.65	*e*
	$Rh^{III/II}$	−0.41	2.1[f,g]
	$Rh^{II/I}$	−0.77[d]	
	$dpp^{0/-}$	−0.99	1.0[f]
$[(bpy)_2Os(dpp)RhCl_2(phen)](PF_6)_3$	$Os^{III/II}$	1.24	*e*
	$Rh^{III/II}$	−0.44	1.9[f,g]
	$Rh^{II/I}$	−0.78[d]	
	$dpp^{0/-}$	−0.98	0.9[f]
$[(tpy)OsCl(dpp)RhCl_2(phen)](PF_6)_2$	$Os^{III/II}$	0.83	*e*
	$Rh^{III/II/I}$	−0.57[d]	2.0[f]
	$dpp^{0/-}$	−0.85	*e*
	$dpp^{-/2-}$	−1.15	*e*

[a] bpy = 2,2'-bipyridine, dpp = 2,3-bis(2-pyridyl)pyrazine, phen = 1,10-phenanthroline, bpm = 2,2'-bipyrimidine, 2,2':6",2'-terpyridine

[b] Potentials were measured in 0.1 M Bu_4NPF_6 acetonitrile with Pt-disk working and Pt-wire auxiliary electrode, and are reported versus Ag/AgCl (3M NaCl), ±0.03 V, v = 100 mV/s. The large ΔE_p for the processes at higher potential are likely due to uncompensated solution resistance

[c] moles of electrons per mole of metal complex as determined by coulometry

[d] E_p^c for an irreversible couple

[e] Values not determined

[f] Followed by an apparent chemical step

[g] First and second reduction were inseparable by CPE

3.2.1. Electrochemical Properties of [(bpy)$_2$Ru(bpm)RhCl$_2$(phen)](PF$_6$)$_3$

The complex $[(bpy)_2Ru(bpm)RhCl_2(phen)](PF_6)_3$ has electrochemical properties similar to $[\{(bpy)_2Ru(bpm)\}_2RhCl_2](PF_6)_5$, but with key differences attributed to the number of light absorbers attached to the *cis*-$Rh^{III}Cl_2$ center. The complex $[(bpy)_2Ru(bpm)RhCl_2(phen)](PF_6)_3$ exhibits a reversible oxidation at $E_{1/2}$ = 1.71 V vs. Ag/AgCl, assigned to $Ru^{III/II}$, Figure 3.7. The first reduction at −0.18 V for $[(bpy)_2Ru(bpm)RhCl_2(phen)](PF_6)_3$ is reversible by cyclic voltammetry. Controlled potential electrolysis (CPE) with coulometry at −0.35 V results in

passage of 0.9 reducing equivalents. Reverse CPE at +0.10 V causes an anodic current with decay consistent with 0.9 reducing equivalents, also consistent with an electrochemically reversible process.

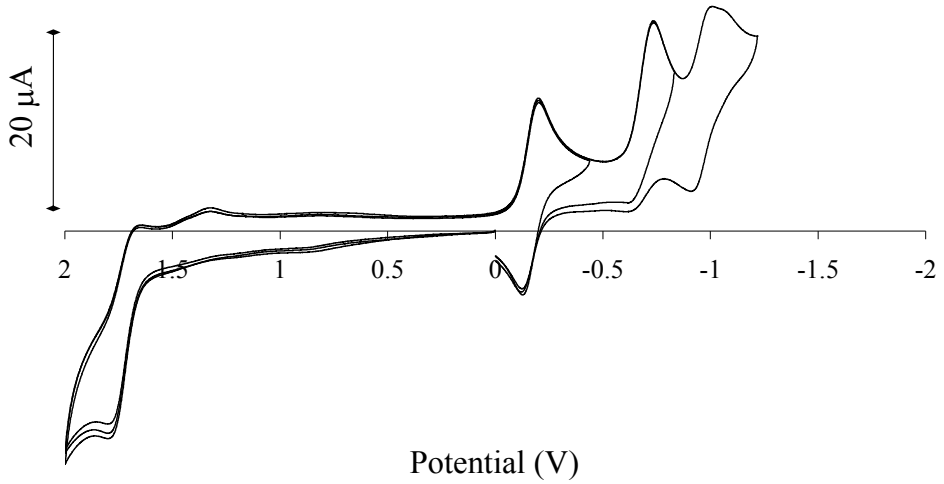

Figure 3.7. Cyclic voltammogram of $[(bpy)_2Ru(bpm)RhCl_2(phen)](PF_6)_3$ in 0.1 M Bu_4NPF_6 acetonitrile at a platinum disc working electrode versus Ag/AgCl (3M NaCl) (−0.46 V vs. $FeCp_2^{+/0}$) and with platinum wire counter electrode. Scan rate (v) = 100 mV/s.

The electrochemical process of $[(bpy)_2Ru(bpm)RhCl_2(phen)](PF_6)_3$ following the first reduction also was studied by spectroelectrochemistry using an OTTLE cell. An absorption at ca. 280 nm in the electronic absorption spectrum decreases in intensity following reduction, consistent with the shift of an underlying bpm($\pi\rightarrow\pi^*$) transition, Figure 3.8.[160] Absorptions at ca. 412 nm and 600 nm assigned as Ru($d\pi$)→bpm(π^*) charge transfer (MLCT) transitions shift to higher energy upon reduction with a new absorption observed at ca. 550 nm, consistent with a $\pi^*\rightarrow\pi^*$ transition of a bpm centered radical anion. Reversal of the spectroelectrochemistry was effected by applying a potential of +400 mV, resulting in 97% recovery of the original spectrum upon re-oxidation ($A_f^{280\ nm}/A_i^{280\ nm}$). The first reduction is therefore assigned to $bpm^{0/-}$.

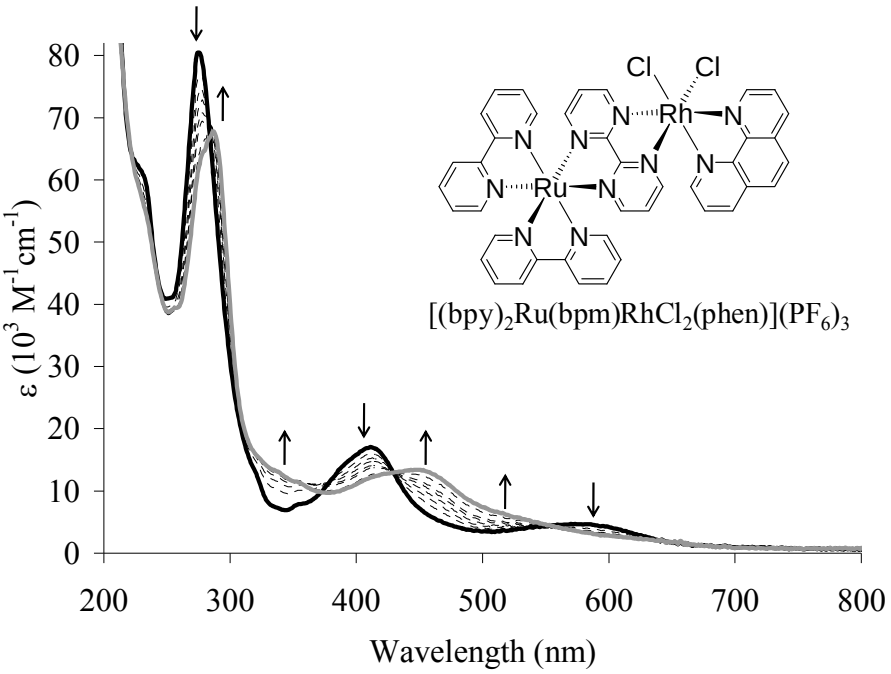

Figure 3.8. Spectroelectrochemistry of $[(bpy)_2Ru(bpm)RhCl_2(phen)](PF_6)_3$ showing electronic absorption spectroscopy in acetonitrile before (bold black line) and after (bold gray line) reduction by one electron at −350 mV at a gold mesh optically transparent thin layer electrode (OTTLE) versus Ag/AgCl (3M NaCl) (−0.46 V vs. $FeCp_2^{+/0}$) and with a platinum wire counter electrode. The arrows indicate spectral shift with reduction and the dotted lines are intermediate spectra.

The second and third reductions of $[(bpy)_2Ru(bpm)RhCl_2(phen)](PF_6)_3$ both show irreversible couples by CPE and correspond by coulometry to passage of a single reducing equivalent for each couple (n = 1.1 and 1.3, respectively). This observation coupled with the growth of an irreversible oxidative wave at 1.2 V, consistent with free chloride in solution, supports assignment of these couples as sequential $Rh^{III/II}$ and $Rh^{II/I}$ reductions. The electrochemical reduction of $[(bpy)_2Ru(bpm)RhCl_2(phen)](PF_6)_3$ follows an EECEC mechanism consistent with a $bpm^{0/-}$ couple, followed by $Rh^{III/II}$ and $Rh^{II/I}$ couples.

3.2.2. Electrochemical Properties $[(bpy)_2Ru(dpp)RhCl_2(phen)](PF_6)_3$

The bimetallic complex $[(bpy)_2Ru(dpp)RhCl_2(phen)](PF_6)_3$ possess the same structural components as the known trimetallic analog $[\{(bpy)_2Ru(dpp)\}_2RhCl_2](PF_6)_5$, but displays different redox properties. The oxidation at 1.65 V vs. Ag/AgCl is reversible, consistent with a stabilized $Ru^{III/II}$ process, Figure 3.9, representing oxidation of a single Ru^{II} light absorbing center. The bimetallic $[(bpy)_2Ru(dpp)RhCl_2(phen)](PF_6)_3$ shows three reductions at −0.39, −0.74 and −0.98 V. Constant potential electrolysis with coulometry past the first or second

reduction results in passage of 2.1 reducing equivalents with evidence of chloride in solution, consistent with Rh based reductions. Conducting cyclic voltammetry at slower scan rates leads to an increase in the cathodic current for the couple at −0.39 V, a concurrent decrease in the couple at −0.74 V and decrease the reversibility of the −0.39 V couple, Figure 3.10. A chemical process is likely responsible for the scan rate dependent electrochemistry. The CPE results suggest both couples coalesce to a process at ca. −0.39 V under these slower bulk methods. Constant potential electrolysis at −1.10 V results in passage of a third reducing equivalent (n = 1.0). The first two couples are therefore assigned as Rh based reductions, followed by reduction of the dpp bridge at −0.98 V.

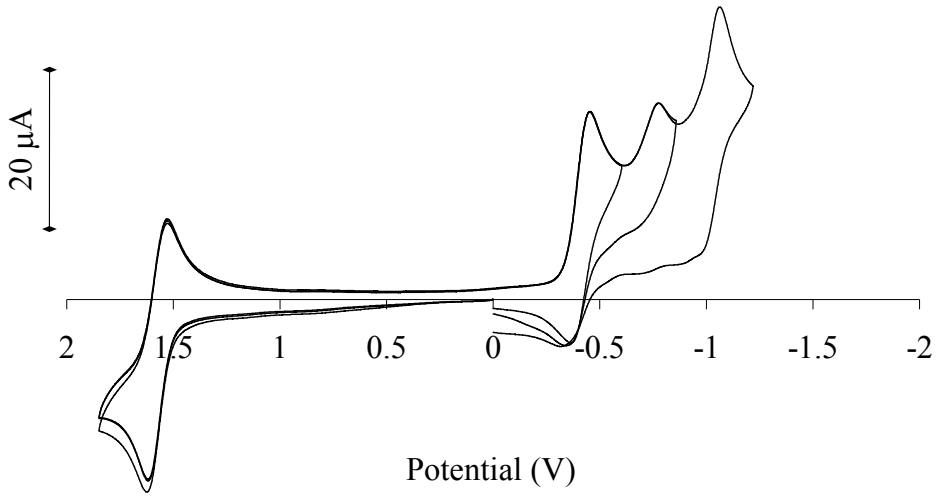

Figure 3.9. Cyclic voltammogram of $[(bpy)_2Ru(dpp)RhCl_2(phen)](PF_6)_3$ in 0.1 M Bu_4NPF_6 acetonitrile at a platinum disc working electrode versus Ag/AgCl (3M NaCl) (−0.46 V vs. $FeCp_2^{+/0}$) and with platinum wire counter electrode. Scan rate (v) = 100 mV/s.

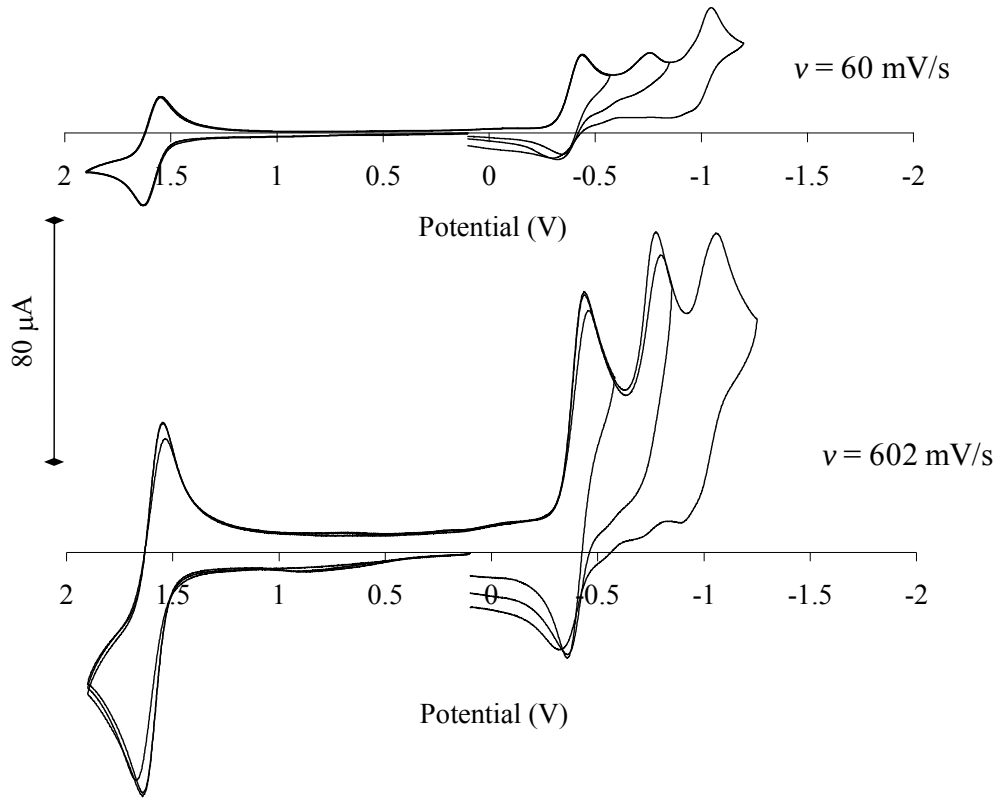

Figure 3.10. Cyclic voltammograms of $[(bpy)_2Ru(dpp)RhCl_2(phen)](PF_6)_3$ (5.0 mM) illustrating the scan rate (ν) dependence of the couples in the reductive region. Voltammograms obtained in 0.1 M Bu_4NPF_6 acetonitrile at a platinum disc working electrode versus Ag/AgCl (3M NaCl) (−0.46 V vs. $FeCp_2^{+/0}$) and with platinum wire counter electrode.

3.2.3. Electrochemical Properties of $[(bpy)_2Os(dpp)RhCl_2(phen)](PF_6)_3$

The electrochemical properties of $[(bpy)_2Os(dpp)RhCl_2(phen)](PF_6)_3$ are reminiscent of the Ru^{II} containing analog, with a shift less positive potential of the metal based oxidation. A reversible oxidation at 1.24 V vs. Ag/AgCl is consistent with a $Os^{III/II}$ couple, Figure 3.11. This shift is reflective of the higher energy dπ orbitals on Os^{II} versus Ru^{II} in the same structural motif. In the reductive region $[(bpy)_2Os(dpp)RhCl_2(phen)](PF_6)_3$ exhibits reductions analogous to $[(bpy)_2Ru(dpp)RhCl_2(phen)](PF_6)_3$.

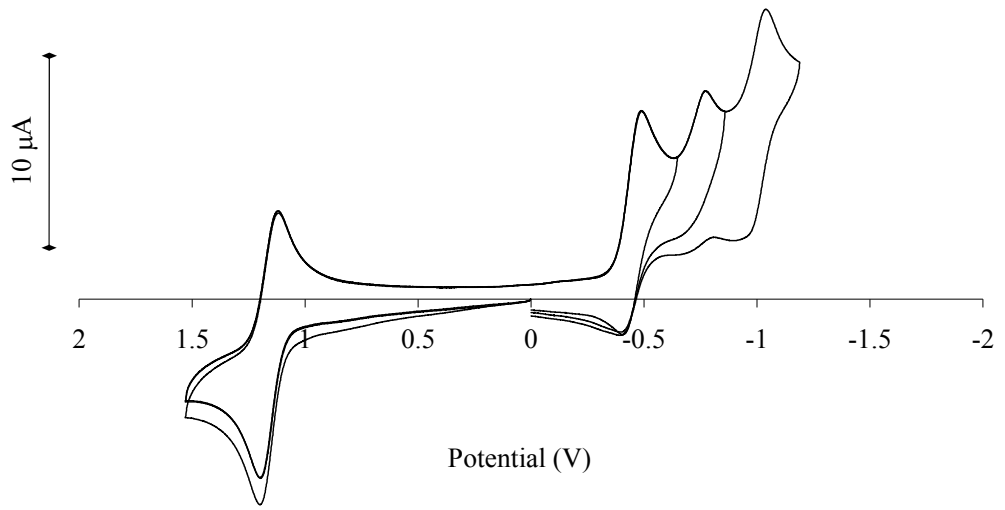

Figure 3.11. Cyclic voltammogram of $[(bpy)_2Os(dpp)RhCl_2(phen)](PF_6)_3$ in 0.1 M Bu_4NPF_6 acetonitrile at a platinum disc working electrode versus Ag/AgCl (3M NaCl) (−0.46 V vs. $FeCp_2^{+/0}$) and with platinum wire counter electrode. Scan rate (ν) = 100 mV/s.

3.2.4. Electrochemical Properties of $[\{(tpy)OsCl(dpp)\}_2RhCl_2](PF_6)_3$ and $[(tpy)OsCl(dpp)RhCl_2(phen)](PF_6)_2$

The electrochemical properties of $[\{(tpy)OsCl(dpp)\}_2RhCl_2](PF_6)_3$ and $[(tpy)OsCl(dpp)RhCl_2(phen)](PF_6)_2$ are characteristic of mixed metal supramolecules containing two or one light absorber subunit linked to a *cis*-$RhCl_2$ center.[34,79] The complexes exhibit reversible $Os^{III/II}$ couples at 0.85 V and 0.86 V for the triad and dyad, respectively, Figures 3.12 and 3.13. The first reduction of $[\{(tpy)OsCl(dpp)\}_2RhCl_2](PF_6)_3$ is irreversible, consistent with known loss of two chlorides following $Rh^{III/II/I}$ reduction in this structural motif.[15] The Os,Rh,Os triad has additional reductive processes attributed to sequential reduction of bridging dpp ligands. A broad desorption spike is observed upon cycling after the third reductive couple. The bimetallic has a irreversible first reduction at −0.57 V at any scan rate studied, contrary to the other bimetallic complexes. CPE with coulometry negative of the first reduction at −0.57 V of $[(tpy)OsCl(dpp)RhCl_2(phen)](PF_6)_2$ results in the passage of two reducing equivalents with observation of a Cl^- loss, consistent with a Rh based reduction.

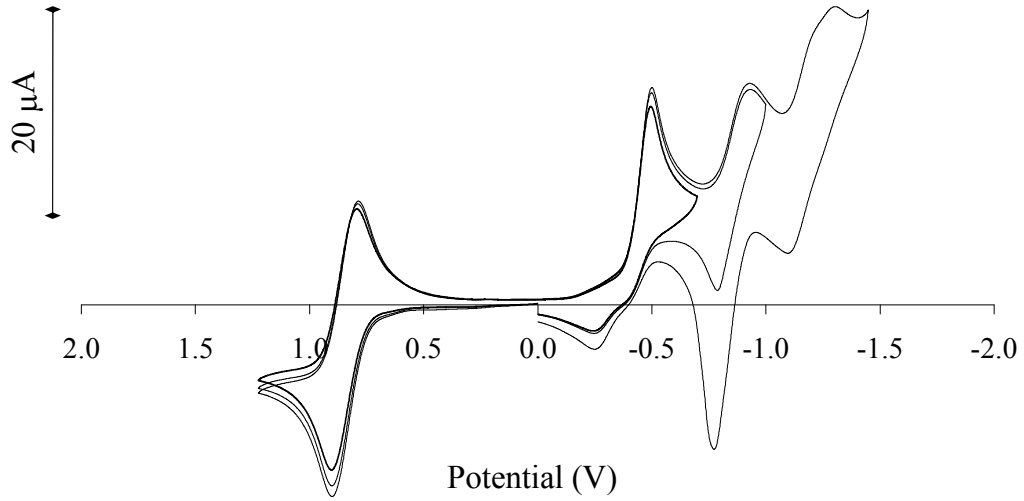

Figure 3.12. Cyclic voltammogram of $[\{(tpy)OsCl(dpp)\}_2RhCl_2](PF_6)_3$ in 0.1 M Bu_4NPF_6 acetonitrile at a platinum disc working electrode versus Ag/AgCl (3M NaCl) (−0.46 V vs. $FeCp_2^{+/0}$) and with platinum wire counter electrode. Scan rate (v) = 100 mV/s.

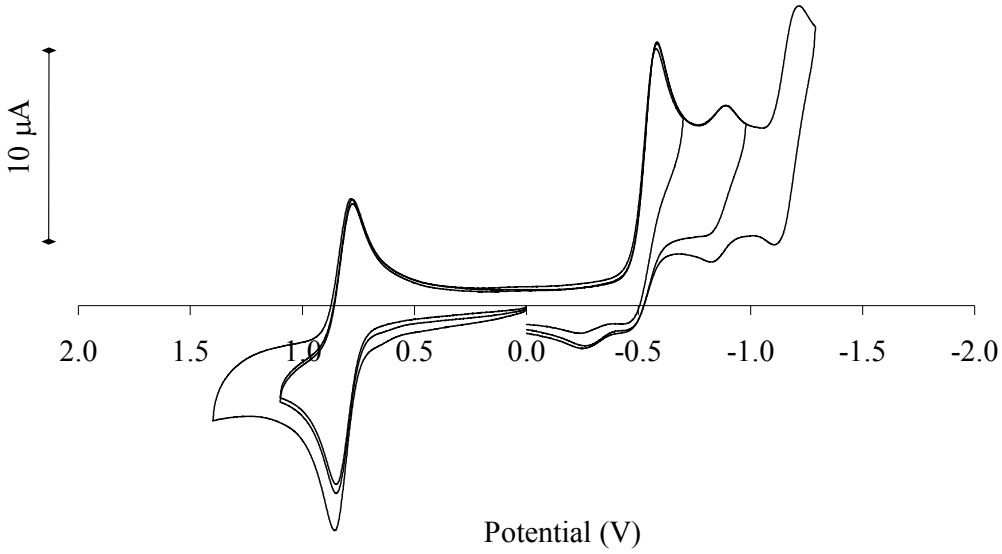

Figure 3.13. Cyclic voltammogram of $[(tpy)OsCl(dpp)RhCl_2(phen)](PF_6)_2$ in 0.1 M Bu_4NPF_6 acetonitrile at a platinum disc working electrode versus Ag/AgCl (3M NaCl) (−0.46 V vs. $FeCp_2^{+/0}$) and with platinum wire counter electrode. Scan rate (v) = 100 mV/s.

3.2.5. Concluding Remarks on the Electrochemistry of Mixed Metal Dyads

The polyazine bridged Ru,Rh and Os,Rh complexes studied herein represent an interesting new class of electroactive complexes with a *cis*-$Rh^{III}Cl_2$ center. The complexes display surprisingly complicated electrochemical processes. The trimetallic analogs of each

mixed metal dyad display electrochemical behavior consistent with their composition and consistent with the electrochemistry of simpler Ru^{II}, Os^{II} and Rh^{III} complexes. Exchange of a LA subunit for the stronger base 1,10-phenanthroline should perturb the Rh(dσ*) acceptor orbital, but gives species with electrochemical properties similar to the trimetallic analogs.

3.3. Electronic Absorption Spectroscopy Measurements

A summary of the electronic absorption properties of each of the mixed metal supramolecules studied is found in Tables 3.3 and 3.4. Each of the complexes is characterized by ligand center $\pi \rightarrow \pi^*$ transitions (internal ligand, IL) in the UV region of the spectrum and metal to ligand charge transfer (MLCT) transitions in the visible region of the spectrum. The molar absorptivity of the IL transitions in the UV region is reflective of the number of bridging and terminal polyazine ligands in the complex of interest. Likewise, the extinction coefficients of the MLCT transitions in the visible region of the spectrum are indicative of the number of Ru or Os centered light absorbing subunits used in the supramolecular architecture. Os^{II} polyazine complexes possess intense low energy absorptions due to spin orbit coupling that relaxes the spin selection rules associated with the formally forbidden $^1GS \rightarrow {}^3MLCT$ transition. Interestingly, each of the bimetallic complexes has transitions in the visible coincident with the trimetallic analog. Therefore, the visible light absorbing properties of the mixed metal complexes differed between those with varying metal centers (Os vs. Ru), terminal ligands (tpy,Cl vs. bpy,bpy) and bridging polyazine ligands (dpp vs. bpm), but not appreciably by the number of visible light absorbing centers (M,Rh,M vs. M,Rh, where M = Ru or Os).

Table 3.3. Electronic absorption properties of polyazine bridged bimetallic **s**upramolecules. [a]

Complex[b]	λ_{max} (nm)[c]	$\varepsilon \times 10^{-3}$ ($M^{-1}cm^{-1}$)	Assignment[d]
$[(bpy)_2Ru(bpm)RhCl_2(phen)](PF_6)_3$	276	78.4	bpy π→π* phen π→π* bpm π→π*
	393(sh)	14.2	Ru(dπ)→bpm(π*) CT
	412	16.6	Ru(dπ)→bpy(π*) CT
	581(br)	4.0	Ru(dπ)→bpm(π*) CT
$[(bpy)_2Ru(dpp)RhCl_2(phen)](PF_6)_3$	279	71.3	bpy π→π* phen π→π*
	338(sh)	23.4	dpp π→π*
	418	8.1	Ru(dπ)→bpy(π *) CT
	509	14.7	Ru(dπ)→dpp(π*) CT
$[(bpy)_2Os(dpp)RhCl_2(phen)](PF_6)_3$	282	71.1	bpy π→π* phen π→π*
	340(sh)	26.5	dpp π→π*
	416	10.8	Os(dπ)→bpy(π *) CT
	521	18.1	Os(dπ)→dpp(π*) CT
	784(br)	2.81	Os(dπ)→dpp(π*) CT
$[(tpy)OsCl(dpp)_2RhCl_2(phen)](PF_6)_3$	275	56.9	phen π→π* tpy π→π*
	322	42.4	tpy π→π* dpp π→π*
	536	21.8	Os(dπ)→dpp(π*) CT
	856(br)	3.2	Os(dπ)→dpp(π*) CT

[a] In room temperature acetonitrile
[b] bpy = 2,2'-bipyridine, dpp = 2,3-bis(2-pyridyl)pyrazine, phen = 1,10-phenanthroline, bpm = 2,2'-bipyrimidine, tpy = 2,2':6',2''-terpyridine
[c] sh = shoulder, br = broad
[d] CT = charge transfer

Table 3.4. Electronic absorption properties of polyazine bridged trimetallic supramolecules.[a]

Complex[b]	λ_{max} (nm)[c]	$\varepsilon \times 10^{-3}$ ($M^{-1}cm^{-1}$)	Assignment[d]
$[\{(bpy)_2Ru(bpm)\}_2RhCl_2](PF_6)_5$ [e]	278	99.0	bpy π→π* bpm π→π*
	412	37.0	Ru(dπ)→bpy(π*) CT Ru(dπ)→bpm(π*) CT
	594(br)	9.9	Ru(dπ)→bpm(π*) CT
$[\{(bpy)_2Ru(dpp)\}_2RhCl_2](PF_6)_5$ [f]	284	97.7	bpy π→π*
	338(sh)	39.3	dpp π→π*
	416	14.9	Ru(dπ)→bpy(π*) CT
	520	26.1	Ru(dπ)→dpp(π*) CT
$[\{(bpy)_2Os(dpp)\}_2RhCl_2](PF_6)_5$ [g]	284	117.0	bpy π→π*
	336(sh)	51.3	dpp π→π*
	412	22.2	Os(dπ)→bpy(π *) CT
	534	36.0	Os(dπ)→dpp(π *) CT
	798(br)	6.1	Os(dπ)→dpp(π *) CT
$[\{(tpy)OsCl(dpp)\}_2RhCl_2](PF_6)_3$ [h]	272	69.9	tpy π→π*
	317	79.3	tpy π→π* dpp π→π*
	426(sh)	13.9	Os(dπ)→tpy(π *) CT
	535	40.6	Os(dπ)→dpp(π*) CT
	856(br)	7.8	Os(dπ)→dpp(π*) CT

[a] In room temperature acetonitrile
[b] bpy = 2,2'-bipyridine, dpp = 2,3-bis(2-pyridyl)pyrazine, phen = 1,10-phenanthroline, bpm = 2,2'-bipyrimidine, tpy = 2,2':6',2''-terpyridine
[c] sh = shoulder, br = broad
[d] CT = charge transfer
[e] From Nallas *et al*.[36]
[f] Based on MLCT reported by Arachchige *et al*.[161]
[g] From Holder *et al.*[79]
[h] This work.

3.3.1. Electronic Absorption Spectroscopy of [{(bpy)$_2$Ru(bpm)}$_2$RhCl$_2$](PF$_6$)$_5$ and [(bpy)$_2$Ru(bpm)RhCl$_2$(phen)](PF$_6$)$_3$

The bpm bridged complexes [{(bpy)$_2$Ru(bpm)}$_2$RhCl$_2$](PF$_6$)$_5$ and [(bpy)$_2$Ru(bpm)RhCl$_2$(phen)](PF$_6$)$_3$ have strikingly similar electronic absorption properties. The electronic absorption spectra are presented in Figure 3.14. The intensity of the electronic absorption bands for each complex reflects the number of Ru(II) light absorbers attached to the Rh(III) center. The lowest lying visible absorbance is Ru(dπ)→bpm(π*) CT in nature with λ_{max} = 594 and 581 nm for [{(bpy)$_2$Ru(bpm)}$_2$RhCl$_2$](PF$_6$)$_5$ and [(bpy)$_2$Ru(bpm)RhCl$_2$(phen)](PF$_6$)$_3$, respectively. Typical of bpm bridged complexes, a higher energy CT band is seen at 412 nm with higher absorptivity, consistent with overlapping Ru(dπ)→bpy(π*) CT and Ru(dπ)→bpm(π*) CT transitions in this region. In the UV-region of the spectrum, a strong absorption band at ca. 270 nm is observed for each complex with intensity reflective of the number of terminal polyazine ligands.

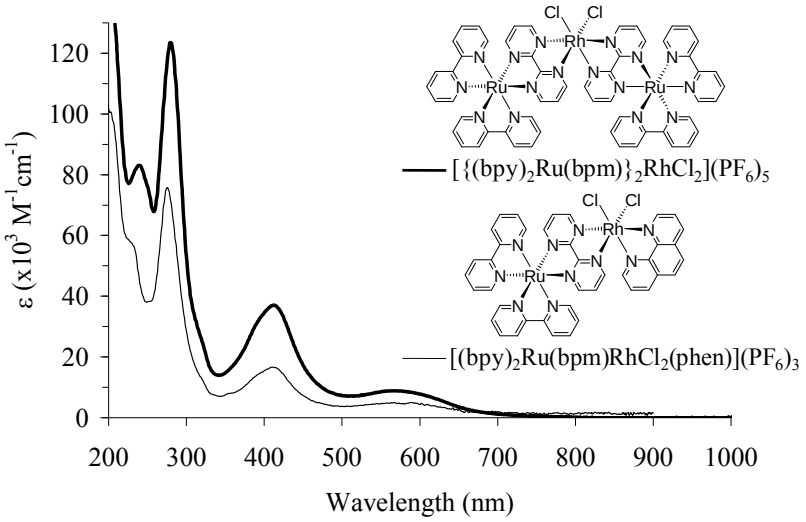

Figure 3.14. Electronic absorption spectra of [{(bpy)$_2$Ru(bpm)}$_2$RhCl$_2$](PF$_6$)$_5$[36] and [(bpy)$_2$Ru(bpm)RhCl$_2$(phen)](PF$_6$)$_3$ in room temperature acetonitrile, bpy = 2,2'-bipyridine, bpm = 2,2'-bipyrimidine, phen = 1,10-phenanthroline.

3.3.2. Electronic Absorption Spectroscopy of [{(bpy)$_2$Ru(dpp)}$_2$RhCl$_2$](PF$_6$)$_5$ and [(bpy)$_2$Ru(dpp)RhCl$_2$(phen)](PF$_6$)$_3$

The complexes [{(bpy)$_2$Ru(dpp)}$_2$RhCl$_2$](PF$_6$)$_5$ and [(bpy)$_2$Ru(dpp)RhCl$_2$(phen)](PF$_6$)$_3$ are both efficient visible light MLCT absorbers. The electronic absorption spectra are presented in Figure 3.15. Typical for (bpy)$_2$Ru^{II}(μ-dpp) subunits, the Ru(dπ)→bpy(π*) CT transition

occurs at ca. 410 nm for the $[(bpy)_2Ru(dpp)RhCl_2(phen)](PF_6)_3$ complex and displays significantly lower absorptivity than the Ru(dπ)→dpp(π*) CT transition. Low energy absorption bands assigned to a Ru(dπ)→dpp(π*) CT transition occur at 520 and 509 nm for the trimetallic and bimetallic respectively, with extinction coefficients consistent with the number of Ru(II) centered chromophores. The hetero-bimetallic complex $[(bpy)_2Ru(dpp)Rh(bpy)_2](PF_6)_5$ displays a lowest lying MLCT transition centered at 514 nm (ε = 14,400 $M^{-1}cm^{-1}$)[73] while the Ru,Ru homo-bimetallic $[(bpy)_2Ru(dpp)Ru(bpy)_2](PF_6)_4$ displays Ru(dπ)→dpp(π*) CT transition at 526 nm (ε = 24,800 $M^{-1}cm^{-1}$).[74] The similar energy of these Ru(dπ)→dpp(π*) CT transitions indicates that $Ru^{II}(bpy)_2$, $Rh^{III}(bpy)_2$, $Rh^{III}Cl_2(phen)$ or $Rh^{III}Cl_2(dpp)$ have similar effect on the energy and oscillator strength of the Ru(dπ)→dpp(π*) CT transitions.

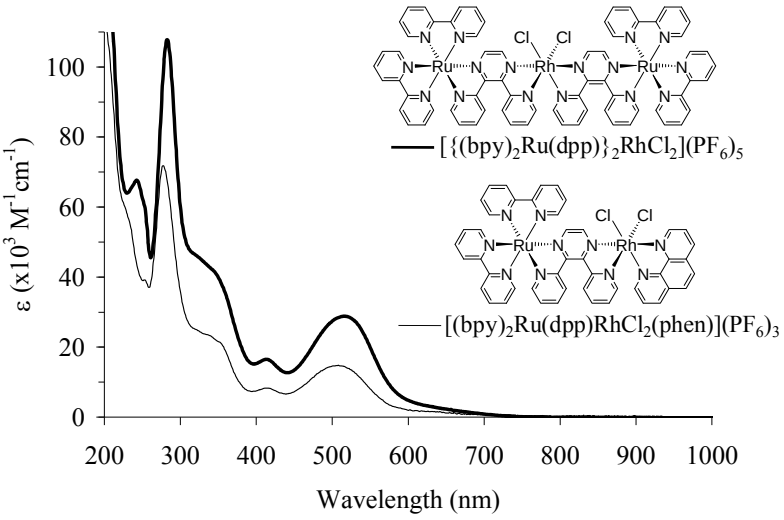

Figure 3.15. Electronic absorption spectra of $[\{(bpy)_2Ru(dpp)\}_2RhCl_2](PF_6)_5$[161] and $[(bpy)_2Ru(dpp)RhCl_2(phen)](PF_6)_3$ in room temperature acetonitrile, bpy = 2,2'-bipyridine, dpp = 2,3-bis(2-pyridyl)pyrazine, phen = 1,10-phenanthroline.

3.3.3. Electronic Absorption Spectroscopy of $[\{(bpy)_2Os(dpp)\}_2RhCl_2](PF_6)_5$ and $[(bpy)_2Os(dpp)RhCl_2(phen)](PF_6)_3$

The Os^{II} centered molecules $[\{(bpy)_2Os(dpp)\}RhCl_2](PF_6)_5$ and $[(bpy)_2Os(dpp)RhCl_2(phen)](PF_6)_3$ have electronic absorption properties reflective of the number and types of chromophores. The electronic absorption spectra of each is presented in Figure 3.16. Each complex absorbs strongly in the UV region of the spectrum, with a prominent transition centered at 285 and 282 nm for the Os,Rh,Os and Os,Rh complexes respectively.

These absorptions are due to the terminal ligand (TL) centered π→π* transitions, where TL = 4 bpy or 2bpy + 1phen. A shoulder at ca. 340 nm for each complex is due to the dpp π→π* transition. Each complex absorbs strongly in the visible region with prominent absorptions at ca. 414 nm assigned as Os(dπ)→bpy(π*) CT transitions, with Os(dπ)→dpp(π*) CT transitions at lower energy. Both $[\{(bpy)_2Os(dpp)\}RhCl_2](PF_6)_5$ and $[(bpy)_2Os(dpp)RhCl_2(phen)](PF_6)_3$ have broad, intense, low energy absorptions due to direct population of the Os(dπ)-dpp(π∗) ^{3}MLCT state, as is typical for Os^{II} polyazine complexes.

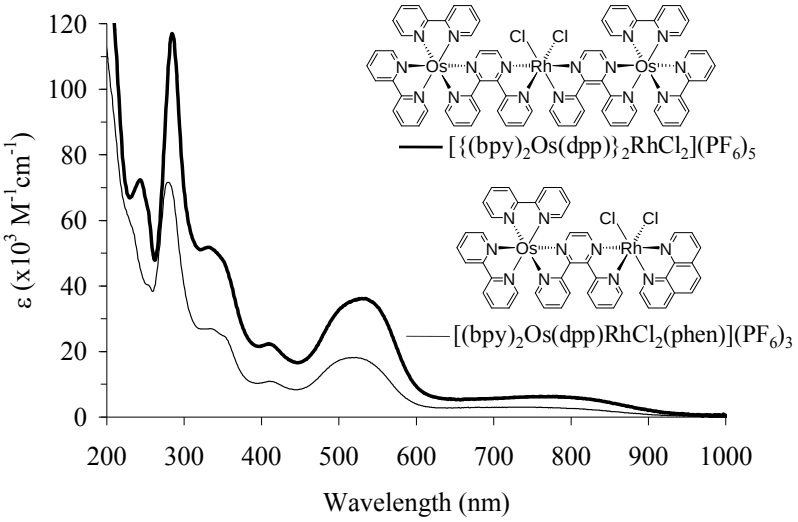

Figure 3.16. Electronic absorption spectra of $[\{(bpy)_2Os(dpp)\}_2RhCl_2](PF_6)_5$[79] and $[(bpy)_2Os(dpp)RhCl_2(phen)](PF_6)_3$ in room temperature acetonitrile, bpy = 2,2'-bipyridine, dpp = 2,3-bis(2-pyridyl)pyrazine, phen = 1,10-phenanthroline.

3.3.4. Electronic Absorption Spectroscopy of $[\{(tpy)OsCl(dpp)\}_2RhCl_2](PF_6)_3$ and $[(tpy)OsCl(dpp)RhCl_2(phen)](PF_6)_2$

Strong metal-to-ligand charge transfer (MLCT) absorptions over the visible region of the electronic absorption spectra of $[(tpy)OsCl(dpp)RhCl_2(phen)](PF_6)_2$ and $[\{(tpy)OsCl(dpp)\}_2RhCl_2](PF_6)_3$ are consistent with other Os(II) polyazine complexes, Figure 3.17. Transitions in the UV region of the spectrum can be assigned to stabilized phen (π→π*) transitions at higher energy, while overlapping tpy(π→π*) and dpp(π→π*) transitions occur ca. 0.67 eV lower. Overlapping tpy and dpp based MLCT transitions occur at 536 nm for the trimetallic and bimetallic. A tail at lower energy is consistent with direct population of a ^{3}MLCT state of each complex.[53]

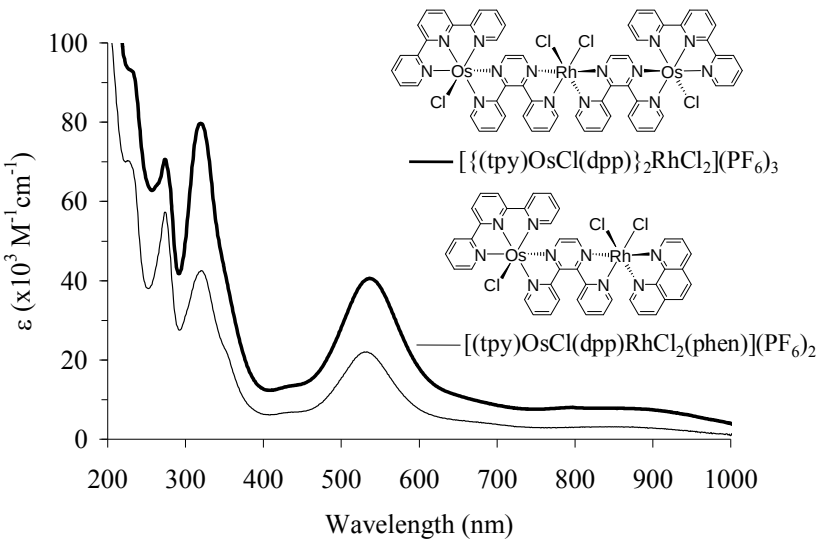

Figure 3.17. Electronic absorption spectra of $[\{(tpy)OsCl(dpp)\}_2RhCl_2](PF_6)_3$ and $[(tpy)OsCl(dpp)RhCl_2(phen)](PF_6)_2$ in room temperature acetonitrile, tpy = 2,2':6',2"-terpyridine, dpp = 2,3-bis(2-pyridyl)pyrazine, phen = 1,10-phenanthroline.

3.3.5. Comparing the Electronic Absorption Spectra of Mixed Metal Dyads

The visible region of the spectrum of polyazine bridged mixed metal complexes are dominated by M(dπ)→BL(π*) CT transitions, with spectral character reflective of the bridge. Complexes containing a Ru(bpm) based light absorber tend to have transitions at lower energy compared to the dpp bridged analogs. Kalyanasundaram and Nazeeruddin reported the Ru,Ru dyads $[(bpy)_2Ru(BL)Ru(bpy)_2]^{4+}$, where BL = dpp or bpm.[74] Separating the two LA units by a *cis*-$Rh^{III}Cl_2$ center is reported to have little impact on the observed spectroscopic features.[36,37] The BL localized LUMO for the bpm complexes lies at lower energy than the dpp bridged complexes, giving rise to a broad, low energy absorption at ca. 600 nm, compared to ca. 520 nm for the dpp bridged complexes.[100,162,163] A Ru(dπ)→bpy(π*) CT transition is observed at higher energy (ca. 410 nm) for complexes bridged by either dpp or bpm. In the case of $[\{(bpy)_2Ru(bpm)\}_2RhCl_2](PF_6)_5$ and $[(bpy)_2Ru(bpm)RhCl_2(phen)](PF_6)_3$ the Ru(dπ)→bpy(π*) CT and Ru(dπ)→bpm(π*) CT transitions overlap giving rise to a peak with greater intensity than the Ru(dπ)→bpm(π*) CT transition at lower energy.

Mixed metal supramolecules with Os^{II} light absorbing centers have electronic transitions in the visible region shifted to lower energy and of greater intensity relative to their Ru^{II} containing analogs. The electronic absorption spectrum of the complex

$[(bpy)_2Os(dpp)RhCl_2(phen)](PF_6)_3$ is dominated in visible region by Os(dπ)→dpp(π*) CT and Os(dπ)→bpy(π*) CT transitions similar to those observed for $[(bpy)_2Ru(dpp)RhCl_2(phen)](PF_6)_3$. The difference in extinction coefficients is consistent with the greater oscillator strength of Os^{II} based MLCT transitions versus Ru^{II} analogs.[164]

The electronic absorption spectra of $[(bpy)_2Os(dpp)RhCl_2(phen)](PF_6)_3$ and $[(tpy)OsCl(dpp)RhCl_2(phen)](PF_6)_2$ are different, as expected with the change in ligands bound to the light absorbing metal. Complexes of the form $[(NNN)MCl(NN)]^+$ have a higher lying M(dπ) based HOMO relative to the $[M(NN)_3]^{2+}$ analog, where NNN = a terpyridine type *mer*-tridentate ligand, M = Os^{II} or Ru^{II}, and where NN = a bidentate polyazine ligand.[24] This shift in orbital energy can be attributed to the weaker field ligands of chloride and tpy versus bpy. The shift in orbital energy also results in shifts to lower energy of related MLCT transitions. The more intense, lower energy absorptions of the $[(tpy)OsCl(dpp)RhCl_2(phen)](PF_6)_2$ compared to $[(bpy)_2Os(dpp)RhCl_2(phen)](PF_6)_3$ result from Os(dπ)→tpy(π*) CT transitions underlying the common Os(dπ)→dpp(π*) CT transitions. The low energy tail attributed to direct population of the ^{3}MLCT state of $[(tpy)OsCl(dpp)RhCl_2(phen)](PF_6)_2$ also extends well into the near-IR region of the spectrum, with significant absorptivity out to 1000 nm. Supramolecules terminated by tpy therefore are interesting candidates as PDT agents absorbing in the therapeutic window.

3.3.6. Comments on the Electronic Absorption Spectra of Mixed Metal Dyads and Triads

The series of mixed metal supramolecules studied is important as they provide a clear illustration of tuning the light absorbing properties of a system. The number of light absorbing units on a supramolecule affects only the molar absorptivity of observed electronic transitions without a significant shift in energy. The visible light absorbing properties are most strongly impacted by the combination of polyazine terminal ligands, bridging ligands and light absorbing metal center. Supramolecules with Os^{II} polyazine chromophores are potent light absorbers with strong absorptions throughout the UV, visible and near IR regions due to their strong spin-orbit coupling. Use of tpy and a weak field ligand such as chloride enhances the lower energy light absorbing properties by shifting the electronic transitions to the red. The electronic absorption properties, when coupled with the results of electrochemical experiments (Section 3.2) strongly suggest that these complexes have many lower lying electronic excited states. Understanding

and controlling electronic excited states and interstate dynamics would be valuable in applications where low energy light activation of the material is preferred, including PDT.

3.4. Photophysical Properties of [{(bpy)$_2$Ru(dpp)}$_2$RhCl$_2$](PF$_6$)$_5$ and [(bpy)$_2$Ru(dpp)RhCl$_2$(phen)](PF$_6$)$_3$

The nature of the observed lowest lying electronic excited states of [(bpy)$_2$Ru(dpp)RhCl$_2$(phen)](PF$_6$)$_3$ and [{(bpy)$_2$Ru(dpp)}$_2$RhCl$_2$](PF$_6$)$_5$ was assessed using a combination of steady state emission spectroscopy, time resolved emission spectroscopy and transient absorption spectroscopy. The photophysical properties were compared to those observed for known complexes. The sum of these observations points to a low lying and reactive Ru(dπ)-dpp(π*) CT state (^{3}MLCT). Low lying electronic states (e.g. ^{3}MMCT, ^{3}LF) were not observed, but are implicated in the observed enhancement of ^{3}MLCT decay relative to a model complex and from the redox properties of the complexes. Emission was not observed at room temperature for [{(bpy)$_2$Ru(bpm)}$_2$RhCl$_2$](PF$_6$)$_5$, [(bpy)$_2$Ru(bpm)RhCl$_2$(phen)](PF$_6$)$_3$, [{(bpy)$_2$Os(dpp)}$_2$RhCl$_2$](PF$_6$)$_5$, [(bpy)$_2$Os(dpp)RhCl$_2$(phen)](PF$_6$)$_3$, [{(tpy)OsCl(dpp)}$_2$RhCl$_2$](PF$_6$)$_3$, [(tpy)OsCl(dpp)RhCl$_2$(phen)](PF$_6$)$_2$ consistent with red shifted, weaker emissions reported for similar complexes.[74]

3.4.1. Steady State Emission at Room Temperature and 77K

The emission spectra of the [(bpy)$_2$Ru(dpp)RhCl$_2$(phen)](PF$_6$)$_3$ and [{(bpy)$_2$Ru(dpp)}$_2$RhCl$_2$](PF$_6$)$_5$ were measured in room temperature acetonitrile and in 4:1 ethanol/methanol glass at 77 K, and compared to the homo-bimetallic [(bpy)$_2$Ru(dpp)Ru(bpy)$_2$](PF$_6$)$_4$ lacking the Rh^{III} acceptor (Φ^{em} = 1.4 x 10^{-3}), Table 3.5 and Figure 3.18.[74] A broad, weak emission was observed for [(bpy)$_2$Ru(dpp)RhCl$_2$(phen)](PF$_6$)$_3$ at 785 nm (Φ^{em} = 2.3 x 10^{-4}) at room temperature. The room temperature emission of [{(bpy)$_2$Ru(dpp)}$_2$RhCl$_2$](PF$_6$)$_5$ was centered at 785 nm with Φ^{em} = 1.9 x 10^{-4}, consistent with the previously reported photophysics of this complex when corrected for PMT response,.[77] In alcoholic glass at 77 K the emission peak remained broad, but shifted to 715 nm for [(bpy)$_2$Ru(dpp)RhCl$_2$(phen)](PF$_6$)$_3$ and to 730 nm for [{(bpy)$_2$Ru(dpp)}$_2$RhCl$_2$](PF$_6$)$_5$, Figures 3.19 and 3.20.

Table 3.5. Photophysical properties of bimetallic and trimetallic metal complexes bridged by dpp

Complex[a]	λ_{max}^{em} (RT)[b] (nm)	$\Phi^{em, c}$ (RT)	τ (RT) (ns)	λ_{max}^{em} (77 K)[d] (nm)	τ (77 K) (μs)
$[(bpy)_2Ru(dpp)Ru(bpy)_2](PF_6)_4$	760	1.4×10^{-3}[e]	125	695	2.5
$[(bpy)_2Ru(dpp)Rh(bpy)_2](PF_6)_5$[f]	780	--	37	685	1.7
$[\{(bpy)_2Ru(dpp)\}_2RhCl_2](PF_6)_5$	785	1.9×10^{-4}	32	730	1.9
$[(bpy)_2Ru(dpp)RhCl_2(phen)](PF_6)_3$	785	2.3×10^{-4}	30	715	1.8

[a] bpy = 2,2'-bipyridine, dpp = 2,3-bis(2-pyridyl)pyrazine, phen = 1,10-phenanthroline

[b] Room temperature (RT) emission data reported in aerated acetonitrile corrected for PMT response

[c] Quantum yield measured versus $[(bpy)_2Ru(dpp)Ru(bpy)_2](PF_6)_4$ using absorbance matched solutions with large associated error

[d] 77 K emission data reported in 4:1 v/v ethanol/methanol glass corrected for PMT response

[e] From Kalyanasundaram, and Nazeeruddin.[74]

[f] From Kalyanasundaram, Gratzel and Nazeeruddin.[73]

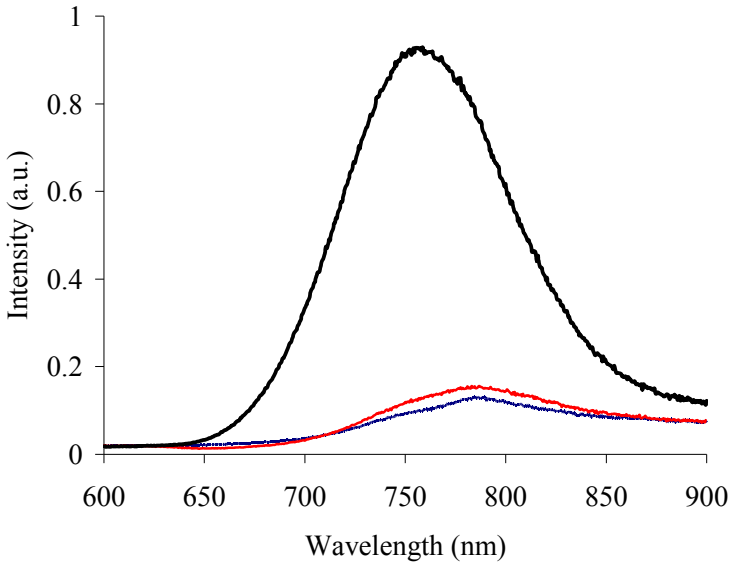

Figure 3.18. The emission spectra of $[(bpy)_2Ru(dpp)Ru(bpy)_2](PF_6)_4$ (black), $[\{(bpy)_2Ru(dpp)\}_2RhCl_2](PF_6)_5$ (blue) and $[(bpy)_2Ru(dpp)RhCl_2(phen)](PF_6)_3$ (red) in deoxygenated room temperature acetonitrile, where each is the raw emission data corrected for instrument response (λ^{ex} = 520 nm, PMT = Hamamatsu 1527 red sensitive photomultiplier tube) and bpy = 2,2'-bipyridine, dpp = 2,3-bis(2-pyridyl)pyrazine, and phen = 1,10-phenanthroline.

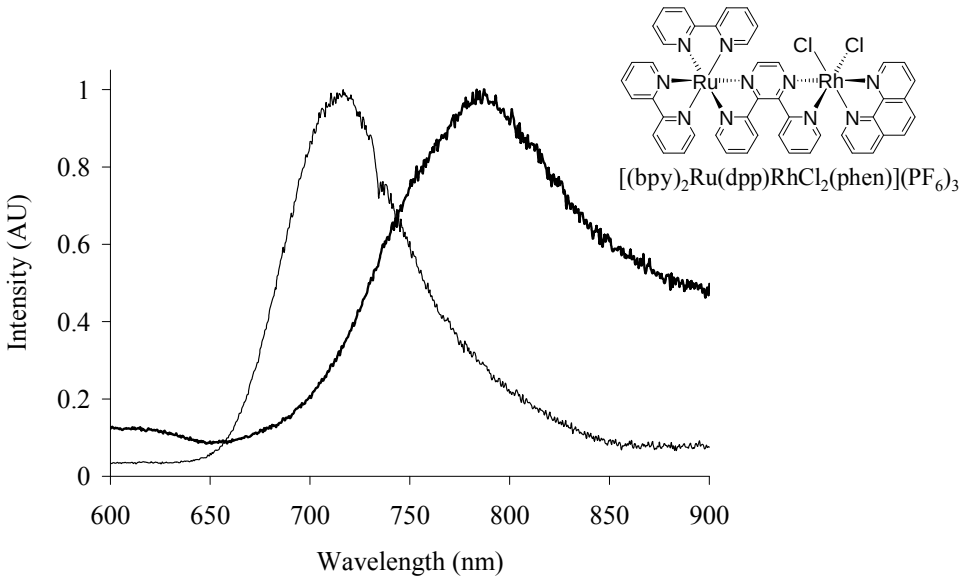

Figure 3.19. The normalized emission spectra of $[(bpy)_2Ru(dpp)RhCl_2(phen)](PF_6)_3$ in deoxygenated room temperature acetonitrile (bold line) and in 4:1 ethanol/methanol glass at 77 K, where each is corrected for instrument response and bpy = 2,2'-bipyridine, dpp = 2,3-bis(2-pyridyl)pyrazine, and phen = 1,10-phenanthroline, λ^{ex} = 520 nm, PMT = red sensitive Hamamatsu 1527.

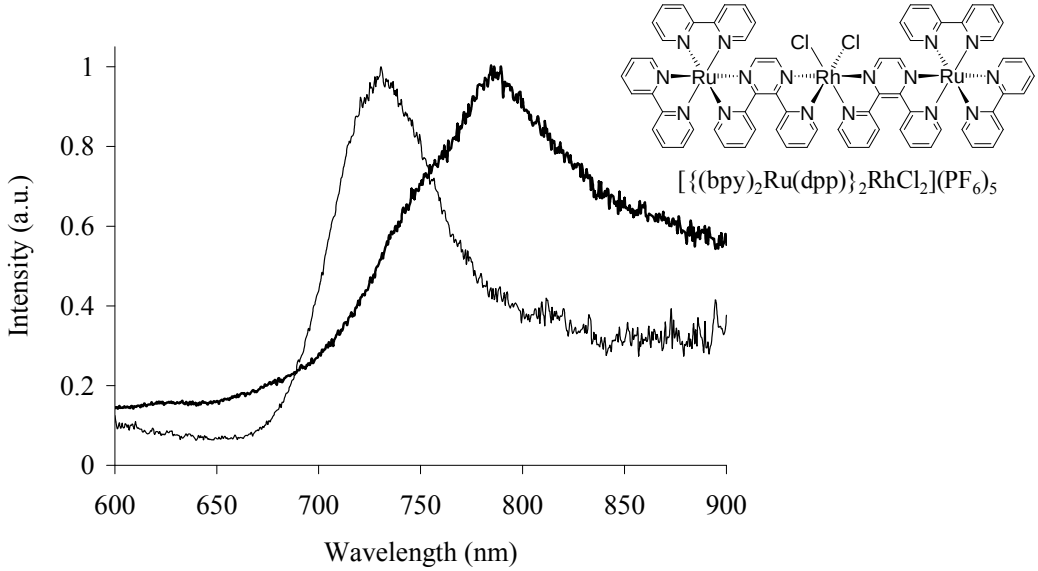

Figure 3.20. The normalized emission spectra of $[\{(bpy)_2Ru(dpp)\}_2RhCl_2](PF_6)_5$ in room temperature acetonitrile (bold line) and in 4:1 ethanol/methanol glass at 77 K, where each is corrected for instrument response and bpy = 2,2'-bipyridine and dpp = 2,3-bis(2-pyridyl)pyrazine, λ^{ex} = 520 nm, PMT = red sensitive Hamamatsu 1527.

The room temperature emission of the Ru,Rh complexes are significantly weaker than that of the Ru,Ru model complex. Both $[\{(bpy)_2Ru(dpp)\}_2RhCl_2](PF_6)_5$ and $[(bpy)_2Ru(dpp)RhCl_2(phen)](PF_6)_3$ have broad, structureless emissions at 785 nm, consistent with emission from a stabilized Ru(dπ)→μ-dpp(π*) CT (^{3}MLCT) state. The complex $[(bpy)_2Ru(dpp)Rh(bpy)_2](PF_6)_5$ possesses a similar reported emission (λ_{max}^{em} = 780 nm) at room temperature.[74] The homonuclear complex $[(bpy)_2Ru(dpp)Ru(bpy)_2](PF_6)_4$ emission is slightly blue-shifted, centered at 760 nm with significantly higher intensity. The quantum yields of the emission of the mixed metal complexes are significantly reduced compared to the homonuclear analog. The Rh containing complexes possess low lying Rh(dσ*) acceptor orbitals. This provides energetically feasible intramolecular electron transfer to give the Ru(dσ)→Rh(dσ*) CT excited state (^{3}MMCT), leading to quenching of the ^{3}MLCT emission. Further, stabilization of the Rh(dσ*) acceptor orbital was noted to result in a red shift of the Rh centered ligand field state (^{3}LF).[33] Therefore intramolecular energy transfer to a low lying ^{3}LF state also may contribute to enhanced decay of the emissive ^{3}MLCT state.

The ^{3}MLCT emission of the dpp bridged mixed metal supramolecules in alcoholic glass was studied and compared to the analogous emission of $[(bpy)_2Ru(dpp)Ru(bpy)_2](PF_6)_4$. The emission of $[(bpy)_2Ru(dpp)Ru(bpy)_2](PF_6)_4$ at 77 K displays some broad structure centered at 695 nm, consistent with previous reports, Figure 3.21.[74] The previously studied Ru,Rh dyad $[(bpy)_2Ru(dpp)Rh(bpy)_2](PF_6)_5$ displayed a similar emission at 77 K blue shifted 10 nm relative to the Ru,Ru analog.[73] The *cis*-$Rh^{III}Cl_2$ containing complexes, however, have emission maxima red-shifted versus $[(bpy)_2Ru(dpp)Ru(bpy)_2](PF_6)_4$. The complex $[(bpy)_2Ru(dpp)RhCl_2(phen)](PF_6)_3$ had an emission centered at 715 nm, while emission at 77 K from $[\{(bpy)_2Ru(dpp)\}_2RhCl_2](PF_6)_5$ was centered at 730 nm. The shift in emission maximum at 77 K likely results from minor stabilization of the dpp(π*) acceptor orbital due to the different ligand environment around the Rh^{III} center.

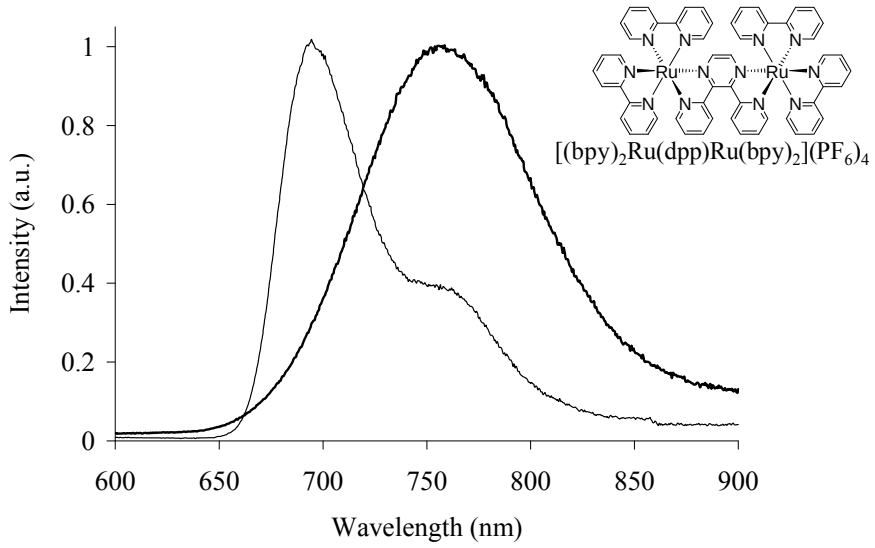

Figure 3.21. The normalized emission spectra of $[(bpy)_2Ru(dpp)Ru(bpy)_2](PF_6)_4$ in room temperature acetonitrile (bold line) and in 4:1 ethanol/methanol glass at 77 K, where each is corrected for instrument response and bpy = 2,2'-bipyridine and dpp = 2,3-bis(2-pyridyl)pyrazine, λ^{ex} = 520 nm, PMT = red sensitive Hamamatsu 1527.

3.4.2. Time Resolved Emission Spectroscopy

Emissive electronic excited state lifetimes were determined by measuring emission decay in acetonitrile at room temperature and in 4:1 ethanol/methanol glass at 77 K, Table 3.5. The decay of the ^{3}MLCT emission fits well to a single exponential decay. In room temperature, fluid solution the excited state lifetime of $[(bpy)_2Ru(dpp)RhCl_2(phen)](PF_6)_3$ was measured to be 30 ns and the lifetime of $[\{(bpy)_2Ru(dpp)\}_2RhCl_2](PF_6)_5$ was determined to be 32 ns. In alcohol glass at 77 K the excited state lifetimes were 1.8 μs and 1.9 μs, for $[(bpy)_2Ru(dpp)RhCl_2(phen)](PF_6)_3$ and $[\{(bpy)_2Ru(dpp)\}_2RhCl_2](PF_6)_5$ respectively.

The lifetime of the emitting states of $[(bpy)_2Ru(dpp)RhCl_2(phen)](PF_6)_3$ and $[\{(bpy)_2Ru(dpp)\}_2RhCl_2](PF_6)_5$ in room temperature solution are significantly shorter than that of $[(bpy)_2Ru(dpp)Ru(bpy)_2](PF_6)_4$. At room temperature, the lifetimes of the emission from the ^{3}MLCT states of $[(bpy)_2Ru(dpp)RhCl_2(phen)](PF_6)_3$ and $[\{(bpy)_2Ru(dpp)\}_2RhCl_2](PF_6)_5$ are ca. 30 ns, similar to the previously reported Ru,Rh complex $[(bpy)_2Ru(dpp)Rh(bpy)_2](PF_6)_5$ (τ = 37 ns).[73] The Ru,Rh complexes all display shorter ^{3}MLCT excited state lifetimes relative to $[(bpy)_2Ru(dpp)Ru(bpy)_2](PF_6)_4$ (τ = 124 ns). This is reflective of quenching of the ^{3}MLCT state by intramolecular electron transfer to generate the ^{3}MMCT state and/or intramolecular energy transfer to a low lying, Rh centered ^{3}LF state. In alcoholic glass at 77 K the excited state lifetime

of $[(bpy)_2Ru(dpp)RhCl_2(phen)](PF_6)_3$ and $[\{(bpy)_2Ru(dpp)\}_2RhCl_2](PF_6)_5$ increase significantly to ca. 1.8 μs, compared to 2.5 μs measured for $[(bpy)_2Ru(dpp)Ru(bpy)_2](PF_6)_4$ under these conditions. Excited state electron transfer is known to be inhibited in rigid matrices due to the large reorganizational energy associated with charge redistribution. For example, the ^{3}MLCT emission of $[(Me_2phen)_2Ru(Mebpy\text{-}CH_2CH_2\text{-}Mebpy)Rh(dmb)_2]^{5+}$ increases from 30 ns to 6.8 μs when studied at 77 K in frozen solution.[72] The large increase in ^{3}MLCT emission for $[(bpy)_2Ru(dpp)RhCl_2(phen)](PF_6)_3$ and $[\{(bpy)_2Ru(dpp)\}_2RhCl_2](PF_6)_5$ at 77 K versus room temperature is indicative of intramolecular electron transfer and population of a ^{3}MMCT state at room temperature being impeded at 77 K in rigid media.

The interstate dynamics proposed previously by Brewer and coworkers for the complex $[\{(bpy)_2Ru(dpp)\}_2RhCl_2](PF_6)_5$, Figure 3.21, is supported by the most recent results of low temperature emission spectroscopy. Population of a low lying ^{3}MMCT state from the emissive ^{3}MLCT state due to intramolecular excited state electron transfer was suggested to result in decreased emission relative to the model complex $[(bpy)_2Ru(dpp)Ru(bpy)_2](PF_6)_4$. The electronic state diagram presented in Figure 3.22 likely applies to the Ru,Rh dyad as well, given its electrochemical, electronic absorption and photophysical similarities to the Ru,Rh,Ru triad. Unfortunately, luminescence spectroscopy has not given direct evidence of any electronic states resulting from the ^{3}MLCT state of $[\{(bpy)_2Ru(dpp)\}_2RhCl_2](PF_6)_5$ and $[(bpy)_2Ru(dpp)RhCl_2(phen)](PF_6)_3$ versus that of $[(bpy)_2Ru(dpp)Ru(bpy)_2](PF_6)_4$.

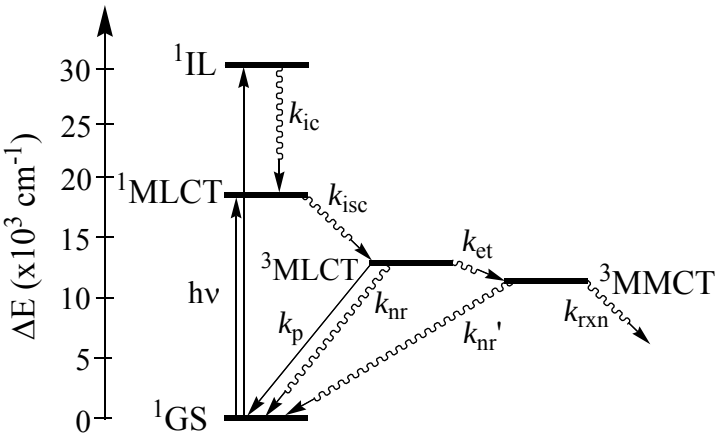

Figure 3.22. Jablonski-type state diagram of $[\{(bpy)_2Ru(dpp)\}_2RhCl_2]^{5+}$ proposed by Brewer and coworkers supported by the results of this work. bpy = 2,2'-bipyridine, dpp = 2,3-bis(2-pyridyl)pyrazine, ^{1}GS = singlet electronic ground state, ^{1}MLCT = singlet metal to ligand charge transfer, ^{3}MLCT = triplet MLCT, ^{1}IL = singlet internal ligand excited state.

3.4.3. Transient Absorption Spectroscopy

The transient electronic absorption spectra of three related dpp bridged supramolecular complexes were studied with the use of instrumentation in the laboratory of Professor Russell H. Schmehl at Tulane University (New Orleans, LA). Continuously deaerated acetonitrile solutions of $[(bpy)_2Ru(dpp)Ru(bpy)_2](PF_6)_4$, $[(bpy)_2Ru(dpp)RhCl_2(phen)](PF_6)_3$, and $[\{(bpy)_2Ru(dpp)\}_2RhCl_2](PF_6)_5$ were pumped with a 520 nm pulse (FWHM ≈ 4 ns) from an optical parametric oscillator (OPO) attenuated, frequency doubled Nd:YAG laser (532 nm). Decay of their absorption difference spectra was used to determine rate constants. Rise time data is meaningless for these measurements because of the relatively long laser pump. The results of the transient absorption experiments indicate that the observed electronic excited state is likely Ru(dπ)-dpp(π*) CT in nature, but other electronic excited states could not be excluded.

The transient absorption spectra of $[(bpy)_2Ru(dpp)Ru(bpy)_2](PF_6)_4$, $[(bpy)_2Ru(dpp)RhCl_2(phen)](PF_6)_3$, and $[\{(bpy)_2Ru(dpp)\}_2RhCl_2](PF_6)_5$ were surprisingly similar to each other, Figures 3.23, 3.24 and 3.25. Each was characterized by a prominent bleach at ca. 540 nm, consistent with loss of the Ru(dπ)→dpp(π*) CT transition as previously described by Berger.[162] A reasonably strong absorption was observed at ca. 390 nm, attributed to a dpp(π*→π*) internal ligand transition of the dpp localized radical anion. A broad weaker absorption at longer wavelengths (600-750 nm) also was consistent with a dpp localized radical.

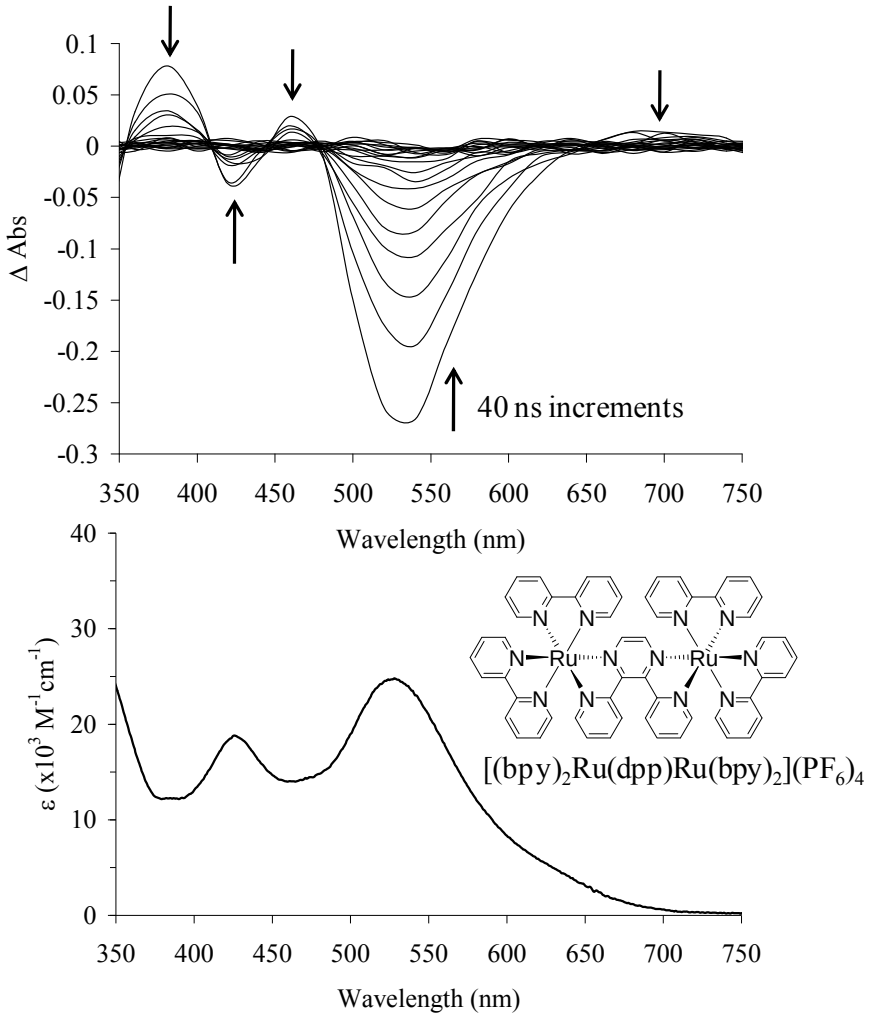

Figure 3.23. Ground state electronic absorption spectrum (lower) and transient absorption difference spectrum of $[(bpy)_2Ru(dpp)Ru(bpy)_2](PF_6)_4$ in deoxygenated, room temperature acetonitrile, bpy = 2,2'-bipyridine and 2,3-bis(2-pyridyl)pyrazine. The arrows indicate the direction of spectroscopic decay following excitation with 520 nm light. The full transient absorption spectrum was reported previously by Berger.[162]

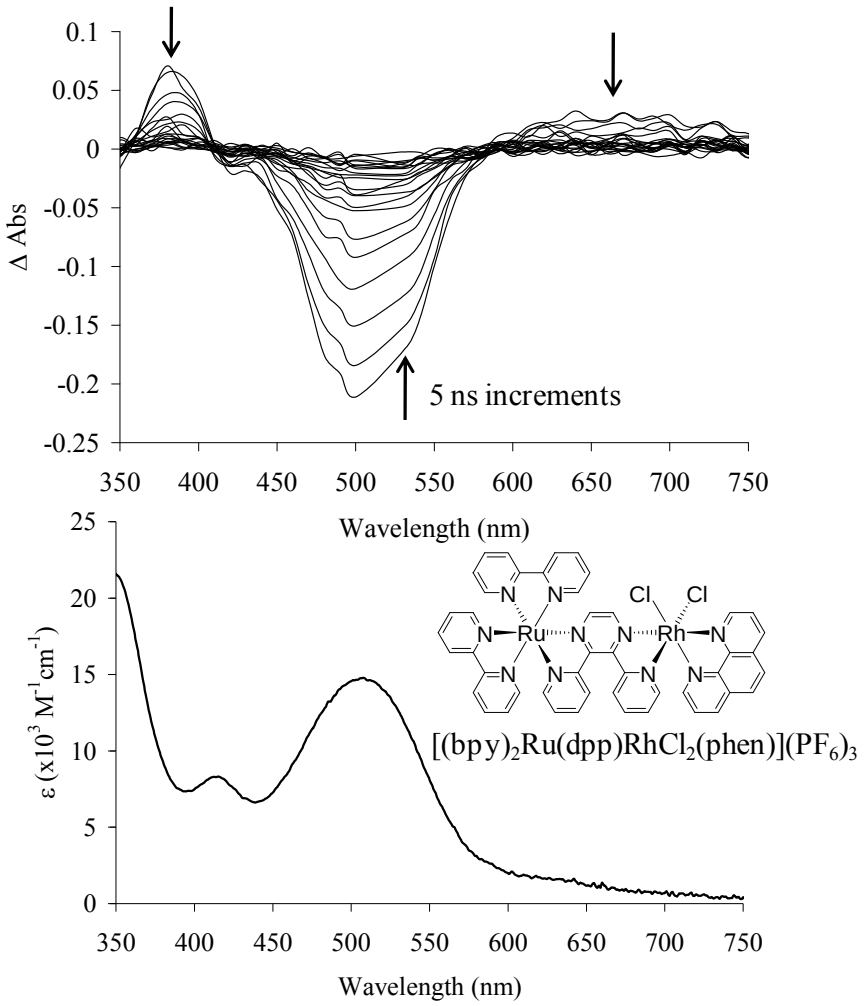

Figure 3.24. Ground state electronic absorption spectrum (lower) and transient absorption difference spectrum of $[(bpy)_2Ru(dpp)RhCl_2(phen)](PF_6)_3$ in deoxygenated, room temperature acetonitrile, bpy = 2,2'-bipyridine, 2,3-bis(2-pyridyl)pyrazine and phen = 1,10-phenanthroline. The arrows indicate the direction of spectroscopic decay following excitation at 520 nm.

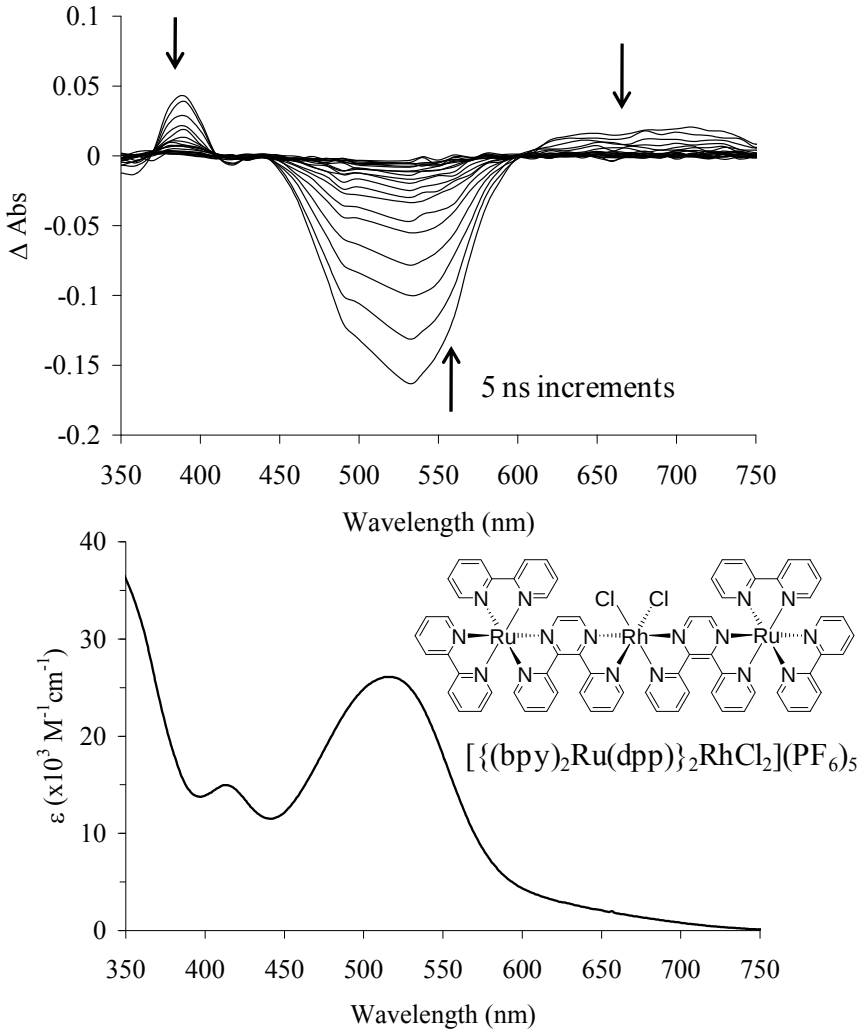

Figure 3.25. Ground state electronic absorption spectrum (lower) and transient absorption difference spectrum of $[\{(bpy)_2Ru(dpp)\}_2RhCl_2](PF_6)_5$ in deoxygenated, room temperature acetonitrile, bpy = 2,2'-bipyridine and 2,3-bis(2-pyridyl)pyrazine. The arrows indicate the direction of spectroscopic decay following 520 nm excitation.

The electronic excited decay measured from the transient absorption spectra indicated interesting excited state decay kinetics consistent with the time resolved emission measurements. Transient decay gave identical kinetics regardless of wavelength, consistent with a single electronic excited state. The absorption decay profiles for the mixed metal complexes were particularly well resolved relative to the analogous emission experiments. The well resolved decays were attributed to the larger signal to noise of the transient absorption measurements and superior temporal resolution of the oscilloscope used to record PMT response decay.

The kinetic data acquired using transient absorption spectroscopy supplemented those determined using excited state emission techniques, giving a more accurate measure of excited state lifetime and identifying a previously unobserved long lived component. The ^{3}MLCT state of $[(bpy)_2Ru(dpp)Ru(bpy)_2](PF_6)_4$ was measured to have a lifetime of 125 ns in room temperature, deoxygenated acetonitrile using both transient emission spectroscopy and transient absorption spectroscopy, consistent with the literature.[74] The complexes $[(bpy)Ru(dpp)RhCl_2(phen)](PF_6)_3$ and $[\{(bpy)_2Ru(dpp)\}_2RhCl_2](PF_6)_5$ each exhibit shorter lived ^{3}MLCT states, 18 ns and 16 ns respectively. Neither mixed metal complex was indicated to possess other electronic excited states during the transient absorption experiments.

The quenching introduced by inclusion of a *cis*-$Rh^{III}Cl_2$ center was assessed by comparing the ^{3}MLCT state decay of the mixed metal complexes to that of $[(bpy)_2Ru(dpp)Ru(bpy)_2](PF_6)_4$. The intrinsic excited state lifetime, τ^o, was calculated using Eq. 3.2.

$$\ln\left[\frac{OD_t^x - OD_\infty^x}{OD_0^x - OD_\infty^x}\right] = -k^o t \qquad (3.1)$$

Here OD is optical density (or absorbance) and the fraction is simply the difference in optical density (ΔOD or ΔAbs) at time t divided by ΔOD initial. The term k^o (reciprocal lifetime, $1/\tau^o$) is the intrinsic decay rate constant typically defined as the sum of all competing decay pathways from a given excited state. For the mixed metal complexes studied this can be reduced to equation 3.2:

$$k^o = \frac{1}{\tau^o} = k_p + k_{nr} + k_{en} + k_{et} \qquad (3.2)$$

where the rate constant of phosphorescence ($k_p = 1.1 \times 10^{-4}$ s^{-1}) and rate constant of other non-radiative processes ($k_{nr} = 8.0 \times 10^{-6}$ s^{-1}) are estimated from decay of the ^{3}MLCT state of $[(bpy)_2Ru(dpp)Ru(bpy)_2](PF_6)_4$. The rate constants of unimolecular excited state energy transfer (k_{en}) and electron transfer (k_{et}), could not be distinguished from the experiments used and were combined into the common intramolecular quenching constant (k_q). Therefore in room temperature solution the calculated k_q of 4.8×10^7 s^{-1} for $[\{(bpy)_2Ru(dpp)\}_2RhCl_2](PF_6)_5$ and 5.4×10^7 s^{-1} for $[(bpy)_2Ru(dpp)RhCl_2(phen)](PF_6)_3$ is in reasonable agreement with the values calculated by Elvington.[159]

3.5. *Supramolecular Photochemistry with DNA using an Array of LEDs*

The development of new compounds that display important light activated bio-reactivity includes systems with light activated DNA cleavage. There are a number of important considerations for assaying DNA photocleavage, including factors impacting light delivery, reaction conditions and DNA analysis. An array of high intensity LEDs was designed, constructed and tested to simultaneously assay multiple photochemical experiments with DNA. Detailed experimental conditions are provided for xenon arc lamp and LED array methods for the assay of DNA photocleavage.

3.5.1. LED Array Design

The design and construction of the LED array for DNA photocleavage assays (or analysis) requires reproducible methods to allow for high-throughput screening. The presented design is a modification of an array developed for solar hydrogen generation that was refined through several generations and analyzed using statistical methods.[145] The LED array presented herein provides for the economical screening of many compounds or conditions for optimization of light activated interactions with DNA. Such rapid screening is important to the development of new systems for DNA manipulation and/or photodynamic therapy.

All of the components used to build the LED array were available from commercial vendors. Parts needed rapidly during construction often were available at the local electronics store. The 6061 aluminum alloy was selected as the material to construct the array because of the alloy's high thermal conductivity, corrosion resistance, and its ease of machining. Architectural grade aluminum alloy (6063) was used for some of the structural pieces.

LED array construction was straightforward after careful planning. A graphical representation of the parts of the LED array is presented in Figure 3.26. The design of the reported array is such that someone with minimal mechanical and electronics knowledge can build it in a relatively short timeframe with high precision. Mechanical variation between LED stations was prevented by only allowing a tolerance of ±0.001" when machining the parts of the array. The LED array is modular for ease of adjusting the wavelength of excitation and number of LED photolysis stations. A simple photolysis system with a single LED could be constructed for $200 in parts. The array was easily moved within the lab due to its small size, relatively light weight and rigid construction. Electronic variation is limited by calibration of the system prior to

use and through the optimized electronic circuitry. The high precision of our LED array ensured little difference in photonic flux between LED photolysis stations.

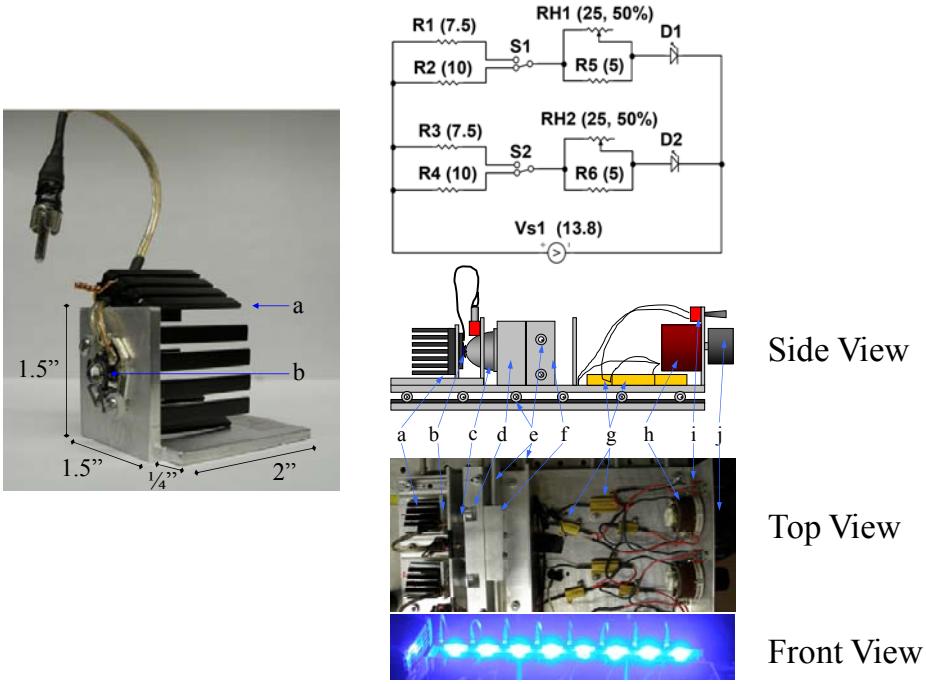

Figure 3.26. Photographic and schematic representations of an eight station, ultra high intensity LED array constructed to perform high throughput screening of the photochemical properties of mixed metal supramolecules with DNA. The letter key is as follows: a = heat sink, b = 5W blue LED star, c = parabolic reflector, d = thermostated cell holder, e = coolant flow, f = heat transfer blocks, g = resistors, h = 25W rheostat, i = single pole, double throw switch, and j = knob to adjust light flux. Reproduced from Prussin, A.J.; Zigler, D.F.; Brown, J.R.; Jain, A.; Winkel, B.S.J.; Brewer, K.J. *J. Inorg. Biochem.* **2008,** *102*, 731-738 with permission from Elsevier.[137]

3.5.2. Validation of the LED Array using Two Chemical Actinometers

Note: Aaron J. Prussin determined the LED light flux for the array using the chemical actinometer, tris(oxalate)ferrate(II).

Photon flux from the LED array was assayed using the tris(oxalate)ferrate(II) chemical actinometer and a DNA photocleavage assay of local design to validate the use of an LED array for DNA photochemical experiments. Photonic flux of each LED was adjusted by first tuning the current to each LED. Fine tuning was performed using an apparatus that collects the light into a fiber optic cable and measures output using a photodiode array. The average total flux of the LEDs was found by Aaron Prussin of the Brewer group to be 1.96 (±0.11) x 10^{19} photons/min using the potassium tris(oxalate)ferrate(II) actinometer, Table 3.6. The flux determined is more than three times that reported for the previous system and with comparable

deviation between LEDs.[145] The greater flux is likely due to light that would otherwise pass through the sample that is reflected back by the aluminum sample holder. An additional assay of relative photon flux was performed by quantitative analysis of the incomplete photocleavage reaction of pUC18 with dissolved $^1O_2$ photosensitized by $[(bpy)_2Ru(dpp)]Cl_2$. The gel electrophoresis results indicate that each of the eight LEDs provides similar quantities of light to each sample, Figure 3.27, consistent with tris(oxalate)ferrate(II) actinometry.

Table 3.6. Results of chemical actinometry assaying photon flux from an eight station LED array

LED Station[a]	SC (% emission)[b]	OC (% emission)[b]	I_o (x10^{19} photons/min)[c]
C 1	95.1	4.9	--
1	55.6	44.4	1.99 ± 0.16
2	57.0	43.0	2.07 ± 0.11
3	59.7	40.3	1.87 ± 0.15
4	62.0	38.0	1.74 ± 0.14
C 2	95.3	4.7	--
5	56.7	43.3	2.07 ± 0.05
6	57.7	42.3	2.03 ± 0.04
7	58.7	41.3	1.93 ± 0.09
8	57.5	42.5	2.01 ± 0.10
Ave±StDev[d]	58.1 ± 2.0	41.9 ± 2.0	1.96 ± 0.11

[a] Photolysis of 15.3 μM (base pairs) solution of supercoiled (SC) pUC18 DNA in 10 mM NaH_2PO_4 aqueous buffer with 3.1 μM $[(bpy)_2Ru(dpp)]Cl_2$, bpy = 2,2'-bipyridine, dpp = 2,3-bis(2-pyridyl)pyrazine. LED stations labeled C1 and C2 were DNA solutions made simultaneously without photolysis.

[b] Relative intensity of the ethidium bromide stained SC or open circular (OC) DNA isolated by gel electrophoresis, Figure 3.28

[c] Determined with potassium trisoxolatoferrate(III) chemical actinometer by Aaron J. Prussin

[d] Average of all LED stations ± standard deviation between stations

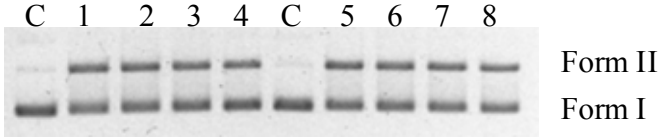

Figure 3.27. Electrophoresis gel comparing the photoproducts resulting from photolysis of pUC18 DNA and $[(bpy)_2Ru(dpp)]Cl_2$ in aerated solution by one of eight LEDs of an LED array (bpy = 2,2'-bipyridine and dpp = 2,3-bis(2-pyridyl)pyrazine). Samples were photolyzed for 26 min prior to analysis. C = pUC18 DNA control and lanes 1-8 are the same 5:1 DNA base pairs: metal complex solutions photolyzed at λ_{max} = 455 nm using each of the eight LEDs in the array. Reproduced from Prussin, A.J.; Zigler, D. F.; Brown, J.R.; Jain, A.; Winkel, B. S. J.; Brewer, K. J. *J. Inorg. Biochem.* **2008,** *102,* 731-739, with permission from Elsevier.[137]

The flux from 1000 W xenon arc lamp with 450 nm cut-on filter, traditionally used for DNA photochemical experiments, was determined for comparison to the LEDs. Flux for the lamp could not be determined directly as chemical actinometry is inaccurate for broad band sources. The photon flux therefore was estimated by measuring flux from the lamp filtered with a 480 nm narrow band pass filter. The percent transmittance of each filter was then used to estimate flux using the 450 nm cutoff filter. Figure 3.28 illustrates the relative flux and spectral pattern of each light source and also the absorbance of a 2.4 μM solution of $[\{(bpy)_2Ru(dpp)\}_2RhCl_2]Cl_5$ in water.

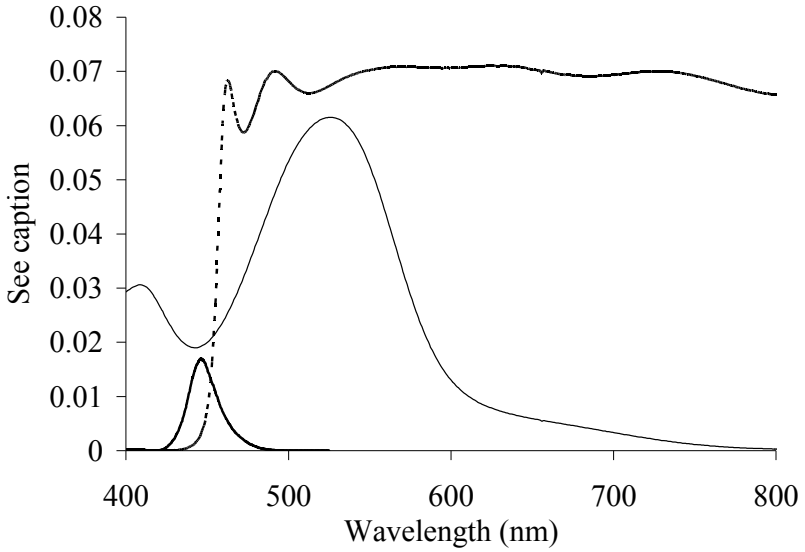

Figure 3.28. Graph comparing photon flux (y-axis units = 10^{19} photons/min) of light from a xenon arc lamp filtered with a 450 nm cutoff filter (broken line) and a 455 nm 5W LED (bold line). Also presented is the visible spectrum (y-axis units = Abs.) of a 3.1 μM solution of $[\{(bpy)_2Ru(dpp)\}_2RhCl_2]Cl_5$ in water (solid line). Reproduced from Prussin, A.J.; Zigler, D. F.; Brown, J.R.; Jain, A.; Winkel, B. S. J.; Brewer, K. J. *J. Inorg. Biochem.* **2008,** *102,* 731-739, with permission from Elsevier.[137]

3.5.3. Methodologies for DNA Photochemical Experiments

A general and convenient method was developed to perform plasmid DNA photocleavage experiments using different light sources. The photolysis and electrophoresis experiments were facilitated by the ready availability and relatively low cost of the reagents used for these experiments. In addition, as was observed from control samples made simultaneously, extraordinarily sterile techniques are unnecessary for performing this assay. DNA controls showed little evidence of DNA cleavage by nuclease contaminants compared to the photocleavage activity of the metal complexes, consistent with previously reported results.[60,79]

Typical glassware cleaning techniques, (e.g. water and acetone) were sufficient to prevent contamination of the DNA solutions by photoproducts from previous reactions or by contamination with nucleases present in the environment. Cuvettes were occasionally treated with an acid bath to remove contaminants adsorbed to the glass surface.

The buffer solutions used during the photolysis and electrophoresis experiments were prepared at standard concentrations. We found that at the standard concentrations the xylene cyanol in the dye solution migrates with the open-circular form of pUC18 (~4,000 bp) and makes visualization of the corresponding band difficult. We therefore used a loading dye containing only the faster running dye, bromophenol blue, giving superior resolution of bands by transilluminator.

Samples in optically matched 1 cm pathlength cuvettes and purged of oxygen by continuous flow of argon were photolyzed by either the xenon arc lamp or the LED. The buffer concentration during photolysis is an important consideration for cationic metal complexes, as higher ionic strengths limit electrostatic association with DNA and slow DNA photocleavage. The DNA concentration of 15.3 μM(bp) in the analyte solutions was convenient because the volume that was loaded per lane in the agarose gel, 4 μL, contained 40 ng of DNA. Loading too much DNA on the electrophoresis gel resulted in poor band resolution, streaking and pixel saturation, while too little DNA was difficult to detect by ethidium bromide staining.[165]

Agarose gel electrophoresis was employed extensively for the study of metal complex/plasmid DNA interactions because it offers a straightforward method for identifying changes in the topology of plasmid DNA.[52,69,113,166-168] The gel electrophoresis conditions used to study the photocleavage of pUC18 make it possible to examine all photoproducts of the pUC18 and $[\{(bpy)_2Ru(dpp)\}_2RhCl_2]Cl_5$ photoreaction. In these experiments, we generally see rapid and complete conversion of the supercoiled pUC18 to the open circular form.[60] Conversion of supercoiled pUC18 DNA to the open circular form is consistent scission of at least one site in the sugar-phosphate backbone of the DNA molecule, suggesting single strand photocleavage.[116]

Metal complexes can cleave DNA through a number of mechanisms including frank sugar phosphate single strand cleavage, cleavage by base modification and double strand scission.[52,69,113,114,123] Cleavage by base oxidation is typically not observed without a follow-up treatment to remove the damaged base and therefore would not be detected with this assay,

which is designed to detect frank DNA cleavage without further treatment.

The results of our DNA photocleavage assay using both a xenon arc lamp and LED array excitation are shown in Figures 3.29 and 3.30. With the use of time course photolysis studies we were able to assess completion of the photocleavage reaction as a function of photolysis time for each of the sources. Aliquots were removed at regular intervals and stored in the dark. We saw no evidence of reaction in the samples of pUC18 that were stored in the dark. Agarose gel electrophoresis was used to assay the time course photolysis studies and compare the xenon arc lamp and LED excitation. The xenon arc lamp broad spectrum source required 20 min to completely cleave pUC18 under our conditions, while the LEDs took 70 min, consistent with higher light flux of the xenon arc lamp, Figure 3.28. These data show that the LED array is a valuable light source for DNA photocleavage providing simple, inexpensive excitation that leads to the same photoreaction as the xenon arc lamp excitation.

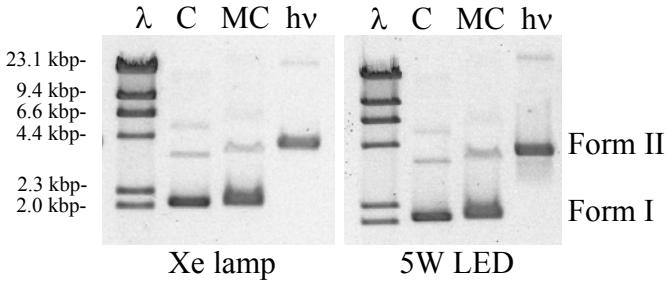

Figure 3.29. Photograph of agarose gels, stained with ethidum bromide, following loading with control and photolyte solutions and electrophoresis. The lanes of each gel are λ = Lambda DNA/*Hin*dIII molecular marker, C = pUC18 DNA (15.3 μM) control (no metal complex or photolysis), MC = pUC18 DNA incubated at room temperature in the dark with $[\{(bpy)_2Ru(dpp)\}_2RhCl_2]Cl_5$ (2.4 μM), hν = the DNA photoproduct of pUC18 DNA and MC when irradiated for 20 min with filtered xenon arc lamp light (>450 nm, left) or when irradiated for 70 min with a 5W LED (λ_{max} = 455 nm, right) under flow of argon. The band labeled Form I = native, supercoiled pUC18 DNA, while Form II = open-circular pUC18. Reproduced from Prussin, A.J.; Zigler, D. F.; Brown, J.R.; Jain, A.; Winkel, B. S. J.; Brewer, K. J. ***J. Inorg. Biochem.*** **2008,** *102,* 731-739, with permission from Elsevier.[137]

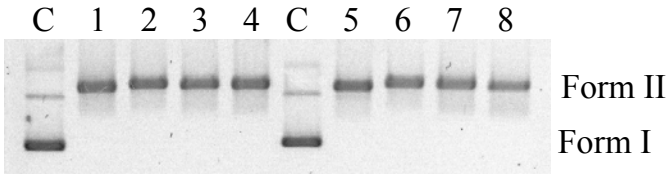

Figure 3.30. Photograph of agarose gel following electrophoresis and staining with ethidium bromide illustrating the application of our new LED array to study DNA photocleavage. C = pUC18 DNA control (no metal complex or photolysis, 15.3 μM in base pairs), 1-8 = $[\{(bpy)_2Ru(dpp)\}_2RhCl_2]Cl_5$ (2.4 μM), 70 min with 5W LED (λ_{max} = 455 nm) under flow of argon, Form I = native, supercoiled pUC18 DNA, Form II = open-circular pUC18. Reproduced from Prussin, A.J.; Zigler, D. F.; Brown, J.R.; Jain, A.; Winkel, B. S. J.; Brewer, K. J. *J. Inorg. Biochem.* **2008,** *102,* 731-739, with permission from Elsevier.[137]

3.5.4. Comments of Photocleavage of DNA with LED Light

The LED array functions well as a light source for assaying DNA photocleavage by potentially new phototherapeutic agents. While photocleavage experiments using the LED source generally took longer to reach completion, the array made it possible to perform multiple photocleavage experiments simultaneously. The high precision of the LED design was evident from identical photolysis that was carried out in each of the eight LED photolysis stations simultaneously, Figure 3.26. In addition, analysis with ImageJ showed that the deviation between pixel intensity of lanes was 9%, with no trend between individual LED stations when comparing multiple gels, Table 3.6. This result illustrates the potential of this array to be used to simultaneously assay eight different conditions for DNA photocleavage.

There are distinct advantages to both xenon arc lamp and LED array excitation for our DNA photocleavage application. The advantage of the xenon arc lamp is that it gives access to a wide spectral range with high light flux. DNA photolysis experiments using the broad spectrum xenon arc source have shorter photolysis times, eliminating potential problems common to extended photochemical experiments. The LED array also provides an inexpensive and mobile means to perform DNA photolysis experiments using monochromatic light. LED arrays are inexpensive to construct and have been shown to be reproducible light sources.[145] The design of the LED array allows for interchange of LEDs, which are commercially available in wide range of nearly monochromatic light. Further, the LED array allows photolysis of multiple analyte

solutions simultaneously, increasing the number of data points obtained and facilitating high-throughput analyses.

3.6. Mixed Metal Supramolecule Photocleavage of and Photobinding to DNA

The photochemical activity of some mixed metal supramolecules was assessed by studying their excited state interaction with DNA. The photochemistry of the mixed metal supramolecules was investigated by gel electrophoresis of and via selective precipitation of DNA photoproducts.

3.6.1. Perturbation of Circular Plasmid DNA Structure and Gel Electrophoresis

Gel electrophoresis is useful for studying single strand cleavage of supercoiled (SC) circular plasmid DNA, while also providing a means to assay other changes to the DNA's size, charge and tertiary structure. DNA migration in gel electrophoresis is governed by its size to charge ratio.[115] Frank cleavage is evidenced by direct conversion of the SC DNA to an open circular (OC) form (See for example Figure 3.27).[113] Perturbation of the DNA supercoil by either metal complex binding to the DNA or by photooxidation of the nucleobases also slows migration of the DNA in the gel, Figure 3.31.[67,123,169-171] Base oxidation relaxes the SC DNA by perturbing the base pair hydrogen bonding.[123] Metal complex binding to DNA bases also contributes to unwinding of the DNA's supercoiled tertiary structure.[125,172] Covalent binding of a positively charged metal complex to the DNA decreases its charge, decreasing the DNA's migration in gel electrophoresis.[115] Co-migration of SC and OC DNA in gel electrophoresis occurs when both forms of DNA have similar tertiary structure. Metal complexes that have multiple binding sites, like the known DNA binder *cis*-$[Pt(NH_3)_2Cl_2]$, can bind multiple adjacent bases and compress the DNA into a positive supercoil.[169] This compression causes the circular plasmid DNA to rewind and migrate in gel electrophoresis as two distinct bands, providing little evidence of strand breakage. The analogous complex $[Pt(NH_3)_3Cl]^+$ has only one labile site, thus contributes less to the unwinding of DNA upon metal complex binding.[173] Changes in the migration velocity to DNA in an electrophoresis gel, resulting from DNA unwinding, are indicative of the number of metal complex molecules bound to each plasmid DNA.[167]

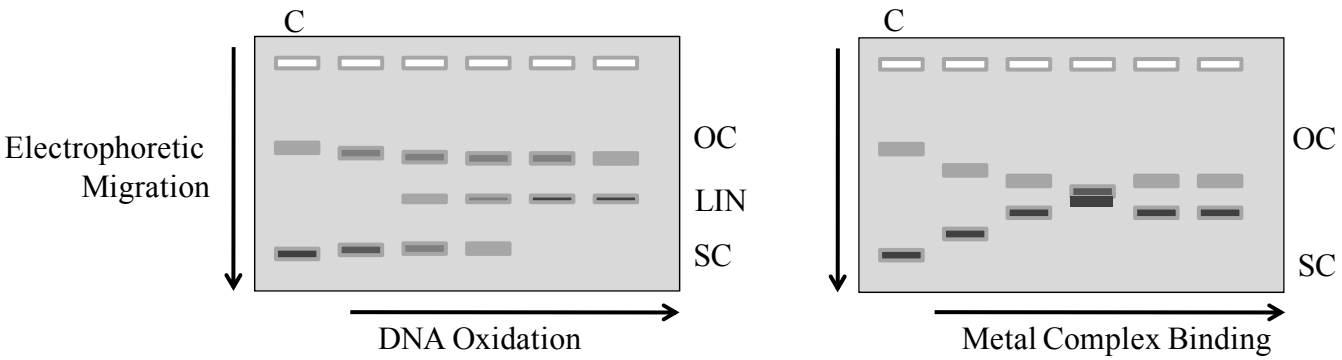

Figure 3.31. Illustrations of electrophoresis gels with circular plasmid DNA (C) following oxidative damage to the DNA (left) or metal complex binding (right). OC = nicked, relaxed circular DNA, LIN = linear plasmid DNA, SC = supercoiled circular plasmid DNA.

3.6.2. Photochemistry of New Mixed Metal Supramolecules with DNA

Agarose gel electrophoresis was used to assay the photochemistry of newly constructed mixed metal supramolecules with circular plasmid DNA, Figure 3.32. Solutions of supercoiled pUC18 DNA in buffer were photolyzed with light from a 5W LED and in the presence of either $[\{(tpy)OsCl(dpp)\}_2RhCl_2]Cl_3$ (Figure 3.32 B), $[(bpy)_2Ru(dpp)RhCl_2(phen)]Cl_3$ (Figure 3.32 C) or $[(tpy)OsCl(dpp)RhCl_2(phen)]Cl_2$ (Figure 3.31 D). The metal complexes were used as the chloride salts because these salts are more soluble in aqueous solution. Solutions were absorbance matched at 455 nm to 2.4 μM solutions of $[\{(bpy)_2Ru(dpp)\}_2RhCl_2]Cl_5$ (Figure 3.32 A). Electrophoretic migration was compared to the DNA based molecular weight marker resulting from the digestion of Lamda DNA with *Hin*dIII endonuclease (λ). Two controls were studied, C was pUC18 DNA without metal complex or photolysis and 0 was metal complex and pUC18 DNA incubated at room temperature in the dark for the duration of the photolyses. Two photolysis time regimes were examined for each metal complex, a short time regime with aliquots removed every 2 or 3 min and 15 min total photolysis time, and a long time regime with aliquots removed every 5, 10, or 20 min with total photolysis time of 60 min. The results of gel electrophoresis confirm that all of the complexes studied are photoactive toward DNA with visible light irradiation.

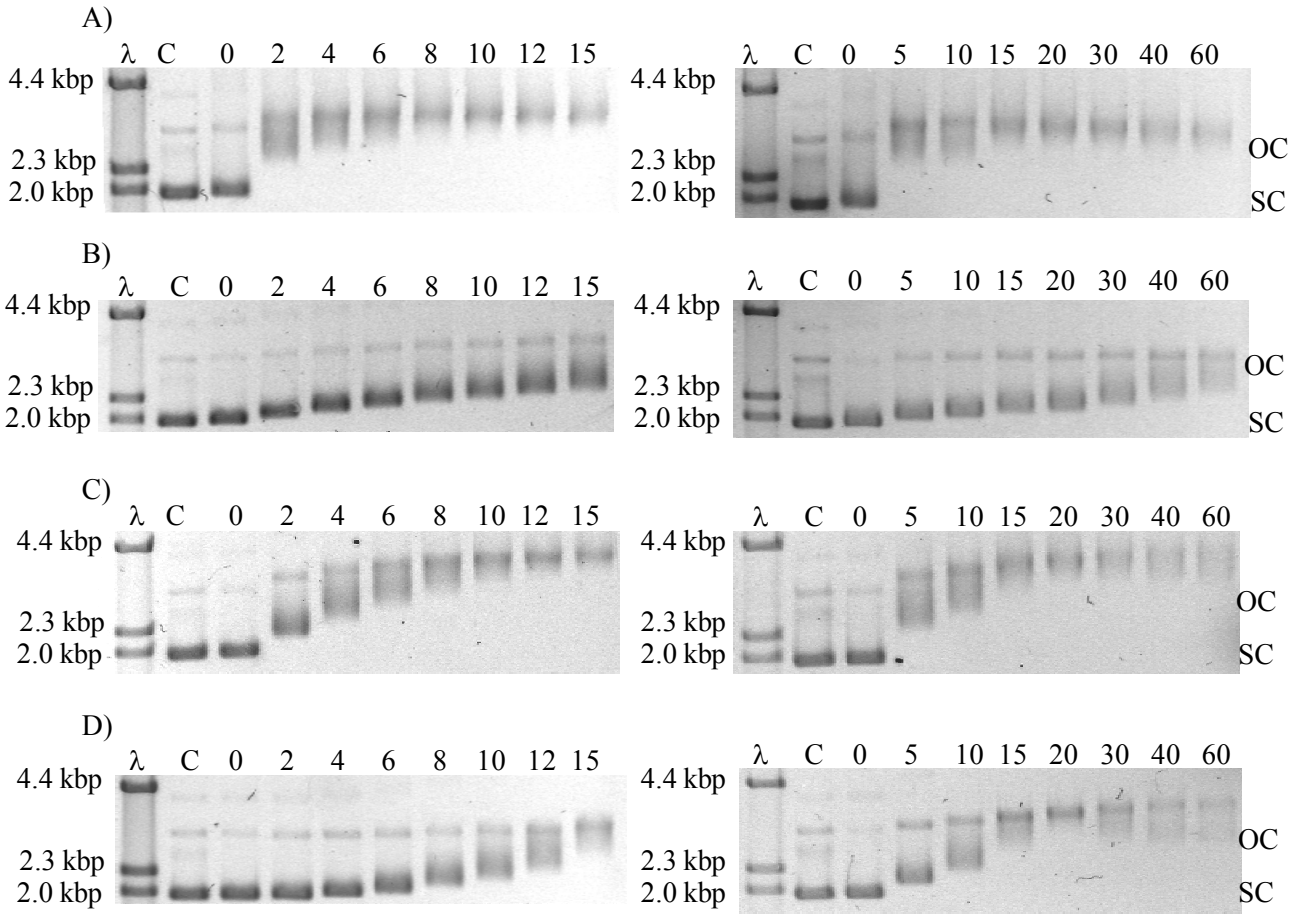

Figure 3.32. Representative electrophoresis gels assaying the DNA photochemistry of A) $[\{(bpy)_2Ru(dpp)\}_2RhCl_2]Cl_5$ (2.4 μM), B) $[\{(tpy)OsCl(dpp)\}_2RhCl_2]Cl_3$ (1.9 μM), C) $[(bpy)_2Ru(dpp)RhCl_2(phen)]Cl_3$ (4.4 μM), D) $[(tpy)OsCl(dpp)RhCl_2(phen)]Cl_2$ (3.7 μM). Solutions were absorbance matched at 455 nm. The DNA used was 15.3 μM (in base pairs) supercoiled pUC18 DNA. Photolysis was performed using 455 nm light from a 5W LED source, with continuous deoxygenation by bubbling with argon. Lane labels are λ = *Lambda* DNA/*Hin*dIII digest molecular weight marker, C is pUC18 control w/o metal complex, and numbers are the photolysis times of DNA solutions with metal complex, OC is nicked circular plasmid DNA and SC is intact supercoiled circular plasmid DNA.

The results of the gel electrophoresis assay of supercoiled circular plasmid DNA following photolysis with the mixed metal supramolecules may suggest that the metal complexes studied react by multiple photochemical pathways. As reported previously, extended photolysis of pUC18 DNA in the presence of $[\{(bpy)_2Ru(dpp)\}_2RhCl_2]Cl_5$, photolysis time > 10 min, resulted in a single band migrating more slowly than SC pUC18 consistent with its OC form, Figure 3.32A.[60] Photoproducts at shorter photolysis time were not consistent with the dark controls, lacking a band corresponding to native SC DNA and suggesting efficient

photochemistry resulting in perturbation of the tertiary structure of pUC18 DNA. These samples taken at earlier photolysis times gave results by gel electrophoresis consistent with more photochemistry than only a frank photocleavage event. As photolysis time was increased, the DNA photoproduct migration was consistent with SC pUC18 with perturbed tertiary structure. The electrophoresis gel did not indicate a change to the DNA following continued photolysis with $[\{(bpy)Ru(dpp)\}_2RhCl_2]Cl_5$ (>15 min), suggesting that any additional photochemistry did not significantly alter the tertiary structure of the plasmid DNA. In addition, the same amount of DNA was loaded into each lane for each sample and the gels were stained under identical conditions. The intensity of the ethidium bromide emission by the DNA photoproduct bands in the gel diminished for the samples photolyzed at longer times. DNA band intensity results from enhanced emission of DNA intercalated ethidium bromide. Changes to the DNA structure that impact the ability of ethidium bromide to intercalate the DNA, species capable of quenching the ethidium emission (by intermolecular excited energy transfer or electron transfer) and metal complex bonding can all decrease the DNA band intensity. Migration of DNA in gel electrophoresis inconsistent with frank photocleavage and quenching of ethidium emission relative to controls are hallmarks of metal complex bound to the DNA.[67,173] The results of the gel electrophoresis assay support DNA photocleavage by the metal complex $[\{(bpy)_2Ru(dpp)\}_2RhCl_2]Cl_5$. Observation of bands between the SC and OC form at 2 or 4 minutes of photolysis were not consistent with simple frank cleavage and suggest perhaps another operative photochemical mechanism.

Gel electrophoresis following photolysis of $[\{(tpy)OsCl(dpp)\}_2RhCl_2]Cl_3$ with pUC18 DNA indicates a lower quantum efficiency for DNA photomodification versus $[\{(bpy)_2Ru(dpp)\}_2RhCl_2]Cl_5$, Figure 3.32 A versus B. The decreased quantum yield of DNA photomodification for the Os,Rh,Os complex versus the Ru,Rh,Ru triad was not unexpected due to the likely shorter lived ^{3}MLCT state populated with visible light excitation. Products at shorter photolysis times were observed as two bands. The faster band was broad and intense, consistent with modified, unnicked DNA, while the slower, faint band was consistent with OC pUC18. Interestingly, as photolysis time was increased, the band corresponding to nicked pUC18 (OC) intensified independently of changes to the migration of the other form(s) of pUC18. The observation of the OC band intensification was consistent with the photocleavage of SC pUC18 DNA. The electrophoretic migration of the OC and SC bands both changed with

photolysis, consistent with modification to the DNA's tertiary structure. Changes to the tertiary structure of the DNA can be induced by different modifications such as DNA binding or oxidative damage to the DNA. Oxidative damage to the DNA tends to give predicatable electrophoresis results since the changes to the DNA tertiary structure typically do not involve significant change in the DNA's mass to charge ratio. This result means that photooxidized OC DNA tends to migrate in the gel with greater velocity than unmodified OC DNA. The OC band from the experiments herein, however, has decreased electrophoretic mobility as a result of visible light photolysis with $[\{(tpy)OsCl(dpp)\}_2RhCl_2]Cl_3$. Therefore, gel electrophoresis results of the pUC18 DNA/$[\{(tpy)OsCl(dpp)\}_2RhCl_2]Cl_3$ photoproducts support both photocleavage of the DNA backbone and photobinding of the positively charged metal complex to the DNA.

Gel electrophoresis results for the photolysis of $[(bpy)_2Ru(dpp)RhCl_2(phen)]Cl_3$ and pUC18 DNA indicated possible alternate photomodification versus the trinuclear species, Figure 3.32 C. At about 15 min of photolysis time, the DNA/metal complex photoproducts co-migrated by gel electrophoresis. Co-migration of DNA photoproducts suggested them to have similar size to charge ratios. Compared to the Ru,Rh,Ru triad, the quantum efficiency of DNA photomodification was similar when considering the photolysis time to reach coalescence (an indication of average photochemical events), Figure 3.32 A versus C. Slight differences were observed at 2 and 4 min, with the photoproduct of pUC18 with $[(bpy)_2Ru(dpp)RhCl_2(phen)]Cl_3$ resolved as two bands while the early time photoproducts with the Ru,Rh,Ru triad were unresolved. The electrophoretic mobility of DNA photoproducts with the Ru,Rh,Ru at photolysis times greater than 20 minutes appeared to be similar, while continued photolysis of pUC18 DNA with the Ru,Rh dyads caused broadening of the photoproducts band. Band broadening is indicative of closed circular plasmid DNA that has not been nicked, but has additional changes to tertiary structure as a result of continued photochemistry. The decreased electrophoretic migration of the DNA photoproduct versus both SC and OC DNA controls supports metal complex photobinding DNA that does not necessarily involve photomodification by cleavage or oxidation, behavior unique compared to the trimetallic.

The results of gel electrophoresis of the DNA/MC photoproduct when photolyzed in the presence of or $[(tpy)OsCl(dpp)RhCl_2(phen)]Cl_2$ indicated DNA photomodification efficiencies similar to the Ru,Rh dyad, Figure 3.32 C versus D. Like the photoproducts of the Ru,Rh dyad, co-migration of photoproducts was observed after about 20 min of visible light photolysis. This

is in contrast to gel electrophoresis results following photolysis of DNA with $[\{(tpy)OsCl(dpp)\}_2RhCl_2]Cl_3$ which suggested inefficient DNA photomodification, Figure 3.32 B versus D. Also similar to the Ru,Rh dyad, photoproducts with the Os,Rh dyad indicated divergence of electrophoretic mobility with continued photolysis. In contrast to $[(bpy)_2Ru(dpp)RhCl_2(phen)]Cl_3$, DNA photoproducts migrated in the gel as two reasonably well resolved bands at photolysis times up to about 10 minutes, indicating decreased photochemical efficiency due to a likely shorter lived ^{3}MLCT state for $[(tpy)OsCl(dpp)RhCl_2(phen)]Cl_2$. Also, photolysis at 60 min gave photoproducts migrating in the gel as two faint, poorly resolved bands, whereas photoproducts with the Ru,Rh dyad gave a single broad DNA band. The photochemical mechanism(s) for DNA photomodification might be similar for $[(bpy)_2Ru(dpp)RhCl_2(phen)]Cl_3$ and $[(tpy)OsCl(dpp)RhCl_2(phen)]Cl_2$, but differing observations by gel electrophoresis might be due to lower positive charge on the Os,Rh dyad.

Significant new observations have been made concerning the change to the electrophoretic mobility of pUC18 DNA when photolyzed with the title mixed metal supramolecules. Early observations showed that after photolysis of pUC18 DNA with $[\{(bpy)_2Ru(dpp)\}_2RhCl_2]Cl_5$ a single, well resolved was obtained by gel electrophoresis.[60] This band, whose electrophoretic migration was significantly reduced relative to the native SC control, was concluded to OC DNA resultant from frank single strand cleavage. Previous studies did not report the changes to electrophoretic migration at shorter photolysis times, and therefore missed more complicated photochemical behavior as evidenced by gel electrophoresis. The current gel electrophoresis results assaying DNA/MC photoproducts indicate changes to the DNA's tertiary supporting more than just DNA photocleavage. DNA migrating between the SC and OC DNA controls could result from DNA oxidation or metal complex photobinding to DNA. DNA photoproducts migrating in the gel slower than the OC band indicates decreased size to charge of the photoproduct, consistent with positively charge metal complex bound to the DNA. Consistent with previous reports, photolysis of pUC18 in the presence of $[\{(bpy)_2Ru(dpp)\}_2RhCl_2]Cl_5$ results in rapid photomodification of the DNA, though DNA migrating between SC and OC forms is noted at shorter photolysis times. The quantum efficiency of DNA photomodification by $[\{(tpy)OsCl(dpp)\}_2RhCl_2]Cl_3$ is significantly reduced relative to the Ru,Rh,Ru triad, likely due to a shorter lived ^{3}MLCT state for the Os complex. Both $[(bpy)_2Ru(dpp)RhCl_2(phen)]Cl_3$ and $[(tpy)OsCl(dpp)RhCl_2(phen)]Cl_2$ have similar DNA

photomodification efficiencies, with both requiring ca. 20 min of photolysis to give co-migrating pUC18 DNA/MC photoproducts. Contrary to $[\{(bpy)_2Ru(dpp)\}_2RhCl_2]Cl_5$, the dyads have evidence by gel electrophoresis of continued photochemistry at photolysis times greater than 20 min. Additional changes to the DNA's tertiary structure can possibly be attributed to photobinding of the bimetallic complexes enhanced relative to photocleavage. Enhanced photobinding might be due the less sterically encumbered *cis*-$Rh^{III}Cl_2$ center of the bimetallic complexes versus the trimetallics.

3.6.3. Assaying the Photobinding of $[\{(tpy)OsCl(dpp)\}_2RhCl_2]Cl_3$ to DNA

The mixed metal complex $[\{(tpy)OsCl(dpp)\}_2RhCl_2]Cl_3$ was studied further to assay potential photobinding to DNA. The metal complex $[\{(tpy)OsCl(dpp)\}_2RhCl_2]Cl_3$ produced the smallest change in DNA migration as a function of photolysis time relative to $[\{(bpy)_2Ru(dpp)\}_2RhCl_2]Cl_5$, $[(bpy)_2Ru(dpp)RhCl_2(phen)]Cl_3$ and $[(tpy)OsCl(dpp)RhCl_2(phen)]Cl_2$.

DNA photobinding experiments were adapted from previously reported procedures.[174] Calf thymus DNA was photolyzed in the presence of $[\{(tpy)OsCl(dpp)\}_2RhCl_2]Cl_3$ with light from a 5W 455 nm light emitting diode (LED). DNA was selectively precipitated by adding 5M NaCl and 95% ethanol to an aliquot of the photolysis solution. Following vortex stirring and centrifugation, a portion of the resulting supernatant was added to deionized water and the absorbance at 530 nm was measured. The change in supernatant absorbance is presented in Figure 3.33.

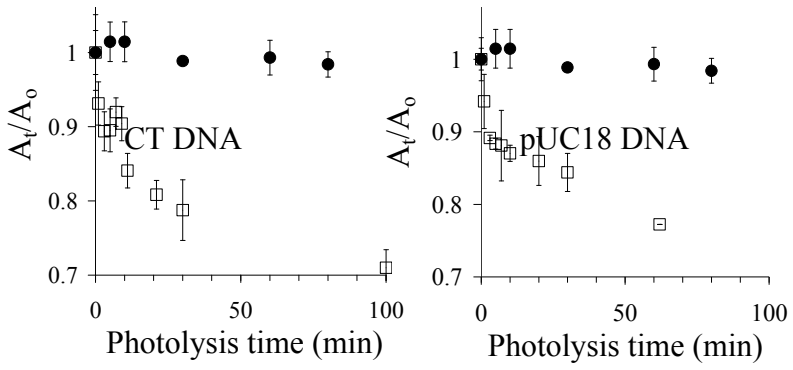

Figure 3.33. Plot of absorbance at 530 nm versus time of $[\{(tpy)OsCl(dpp)\}_2RhCl_2]Cl_3$ (27 μM initial concentration) remaining in the ethanolic supernatant following photolysis and selective precipitation of calf thymus DNA (CT, left) or pUC18 DNA (right) (each at 120 μM,). Samples were photolyzed with 455 nm light from a 5W LED, tpy = 2,2':6',2"-terpyridine, dpp = 2,3-bis(2-pyridyl)pyrazine. Sample points (□) are compared to a dark control (●). Values are the average of at least 4 separate experiments, with standard deviation error bars.

The metal complex $[\{(tpy)OsCl(dpp)\}_2RhCl_2]Cl_3$ that precipitate with the DNA increased with increasing photolysis time. The absorbance of the photolyte solutions did not change during photolysis indicating that the photoproducts were soluble in aqueous 55 mM NaH_2PO_4 buffer. After selective precipitation of the DNA, however, the amount of metal complex remaining in the supernatant decreased with photolysis time, Figure 3.33. At longer photolysis times, the concentration of the metal complex remaining in the supernatant approached ~70% of the original value. This spectroscopically observed endpoint of photobinding is consistent with saturation of the major grove of the DNA with $[\{(tpy)OsCl(dpp)\}_2RhCl_2]Cl_3$ spanning 10 to 12 base pairs (3 nm). Preliminary photobinding experiments using the more expensive pUC18 DNA were concluded to allow direct comparison of the spectroscopic precipitation study with a gel electrophoresis assay. This pUC18 study gave an A_t/A_o vs. t plot within error of the plot generated using CT DNA. The results of a gel electrophoresis assay of pUC18 when photolyzed at 120 μM(bp) in the presence of 27 μM metal complex and in 55 mM NaH_2PO_4 is shown in Figure 3.34. Interestingly, intensification of the OC band was seen upon photolysis as well as a change in the migration of the SC band. This supports two mechanisms of action, frank photocleavage and also photobinding of the metal complex. The results vary slightly compared to the gel shown in Figure 3.32 B, but this variance is attributable to changes to the photolysis conditions required for the precipitation studies versus the gel electrophoresis studies. This implies that these complexes have quite complicated photochemical kinetics, involving terms not just for reactant concentration, but also for ionic strength.

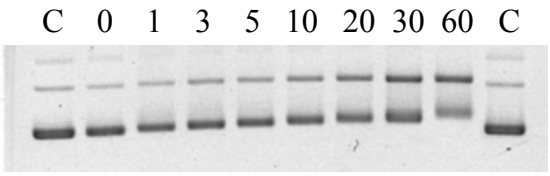

Figure 3.34. Electrophoresis gel of pUC18 DNA (120 μM bp) when photolyzed with 455 nm light from a 5W LED and in the presence of $[\{(tpy)OsCl(dpp)\}_2RhCl_2]Cl_3$ (27 μM) in aqueous NaH_2PO_4 buffer (55 mM). C = pUC18 DNA control. The photolysis solutions were more concentrated compared to the experiments giving the gel electrophoresis results in Figure 3.30 B. Numbers indicate photolysis time with metal complex in minutes and are aliquots removed during the photobinding study (see Figure 3.31, pUC18).

3.6.4. Proposed Mechanism of Supramolecular Photochemistry with DNA

Photolysis experiments of the mixed metal complexes $[\{(bpy)_2Ru(dpp)\}_2RhCl_2]Cl_5$, $[\{(tpy)OsCl(dpp)\}_2RhCl_2]Cl_3$, $[(bpy)_2Ru(dpp)RhCl_2(phen)]Cl_3$ and $[(tpy)OsCl(dpp)RhCl_2(phen)]Cl_2$ with DNA suggest that these complexes react by multiple photochemical mechanisms. Precipitation studies of $[\{(tpy)OsCl(dpp)\}_2RhCl_2]Cl_3$ suggest covalent binding of the metal complex to DNA following photolysis. Gel electrophoresis suggests that the four mixed metal complexes studied covalently bind to the DNA, Figure 3.32, supported by early results from a DNA/metal complex precipitation study, Figure 3.33. Covalent binding of the bimetallics and trimetallics upon photolysis to DNA suggests photo-induced chloride loss from the *cis*-$Rh^{III}Cl_2$ moiety of these complexes.[57] Both a Rh centered ^{3}LF state and a ^{3}MMCT state could be labile toward chloride substitution, providing viable electronic excited state decay pathways leading to the supramolecules photobinding to DNA. Photocleavage of the DNA, however, is expected to be solely from a ^{3}MMCT excited state. Gel electrophoresis of the photoproducts supports photocleavage of DNA by the mixed metal complexes in addition to photobinding. The relative quantum efficiency for DNA photocleavage versus DNA photobinding, as suggested by gel electrophoresis, however is blurred by effects such as co-migration of photoproducts in the gel and quenching of ethidium emission. A general state diagram for the mixed metal complexes is proposed based on the results of the photochemical experiments, Figure 3.35. The energy of the proposed Rh centered ^{3}LF state (14,100 cm^{-1}) is estimated from the known emission of $[(dpp)_2RhBr_2](PF_6)$ (707 nm)[33] and of $[(dpp)_2RhCl_2](PF_6)$ (704 nm)[73] in 77 K glass.

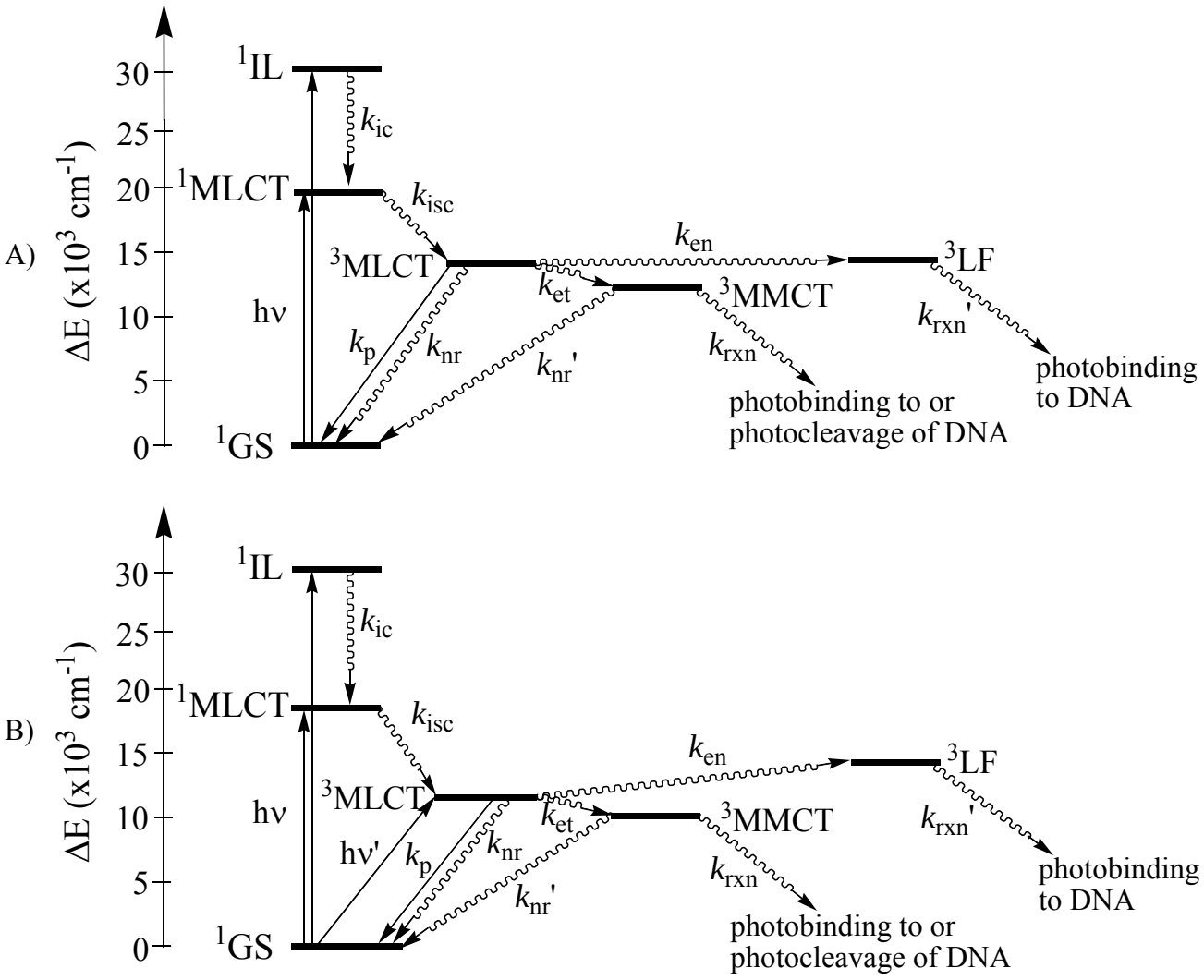

Figure 3.35. Proposed state diagram applicable to the mixed metal complexes A) $[\{(bpy)_2Ru(dpp)\}_2RhCl_2]Cl_5$ and $[(bpy)_2Ru(dpp)RhCl_2(phen)]Cl_3$, and B) $[\{(tpy)OsCl(dpp)\}_2RhCl_2]Cl_3$ and $[(tpy)OsCl(dpp)RhCl_2(phen)]Cl_2$. Relative state energies are approximate and estimated from the complexes' electronic spectroscopy. bpy = 2,2'-bipyridine, dpp = 2,3-bis(2-pyridyl)pyrazine, ^{1}GS = singlet electronic ground state, ^{1}MLCT = singlet metal to ligand charge transfer, ^{3}MLCT = triplet MLCT, ^{1}IL = singlet internal ligand, ^{3}MMCT = triplet Ru(dπ)→Rh(dσ*) metal to metal CT, and ^{3}LF = Rh centered triplet ligand field excited state.

Chapter 4: Conclusions and Future Directions

Mixed metal supramolecules were synthesized, characterized and studied by electrochemistry, electronic absorption spectroscopy, luminescence spectroscopy, and transient absorption spectroscopy. A new structural motif was created during the course of this work incorporating a *cis*-$Rh^{III}Cl_2$ site bridged by a polyazine ligand to a single Ru^{II} or Os^{II} polyazine light absorber. Development of this structural motif provides a general synthetic methodology and this motif represents a series of simplified molecular systems that will allow more detailed analysis of excited state properties and reactivity. Supramolecules with the new architecture, $[(bpy)_2Ru(bpm)RhCl_2(phen)](PF_6)_3$, $[(bpy)_2Ru(dpp)RhCl_2(phen)](PF_6)_3$, $[(bpy)_2Os(dpp)RhCl_2(phen)](PF_6)_3$ and $[(tpy)OsCl(dpp)RhCl_2(phen)](PF_6)_2$, displayed electronic absorption properties that were remarkably similar to their trimetallic analogs, $[\{(bpy)_2Ru(bpm)\}_2RhCl_2](PF_6)_5$, $[\{(bpy)_2Ru(dpp)\}_2RhCl_2](PF_6)_5$, $[\{(bpy)_2Os(dpp)\}_2RhCl_2](PF_6)_5$ and $[\{(tpy)OsCl(dpp)\}_2RhCl_2](PF_6)_3$. The electrochemical properties of the bimetallic complexes were also similar to the trimetallic analogs. The complex $[(bpy)_2Ru(bpm)RhCl_2(phen)](PF_6)_3$ displays a bpm based first reduction, consistent with a bridging ligand localized lowest unoccupied molecular orbital (LUMO). Reductions further negative are consistent with occupation of higher lying Rh($d\sigma^*$) orbitals. The dpp bridged complexes all have electrochemistry consistent a Rh($d\sigma^*$) LUMO suggesting low lying Ru($d\pi$)-Rh($d\sigma^*$) charge transfer (^{3}MMCT) states. Excited state emission spectroscopy indicated that the complexes $[\{(bpy)_2Ru(dpp)\}_2RhCl_2](PF_6)_5$ and $[(bpy)_2Ru(dpp)RhCl_2(phen)](PF_6)_3$ have an emissive electronic excited state consistent with a quenched ^{3}MLCT state. The lifetime of this state at room temperature was surprisingly similar for the Ru,Rh,Ru triad and Ru,Rh dyad, indicating little impact of the additional light absorber on the photophysical properties of theses complexes. The emissive excited states of both mixed metal complexes also had similar lifetimes at 77K in alcoholic glass. Transient absorption spectroscopy supported assignment of the emissive electronic excited state to a ^{3}MLCT state when compared to $[(bpy)_2Ru(dpp)Ru(bpy)_2](PF_6)_4$, a model complex lacking the *cis*-$Rh^{III}Cl_2$ moiety. The shorter ^{3}MLCT state lifetime measured for the Ru,Rh,Ru triad and Ru,Rh dyad versus the model Ru,Ru complex suggests the mixed metal complexes possess a low lying electronic excited state that deactivates the ^{3}MLCT state. Electrochemistry showing a Ru^{II} based first oxidation and Rh^{III} based reduction supports a low lying ^{3}MMCT state that can be populated by intramolecular

electron transfer from a ^{3}MLCT state.

Methods of inducing DNA photocleavage by a mixed-metal supramolecular complex were tested using light from either a filtered xenon arc lamp or a 5W LED. In these experiments, agarose gel electrophoresis was used to assay the extent of photocleavage induced using these two light sources. The analyte solution concentrations and photolysis conditions proved to be generally applicable, regardless of the excitation source. A multi-station LED array was designed and constructed that allowed use of commercially available, absorbance matched, 1 cm cuvettes for the performance of multiple photochemical experiments at once. This is especially important for DNA studies as it allows simultaneously analysis of all samples. The methods described have general applicability to qualitatively assay photocleavage of supercoiled pUC18 DNA, even under anaerobic conditions.

The known photochemistry of the complex $[\{(bpy)_2Ru(dpp)\}_2RhCl_2]Cl_5$ with DNA was explored further and compared to the new complexes $[\{(tpy)OsCl(dpp)\}_2RhCl_2]Cl_3$, $[(bpy)_2Ru(dpp)RhCl_2(phen)]Cl_3$, and $[(tpy)OsCl(dpp)RhCl_2(phen)]Cl_2$. In addition to the previously described photocleavage of supercoiled (SC) plasmid DNA, evidence to suggest photobinding to DNA was observed. Photolysis of SC pUC18 DNA in the presence of mixed metal supramolecules causes DNA migration in gel electrophoresis consistent with metal complex covalently bound to DNA. Following photolysis in the presence of calf thymus DNA or pUC18 DNA and selective precipitation of the DNA photoproducts, the concentration of $[\{(tpy)OsCl(dpp)\}_2RhCl_2]Cl_3$ remaining in solution decreased with photolysis time, also supporting photobinding to DNA. Two proposed low lying electronic excited states, ^{3}MMCT or ^{3}LF, could be expected to be labile toward Cl^- substitution, facilitating DNA photobinding. The ^{3}MMCT, with a formally reduced Rh center and oxidized Ru or Os center, is likely the reactive electronic excited state responsible for the observed photocleavage of DNA.

4.1. Future Directions

Mixed metal supramolecules like those presented herein show efficient photochemistry with DNA, making them interesting biologically relevant photochemicals. In addition, mixed metal complexes such as these generate hydrogen photocatalytically from water and an electron donor. Questions remain regarding these molecules redox properties, basic photochemical function and their photophysical properties. Future work aims to explore basic physical

properties of polyazine bridged mixed metal dyads such as those above and to investigate their applications in photochemical and photobiological realms.

The research presented in this dissertation unveils many questions. The new bimetallic structural motif allows for the facile tuning of the Rh center by variation of the terminal ligand now bound to this site. Studies are underway to examine the effect of exchanging the terminal phenanthroline ligand with other chelating polyazine ligands to assess their impact on the observed electrochemical, photophysical and photochemical properties of these complexes. In addition, the *cis*-$Rh^{III}Cl_2$ attached to terminal polyazine ligands that have aliphatic protons or other NMR active labels would be useful in understanding the mixed metal dyads' architecture, and geometric and diastereomeric distributions. We might better understand the effect that the structure around the rhodium center has on the orbital energetics of the supramolecule as a whole. Further, better knowledge about the structure of these complexes could improve the understanding of the mode of photochemistry, e.g. photomodification of DNA. One strategy to reach a diastereomerically defined supramolecule might employ the reaction of two structurally defined subunits, Figure 4.1, achieved by chiral separation of $[(BL)RhCl_2(TL)]^+$ into enantiomers prior to reaction with a single enantiomer of $[(TL)_2RuCl_2]$.

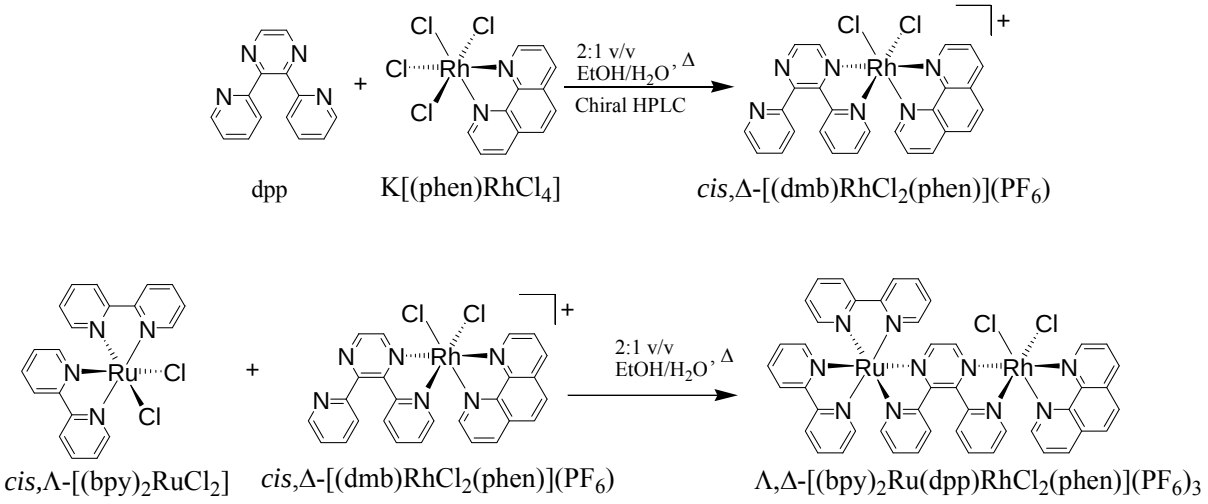

Figure 4.1. Proposed synthetic strategy to produce stereochemically defined polyazine bridged mixed metal supramolecules.

The electrochemical properties of the bimetallic complexes, though similar to those of the trimetallic analogs, require further examination of the associated electrochemical mechanism. Some of the electrochemical experiments include extending the variable scan rate studies,

studying the impact of solvent on electrochemical processes, more in depth spectroelectrochemical studies and a continuation of controlled potential electrolysis experiments to analyze the electrochemical products by ESI mass spectrometry. Together these may allow for study of key redox products that may be important in applications of these complexes.

The photophysical properties of the complexes need to be evaluated for the complexes other than $[\{(bpy)_2Ru(dpp)\}_2RhCl_2](PF_6)_5$ and $[(bpy)_2Ru(dpp)RhCl_2(phen)](PF_6)_3$. Complexes without measureable emissive electronic excited states can be studied using transient absorption spectroscopy. Transient absorption spectroscopy is also useful for investigating the changes to the electronic excited states in different solvent environments and in the presence of various quenchers, including DNA. Reductive quenchers such as *N*,*N*-dimethylaniline are especially interesting for transient absorption quenching studies because the radical redox products tend to have characteristic electronic absorption spectra and known decomposition pathways. Identifying the metal complex redox products from these reactions is key to understanding the complexes' photochemistry, including reactions resulting in photocleavage or photooxidation of DNA.

Particularly interesting is the nature of the Rh based electrochemical and photophysical properties. Currently, few model complexes are available to compare the electrochemistry and photophysics of polyazine bridged mixed metal complexes. Complexes composed of two rhodium subunits sharing a ligand bridge, i.e. $[(TL)RhCl_2(BL)RhCl_2(TL)]^{2+}$, could posses interesting electrochemical and photophysical properties that better characterize the orbital energetics and electronic excited state properties of the heteroleptic Rh center. These complexes possess analogous components to the heterometallic dyads, but lack the visible light absorbing subunit. A Rh,Rh dyad could be studied in solid solution at 77 K to observed low lying, emissive ligand field states like those proposed above. Additionally, weakly absorbing transitions in the UV region that are normally swamped by intense Ru^{II} or Os^{II} based MLCT transitions could be characterized. The comparison between the Rh,Rh dyad and well known monometallic Rh^{III} polyazine complexes such as *cis*-$[(phen)_2RhCl_2]^+$ could provide insight into the excitation pathways giving rise to the observed photochemistry with DNA.

Given the interesting preliminary results of DNA photochemistry, these complexes are potentially interesting in photo-induced cell killing schemes. The complexes $[\{(bpy)_2M(dpp)\}_2RhCl_2]Cl_5$, M = Ru^{II} or Os^{II}, kill cells with photolysis, but do not impede cell

growth in the absence of light, Figure 4.2.[175] The Ru,Rh,Ru and Os,Rh,Os complexes also are efficient at DNA photomodification.[60,79] Complexes with the new molecular architecture should also be investigated for their photobiological activity. Their efficient photomodification of DNA as observed with gel electrophoresis supports their function as DNA photokilling agents. Related to these studies would be photo-killing studies examining cytospecificity (cancer cell lines), cellular uptake and cellular metabolism of these complexes. General knowledge of cellular uptake and metabolism gives hints to the *in vivo* stability of these complexes and their retention time within an organism.

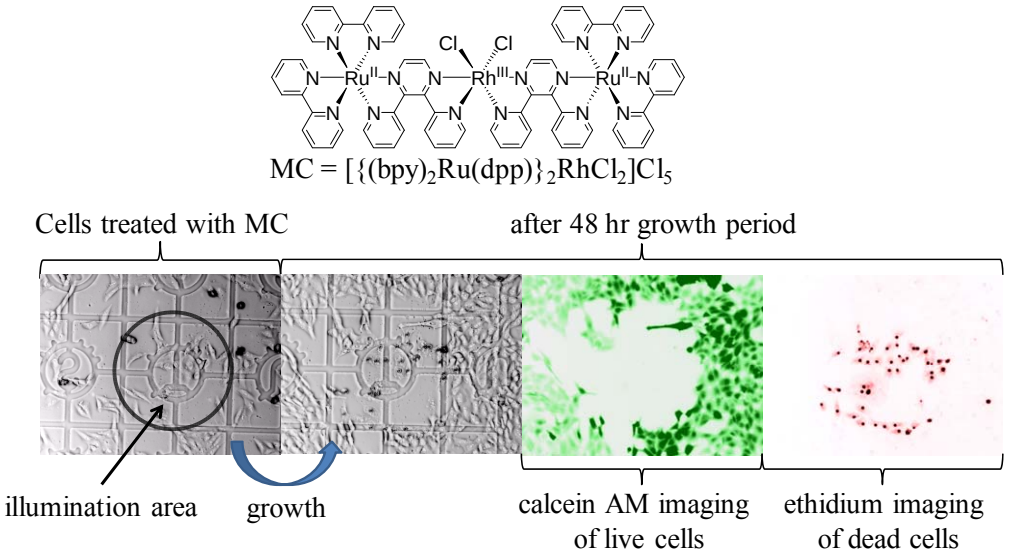

Figure 4.2. Micrographs of *Vero* cells pretreated with $[\{(bpy)_2Ru(dpp)\}_2RhCl_2]Cl_5$, rinsed, and illuminated with 400-1000 nm light showing the high level of light activated cell killing [bpy = 2,2'-bipyridine, dpp = 2,3-bis(2-pyridyl)pyrazine]. (from left to right) Immediately after photolysis (light exposure within circle); after 48 hour growth period; live cell (green) visualized with calcein AM fluorescent dye; dead cell (red) visualized with ethidium homodimer-1 fluorescent dye. Reproduced from Zigler, D.F.; Brewer, K.J. "Toward Photodynamic Therapy of Cancer with Platinum Group Metal Polyazine Complexes" in *Metal-Complexes-DNA Interactions*, Wiley-Blackwell, In press, with permission from Wiley-Blackwell.[48]

Additional studies should be performed to assess the feasibility of polyazine bridged mixed metal supramolecules as photodynamic therapy agents. Animal trials can be used to assess their general toxicity, stability *in vivo* and initial treatment regimes. Animal trials will also give insight into retention time within the body. Photofrin®, a commonly used PDT agent, suffers from the fact that it has only about a two-fold increase in toxicity upon irradiation with

visible light. Passage of the drug also is very slow, leaving PDT patients treated with Photofrin® sensitive to light for up to 8 weeks. Photofrin® is a neutral, fat soluble compound that has slow passage from the body. Charged species such as the title supramolecules offer an alternate molecular architecture with significant charge that would not likely build up in fat stores as readily as Photofrin®.

References

1. Balzani, V.; Scandola, F. "Photophysical and photochemical devices" In *Comprehensive Supramolecular Chemistry*; Reinhoudt, D. H., Ed.; Permagon: New York, 1996; Vol. 10, p 687-746.
2. Balzani, V.; Moggi, L.; Scandola, F. "Towards a supramolecular photochemistry: Assembly of molecular component to obtain photochemical molecular devices" In *Supramolecular Photochemistry*; Balzani, V., Ed.; D. Reidel Publishing Company: 1987, p 1-28.
3. Balzani, V.; Credi, A.; Venturi, M. "Photochemical conversion of solar energy" *Chem. Sus. Chem.* **2008**, *1*, 26-58.
4. Balzani, V.; Juris, A.; Venturi, M.; Campagna, S.; Serroni, S. "Luminescent and Redox-Active Polynuclear Transition Metal Complexes" *Chem. Rev.* **1996**, *96*, 759-834.
5. Campagna, S.; Puntoriero, F.; Nastasi, F.; Bergamini, G.; Balzani, V. "Photochemistry and photophysics of coordination compounds: Ruthenium" *Top. Curr. Chem.* **2007**, *280*, 117-214.
6. Kumaresan, D.; Shankar, K.; Vaidya, S.; Schmehl, R. H. "Photophysics and photochemistry of coordination compounds: Osmium" *Top. Curr. Chem.* **2007**, *281*, 101-142.
7. Indelli, M. T.; Chiorboli, C.; Scandola, F. "Photochemistry and photophysics of coordination compounds: Rhodium" *Top. Curr. Chem.* **2007**, *280*, 215-255.
8. Allison, R. R.; Downie, G. H.; Cuenca, R.; Hu, X.-H.; Childs, C. J. H.; Sibata, C. H. "Photosensitizers in clinical PDT" *Photodiagn. Photodyn. Ther.* **2004**, *1*, 27-42.
9. Caspar, J. V.; Kober, E. M.; Sullivan, B. P.; Meyer, T. J. "Application of the Energy Gap Law to the Decay of Charge-Transfer Excited States" *J. Am. Chem. Soc.* **1982**, *104*, 630-632.
10. Englman, R.; Jortner, J. "The energy gap law for radiationless transitions in large molecules" *Mol. Phys.* **1970**, *18*, 145-164.
11. Triesscheijn, M.; Baas, P.; Schellens, J. H. M.; Stewart, F. A. "Photodynamic therapy in oncology" *Oncologist* **2006**, *11*, 1034-1044.
12. Ali, H.; van Lier, J. E. "Metal complexes as photo- and radiosensitizers" *Chem. Rev.* **1999**, *99*, 2379-2450.
13. Szacilowski, K.; Macyk, W.; Drzewiecka-Matuszek, A.; Brindell, M.; Stochel, G. "Bioinorganic photochemistry: Frontiers and mechanisms" *Chem. Rev.* **2005**, *105*, 2647-2694.
14. Kalyanasundaram, K. *Photochemistry of Polypyridine and Porphyrin Complexes*; Academic Press: San Diego, 1992.
15. Kew, G.; DeArmond, K.; Hanck, K. ""Electrochemistry of Rhodium-Dipyridyl Complexes"" *J. Phys. Chem.* **1974**, *78*, 727-734.
16. Roffia, S.; Ciano, M. "Voltammetric behaviour of dichlorobis(2,2'-bipyridine)iridium(III) and dichlorobis(1,10-phenanthroline)iridium(III) complexes" *J. Electroanal. Chem.* **1978**, *87*, 267-274.
17. Kahl, J. L.; Hanck, K. W.; DeArmond, K. "Electrochemistry of iridium-bipyridine complexes" *J. Phys. Chem.* **1978**, *82*, 540-545.
18. Bard, A. J.; Faulkner, L. R. *Electrochemical Methods: Fundamentals and Applications*; Second ed.; John Wiley & Sons, Inc.: New York, 2001.

19. Nicholson, R. S.; Shain, I. "Theory of stationary electrode polarography: Single scan and cyclic methods applied to reversible, irreversible and kinetic systems" *Anal. Chem.* **1964**, *36*, 706-723.
20. Smith, W. H.; Bard, A. J. "Electrochemical reactions of organic compounds in liquid ammonia. II. Nitrobenzene and nitrosobenzene" *J. Am. Chem. Soc.* **1975**, *97*, 5203-5210.
21. Juris, A.; Balzani, V.; Barigletti, F.; Campagna, S.; Belser, P.; Von Zelewsky, A. "Ru(II) polypyridine complexes photophysics, photochemistry, electrochemistry, and chemiluminescence" *Coord. Chem. Rev.* **1988**, *84*, 85-277.
22. Johnson, S. R.; Westmoreland, T. D.; Caspar, J. V.; Barqawi, K. R.; Meyer, T. J. ""Influence of variations in the chromophoric ligand on the properties of metal-to-ligand charge-transfer excited states"" *Inorg. Chem.* **1988**, *27*, 3195-3200.
23. Elliot, C. M.; Hershenhart, E. J. "Electrochemical and spectral investigations of ring-substituted bipyridine complexes of ruthenium(II)" *J. Am. Chem. Soc.* **1982**, *104*, 7519-7526.
24. Kober, E. M.; Caspar, J. V.; Sullivan, B. P.; Meyer, T. J. "Synthetic Routes to New Polypyridyl Complexes of Osmium(II)" *Inorg. Chem.* **1988**, *27*, 4587-4598.
25. Berger, R. M.; McMillin, D. R. "Localized states in reduced and excited-state ruthenium(II) terpyridyls" *Inorg. Chem.* **1988**, *27*, 4245-4249.
26. Swavey, S.; Fang, Z.; Brewer, K. J. "Mixed-metal supramolecular complexes coupling phosphine-containing Ru(II) light absorbers to a reactive Pt(II) through polyazine bridging ligands" *Inorg. Chem.* **2002**, *41*, 2598-2607.
27. Demadis, K. D.; El-Samanody, E.-S.; Meyer, T. J.; White, P. S. ""Structural and Redox Chemistry of Osmium(III) Chloro Complexes Containing 2,2':6'2"-terpyridyl and *tris*-pyrazolyl borate ligands"" *Polyhedron* **1999**, *18*, 1587-1594.
28. Saji, T.; Aoyagui, S. "Polarographic studies on bipyridine complexes. 1. Correlation between reduction potentials of iron(II), ruthenium(II) and osmium(II) complexes and those of free ligands" *J. Electroanal. Chem.* **1975**, *58*, 401-410.
29. Bolinger, C. M.; Story, N.; Sullivan, B. P.; Meyer, T. J. "Electrocatalytic reduction of carbon dioxide by 2,2'-bipyridine complexes of rhodium and iridium" *Inorg. Chem.* **1988**, *27*, 4582-4587.
30. Kew, G.; Hanck, K.; DeArmond, K. "Voltammetry of rhodium-1,10-phenanathroline complexes" *J. Phys. Chem.* **1975**, *79*, 1828-1835.
31. Schwarz, H. A.; Creutz, C. "Reactions of tris- and bis(2,2'-bipyridine)rhodium(II) complexes in aqueous solution" *Inorg. Chem.* **1983**, *22*, 707-713.
32. Oliveira, I. M. F.; Moutet, J.-C.; Vlachopoulos, N. "Poly(pyrrole-2,2'-bipyridyl rhodium(III) complexes) modified electrodes: Molecular materials for hydrogen evolution and electrocatalytic hydrogenation" *J. Electroanal. Chem.* **1990**, *291*, 243-249.
33. Rasmussen, S. C.; Richter, M. M.; Yi, E.; Place, H.; Brewer, K. J. ""Synthesis and characterization of a series of novel rhodium and iridium complexes containing polypyridyl bridging ligands: potential uses in the development of multimetal catalysts for carbon dioxide reduction"" *Inorg. Chem.* **1990**, *29*, 3926-3932.
34. Swavey, S.; Brewer, K. J. "Synthesis and study of Ru,Rh,Ru Triads: Modulation of orbital energies in a supramolecular architecture" *Inorg. Chem.* **2002**, *41*, 4044-4050.
35. Nallas, G. N. A. "Heteronuclear trimetallic polyazine complexes of iridium(III) or rhodium(III) as electrocatalysts for the reduction of CO_2" Ph.D thesis, Virginia Polytechnic Institute and State University, 1993.

36. Nallas, G. N. A.; Jones, S. W.; Brewer, K. J. ""Bipyrimidine-bridged mixed-metal trimetallic complexes of ruthenium(II) with rhodium(III) or irdium(III), $\{[(bpy)_2Ru(bpm)]_2RhCl_2\}^{5+}$"" *Inorg. Chem.* **1996**, *35*, 6974-6980.
37. Molnar, S. M.; Jensen, G. E.; Volger, L. M.; Jones, S. W.; Laverman, L.; Bridgewater, J. S.; Richter, M. M.; Brewer, K. J. "Photochemical Properties of mixed-metal Supramolecular Complexes" *J. Photochem. Photobiol. A* **1994**, *80*, 315-322.
38. Lee, J.-D.; Vrana, L. M.; Bullock, E. R.; Brewer, K. J. ""A tridentate bridged ruthenium-rhodium complex as a stereochemically defined light-absorber-electron-acceptor dyad"" *Inorg. Chem.* **1998**, *37*, 3537-3580.
39. Caldararu, H.; DeArmond, M. K.; Hanck, K. W.; Sahini, V. E. "Electron spin resonance of electrochemically generated rhodium(0) complexes" *J. Am. Chem. Soc.* **1976**, *98*, 4455-4457.
40. Shinozaki, K.; Takahashi, N. ""Molecular orbital calculation and spectroscopic study of the photochemical generation of bis(2,2'-bipyridine)rhodium(I) from bis(2,2'-bipyridine)(oxalato)rhodium(III)"" *Inorg. Chem.* **1996**, *35*, 3917-3924.
41. Chou, M.; Creutz, C.; Mahajan, D.; Sutin, N.; Zipp, A. P. ""Nature of bis(2,2'-bipyridine)rhodium(I) in aqueous solutions"" *Inorg. Chem.* **1982**, *21*, 3989-3997.
42. Bridgewater, J. S.; Vogler, L. M.; Molnar, S. M.; Brewer, K. J. "Tuning the spectroscopic and electrochemical properties of polypyridyl bridged mixed-metal trimetallic ruthenium(II), iridium(III) complexes: a spectroelectrochemical study" *Inorg. Chim. Acta* **1993**, *208*, 179-188.
43. Kahl, J. L.; Hanck, K. W.; DeArmond, K. "Electrochemistry of iridium-bis(phenanthroline) complexes" *J. Phys. Chem.* **1979**, *83*, 2606-2611.
44. Divisia-Blohorn, B. "Solvent effects on the electrochemical properties of $IrCl_2(bpy)_2$" *Inorg. Chim. Acta* **1986**, *117*, 97-101.
45. Divisia, B.; Ford, P. C.; Watts, R. J. "Determination of rate constants for photosolvation reactions: Solvent dependence of chloride substitution rates for excited states of *cis*-dichlorobis(2,2'-bipyridine)iridium(III)" *J. Am. Chem. Soc.* **1980**, *102*, 7264-7268.
46. Kahl, J. L.; Hanck, K. W.; DeArmond, K. "Electrochemistry of iridium tris- and bisesquis(phenanthroline) complexes" *J. Phys. Chem.* **1979**, *83*, 2611-2615.
47. Atkins, P.; de Paula, J. In *Physical Chemistry*; Seventh ed.; W. H. Freeman & Co.: New York, 2002, p 540-578, 686-718.
48. Zigler, D. F.; Brewer, K. J. "Toward Photodynamic Therapy of Cancer with Platinum Group Metal Polyazine Complexes" In *Metal-Complexes-DNA Interactions*; Wiley-Blackwell: Oxford, UK, In Press.
49. Kirsch-De Mesmaeker, A.; Lecomte, J.-P.; Kelly, J. M. "Photoreactions of metal complexes with DNA, especially those involving a primary photo-electron transfer" *Top. Curr. Chem.* **1996**, *177*, 25-76.
50. Singh, T. N.; Turro, C. "Photoinitiated DNA binding by cis-$[Ru(bpy)_2(NH_3)_2]^{2+}$" *Inorg. Chem.* **2004**, *43*, 7260-7262.
51. Kumar, C. V.; Barton, J. K.; Turro, N. J. "Photophysics of ruthenium complexes bound to double helical DNA" *J. Am. Chem. Soc.* **1985**, *107*, 5518-5523.
52. Fleisher, M. B.; Waterman, K. C.; Turro, N. J.; Barton, J. K. "Light-Induced Cleavage of DNA by Metal Complexes" *Inorg. Chem.* **1986**, *25*, 3549-3551.
53. Kober, E. M.; Meyer, T. J. "Conerning the Absorption Spectra of the Ions $M(bpy)_3^{2+}$ (M = Fe, Ru, Os; bpy = 2,2'-Bipyridine" *Inorg. Chem.* **1982**, *21*, 3967-3977.

54. Kober, E. M.; Caspar, J. V.; Lumpkin, R. S.; Meyer, T. J. "Application of the energy gap law to excited-state decay of osmium(II)-polypyridine complexes: Calculation of relative nonradiative decay rates from emission spectral profiles" *J. Phys. Chem.* **1986**, *90*, 3722-3734.
55. Blasiu, R.; Nierengarten, H.; Luhmer, M.; Constant, J.-F.; Defrancq, E.; Dumy, P.; van Dorsselaer, A.; Moucheron, C.; Kirsch-De Mesmaeker, A. "Photoreaction of $[Ru(hat)_2phen]^{2+}$ with guanosine-5'-monophosphate and DNA: Formation of new types of photoadducts" *Chem. Euro. J.* **2005**, *11*, 1507-1517.
56. Sitlani, A.; Long, E. C.; Pyle, A. M.; Barton, J. K. "DNA photocleavage by phenanthrene diimine complexes of rhodium(III): Shape selective recognition and reaction" *J. Am. Chem. Soc.* **1992**, *114*, 2303-2312.
57. Mahnken, R. E.; Billadeau, M. A.; Nikonowicz, E. P.; Morrison, H. "Toward the development of photo *cis*-platinum reagents. Reaction of *cis*-dichlorobis(1,10-phenanthroline)rhodium(III) with calf thymus DNA, nucleotides, and nucleosides" *J. Am. Chem. Soc.* **1992**, *114*, 9253-9265.
58. Angeles-Boza, A. M.; Bradley, P. M.; Fu, P. K.-L.; Shatruk, M.; Hilfiger, M. G.; Dunbar, K. R.; Turro, C. "Phototoxicity of a new Rh_2(II,II) complex: Increase in cytotoxicity upon irradiation similar to that of PDT agent hematoporphyrin" *Inorg. Chem.* **2005**, *44*, 7262-7264.
59. Miao, R.; Mongelli, M. T.; Zigler, D. F.; Winkel, B. S. J.; Brewer, K. J. "A multifunctional tetrametallic Ru-Pt supramolecular complex exhibiting both DNA binding and photocleavage" *Inorg. Chem.* **2006**, *45*, 10413-10415.
60. Swavey, S.; Brewer, K. J. "Visible Light Induced Photocleavage of DNA by a Mixed-Metal Supramolecular Complex: $[\{(bpy)_2Ru(dpp)\}_2RhCl_2]^{5+}$" *Inorg. Chem.* **2002**, *41*, 6196-6198.
61. Demas, J. N.; Taylor, D. G. "Intersystem crossing' yields in ruthenium(II) and osmium(II) photosensitizers" *Inorg. Chem.* **1979**, *18*, 3177-3179.
62. Ford, P. C.; Wink, D.; Dibenedetto, J. "Mechanistic aspects of the photosubstitution and photoisomerization reactions of d^6 metal complexes" In *Progress in Inorganic Chemistry*; Lippard, S. J., Ed.; John Wiley & Sons, Inc.: New York, 1983; Vol. 30, p 213-271.
63. Crosby, G. A. "Spectroscopic Investigations of Excited States of Transition-Metal Complexes" *Acc. Chem. Res.* **1975**, *8*, 231-238.
64. Crosby, G. A.; Elfring, W. H., Jr. "Excited states of mixed ligand chelates of ruthenium(II) and rhodium(III)" *J. Phys. Chem.* **1976**, *80*, 2206-2211.
65. Demas, J. N.; Crosby, G. A. "Quantum efficiencies of transition-metal complexes. I. d-d luminescence" *J. Am. Chem. Soc.* **1970**, *92*, 7262-7270.
66. Muir, M. M.; Huang, W.-L. "Photoaquation of some complexes of rhodium(III)" *Inorg. Chem.* **1973**, *12*, 1831-1835.
67. Sherman, S. E.; Lippard, S. J. "Structural aspects of platinum anticancer drug interactions with DNA" *Chem. Rev.* **1987**, *87*, 1153-1181.
68. Bradley, P. M.; Fu, P. K.-L.; Turro, C. "Excited state properties of $Rh_2(O_2CCH_3)_4$: Solution photochemistry and photoinitiated DNA cleavage" *Comments Inorg. Chem.* **2001**, *22*, 393-426.
69. Angeles-Boza, A. M.; Bradley, P. M.; Fu, P. K.-L.; Wicke, S. E.; Bacsa, J.; Dunbar, K. R.; Turro, C. "DNA binding and photocleavage *in vitro* by new dirhodium(II) dppz

complexes: Correlation to cytotoxicity and photocyotoxicity" *Inorg. Chem.* **2004**, *43*, 8510-8519.
70. De Cola, L.; Belser, P. "Photoinduced energy and electron transfer processes in rigidly bridged dinuclear Ru/Os complexes" *Coord. Chem. Rev.* **1998**, *177*, 301-346.
71. Furue, M.; Hirata, M.; Kinoshita, S.; Kushida, T.; Kamachi, M. "Intramolecular electron-transfer of covalently-linked polypyridine ruthenium(II)/rhodium(III) binuclear complexes in the excited state. Observation of the Marcus inverted region" *Chem. Lett.* **1990**, 2065-2069.
72. Indelli, M. T.; Bignozzi, C. A.; Harriman, A.; Schoonover, J. R.; Scandola, F. "Four intercomponent processes in a Ru(II)-Rh(III) polypyridine dyad: Electron transfer from excited donor, electron transfer to excited acceptor, charge recombination, and electronic energy transfer" *J. Am. Chem. Soc.* **1994**, *116*, 3768-3779.
73. Kalyanasundaram, K.; Gratzel, M.; Nazeeruddin, M. K. "Excited-state interactions in ligand-based chromophore-quencher complexes containing rhodium(III) and ruthenium(II) polypyridyl units" *J. Phys. Chem.* **1992**, *96*, 5865-5872.
74. Kalyanasundaram, K.; Nazeeruddin, M. K. "Photophysics and photoredox reactions of ligand-bridged binuclear polypyridyl complexes of ruthenium(II) and their monomeric analogues" *Inorg. Chem.* **1990**, *29*, 1888-1897.
75. Kleverlaan, C. J.; Indelli, M. T.; Bignozzi, C. A.; Pavanin, L.; Scandola, F.; Hasselman, G. M.; Meyer, G. J. "Stepwise charge separation in heterotriads. Binuclear Ru(II)-Rh(III) complexes on nanocrystalline titanium dioxide" *J. Am. Chem. Soc.* **2000**, *122*, 2840-2849.
76. Fuchs, Y.; Lofters, S.; Dieter, T.; Shi, W.; Morgan, R.; Strekas, T. C.; Gafney, H. D.; Baker, A. D. "Spectroscopic and Electrochemical Properties of dimeric Ruthenium(II) Diimine complexes and determination of Their Excited State Redox Properties" *J. Am. Chem. Soc.* **1987**, *109*, 2691-2697.
77. Elvington, M.; Brewer, K. J. "Photoinitiated electron collection at a metal in a rhodium centered mixed-metal supramolecular complex" *Inorg. Chem.* **2006**, *45*, 5242-5244.
78. Elvington, M.; Brown, J. R.; Arachchige, S. M.; Brewer, K. J. "Photocatalytic hydrogen production from water employing a Ru, Rh, Ru molecular device for photointiated electron collection" *J. Am. Chem. Soc.* **2007**, *129*, 10644-10645.
79. Holder, A. A.; Swavey, S.; Brewer, K. J. "Design aspects for the development of mixed-metal supramolecular complexes capable of visible light induced photocleavage of DNA" *Inorg. Chem.* **2004**, *43*, 303-308.
80. Erkkila, K. E.; Odom, D. T.; Barton, J. K. "Recognition and reaction of metallointercalators with DNA" *Chem. Rev.* **1999**, *99*, 2777-2795.
81. Moucheron, C.; Kirsch-De Mesmaeker, A.; Kelly, J. M. "Photoreactions of ruthenium(II) and osmium(II) complexes with deoxyribonucleic acid (DNA)" *J. Photochem. Photobiol. B* **1997**, *40*, 91-106.
82. Marcus, R. A. "Chemical and electrochemical electron transfer theory" *Annu. Rev. Phys. Chem.* **1964**, *15*, 155-196.
83. Demas, J. N.; DeGraff, B. A. "Applications of luminescent transition platinum group metal complexes to sensor technology" *Coord. Chem. Rev.* **2001**, *211*, 317-351.
84. Foote, C. S. "Definition of type I and type II photosensitized oxidation" *Photochem. Photobiol.* **1991**, *54*, 659.

85. Forster, T. "Transfer mechanisms of electronic excitation" *Discuss. Faraday Soc.* **1959**, *27*, 7-17.
86. Dexter, D. L. "A theory of sensitized luminescence in solids" *J. Chem. Phys.* **1953**, *21*, 836-850.
87. Speiser, S. "Photophysics and Mechanisms of Intramolecular Electronic Energy Transfer in Bichromophoric Molecular Systems: Solution and Supersonic Jet Studies" *Chem. Rev.* **1996**, *96*, 1953-1976.
88. Closs, G. L.; Miller, J. R. ""Intramolecular Long-Distance Electron Transfer in Organic Molecules"" *Science* **1988**, *240*, 440-447.
89. Katayama, H.; Maruyama, S.; Ito, S.; Tsuju, Y.; Tsuchida, A.; Yamamoto, M. ""Triplet Energy Transfer of the Intramolecular System Having Benzophenone and Dibenz[*b,f,*]azepine at the Chain Ends: Chain Length Dependence"" *J. Phys. Chem.* **1991**, *95*, 3480-3486.
90. Newton, M. D. "Quantum Chemical Probes of Electron-Transfer Kinetics: The nature of Donor-Acceptor Interactions" *Chem. Rev.* **1991**, *91*, 767-792.
91. Balzani, V.; Bolletta, F.; Scandola, F. "Vertical and 'Nonvertical' Energy Transfer Processes. A General Classical Treatment" *J. Am. Chem. Soc.* **1980**, *102*, 2152-2163.
92. Demas, J. N.; Diemente, D.; Harris, E. W. "Oxygen quenching and charge-transfer excited states of ruthenium(II) complexes. Evidence for singlet oxygen production" *J. Am. Chem. Soc.* **1973**, *95*, 6864-6865.
93. Denti, G.; Campagna, S.; Sabatino, L.; Serroni, S.; Ciano, M.; Balzani, V. "Luminescent and redox-reactive building blocks for the design of photochemical molecular devices: Mono-, di-, tri-, and tetranuclear ruthenium(II) polypyridine complexes" *Inorg. Chem.* **1990**, *29*, 4750-4758.
94. Balzani, V.; Campagna, S.; Denti, G.; Juris, A.; Serroni, S.; Venturi, M. "Designing Dendrimers based on transition-metal complexes. Light-harvesting properties and predetermined redox patterns" *Acc. Chem. Res.* **1998**, *31*, 26-34.
95. Seneviratne, D. S.; Uddin, M. J.; Swayambunathan, V.; Schlegel, H. B.; Endicott, J. F. "Characteristics and properties of metal-to-ligand charge-transfer excited states in 2,3-bis(2-pyridyl)pyrazine and 2,2'-bipyridine ruthenium complexes. Perturbation-theory-based correlations of optical absorption and emission parameters with electrochemistry and thermal kinetics and related ab initio calculations" *Inorg. Chem.* **2002**, *41*, 1502-1517.
96. Puntoriero, F.; Serroni, S.; Licciardello, A.; Venturi, M.; Juris, A.; Ricevuto, V.; Campagna, S. "New ruthenium(II) and osmium(II) trinuclear dendrons. Synthesis, redox behavior, absorption spectra, and luminescence properties" *J. Chem. Soc., Dalton Trans.* **2001**, 1035-1042.
97. Roffia, S.; Marcaccio, M.; Paradisi, C.; Paulucci, F.; Balzani, V.; Denti, G.; Serroni, S.; Campagna, S. "Electrochemical reduction of (2,2'-bipyridine)- and bis((2-pyridyl)pyrazine)ruthenium(II) complexes used as building blocks for supramolecular species. Redox series made of 8, 10, and 12 redox steps" *Inorg. Chem.* **1993**, *32*, 3003-3009.
98. Nozaki, K.; Ohno, T.; Haga, M.-a. "Intramolecular electron transfer in photoexcited Ru(II)-Rh(III) binuclear compounds" *J. Phys. Chem.* **1992**, *96*, 10880-10888.
99. Sauvage, J.-P.; Collin, J.-P.; Chambron, J.-C.; Guillerez, S.; Coudret, C.; Balzani, V.; Barigletti, F.; Cola, L. D.; Flamigni, L. "Ruthenium (II) and osmium(II) bis(terpyridine)

complexes in covalently-linked multicomponent systems: synthesis, electrochemical behavior, absorption spectra, and photochemical and photophysical properties" *Chem. Rev.* **1994**, *94*, 993-1019.
100. Endicott, J. F.; Schlegel, H. B.; Uddin, M. J.; Seniveratne, D. S. "MLCT excited states and charge delocalization in some ruthenium-ammine-polypyridyl complexes" *Coord. Chem. Rev.* **2002**, *229*, 95-106.
101. Endicott, J. F.; Song, X.; Watzky, M. A.; Buranda, T. "Photoinduced electron transfer in linked transition metal donor-acceptor complexes" *J. Photochem. Photobiol. A* **1994**, *82*, 181-190.
102. Indelli, M. T.; Scandola, F.; Collin, J.-P.; Sauvage, J.-P.; Sour, A. "Photoinduced electron and energy transfer in rigidly bridged Ru(II)-Rh(III) binuclear complexes" *Inorg. Chem.* **1996**, *35*, 303-312.
103. Indelli, M. T.; Scandola, F.; Flamigni, L.; Collin, J.-P.; Sauvage, J.-P.; Sour, A. "Photoinduced electron transfer in ruthenium(II)-rhodium(III) terpyridine dyads" *Inorg. Chem.* **1997**, *36*, 4247-4250.
104. Scandola, F.; Argazzi, R.; Bignozzi, C. A.; Indelli, M. T. "Photoinduced energy and electron transfer in inorganic covalently linked systems" *J. Photochem. Photobiol. A* **1994**, *82*, 191-202.
105. Creutz, C.; Newton, M. D.; Sutin, N. "Metal-ligand and metal-metal coupling elements" *J. Photochem. Photobiol. A* **1994**, *82*, 47-59.
106. Endicott, J. F.; Song, X.; Watzky, M. A.; Buranda, T.; Lei, Y. "Electrochemical and spectroscopic manifestations of donor-acceptor coupling in cyanide bridged transition metal complexes: contrasts between Ru-CN-Ru, Co-CN-Ru and Rh-CN-Ru systems" *Chem. Phys.* **1993**, 427-438.
107. Lei, Y.; Buranda, T.; Endicott, J. F. "Photoinduced energy transfer in multinuclear transition-metal complexes. Reversible and irreversible energy flow between charge-transfer and ligand field excited states of cyanide-bridged ruthenium(II)-chromium(III) and ruthenium(II)-rhodium(III) complexes" *J. Am. Chem. Soc.* **1990**, *112*, 8820-8833.
108. Andersson, J.; Puntoriero, F.; Serroni, S.; Yartsev, A.; Pascher, T.; Polivka, T.; Campagna, S.; Sundstrom, V. "New paradigm of transition metal polypyridine complex photochemistry" *Faraday Discuss.* **2004**, 295-305.
109. Andersson, J.; Puntoriero, F.; Serroni, S.; Yartsev, A.; Pascher, T.; Polivka, T.; Campagna, S.; Sundstrom, V. "Ultrafast singlet energy transfer competes with intersystem crossing in a multi-center transition metal polypyridine complex" *Chem. Phys. Lett.* **2004**, *386*, 336-341.
110. Leveque, J.; Elias, B.; Moucheron, C.; Kirsch-De Mesmaeker, A. "Dendritic tetranuclear Ru(II) complexes based on the nonsymmetrical PHEHAT bridging ligand and their building blocks: Synthesis, characterization, and electrochemical and photophysical properties" *Inorg. Chem.* **2005**, *44*, 393-400.
111. Larsen, J.; Puntoriero, F.; Pascher, T.; McClenaghan, N. D.; Campagna, S.; Akesson, E.; Sundstrom, V. "Extending the light-harvesting properties of transition-metal dendrimers" *Chem. Phys. Chem.* **2007**, *8*, 2643-2651.
112. Zeglis, B. M.; Pierre, V. C.; Barton, J. K. "Metallo-intercalators and metallo-insertors" *Chem. Commun.* **2007**, 4565-4579.
113. Armitage, B. "Photocleavage of Nucleic Acids" *Chem. Rev.* **1998**, *98*, 1171-1200.

114. Pogozeleski, W. K.; Tullius, T. D. "Oxidative Strand Scission of Nucleic Acids: Routes Initiated by Hydrogen Abstraction from the Sugar Moiety" *Chem. Rev.* **1998**, *98*, 1098-1107.
115. Calladine, C. R. *Understanding DNA: The molecule and how it works*; 3rd ed.; Elsevier Academic Press San Diego, CA, 2004.
116. Vinograd, J.; Lebowitz, J. "Physical and topological properties of circular DNA" *J. Gen. Physiol.* **1966**, *49*, 103-125.
117. van der Maarel, J. R. C.; Zakharova, S. S.; Jesse, W.; Backendorf, C.; Egelhaaf, S. U.; Lapp, A. "Supercoiled DNA; Plectonemic Structure and Liquid Crystal Formation" *J. Phys.: Condens. Matter* **2003**, *15*, S183-S189.
118. Mei, H. Y.; Barton, J. K. "Chiral probe for A-form helices of DNA and RNA: tris(tetramethylphenanthroline)ruthenium(II)" *J. Am. Chem. Soc.* **1986**, *108*, 7414-7416.
119. Barton, J. K. "Metals and DNA: Molecular left-handed compliments" *Science* **1986**, *233*, 727-734.
120. Manning, G. S.; Ray, J. "Counterion condensation revisited" *J. Biomol. Struct. Dyn.* **1998**, *16*, 461-476.
121. Friedman, A. E.; Chambron, J.-C.; Sauvage, J.-P.; Turro, N. J.; Barton, J. K. "Molecular "light switch" for DNA; $Ru(bpy)_2(dppz)^{2+}$" *J. Am. Chem. Soc.* **1990**, *112*, 4960-4692.
122. Junicke, H.; Hart, J.; Kisko, J.; Glebov, O.; Kirsch, I. R.; Barton, J. K. "Bioinorganic chemistry special feature: A rhodium complex for high-affinity DNA base-pair mismatch recognition" *Proc. Natl. Acad. Sci. USA* **2003**, *100*, 3737-3742.
123. Burrows, C. J.; Muller, J. G. "Oxidative Nucleobase Modifications Leading to Strand Scission" *Chem. Rev.* **1998**, *98*, 1109-1151.
124. Clarke, M. J. "Non-platinum chemotherapeutic metallopharmaceuticals" *Chem. Rev.* **1999**, *99*, 2511-2533.
125. Poklar, N.; Pilch, D. S.; Lippard, S. J.; Redding, E. A.; Dunham, S. U.; Breslauer, K. "Influence of cisplatin intrastrand crosslinking on the conformation, thermal stability, and energetics of a 20-mer DNA duplex" *Proc. Natl. Acad. Sci. USA* **1996**, *93*, 7606-7611.
126. Morrison, H.; Harmon, H. ""Hot spots" associated with the photoinduced binding of *cis*-dichloro bis(1,10-phenanthroline)rhodium(III) chloride to HIV-1 and c-raf DNA" *Photochem. Photobiol.* **2000**, *72*, 731-738.
127. Menon, E. L.; Perera, R.; Navarro, M.; Kuhn, R. J.; Morrison, H. "Phototoxicity against tumor cells and Sindbis virus by an octahedral rhodium bisbipyridyl complex and evidence for the genome as a target in viral photoinactivation" *Inorg. Chem.* **2004**, *43*, 5373-5381.
128. Loganathan, D.; Morrison, H. "Effect of ring methylation on the photophysical, photochemical and photobiological properties of *cis*-dichlorobis(1,10-phenanthrolin)rhodium(III)chloride" *Photochem. Photobiol.* **2006**, *82*, 237-247.
129. Ortmans, I.; Elias, B.; Kelly, J. M.; Moucheron, C.; Kirsch-De Mesmaeker, A. "$[Ru(TAP)_2(dppz)]^{2+}$: a DNA intercalating complex, which luminesces strongly in water and undergoes photo-induced proton-coupled electron transfer with guanosine-5'-monophosphate" *Dalton Trans.* **2004**, 668-676.
130. Kawanishi, S.; Oikawa, S.; Murata, M.; Tsukitome, H.; Saito, I. "Site-specific oxidation at GG and GGG sequences in double-stranded DNA by benzoyl peroxide as a tumor promoter" *Biochemistry* **1999**, *38*, 16733-16739.

131. Prat, F.; Houk, K. N.; Foote, C. S. "Effect of Guanine Stacking on the Oxidation of 8-Oxoguanine in B-DNA" *J. Am. Chem. Soc.* **1998**, *120*, 845-846.
132. Saito, I.; Takayama, M.; Sugiyama, H.; Nakatani, K. "Photoinduced DNA Cleavage via Electron Transfer: Demonstration That Guanine Residues Located 5' to Guanine are the most Electron-Donating Sites" *J. Am. Chem. Soc.* **1995**, *117*, 6406-6407.
133. Sugiyama, H.; Saito, I. "Theoretical studies of GG-specific photocleavage of DNA via electron transfer: Significant lowering of ionization potential and 5'-localization of HOMO of stacked GG bases in B-form DNA" *J. Am. Chem. Soc.* **1996**, *118*, 7063-7068.
134. Mongelli, M. T.; Heinecke, J.; Mayfield, S.; Okyere, B.; Winkel, B. S. J.; Brewer, K. J. "Variation of DNA photocleavage efficiency for $\{(TL)_2Ru(dpp)]Cl_2$ complexes where TL = 2,2'-bipyridine, 1,10-phenanthroline, or 4,7-diphenyl-1,10-phenanthroline" *J. Inorg. Biochem.* **2006**, *100*, 1983-1987.
135. Hergueta-Bravo, A.; Jimenez-Hernandez, M. E.; Montero, F.; Oliveros, E.; Orellana, G. "Singlet-oxygen mediated DNA photocleavage with Ru(II) polypyridyl complexes" *J. Phys. Chem. B* **2002**, *106*, 4010-4017.
136. Chouai, A.; Wicke, S. E.; Turro, C.; Bacsa, J.; Dunbar, K. R.; Wang, D.; Thummel, R. P. "Ruthenium(II) complexes of 1,12-diazaperylene and their interactions with DNA" *Inorg. Chem.* **2005**, *44*, 5996-6003.
137. Prussin, A. J.; Zigler, D. F.; Brown, J. R.; Winkel, B. S. J.; Brewer, K. J. "Photochemical Methods to Assay DNA Photocleavage using Supercoiled pUC18 DNA and LED or Xenon Arc Lamp Excitation" *J. Inorg. Biochem.* **2008**, *102*, 731-739.
138. Braunstein, C. H.; Baker, A. D.; Strekas, T. C.; Gafney, H. D. "Spectroscopic and electrochemical properties of the dimer tetrakis(2,2'-bipyridine)(μ-2,3-bis(2-pyridyl)pyrazine)diruthenium(II) and its monomeric analog" *Inorg. Chem.* **1984**, *23*, 857-864.
139. Richter, M. M.; Brewer, K. J. "Synthesis and characterization of osmium(II) complexes incorporating polypyridyl bridging ligands" *Inorg. Chem. Acta* **1991**, *180*, 125-131.
140. McKenzie, E. D.; Plowman, R. A. ""Rhodium(III) compounds with 1,10-phenanthroline and 2,2'-bipyridyl"" *J. Inorg. Nucl. Chem.* **1970**, *32*, 199-212.
141. Winter, M. *University of Sheffield, ChemPuter*, 1993-2001, http://winter.group.shef.ac.uk/chemputer/.
142. *ChemDraw Ultra 8.0*, CambridgeSoft Corporation, 2003.
143. Gennett, T.; Milner, D. F.; Weaver, M. J. "Role of solvent reorganization dynamics in electron-transfer processes. Theory-experiment comparisons for electrochemical and homogeneous electron exchange involving metallocene redox couples" *J. Phys. Chem.* **1985**, *89*, 2787-2794.
144. Wang, X.-Y.; Del Guerzo, A.; Tunuguntla, H.; Schmehl, R. H. "Photophysical behaviour of Ru(II) and Os(II) terpyridyl phenylene vinylene complexes: Perturbation of MLCT state by intra-ligand charge transfer state" *Res. Chem. Intermed.* **2007**, *63-77*.
145. Brown, J. R.; Elvington, M.; Mongelli, M. T.; Zigler, D. F.; Brewer, K. J. ""Analytical methods development for supramolecular design in solar hydrogen production"" *Proc. of SPIE* **2006**, *6340-17*, 1-10.
146. Rurainski, H. J.; Mader, G. "Light-emitting diodes as a light source in photochemical and photobiological work" In *Methods in Enzymology Part C: Photosynthesis and Nitrogen Fixation*; San Pietro, A., Ed.; Elsevier, Inc.: Knoxville, TN, 1980; Vol. 69, p 667-675.

147. Bernhard, S.; Goldsmith, J. I.; Hudson, W. R.; Lowry, M. S.; Anderson, T. H. "Discovery and high-throughput screening of herteroleptic iridium complexes for photoinduced hydrogen production" *J. Am. Chem. Soc.* **2005**, *127*.
148. Kuhn, H. J.; Braslavsky, S. E.; Schmidt, R. "Chemical actinometry (IUPAC technical report)" *Pure Appl. Chem.* **2004**, *76*, 2105-2146.
149. Rasband, W. S. *ImageJ*, National Institutes of Health, 1997-2007, http://rsb.info.nih.gov/ij/.
150. Brewer, R. G.; Jensen, G. E.; Brewer, K. J. ""Long-Lived Osmium(II) Chromophores Containing 2,3,5,6-Tetrakis(2-pyridyl)pyrazine"" *Inorg. Chem.* **1994**, *33*, 124-129.
151. Yoshikawa, N.; Matsumura-Inoue, T.; Kanehisa, N.; Kai, Y.; Takashima, H.; Tsukahara, K. "Electrochemical and luminescent properties of new ruthenium(II) and binuclear iridum (III)-ruthenium(II) complexes" *Anal. Sci.* **2004**, *20*, 1639-1644.
152. Buckingham, D. A.; Dwyer, F. P.; Sargeson, A. M. ""Mono- and Bis-(2,2'-Bipyridine) and (1,10-Phenanthroline) Chelates of Ruthenium and Osmium. V. Mixed 2,2'-Bipyridine and 2,2',2"-terpyridine Chelates of Bivalent and Tervalent Osmium"" *Aust. J. Chem* **1964**, *17*, 622-631.
153. Brewer, R. G.; Jensen, G. E.; Brewer, K. J. "Long-Lived Osmium(II) Chromophores Containing 2,3,5,6-Tetrakis(2-pyridyl)pyrazine" *Inorg. Chem.* **1994**, *33*, 124-129.
154. Broomhead, J. A.; Grumley, W. ""Iridium(III) and rhodium(III) mono- and bis-(1,10-phenanthroline) complexes and optical isomers of iridium(III), rhodium(III), chromium(III), and cobalt(III) dihalogenbis(1,10-phenanthroline) complex cations"" *Inorg. Chem.* **1971**, *10*, 2002-2009.
155. McKenzie, E. D.; Plowman, R. A. "Rhodium(III) compounds with 1,10-phenanthroline and 2,2'-bipyridyl" *J. Inorg. Nucl. Chem.* **1970**, *32*, 199-212.
156. McKenzie, E. D. ""The steric effect in bis(2,2'-bipyridyl) and bis(1,10-phenanthroline) metal complexes"" *Coord. Chem. Rev.* **1971**, *6*, 187-216.
157. Amarante, D.; Cherian, C.; Emmel, C.; Chen, H.-Y.; Dayal, S.; Koshy, M.; Megehee, E. G. ""Improved synthetic routes to rhodium bipyridine complexes: Comparison of microwave vs. conventional synthesis"" *Inorg. Chim. Acta* **2005**, *358*, 2231-2238.
158. Kulasingam, G. C.; McWhinnie, W. R.; Miller, J. D. ""The mechanism of formation and the stereochemistry of mono- and bis-complexes of rhodium(III) with 1,10-phenanthroline"" *J. Chem. Soc. A* **1969**, 521-524.
159. Elvington, M. "A rhodium centered supramolecular complex as a photoinitiated electron collector", Virginia Polytechnic Institute and State University, 2007.
160. Krejcik, M.; Vlcek, A. A. "Electrochemistry of $[(Ru(bpy)_2)_2bpm](PF_6)_4$. Complete assignment of individual reduction steps" *Inorg. Chem.* **1992**, *31*, 2390-2395.
161. Arachchige, S. M.; Brown, J. R.; Brewer, K. J. "Photochemical hydrogen production from water using the new photocatalyst $[\{(bpy)_2Ru(dpp)\}_2RhBr_2](PF_6)_5$" *J. Photochem. Photobiol. A* **2008**, *197*, 13-17.
162. Berger, R. M. "Excited-state absorption spectroscopy and spectroelectrochemistry of tetrakis(2,2'-bipyridine)(μ-2,3-bis(2-pyridyl)pyrazine)diruthenium(II) and its mononuclear counterpart: A comparative study" *Inorg. Chem.* **1990**, *29*, 1920-1924.
163. Endicott, J. F.; Chen, Y.-J. "Charge transfer-excited state emission spectra of mono- and bi-metallic coordination complexes: Band shapes, reorganizational energies and lifetimes" *Coord. Chem. Rev.* **2007**, *251*, 328-350.

164. Kober, E. M.; Sullivan, B. P.; Meyer, T. J. "Solvent Dependence of Metal-to-Ligand Charge Transfer Transitions. Evidence for Initial Electron Localization in MLCT Excited States of 2,2'-Bipyridine Complexes of Ruthenium(II) and Osmium(II)" *Inorg. Chem.* **1984**, *23*, 2098-2104.
165. Sunada, W. M.; Blanch, H. W. "A theory for the electrophoretic separation of DNA in polymer solutions" *Electrophoresis* **1998**, *19*, 3128-3136.
166. Carnevali, F.; Caserta, M.; Di Mauro, E. "Transitions in topological organization of supercoiled DNA domains as a potential regulatory mechanism" *J. Biol. Chem.* **1984**, *259*, 12633-12643.
167. Cohen, G. L.; Bauer, W. R.; Barton, J. K.; Lippard, S. J. "Binding of *cis*- and *trans*-dichlorodiammineplatinum(II) to DNA: Evidence for unwinding and shortening of the double helix" *Science* **1979**, *203*, 1014-1016.
168. Molloy, M. J.; Hall, V. S.; Bailey, S. I.; Griffin, K. J.; Faulkner, J.; Uden, M. "Effective and robust plasmid topology analysis and subsequent characterization of the plasmid isoforms thereby observed" *Nucleic Acids Res.* **2004**, *32*, e129.
169. Zhang, B.; Seki, S.; Akiyama, K.; Tsutsui, K.; Li, T.; Nagao, K. "Detection and analyses by gel electrophoresis of cisplatin-mediated DNA damage" *Acta Med. Okayama* **1992**, *46*, 427-434.
170. Cohen, G. L.; Ledner, J. A.; Bauer, W. R.; Ushay, H. M.; Caravana, C.; Lippard, S. J. "Sequence dependent binding of *cis*-dichlorodiammineplatinum(II) to DNA" *J. Am. Chem. Soc.* **1980**, *102*, 2487-2488.
171. Pinak, M. "Impact of the 8-Oxoguanine on B-DNA Molecule--Molecular Dynamics Study" *J. Mol. Struct.* **2002**, *583*, 189-197.
172. den Hartog, J. H. J.; Altona, C.; van Boom, J. H.; van der Marel, G. A.; Haasnoot, C. A. G.; Reedjik, J. "*cis*-Diamminedichloroplatinum(II) induced distortion in a double-helical DNA fragment" *J. Am. Chem. Soc.* **1984**, *106*, 1528-1530.
173. Keck, M. V.; Lippard, S. J. "Unwinding of supercoiled DNA by platinum-ethidium and related complexes" *J. Am. Chem. Soc.* **1992**, *114*, 3386-3390.
174. Williams, R. L.; Toft, H. N.; Winkel, B.; Brewer, K. J. "Synthesis, characterization, and DNA binding properties of a series of Ru, Pt mixed-metal complexes" *Inorg. Chem.* **2003**, *42*, 4394-4400.
175. Holder, A. A.; Zigler, D. F.; Tarrago-Trani, M. T.; Storrie, B.; Brewer, K. J. "Photobiological impact of $[\{(bpy)_2Ru(dpp)\}_2RhCl_2]Cl_5$ and $[\{(bpy)_2Os(dpp)\}_2RhCl_2]Cl_5$ [bpy = 2,2'-bipyridine; dpp = 2,3-bis(2-pyridyl)pyrazine] on Vero cells" *Inorg. Chem.* **2007**, *46*, 4760-4762.

Appendix

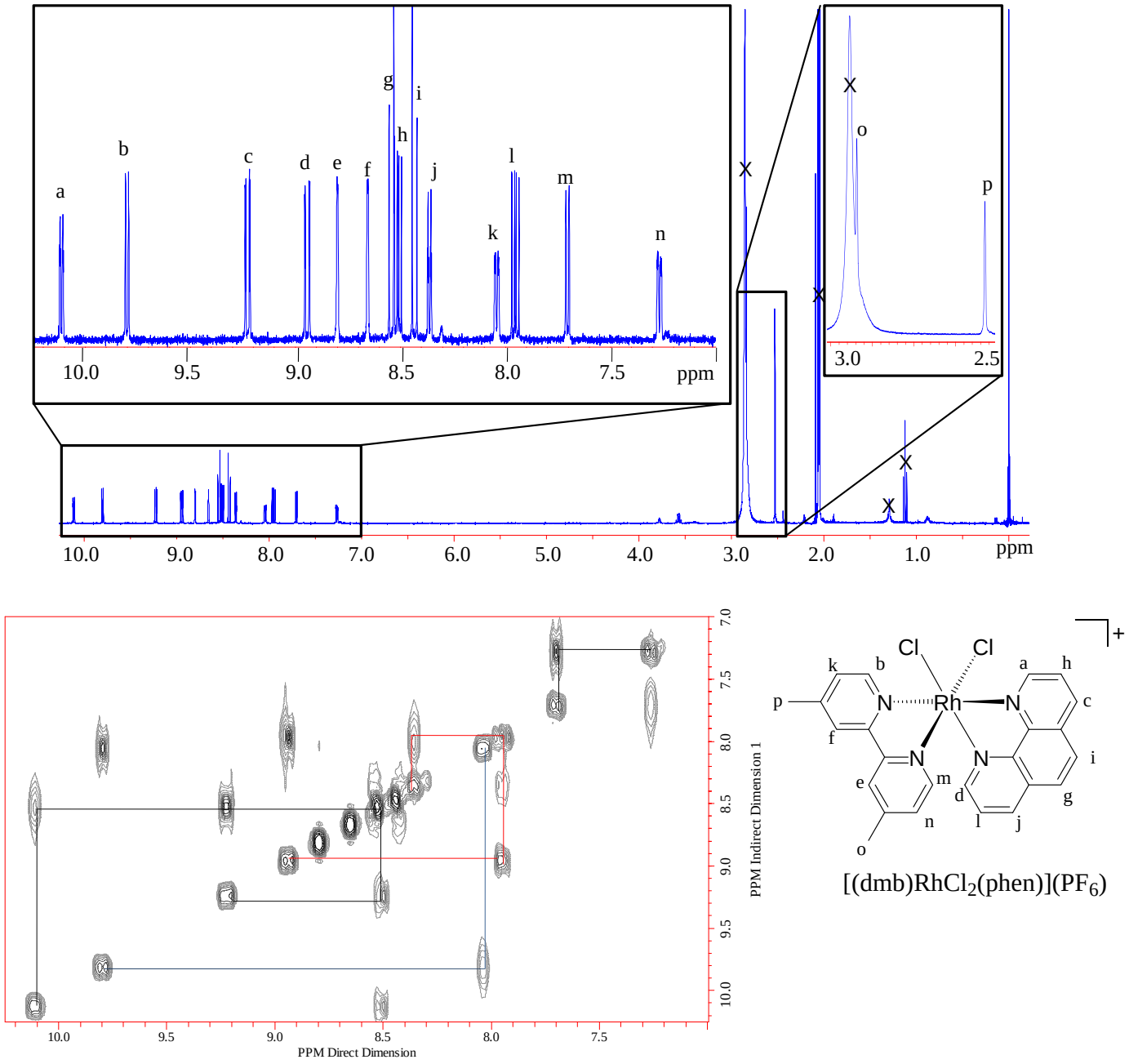

Figure A-1. ^{1}H-NMR spectrum and ^{1}H-^{1}H COSY spectrum of [(phen)RhCl$_2$(dmb)](PF$_6$) saturated solution in d$_6$-acetone with assignments. The "X" denotes peaks due to solvent.

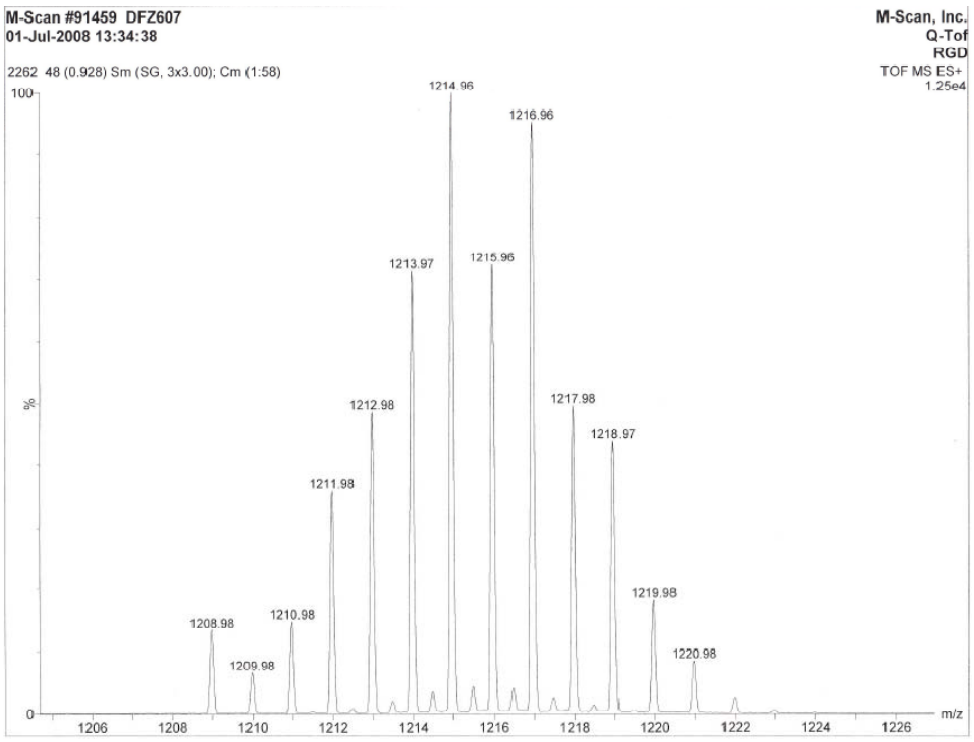

Figure A-2. Mass spectrum of $[(bpy)_2Ru(bpm)RhCl_2(phen)](PF_6)_2^+$ showing isotopic distribution pattern as acquired by M-Scan, Inc, bpy = 2,2'-bipyridine, bpm = 2,2'-bipyrimidine, phen = 1,10-phenanthroline.

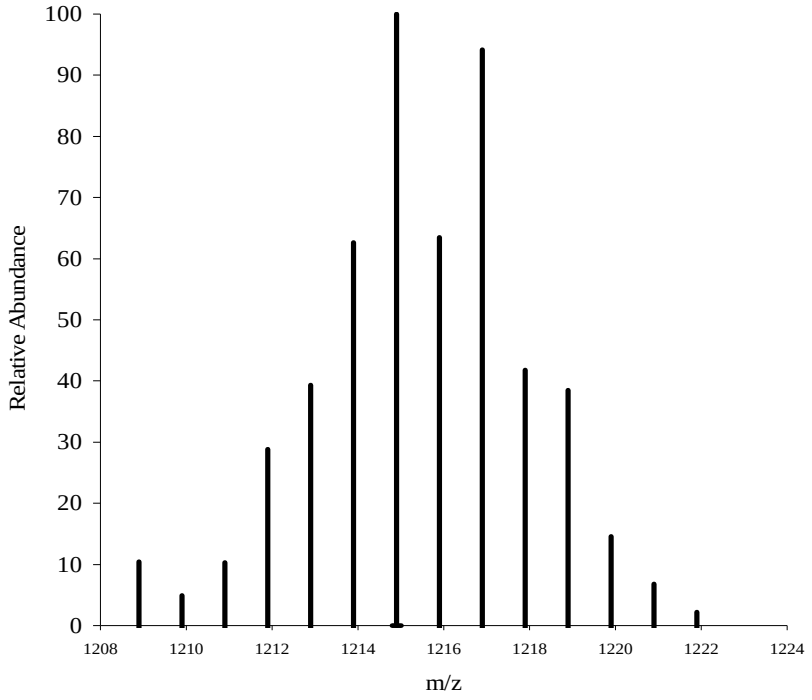

Figure A-3. Mass spectrum of $[(bpy)_2Ru(bpm)RhCl_2(phen)](PF_6)_2^+$ showing isotopic distribution pattern as calculated with the Sheffield Chemputer. bpy = 2,2'-bipyridine, bpm = 2,2'-bipyrimidine, phen = 1,10-phenanthroline.

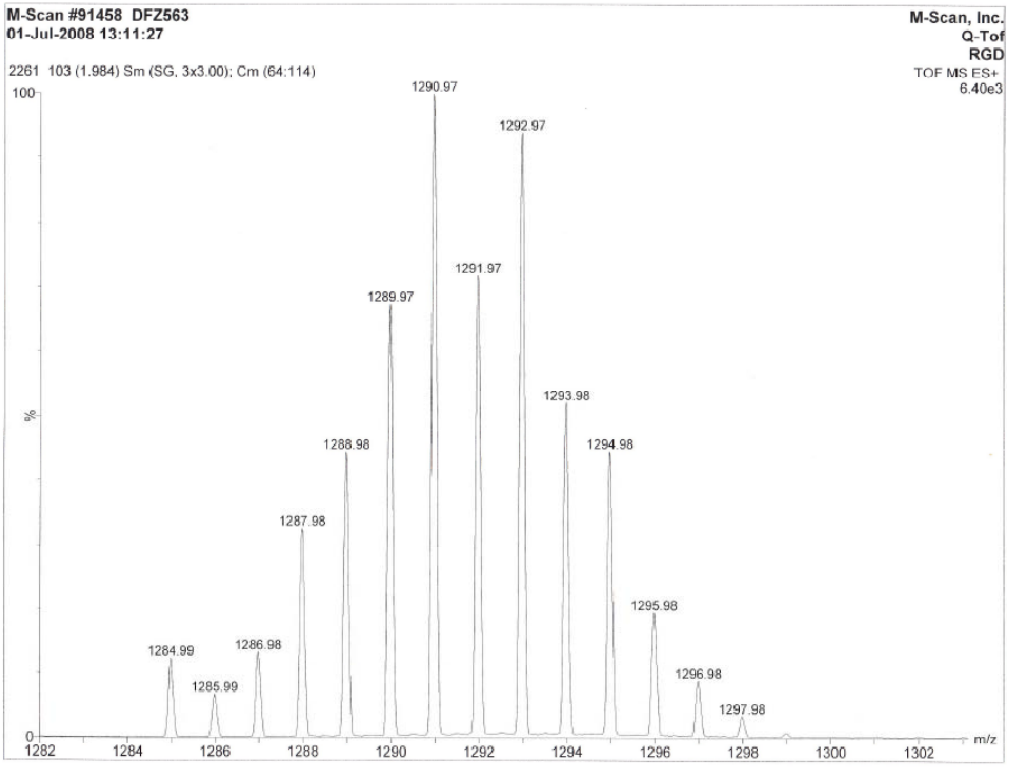

Figure A-4. Mass spectrum of $[(bpy)_2Ru(dpp)RhCl_2(phen)](PF_6)_2^+$ showing isotopic distribution pattern as acquired by M-Scan, Inc, bpy = 2,2'-bipyridine, dpp = 2,3-bis(2-pyridyl)pyrazine, phen = 1,10-phenanthroline.

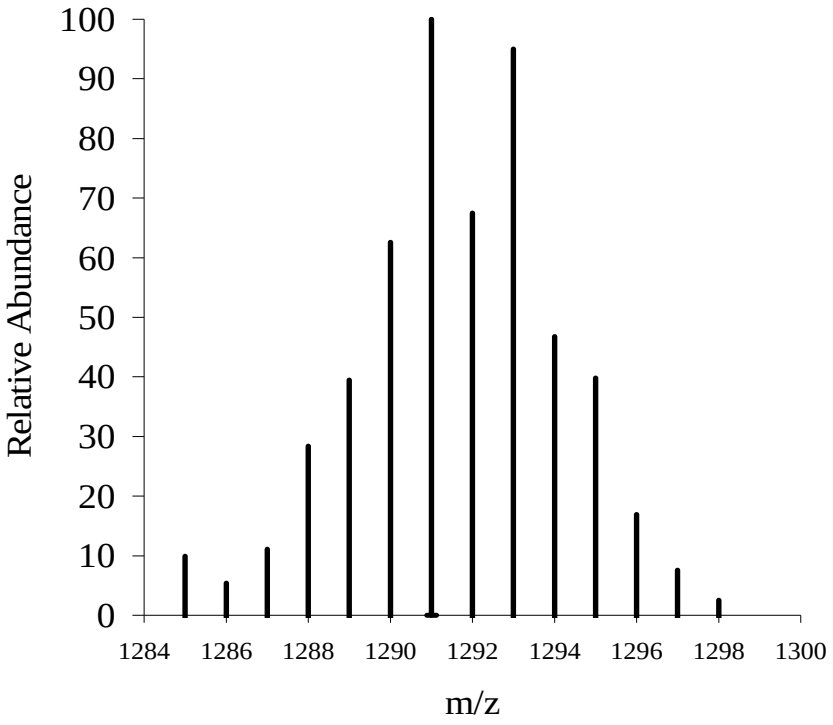

Figure A-5. Mass spectrum of $[(bpy)_2Ru(dpp)RhCl_2(phen)](PF_6)_2^+$ showing isotopic distribution pattern as calculated with the Sheffield Chemputer. bpy = 2,2'-bipyridine, dpp = 2,3-bis(2-pyridyl)pyrazine, phen = 1,10-phenanthroline.

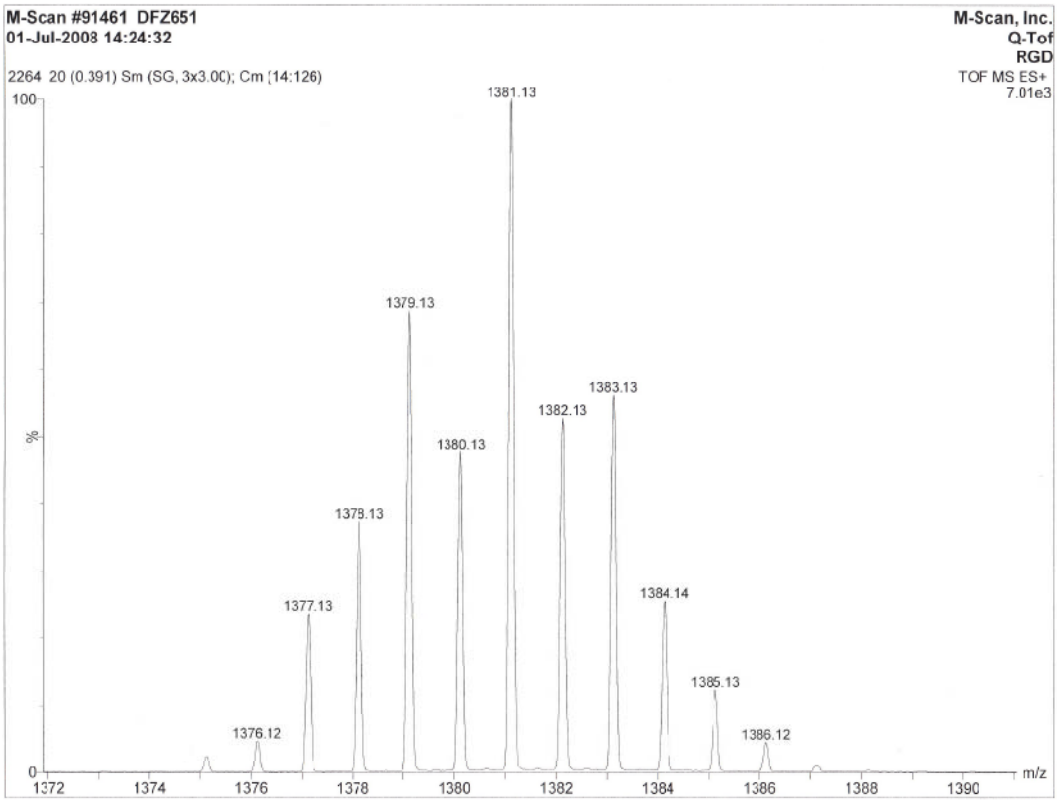

Figure A-6. Mass spectrum of $[(bpy)_2Os(dpp)RhCl_2(phen)](PF_6)_2^+$ showing isotopic distribution pattern as acquired by M-Scan, Inc, bpy = 2,2'-bipyridine, dpp = 2,3-bis(2-pyridyl)pyrazine, phen = 1,10-phenanthroline.

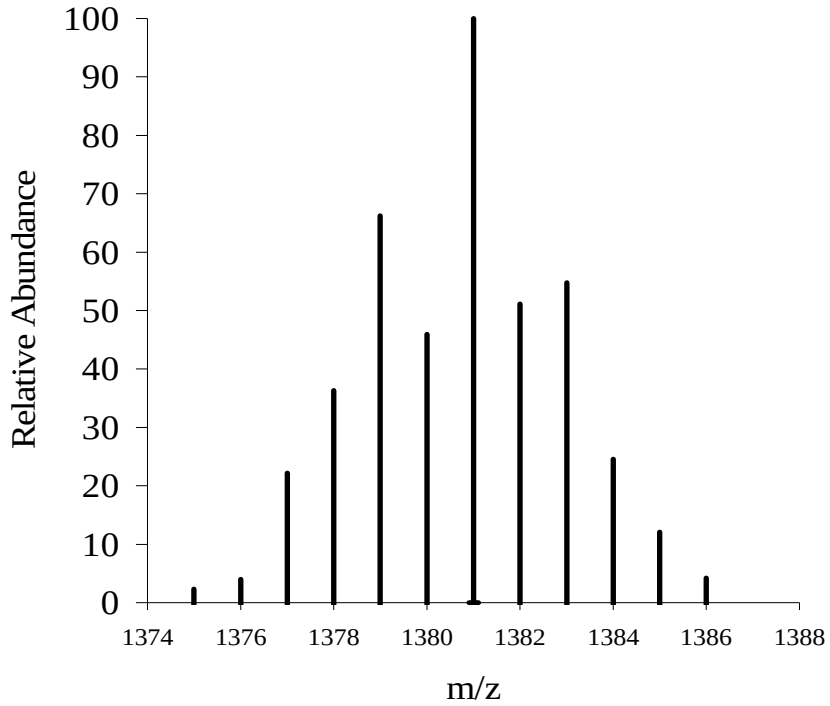

Figure A-7. Mass spectrum of $[(bpy)_2Os(dpp)RhCl_2(phen)](PF_6)_2^+$ as calculated with the Sheffield Chemputer. bpy = 2,2'-bipyridine, dpp = 2,3-bis(2-pyridyl)pyrazine, phen = 1,10-phenanthroline.

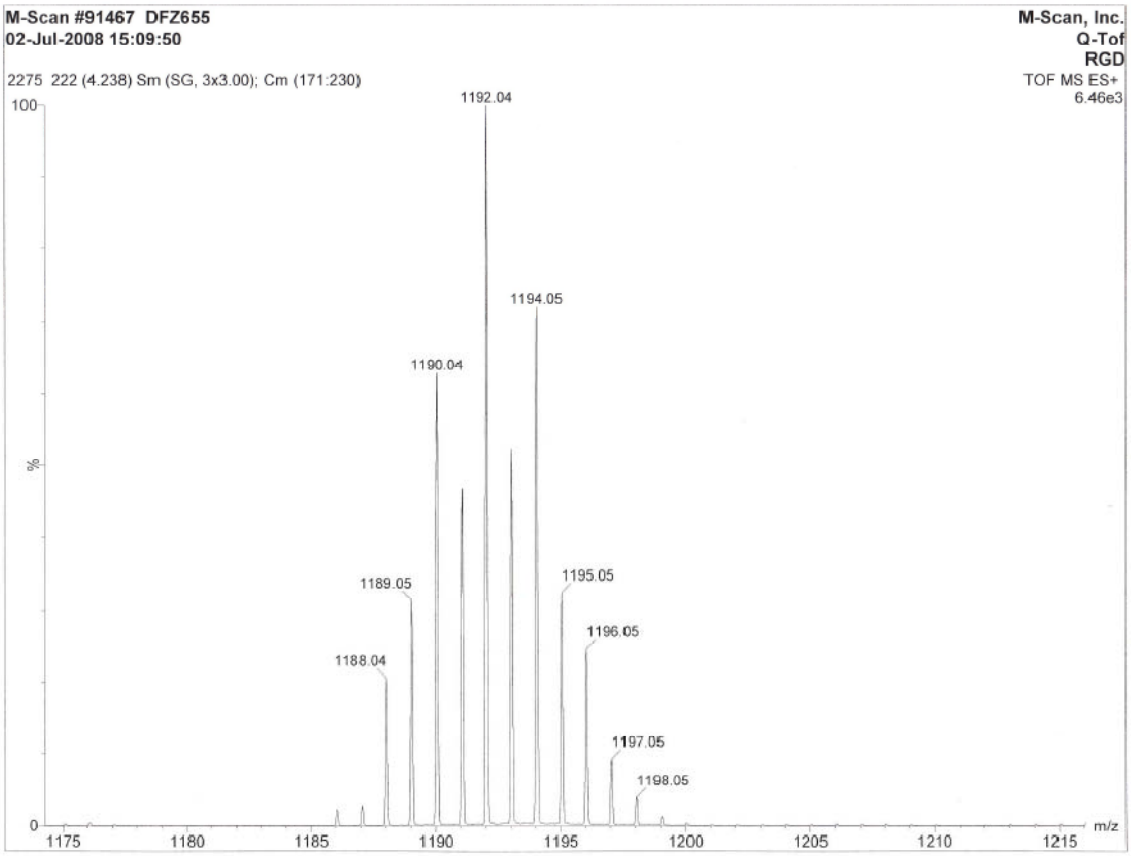

Figure A-8. Mass spectrum of $[(tpy)OsCl(dpp)RhCl_2(phen)](PF_6)^+$ showing isotopic distribution pattern as acquired by M-Scan, Inc, tpy = 2,2':6',2''-terpyridine, dpp = 2,3-bis(2-pyridyl)pyrazine, phen = 1,10-phenanthroline.

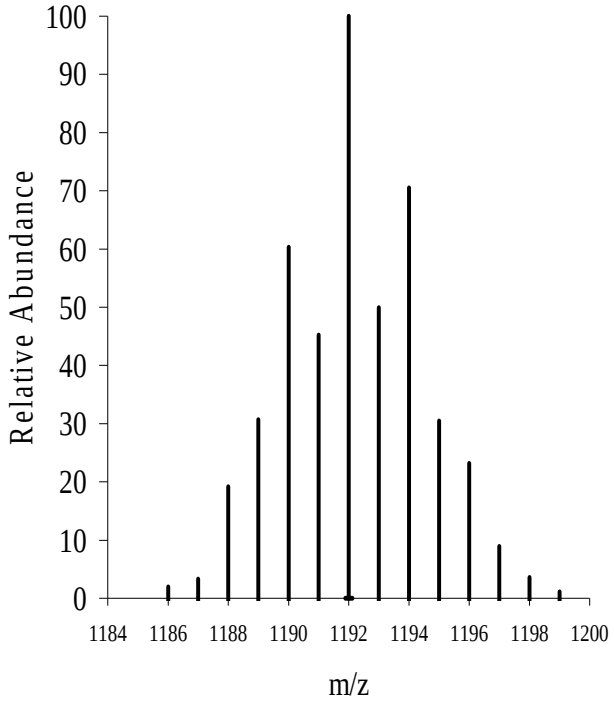

Figure A-9. Mass spectrum of $[(tpy)OsCl(dpp)RhCl_2(phen)](PF_6)^+$ showing isotopic distribution pattern as calculated with the Sheffield Chemputer. tpy = 2,2':6',2''-terpyridine, dpp = 2,3-bis(2-pyridyl)pyrazine, phen = 1,10-phenanthroline.

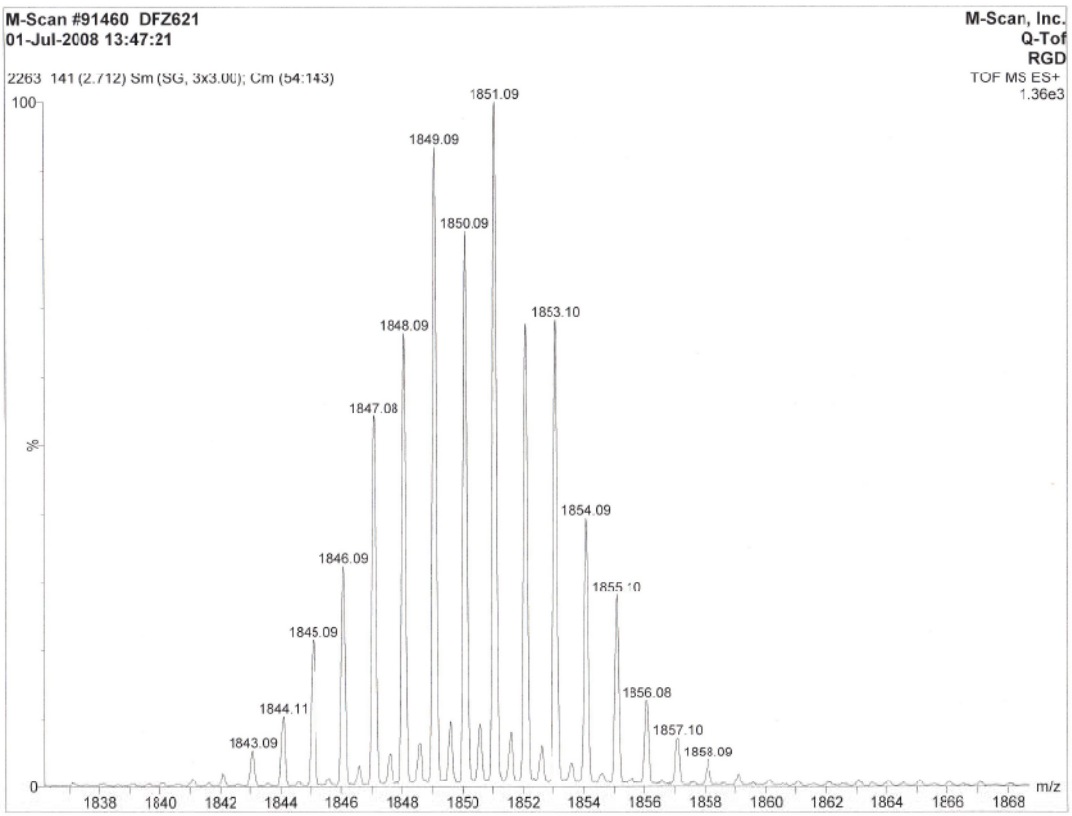

Figure A-10. Mass spectrum of $[\{(tpy)OsCl(dpp)\}_2RhCl_2](PF_6)_2^+$ showing isotopic distribution pattern as acquired by M-Scan, Inc, tpy = 2,2':6',2''-terpyridine, dpp = 2,3-bis(2-pyridyl)pyrazine, phen = 1,10-phenanthroline.

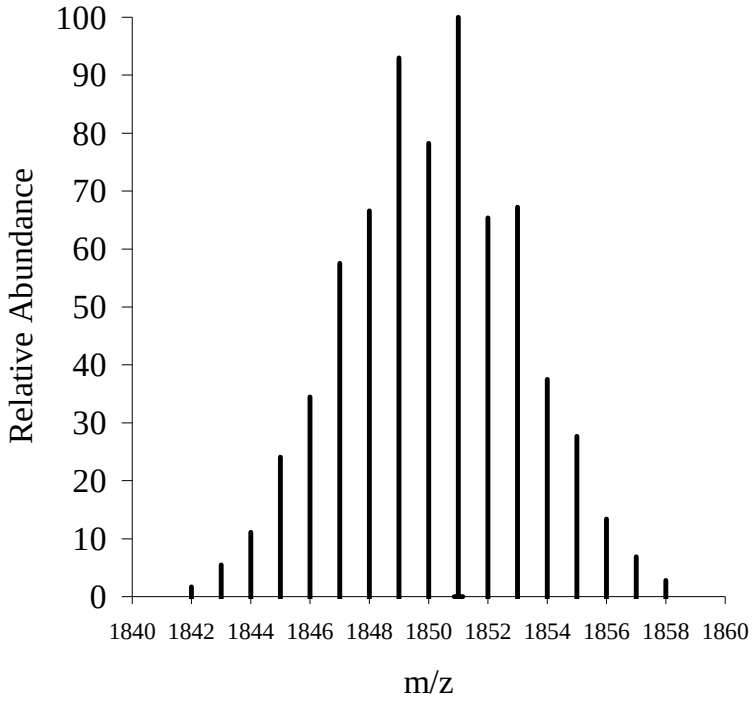

Figure A-11. Mass spectrum of $[\{(tpy)OsCl(dpp)\}_2RhCl_2(phen)](PF_6)_2^+$ showing isotopic distribution pattern as calculated with the Sheffield Chemputer. tpy = 2,2':6',2''-terpyridine, dpp = 2,3-bis(2-pyridyl)pyrazine, phen = 1,10-phenanthroline.

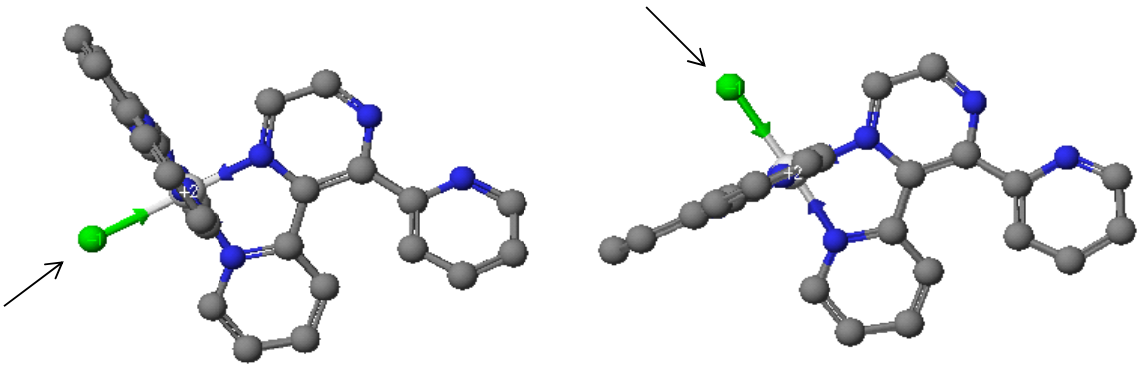

Figure A-12. Possible geometric isomers of [(tpy)OsCl(dpp)](PF_6) with arrow to denote chloride. Hydrogens are omitted and the bound terminal ligand 2,2:6,2-terpyridine is present perpendicular to the plane of the paper for clarity.

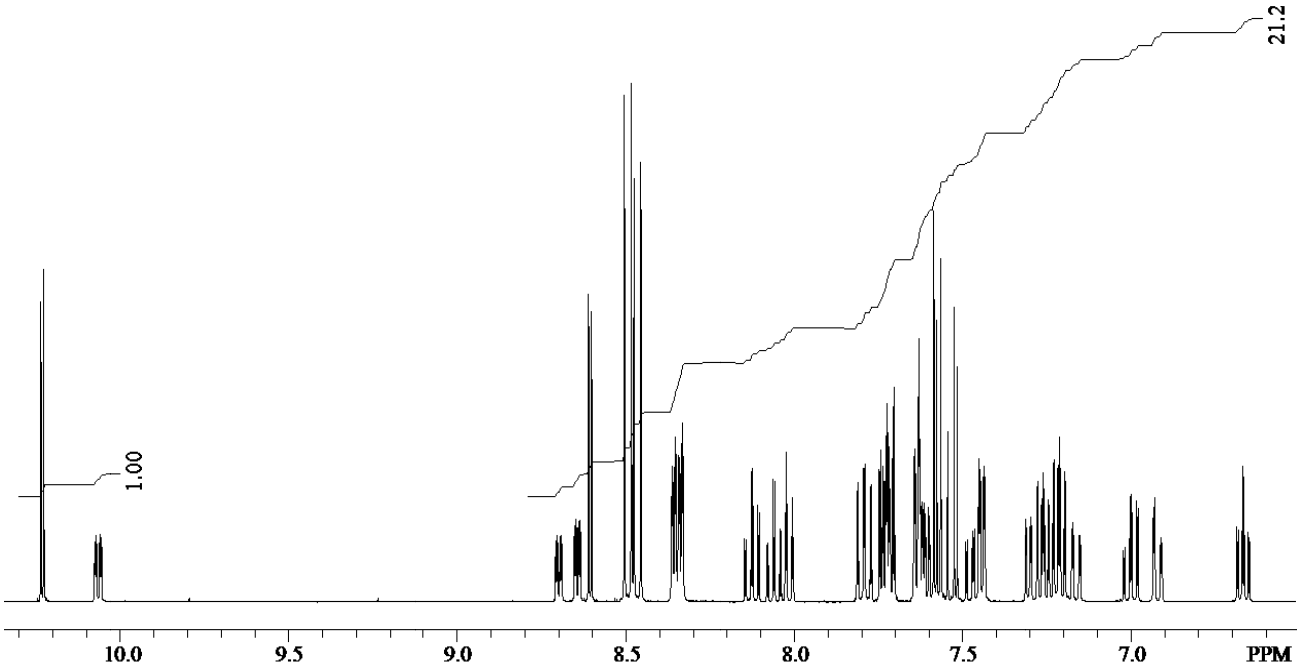

Figure A-13. Expanded aromatic region of the ^{1}H-NMR spectrum of [(tpy)OsCl(dpp)](PF_6) in CD_3CN with peak integrations.